SDL-6-588-1

INFLUENCE OF CO^{60} GAMMA IRRADIATION ON THE BULK AND SURFACE RECOMBINATION RATES IN SILICON

NASA GRANT NsG-588

Theoretical and Experimental Studies of Radiation Damage to Semiconductor Surfaces and the Effect of this Damage on Semiconductor Device Performance

1 March 1967

by

Michael A. Littlejohn
Robert W. Lade (Advisor)

Semiconductor Device Laboratory
Department of Electrical Engineering
North Carolina State University
at
Raleigh, North Carolina

ABSTRACT

LITTLEJOHN, MICHAEL ANTHONY. Influence of Co^{60} Gamma Irradiation on the Bulk and Surface Recombination Rates in Silicon. (Under the direction of ROBERT WALTER LADE).

The technique of photoconductive decay in rectangular semiconductor filaments was used to measure the bulk and surface lifetimes and surface recombination velocity of 100 ohm-cm n- and p-type float zone refined silicon doped with phosphorous and boron, respectively. The influence of Co^{60} gamma radiation on these important material parameters was investigated, and a more complete mathematical model for surface recombination velocity was formulated. This model includes the effects of recombination in the space charge region near the surface, and it is shown that this effect can have a significant contribution to the total surface recombination velocity.

The recombination center which dominates the bulk lifetime in n-type material was found to be different from the one which controls the lifetime in p-type material. In n-type material the recombination center created by gamma radiation was found to be located at 0.40 eV below the conduction band edge, and is associated with a phosphorous-vacancy complex in the crystal. In p-type material, the center was located at 0.18 eV above valence band edge. It is believed that this is the first time such a recombination center has been observed in p-type float zone refined material.

Irradiation by gamma rays had a drastic effect on the surface recombination velocity in n-type silicon, while in p-type silicon there was only a slight variation of this parameter with radiation. In n-type material the surface recombination velocity exhibited a relative minima with gamma ray exposure. In p-type material there was a slow monotonic increase in the surface recombination velocity as each sample was irradiated.

The surface lifetime obeyed the one level Shockley-Read equation for the lifetime. No single energy level could be located at the surface since the position of this level changed with each additional exposure to gamma radiation. This behavior cannot be explained with the data and models used in these experiments.

INFLUENCE OF Co^{60} GAMMA IRRADIATION ON THE BULK AND SURFACE RECOMBINATION RATES IN SILICON

by

MICHAEL ANTHONY LITTLEJOHN

A thesis submitted to the Graduate Faculty of
North Carolina State University at Raleigh
in partial fulfillment of the
requirements for the Degree of
Doctor of Philosophy

DEPARTMENT OF ELECTRICAL ENGINEERING

RALEIGH

1 9 6 7

APPROVED BY:

_____

Chairman of Advisory Committee

SDL-6-588-1

INFLUENCE OF CO^{60} GAMMA IRRADIATION ON THE BULK AND SURFACE RECOMBINATION RATES IN SILICON

NASA GRANT NsG-588

Theoretical and Experimental Studies
of Radiation Damage to Semiconductor
Surfaces and the Effect of this Damage
on Semiconductor Device Performance

1 March 1967

by

Michael A. Littlejohn
Robert W. Lade (Advisor)

Semiconductor Device Laboratory
Department of Electrical Engineering
North Carolina State University
at
Raleigh, North Carolina

ACKNOWLEDGEMENTS

The author extends his deep appreciation to Dr. Robert W. Lade for the continuous help, guidance, criticism, and inspiration which was offered during the course of this research.

Dr. N. F. J. Matthews deserves many thanks for help with the computer programming and for his critical proof reading of the rough draft of this thesis.

The author's gratitude is expressed collectively to all his fellow graduate students for the pleasure of their friendships and the many discussions which were always instructive and interesting.

Finally, the author would like to offer more than just thanks to his wife Kathy, who bore the brunt of his many moods and temperaments, typed the rough draft of this thesis, and helped provide the family income.

Acknowledgement is made to the National Aeronautics and Space Administration for financial support of this work.

TABLE OF CONTENTS

TABLE OF CONTENTS (Continued)

LIST OF TABLES

LIST OF FIGURES

LIST OF FIGURES (Continued)

LIST OF FIGURES (Continued)

LIST OF FIGURES (Continued)

LIST OF FIGURES (Continued)

LIST OF FIGURES (Continued)

LIST OF FIGURES (Continued)

LIST OF FIGURES (Continued)

LIST OF FIGURES (Continued)

CHAPTER I

1. INTRODUCTION

Semiconductor and solid state electronic devices have had a vast impact on the space capabilities of the United States and other countries as well. These devices have reduced the size requirements of electronic packages used in space vehicles, increased the reliability of electronic instruments and equipment in space environments, and they are probably the most important single contributing factor in man's conquest of outer space.

However, before the picture becomes too enticing, it should be pointed out that many new and interesting problems have arisen concerning the performance of solid state devices in the environment of outer space. Even if the technological problems involved in producing and manufacturing these devices can be solved, environmental problems will remain as the most challenging barriers in pursuit of the electrical and electronic slice of the "aerospace pie".

In recent years much research has been carried out with the purpose of studying the effects of irradiation induced damage to semiconductor materials and devices. However, most of this effort has been in the investigation of bulk material variations (induced lattice defect concentrations, reduced bulk minority carrier lifetime, conductivity and mobility variations, etc., as a function or the irradiation exposure) and study of device terminal volt-ampere characteristics. These latter

studies are, for the most part, being carried out on production line state-of-the-art devices.

Present day technology has minimized the effects of bulk properties on the behavior of many semiconductor devices, and in many cases it is the physical surface of the structure which limits its optimum performance. Therefore, studies of the influence of nuclear irradiations on the surface properties of semiconductor materials are in order.

It is the purpose of this thesis to conduct such an undertaking. To limit the scope of the problem only the effects of irradiations with gamma rays on n- and p-type material of one hundred ohm cm resistivity will be investigated, To investigate the surface properties by the experimental techniques utilized requires a knowledge of certain bulk parameters. Therefore, some information concerning bulk damage due to gamma irradiations will be presented.

The experimental work reported herein has pointed out other fruitful areas of investigation, and some of these areas have already been investigated (Mattauch, 1966), while others are being examined at the present.

Probably the most salient feature of this work has been a clearer understanding of the concept of surface recombination velocity, along with a more complete mathematical theory for this parameter than previously reported.

CHAPTER II

2. IMPERFECTIONS IN SILICON

2.1 Lattice Structure of Silicon

Silicon is an element in the fourth column of the periodic table having four valence or outer shell electrons (i.e., silicon has a valency of four). It is known as an elemental or group IV semiconductor. The atomic arrangement of a perfect silicon crystal in thermal equilibrium is such that each atom is surrounded by four equidistant neighboring atoms. The equilibrium spacing between nearest neighbors is 5.429 A^{o} (Rhodes, 1964). Each atom forms what is known as a co-valent or homopolar bond with each of its four nearest neighbors. This means that two electrons are shared between two identical atoms, which results in a group of eight electrons associated with each atom. A very stable structure results. It will be recalled that eight electrons in an outer shell results in the shell being closed, or chemically complete. (For a complete quantum mechanical discussion of the homopolar bond, see Heitler, 1956.) For such a regular arrangement of atoms, the perfect silicon crystal would be electrically neutral, and no conduction could result at low temperatures. In reality, a perfect crystal is impossible to obtain, and deviations from this ideal structure do occur. These deviations, which are in the form of substitutional impurity atoms, broken co-valent bonds, lattice vacancies and interstitials are responsible for the semiconducting properties of elements in group IV.

Since space environments and their radiation fields produce some of the above-mentioned deviations from a perfect crystal, a general discussion of imperfections in silicon follows. After this discussion, a method which allows the general examination of all types of imperfections in terms of the electrical properties of silicon will be reviewed. This method is the energy-band-theory of solids.

2.2 Types of Imperfections Pertinent to this Discussion

The term "single crystal" is used to describe a solid with a high degree of crystalline purity, while the term "imperfection" is used to describe any manner in which a single crystalline solid departs from absolute perfection. The study of imperfections in crystals admits to the fact that a truly perfect crystal does not exist. There are three types of imperfections which will prove to be important in the material presented in this thesis. They are: a) electrons and holes; b) foreign atoms and chemical impurities; and c) lattice defects.

2.2.1 Electrons and Holes

Electrons and holes result in a silicon crystal when there is sufficient thermal or optical (and other forms of energy as well) energy to break a co-valent bond. The electrons become free and are available for conduction; thus, the term conduction electrons. A freed electron leaves behind a localized positive charge, and this "position" in the lattice

is attractive to other electrons. By attracting other electrons this "hole" or positive charge is available for conduction also, in that the attracted electrons leave behind other net positive charges. These electrons and holes thus cause the conductivity to be some finite number instead of identically zero as indicated for the perfect silicon crystal. For this reason electrons and holes which result from broken co-valent bonds are called intrinsic carriers. For any temperature other than absolute zero, there will always be some intrinsic carriers present in a real silicon crystal. For example, at room temperature ($300^{o}K$), the intrinsic resistivity of silicon is 2.3×10^{5} ohm cm. In this sense intrinsic electrons and holes are, in fact, imperfections.

2.2.2 Foreign Atoms and Chemical Impurities

Any foreign atom in the lattice, whether it is purposely introduced or not, constitutes an imperfection in the crystal. The presence of these chemical impurities is unavoidable, since crystals are prepared from impure ores.

There are two ways in which chemical impurities may enter a perfect crystal and form an alloy. The impurity may simply occupy a lattice site normally occupied by a silicon atom, in which case the impurity is said to be "substitutional". Also, it may occupy a position intermediate to other silicon atoms, in which case it is called an "interstitial" impurity. The substitutional impurities do not grossly disturb the crystal lattice, while interstitial atoms usually create chemical

complexes which locally distort the periodicity of the crystal. Either of these two types of impurities may be introduced into a crystal at the time it is grown, or at some later time by additional processing. The term "doping" is used to denote the intentional introduction of impurities into the crystalline lattice.

2.2.3 Lattice Defects

Lattice defects are created any time the periodicity of the lattice is disturbed by misplaced atoms. Thus, an interstitial atom could be treated as a lattice defect. Also, an empty space in the lattice, or a vacancy, is a second type of lattice defect. These two types of defects are classified as Schottky defects and Frenkel defects, respectively. A Schottky defect is equivalent to a simple vacancy in the crystal, where the atom has been extracted from the crystal (e.g., by an electric field). A Frenkel defect is produced when an atom is removed from a lattice site to an interstitial position. Thus, there results two types of lattice defects which are classified as one. It should be noted that lattice defects may be produced in the same manner as electrons and holes, with much more energy required in the former process.

It is possible to judge the quality of a crystal by the types and numbers of imperfections which are present. The electrical properties of a crystal generally provide a very sensitive indication of the presence of imperfections, with some properties being more sensitive indicators than others.

2.3 Crystal Surfaces

There exists one more natural and very important type of imperfection which should be discussed. This imperfection plays a major role in the material contained in this thesis.

Every real crystal has surfaces or terminations of the lattice structure. Since the periodicity of the lattice is certainly disturbed, the crystal surface is a true imperfection, and an unavoidable one in any practical situation. The effects amd implications of this type of imperfection can be fully understood only after the band theory of solids and its relationship to imperfections in the crystal lattice is discussed.

2.4 The Band Theory of Solids and the Relation of Imperfections

A complete discussion of the regular arrangement of atoms in a crystal involves an introduction to the theory of crystallography and quantum mechanics. A complete discussion would be pointless since we are interested primarily in the electrical properties of silicon. It will suffice to say that, whereas in ordinary empty space (the "vacuum") all points are equivalent, in crystal space this is not true. Any crystalline solid requires the development of certain symmetry properties which are characteristic of the "crystal space" for the solid involved. Then using this crystal space and its symmetry properties, we can develop a mathematical theory for the description of the motion of particles in this crystal space. In other words, we could develop a theory of mechanics for the

particles in the crystal. Very fortunately, this theory has been developed; for due to the microscopic nature of the system, the particles in the system obey the laws of quantum mechanics. A fundamental outgrowth of the laws of quantum mechanics is the energy band theory of solids. The results of the band theory of solids as applied to electrons and holes in silicon tells us that the energies which these particles can have are quantized, or restricted to certain allowed values. For particles in a periodic lattice such as silicon, the energies are spread out into quasi-continuous bands. For convenience, the valence band is defined as that energy band which has the highest energy and is completely filled at $T = 0^{o}K$. The band of lowest energy which is empty at $T = 0^{o}K$ is called the conduction band. (In these definitions, a perfect crystal is implied.) The difference between the lowest and highest energies is called the forbidden region or band. In order for electrical conduction to exist, some form of energy is required to change the energy of electrons in the valence band. If the temperature is greater than $0^{o}K$, or if optical energy is supplied to the system, then valence electrons can become conduction electrons. Note that these results from band theory are in agreement with the quantitative discussion given in 2.2.1. A silicon crystal is thus able to be viewed in terms of the very simple energy band model shown in Figure 2.1.

This figure shows energy versus distance assuming that the crystal is homogeneous throughout; that is the energy levels do not vary with position in the crystal.

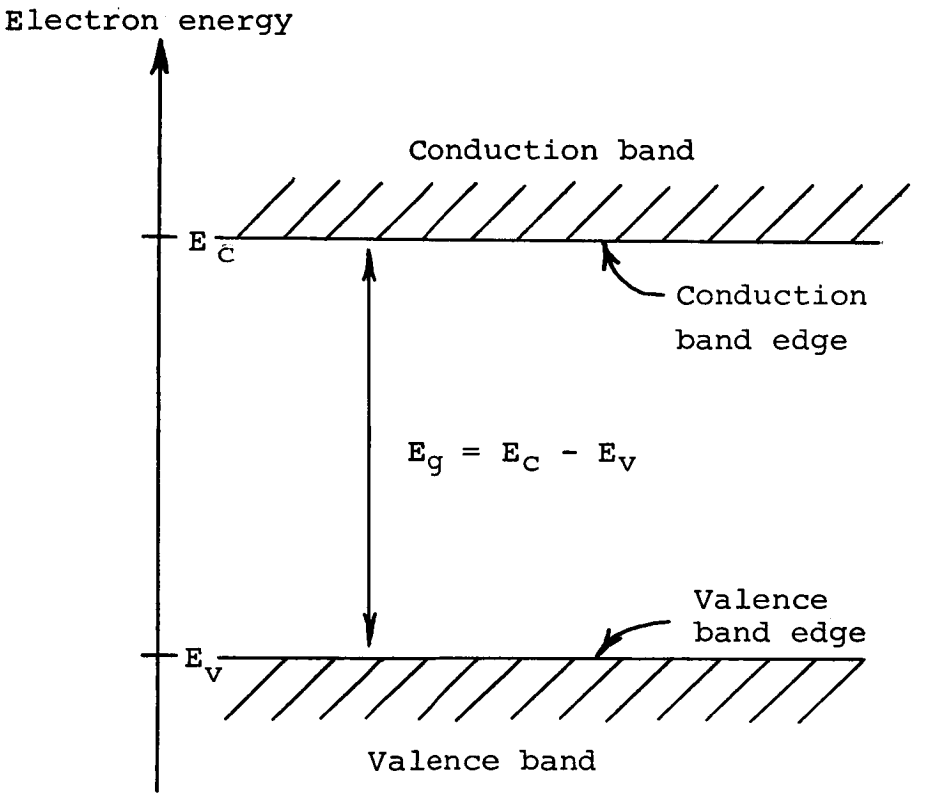

Figure 2.1. A simple energy band diagram of a semiconductor

Now, it can be generally stated that imperfections in a crystal introduce allowed energy levels into the forbidden band. That is, imperfections create allowed energy levels in the forbidden band which are consistent with the quantum mechanical description of an electron in the crystal. For example, if one introduces an atom from group V of the periodic table (e.g., phosphorous) into the silicon lattice, an additional valence electron exists apart from the four required to complete the homopolar bonds. This additional electron is very weakly bound to its phosphorous atom, and only a small amount of energy is required to remove it from the vicinity of the phosphorous atom. The electron is then available for conduction. In the energy band scheme we would represent such an imperfection (substitutional impurity) as having an energy somewhat below the conduction band edge. Calculations show that this level is approximately 10^{-2} ev. below the conduction band edge (Nussbaum, 1962).

As mentioned previously, the surface of a crystal is an imperfection, and when treated from the energy band theory, the surface also creates allowed energy levels in the forbidden region. A complete review of this treatment is presented in Many et. al., (1965).

The fact that all types of imperfections, including surfaces, introduce allowed energy levels in the forbidden band is one of the most important results of the theory of solids. These energy levels, along with other information

from the theory of statistical mechanics, allow the computation of many of the electrical parameters of semiconductors. The parameters that are not directly computable are related to those that are.

2.5 Summary

The energy band concept allows the discussion of imperfections in terms of the energy levels which they introduce into the forbidden band. Most electrical properties of semiconductors are related either directly or indirectly to these energy levels. Thus, it appears that electrical measurements can give information relating to these energy levels. One must admit that these levels give no information concerning the crystalographic structure of a given imperfection. However, the establishment of a cause and effect relation can be obtained. It is this cause and effect relation that is to be examined in this thesis.

CHAPTER III

3. IRRADIATION INDUCED IMPERFECTIONS IN SILICON

3.1 Historical Development

The field of study of irradiation damage to semiconductor crystals began in 1947 when Lark-Horowitz et. al., (1948) and Johnson and Lark-Horowitz, (1949) at Oak Ridge and Purdue University exposed silicon and germanium to reactor irradiations and cyclotron particles. It should be noted that this work began even before the invention of the transistor, and was probably an outgrowth of the utilization of solid-state rectifiers during World War II.

The original goal was a complete and thorough description of the defect structure produced by nuclear irradiations. So far, this goal has not been achieved, and subsequent studies, along with the understanding that these studies have produced, indicate that the original goal was unrealistic. First of all, it has become evident that the defect configurations produced from a single energetic collision can be maintained only at very low temperatures. Second, imperfections remaining at room temperature are likely to be complexes resulting from interactions between imperfections caused by irradiation and imperfections already present in the lattice. Finally, it was recognized that an understanding of the relation between defect structure and physical behavior as well as the interactions between imperfections was very important to a better basic understanding of solids. For these reasons, the primary

emphasis in such studies has changed from the use of semiconductors as a medium in which to study radiation damage to the use of radiation as a tool for investigating defect and defect interactions in these materials (Crawford, 1964).

3.2 Methods Used to Study Radiation Damage

The principle techniques which have been used to study radiation damage in silicon are electron spin resonance, optical absorption, Hall effect and resistivity variations, photoconductivity and various lifetime measurements.

Electron spin resonance is a phenomenon in which electromagnetic energy is resonantly absorbed by electrons in a magnetic field. Electrons near an impurity atom can be excited into the conduction band if photons whose energy corresponds to the energy separation between the impurity level and the conduction band edge are incident on the crystal. This excitation results in a resonance or absorption peak in the spin resonance signal. For silicon, spin resonance is usually examined by placing the sample in a resonant cavity excited by a microwave oscillator. As the magnetic field is varied through the resonant condition, pronounced absorption or reduction in the Q of the cavity occurs. While this technique allows the determination of the energy separation between an imperfection and a band edge, it identifies neither the band nor imperfection.

Optical absorption is similar to spin resonance in that it also utilizes the result that absorption occurs when transitions from impurity centers are induced by energetic photons.

In this technique the transmission of photons through a crystal is measured and the absorption spectra observed (transmission versus energy of the photons). This method also does not identify the band with which interactions occurs.

The Hall effect, when combined with resistivity measurements, gives a fairly straight-forward method for analyzing data concerning the energy levels of irradiation induced imperfections. The Hall co-efficient is inversely proportional to the majority carrier concentration. The Hall mobility is the ratio of the Hall co-efficient and the resistivity. It provides information concerning the imperfections since the mobility is influenced by the scattering of charge carriers due to these imperfections. If the Hall co-efficient and the resistivity are measured as function of temperature, energy level positions can be determined. However, since this is a majority carrier measurement, only levels in the upper half of the gap can be determined in n-type material and levels in the lower half of the gap in p-type material.

Photoconductivity is, in a sense, an extension of optical absorption. If light of the proper frequency is incident on a crystal, the conductivity increases due to an increase in carrier concentration. If photons of various energies are used there will be changes in the photoconductivity when carriers are excited into the bands from levels due to imperfections. By observing photoconductivity as a function of photon energy,these energy levels can be located with respect to a band edge.

The above mentioned techniques all have distinct advantages and disadvantages. However, there is one major disadvantage that precluded their use in this research. In order to obtain data easily interpretable by the above techniques it is necessary to excessively damage the crystal with irradiation. Since these techniques are primarily majority carrier ones, the crystal must be damaged to the extent that the number of defects are of the same order of magnitude as the majority carrier concentration. Also, the experimental equipment required is very expensive, if precise measurements are to be made.

Probably the simplist and one of the most successful techniques used to study irradiation damage in semiconductors is the measurement of minority carrier lifetime. When excess carriers are created in the bands, the laws of thermodynamics require that an equilibrium (or steady state) be established. The rate at which an equilibrium is achieved governs the lifetime of created excess carriers.

There are many techniques for the measurement of carrier lifetime. Several methods utilize p-n junction measurements (Kingston, 1954); and there are many bulk methods. In the p-n junction there are various parameters which are strongly dependent on the lifetimes in the bulk regions. The filamentary transistor technique of Haynes and Shockley, (1951) is also utilized, and has the advantage that mobilities can be measured in the same experiment.

The method chosen here to investigate radiation-induced imperfections in silicon is the method of photoconductive decay. Excess carriers are created by a short pulse of light and the decay of these carriers back to thermal equilibrium is observed. The rate of decay gives a lifetime which is the sum of both bulk and surface contributions. Proper experimental conditions allow the investigation of both bulk and surface properties (See Appendix I). While this is a distinct advantage, junction techniques were not utilized due to the fact that additional imperfections are created during the processing steps used to fabricate the devices.

3.3 Effects of Irradiation Sources Utilized in Radiation Damage Experiments

The type of damage created in any material depends to a great extent on the type of irradiation employed. Heavy particles, such as neutrons, tend to create large disordered regions and isolated point defects. The reason for this is that the mass of the incident particle is of the same order of magnitude as the silicon atom. Thus, an appreciable portion of the incident particle energy can be transferred to a silicon atom. Unless the energy of the incident particle is very low, the displaced silicon atom usually possesses enough energy to cause other displacements in the lattice.

Electrons and gamma rays, on the other hand, can transfer much less of their energy to the silicon atoms because of their much smaller mass, and the damage produced is more uniform.

In this research, heavy particles were not desirable as a source of radiation damage because it was desired to have as uniform a damage mechanism as possible. With electrons, the damage is still slightly non-uniform, while not nearly as drastic as neutrons. It was felt that gamma rays would probably produce the most uniform damage, and since several convenient sources of Co^{60} gamma rays were available, this is the source of irradiation used. Also, it was realized that gamma rays and electrons create similar types of damage in silicon since the principle damage mechanism caused by gamma rays result from Compton electrons.

3.4 Characteristics of Gamma Rays

Gamma rays are electromagnetic radiations produced during nuclear reactions. The emission of gamma rays is a mechanism by which the energy of excitation of a nucleus is removed. Gamma rays accompanying a particular type of nuclear reaction are composed of photons with either a single energy or a group of discrete energies. Typical energies range from a few Kev to several Mev (Price, 1964).

Gamma rays interact with matter primarily through three mechanisms, the photoelectric effect, Compton scattering, and pair production. In the photoelectric effect, the gamma photon interacts with the atom as a whole. In Compton scattering the primary photon interacts with one of the orbital electrons of the atom. The interaction may be treated as an elastic collision between the photon and the electron. In pair production

the primary photon disappears and its energy goes into rest mass energy and the kinetic energy of the hole and electron produced (Price, 1964). Figure 3.1 shows a plot of the atomic number of the photon absorber as a function of the photon energy. Silicon has an atomic number of 14 and the gamma source used (to be discussed in Chapter IV) has a mean energy of 1.25 MeV. Thus it can be seen that the Compton effect is the mechanism by which gamma rays interact with silicon.

3.5 Energy Levels Observed in Gamma Irradiated Silicon

A survey of the literature shows that there have been many various defects observed in gamma ray irradiated silicon. These defects are generally classified by their energy level position in the forbidden region. The literature is summarized in Table 3.1. It should be pointed out that these energy level positions are all located in the bulk of the material. No information has been found concerning surface damage to silicon which has had no processing steps before the measurements were made. The primary purpose of this research is to examine the effects of gamma irradiation to the surface of silicon. The bulk properties obtained will be useful in the analysis of the data, and will be presented for completeness.

3.6 Summary

A brief resumé of the historical aspects of radiation damage studies in semiconductors has been presented, along with some of the techniques used to investigate such damage in silicon.

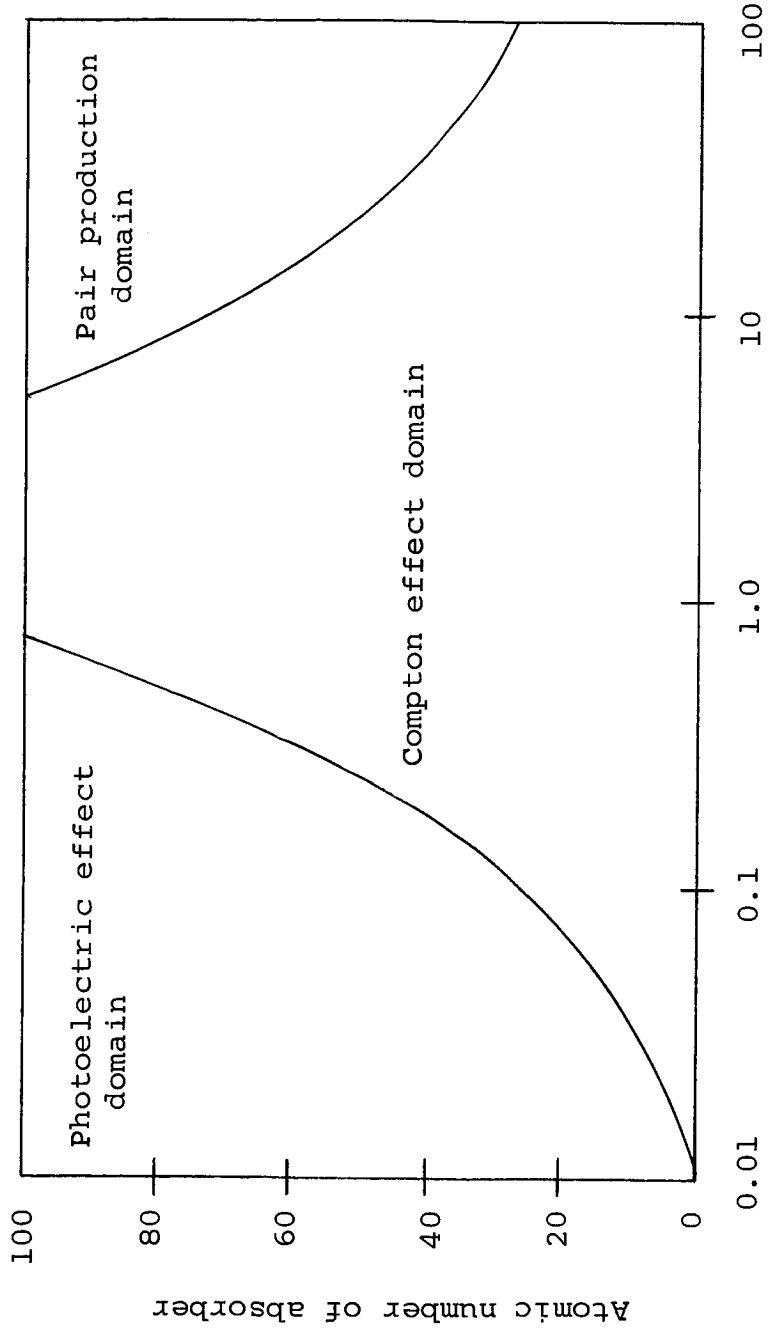

Figure 3.1. Diagram showing energies at which each of the principal gamma ray processes becomes dominant (Source: Evans 1955, p. 712)

Table 3.1 Irradiation induced defects in silicon caused by gamma rays

Level Position (Ec-Er) eV	Material	Resistivity (ohm-cm)	Technique	Reference
	Levels in the upper half of the forbidden region			
.10	n	-	Microwave lifetime	Inuishi & Matsuura
.146 to .173	nPC, nFZ	.1 - 56	Hall Effect	Sonder & Templeton
.16	n	-	Hall Effect	Inuishi & Matsuura
.17	nFZ	2.8 - 140	Hall Effect	Saito, et. al.
.16	nPC, nFZ	80	Hall Effect	Nakana & Inuisha
.16	nPC, nFZ	60 - 250	Hall Effect	Tanaka & Inuisha
.16	nFZ	32,77	Photoconductive Decay	Glaenzer & Wolk
.23	n	-	Microwave lifetime	Inuisha & Matsuura
.38	n	-	Hall Effect	Tanaha & Inuisha
.40	nFZ	2.8 - 140	Hall Effect	Sito, et. al.
.40	nPC, nFZ	80	Hall Effect	Nakana & Inuishi
.40	nFZ	32,77	Photoconductive Decay	Glaenzer & Wolk
.42	n	-	Hall Effect	Tanaka & Inuisha
.43	n(sB doped)	-	Hall Effect	Sonder & Templeton
.47	n(P doped)	-	Hall Effect	Sonder & Templeton

(Continued)

Table 3.1 Continued

Level Position (E_r-E_v) eV	Material	Resistivity (ohm-cm)	Technique	Reference
	Levels in the lower half of the forbidden region			
.35	pPc	-	Hall Effect	Sonder & Templeton
.28	pFZ	-	Hall Effect	Sonder & Templeton
.28	-	-	Microwave lifetime	Inuishi & Matsuura
.27	pPC	-	Microwave lifetime	Nakana, et. al.
.27	pPC, pFZ	-	Hall Effect	Tanaka & Inuishi
.21	pPC	-	Microwave lifetime	Nakana, et. al.
.21	pFZ	-	Hall Effect	Soner & Templeton
.12	p	-	Microwave lifetime	Inuishi & Matsuura

nPC = n-type pulled crucible material
nFZ = n-type float zone refined material
pPC = p-type pulled crucible material
pFZ = p-type float zone refined material

The type of damage produced by the various nuclear radiations has been discussed, and some of the measurement techniques have been analyzed. From the above mentioned results, it was decided that the method of the measurement of lifetime due to the photo-conductive decay would be utilized to study the effects of gamma irradiation on the surface and bulk properties of silicon.

CHAPTER 4

4. EXPERIMENTAL TECHNIQUES

4.1 Preparation of Materials and Samples

Single crystal ingots of silicon were purchased from the Electronic Chemicals Division of Merck and Company, Inc., Rahway, New Jersey, and from the Monsanto Company of St. Louis, Missouri. These ingots were float zone refined by the Czochralski technique and both n- and p-type crystals were obtained.

Upon receiving the ingots, they were mounted on a piece of ceramic tile with the aid of glycholpthaiolate wax as an adheshive. The ingots were then placed in a Micro Mech diamond saw, and a slice was cut parallel to the longitudinal axis of the ingot. This slice provided a reference edge, and all processing of samples was carried out with respect to this plane. Next, two slices were cut perpendicular to the longitudinal axis of the ingot. The thickness of these slices was approximately .205 inches, and they were labelled according to their position on the ingot. After lapping with #120 grit (approximately 110 micron particle size) silicon carbide abrasive, the resistivity was measured using the standard four point probe technique. These two slices were then mounted on a piece of ceramic tile, one slice upon the other, and three rectangular bars were cut from each with the diamond saw. Each bar was labelled according to the slice from which it was cut and

according to its position on the slice with respect to the reference edge. Each bar had dimensions of .205 inches x .205 inches x .610 inches. Figure 4.1 shows a graphical sketch of the ingot, its reference edge, and the relative position of each sample cut from a slice from the ingot. Each sample was next lapped on all sides and ends with #120 grit until there was no further indication of damage on the surfaces caused by the cutting action of the diamond saw blade. Care was taken to insure that the samples remained rectangular. The samples were scrubbed in hot water and alconox detergent to remove any particles and residue which remained after lapping. After a five minute ultrasonic bath in methanol, the samples were given a degreasing treatment, which consisted of a five minute bath in boiling acetone and another bath of the same duration in boiling trichlorethaline. The above treatments were necessary to insure that the samples were completely free of all residue which resulted from the lapping process. Cleanliness is the most important step in fabricating good ohmic contacts to the samples. The previous process, especially the ultrasonic bath, was the one that gave the best results and the most reproducible ohmic contacts. It was deduced primarily by trial and error.

The technique used to apply ohmic contacts to the sample was the electroless nickel plating method as described by Sullivan and Eigler (1957). The electroless nickel plating solution consists of proportions of the following constituents:

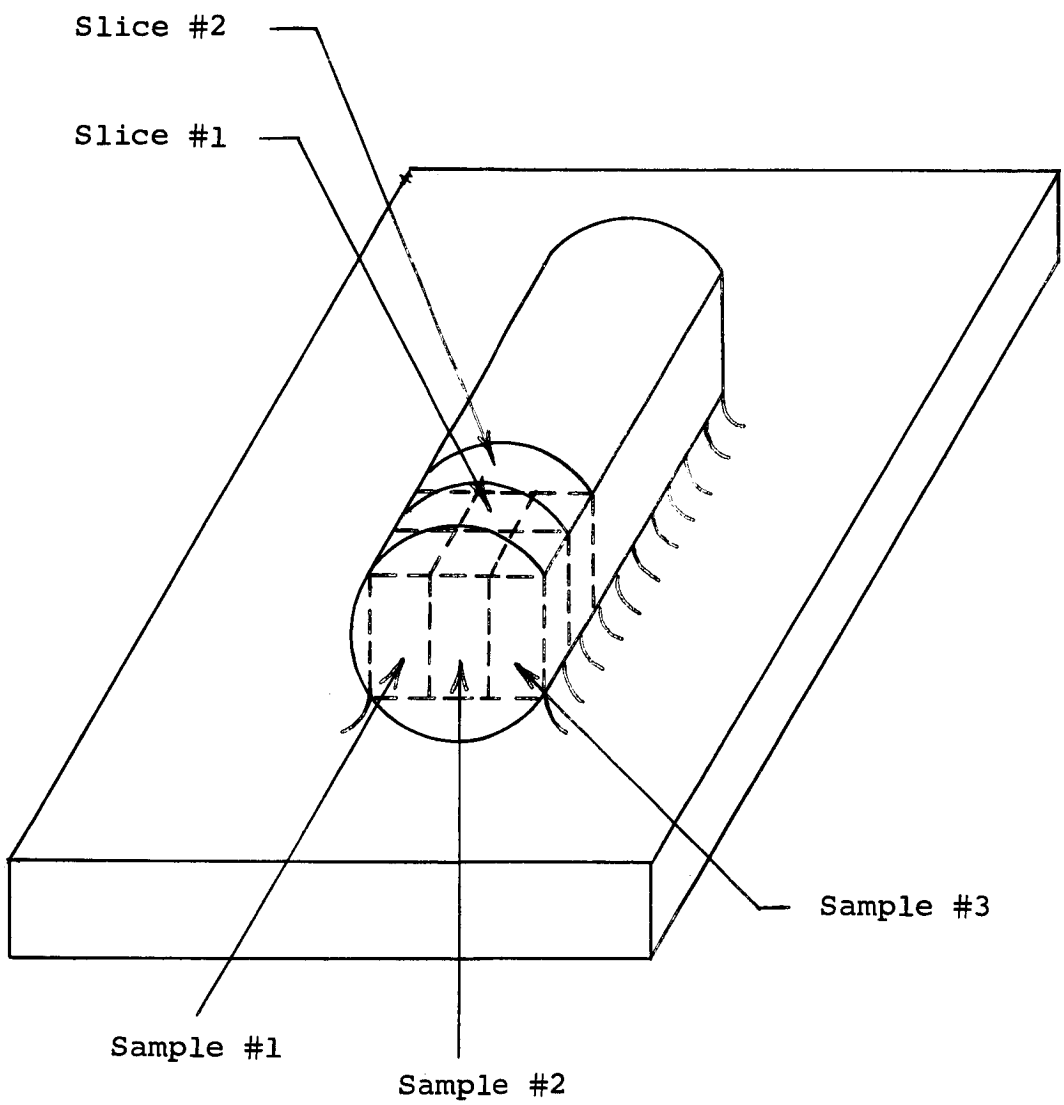

Figure 4.1. Isometric drawing of sample orientation on a silicon ingot

a) 30 gm/liter - Nichelous chloride ($NiCl_2 \cdot 6H_2O$)

b) 50 gm/liter - Ammonium chloride (NH_4Cl)

c) 65 gm/liter - Ammonium citrate ($[NH_4]_2 HC_6H_5O_7$)

d) 10 gm/liter - Sodium Hypophosphite ($NaH_2PO_2 \cdot H_2O$)

The reagent grade chemicals are mixed with one liter of demineralized water to form the nickel plating solution. In order that contacts may be made to the samples, the solution is heated to approximately 80° to $90^{\circ}C$, and enough sodium hydroxide (N_aOH) is added to turn the solution a bright blue color. The sodium hydroxide activates the solution by changing its pH. The samples are left in the nickel plate for three minutes and after removal, they are rinsed in deionized water. Because the samples are nickel plated on all sides and ends, it is necessary to remove the nickel from the sides, leaving only the ends plated. This can be done in two ways. One is to mask the ends of the sample with apiezon wax and then etch the sides chemically with a mixture of 95% nitric acid and 10% hydroflouric acid. Another way is to simply lap the sides of the sample until all the nickel is removed. It is important that all the nickel plate be removed since its presence would affect the electrical properties of the surface. This latter method was chosen, after tests showed that if care was taken to remove all the nickel plate, no difference in lifetime was observed for samples treated by either of the two techniques, and the lapping technique was considerably faster. After the nickel plate is removed from the sides of the samples, they are given a cleanup process and

the nature of the contacts is examined. This is done by observing the voltage versus current using a Textronic 575 curve tracer. Figure 4.2 shows typical v-i characteristics obtained from this instrument for p- and n-type samples. The contacts for the p-type material were not as good as those for the n-type due to the presence of a significant amount of phosphorous in the nickel plating solution. Phosphorous is a donor atom in silicon and thus tends to create a junction if the proper amount is added to p-type material. A careful examination of the properties of the contacts to p-type material showed that they would be sufficient if care was taken to not overheat the sample during plating. Any deviation from ohmicity resulted in the samples being rejected.

The minority carrier lifetime was measured by the method of photo-conductive decay, as mentioned previously. The theory for this measurement is given in Appendix I, and the instrumentation and equipment involved is discussed in section 4.2. The lifetimes for all six of the samples shown in Figure 4.1 were measured and recorded. It was observed that the lifetime varies considerably with radial distance in the silicon ingots used, and thus the orientation of the samples cut from slices 1 and 2 in Figure 4.1 cannot be arbitrary. This is the primary reason for the reference edge. In order for the samples to be acceptable, the lifetimes of corresponding samples on slices 1 and 2 must not deviate from each other by more than 10%. (This was set as the maximum allowable deviation for the experiments performed.) If all corresponding sample lifetimes fell within

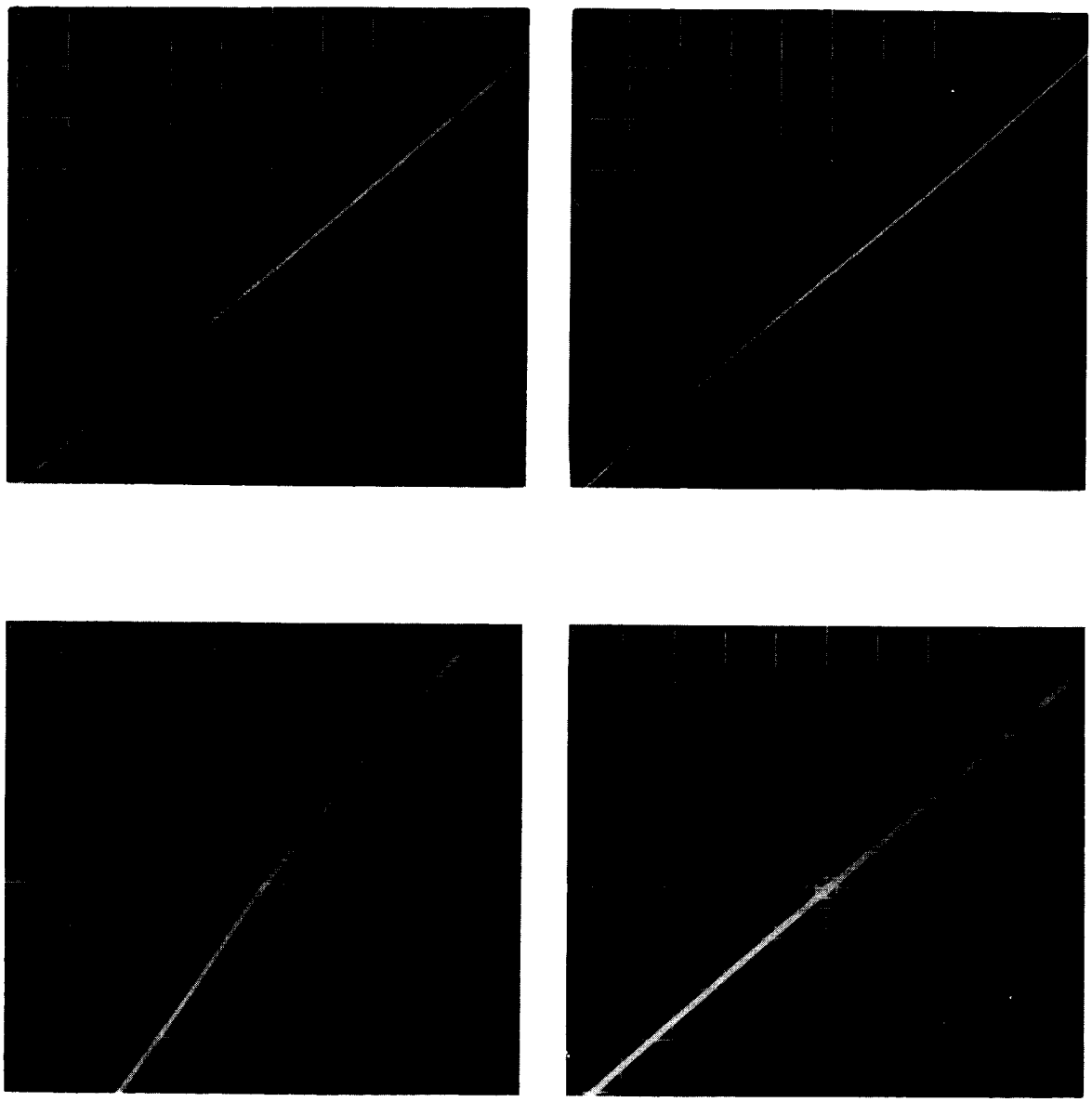

Figure 4.2. Photographs of v-i characteristics of n-type (two top photos) and p-type (two bottom photos) samples. The scale on the left photos are 2 ma/div horizontal and 1 volt/div vertical. The scales on the right photo are reduced by a factor of ten

this limit, then the samples from slice 2 were chosen to be made into thin filaments for the surface parameter measurements.

The three rectangular bars from slice 2 were mounted on ceramic tile and each bar was cut into three thin filaments. The dimensions of the thin filaments were .610 inches x .205 inches x .025 inches. This latter dimension was changed for some of the samples. This will be noted when these samples are referred to in the text.

Each thin filament was carried through several surface preparation processes prior to the final chemical polish. First, these samples were lapped for 15 minutes on each side with #400 grit (approximately 25 micron particle size) silicon carbide abrasive. This was followed by another 15 minute lapping of both sides with #600 grit (approximately 15 micron particle size) silicon carbide abrasive, and then each side of the samples was given a rough mechanical polish by lapping with S. S. White and Company's 10 micron polishing alumina for thirty minutes. The surfaces of each sample were free from all saw dislocations. After baths in boiling acetone and trichlorethylene, the ends of the samples were coated with apiezon wax dissolved in trichlorethylene to protect their contacts, and the samples were placed in a culture dish overnight to allow the wax to dry. This was necessary to assure that the apiezon would not be removed from the contacts during subsequent chemical etching.

The chemical polishing of the samples was accomplished with an etch solution consisting of 90% hydroflouric acid and

10% nitric acid. Figure 4.3 shows the apparatus used to chemically polish the samples. The agitation caused by the movement of the turntable revolving at 33-1/3 r.p.m. was sufficient to insure that the surface of the sample was uniformly etched. Strong illumination during etching seemed to improve the surface polish. The normal etching time was ten minutes. However, this was also changed for several samples, and will be noted for specific cases. The surfaces which resulted from this technique, while not optically flat, were deemed satisfactory for this work. After the chemical polish, the apiezon was removed with trichlorethylene and the samples were cleaned by boiling in acetone and trichlorethylene. The sample preparation was then complete, and the samples were ready for measurements.

4.2 Instrumentation and Measurement Techniques

The primary quantity which was measured in this research was the decay time constant of the photoconductivity of a semiconductor bar. Figure 4.4 shows the instrumentation used to take this measurement.

The sample tester consists of a variable constant current source with provisions for polarity reversal and accomodations for the sample holder. Two different sample holders were used. One holder would accept only a single sample while the other had provisions for a total of twelve samples. The former holder was used when only room temperature measurements were made while the latter was used to take measurements as the temperature

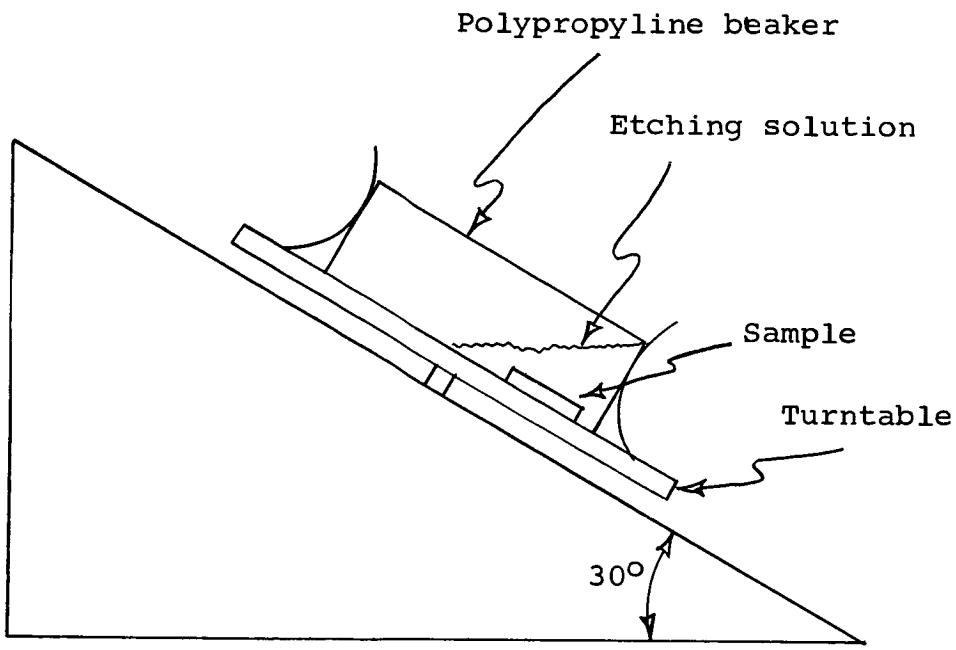

Figure 4.3. Diagram of the angled turntable used for chemically polishing samples

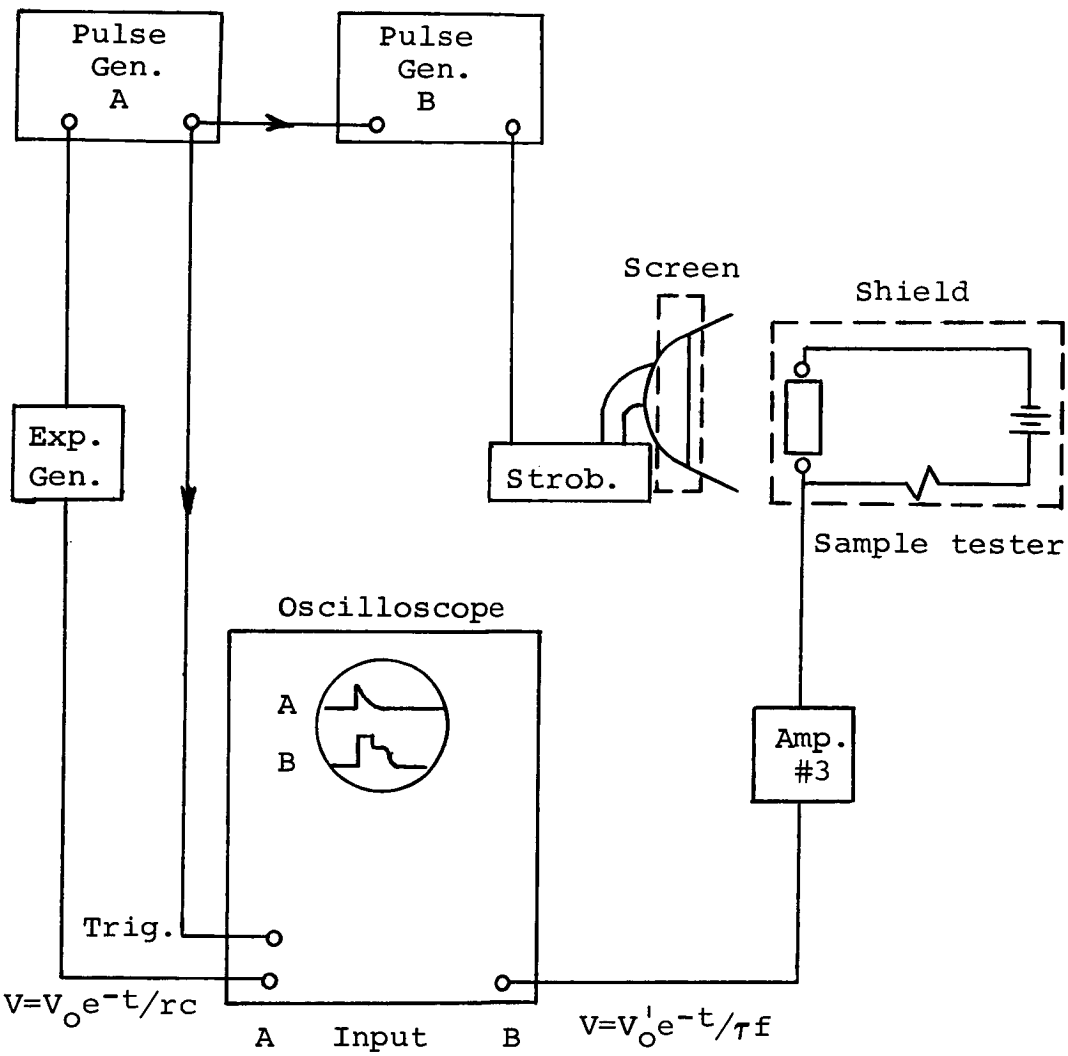

Figure 4.4. Lifetime measurement apparatus

of the sample was varied between 200°K - 400°K. Both were made of bakelite and had spring loaded brass bars to provide pressure contact to the nickel plated ends of the sample. The larger holder had an aluminum base, and a gear arrangement was designed to allow sample selection.

The amplifier was transistorized with a frequency response from 50 Hz to approximately 1MHz and a variable gain of 10 to 100. Figure 4.5 shows a schematic of the circuit employed. The transistors were hand picked in order to minimize the equivalent short circuit input noise to the amplifier. Power was supplied to the amplifier with a dry cell in order to eliminate 60 Hz noise and ripple caused by an a-c operated power supply.

The light source was the General Radio type 1531-A electronic stroboscope, which includes a Strobotron lamp and reflector system, an electronic pulse generator which controls the flashing rate, and a power supply. A pulse of light at various repitition rates can be supplied at three separate light intensities. Figure 4.6 shows the output of the stroboscope at two of three light intensities as measured by the response of a photomultiplier tube displayed on an oscilloscope screen. The reflector of the lamp was enclosed in a copper wire mesh electrostatic shield to reduce low frequency noise from the lamp. A thin silicon filter (approximately 0.050 inches thick) was placed between the lamp and the sample being measured so that the light frequencies with high absorption coefficient would not affect the measurements. This tends

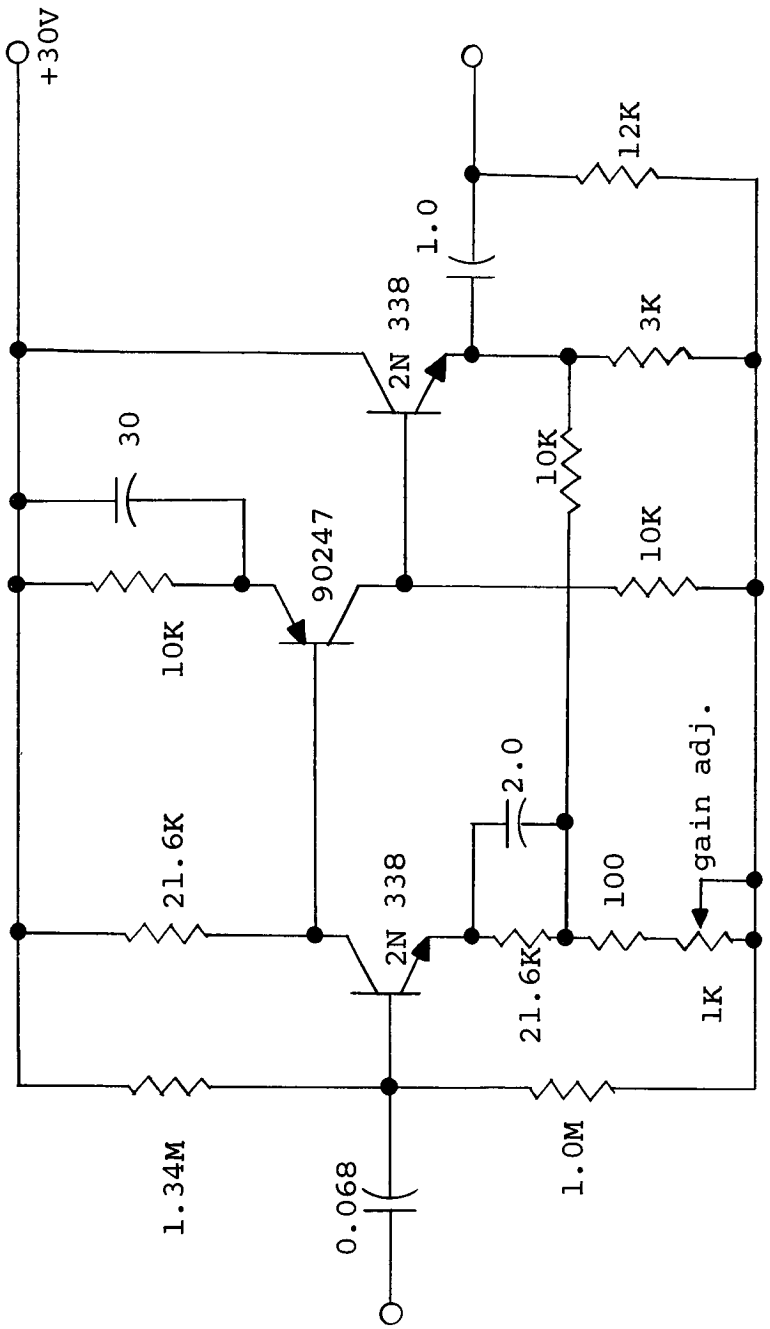

Figure 4.5. Schematic of amplifier used in measurement of lifetime

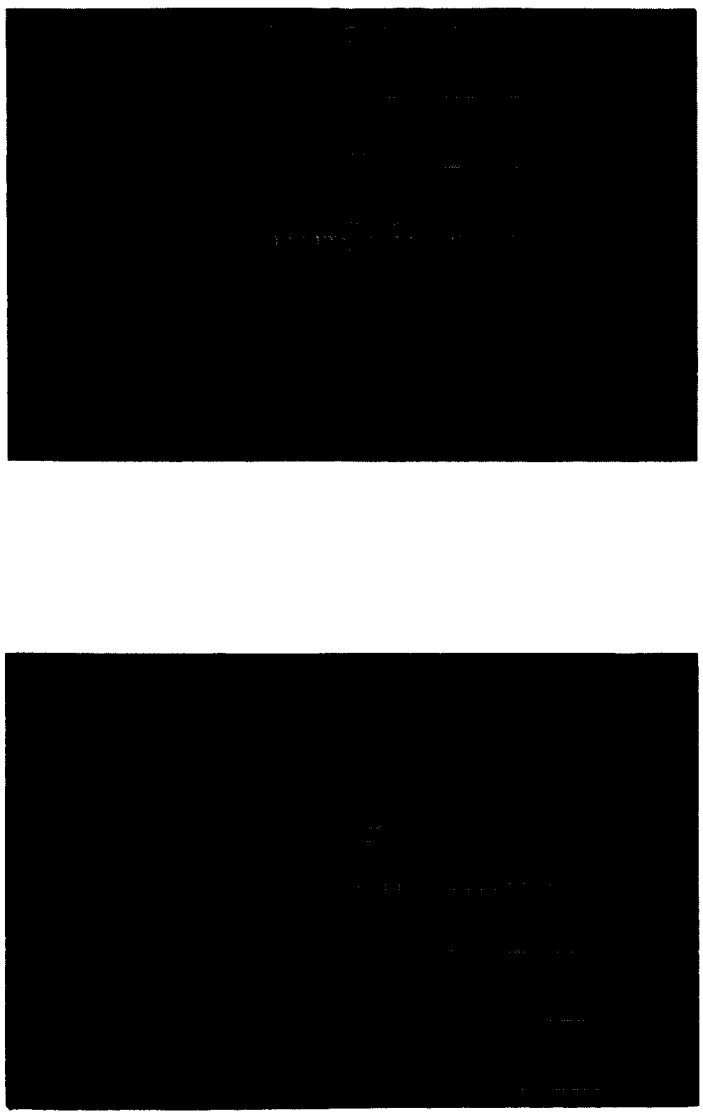

Figure 4.6. Light output of Strobatac. The top photo represents 2.1×10^5 lux and the bottom photo represents 1.2×10^6 lux at a distance of 1 meter from the center of the beam. The horizontal scale is 0.5 μsec/div

to make the light more monochromatic as far as the silicon samples are concerned, in that the long wavelength photons are absorbed in the filter, and the low absorption photons have very little effect on the photoconductivity.

The pulse generators shown in Figure 4.4 were Dumont Laboratories Type 404-R instruments, which provided a fifty volt (maximum) output pulse into a fifty ohm load. The main feature of this generator was the fact that the output pulse could be delayed with respect to the initiation of the instrument. The value of this function will be discussed later. The generator would be initiated either internally or externally, and a trigger pulse was also available with a fixed five microsecond delay with respect to initiation, so that other equipment could be triggered externally.

A circuit diagram of the exponential generator is shown in Figure 4.7. It is a simple diode - RC circuit driven by a pulse with a short duty cycle. The output voltage is governed by the voltage decay of the RC network and is purely exponential in time. The resistance is a precision ten turn Helipot manufactured by Beckman Instruments. The linearity of the potentiometer is accurate to 1/4%, and the total resistance was two kilohms. Precision capacitors were also used, and both the resistance and capacitance valves were measured on a General Radio type 1650-A impedance bridge. The time constant of the exponential generator is simply the resistance-capacitance product. Figure 4.8 shows a plot of exponential time constant versus the potentiometer setting, for a constant value of capacitance.

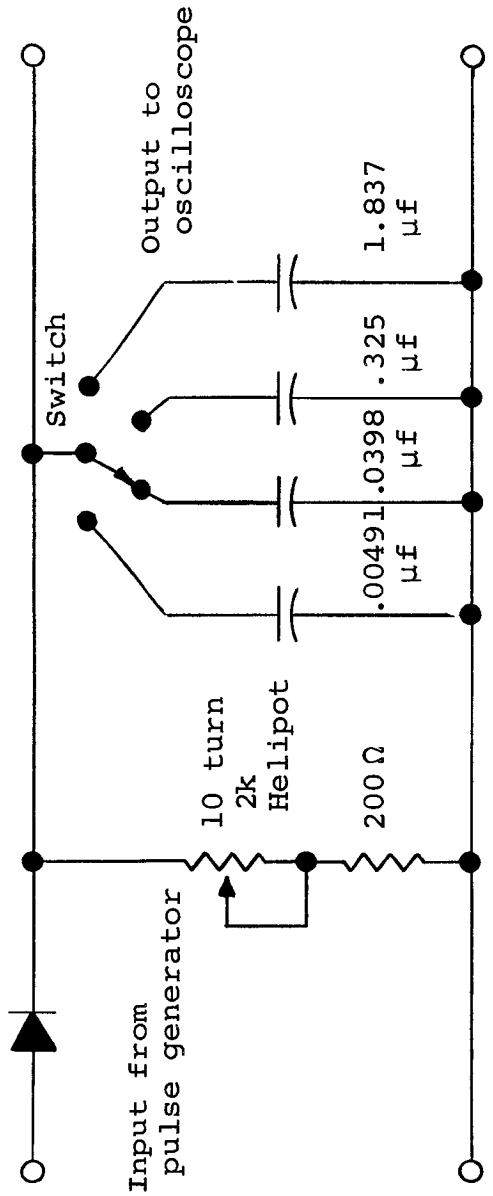

Figure 4.7. Schematic of exponential generator circuit

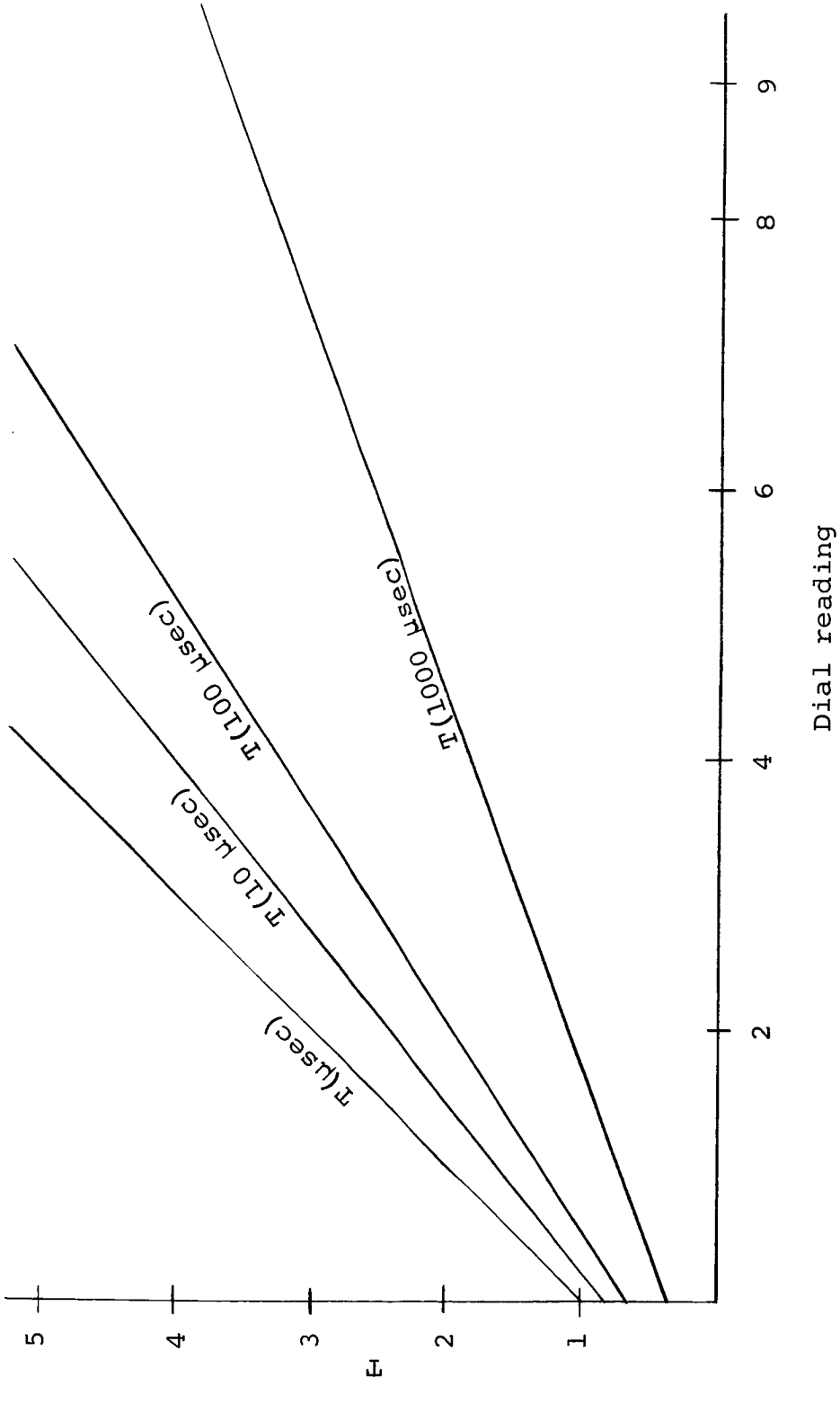

Figure 4.8. Lifetime vs. Heliopot dial setting

The oscilloscope was a Textronix 561-A dual trace instrument with the type 3A1 dual trace amplifier and type 3B3 time base plug-in units. The frequency response of the amplifier was from d.c. to 10 MHz and its risetime was thirty-five nanoseconds. These characteristics were sufficient for measuring lifetimes down to less than one microsecond, and the lowest values encountered in this research were near four microseconds. The 3A1 amplifier unit allowed the examination of each separate trace on the scope, both traces simultaneously, and the addition or subtraction of the two traces. This feature proved to be invaluable in measuring the lifetime.

Figure 4.4 shows how the system was arranged in order to measure the lifetime using the oscilloscope. Pulse generator A was initiated internally. Five microseconds after initiation, its trigger pulse output was used to externally initiate pulse generator B and to trigger the oscilloscope sweep. The output pulse from generator A (attenuated 20 db) was applied to the exponential generator, whose output was displayed on one trace of the oscilloscope. Because of the previously mentioned variable delay between the output pulse and the trigger pulse from generator A, this exponential signal could be continuously varied in time with respect to the point at which the scope was triggered (or the point at which this trace appeared on the oscilloscope screen). The fifty volt output pulse from generator B was used to trigger the Strobotac, producing a light pulse which also could be delayed with respect to the point at which the oscilloscope was triggered. The light pulse modulated

the conductivity of the silicon sample. If the current flowing through the sample is constant, the voltage across the sample is proportional to the change in the conductivity, if the change in conductivity is small (see Appendix III). The sample voltage is amplified, and displayed on the other trace of the oscilloscope. Note again that both voltages can be delayed in time with respect to the point at which the oscilloscope is triggered, and these delays are variable externally on each of the pulse generators. Under ideal conditions, the voltage across the sample is exponential in time, with a time constant equal to the lifetime of minority carriers in the sample. Thus the two signals displayed on the oscilloscope are exponential in time, and if the two can be accurately matched, the minority carrier lifetime is determined from the resistance-capacitance product of the exponential generator.

According to the IRE standards on the measurement of minority carrier lifetime by the method of photoconductivity decay (see Appendix I), the decay time of the photoconductivity should be measured between 50% and 10% of the maximum value. This standard was adherred to throughout these experiments.

Figure 4.9 shows photographs taken from the screen of the oscilloscipe, illustrating the techniques used to measure the minority carrier lifetime of the sample. First, the photoconductive decay curve from the silicon bar is adjusted to correspond to approximately six divisions on the oscilloscope screen. The sweep is adjusted so that the signal covers as much of the screen as possible. Next the signal from the

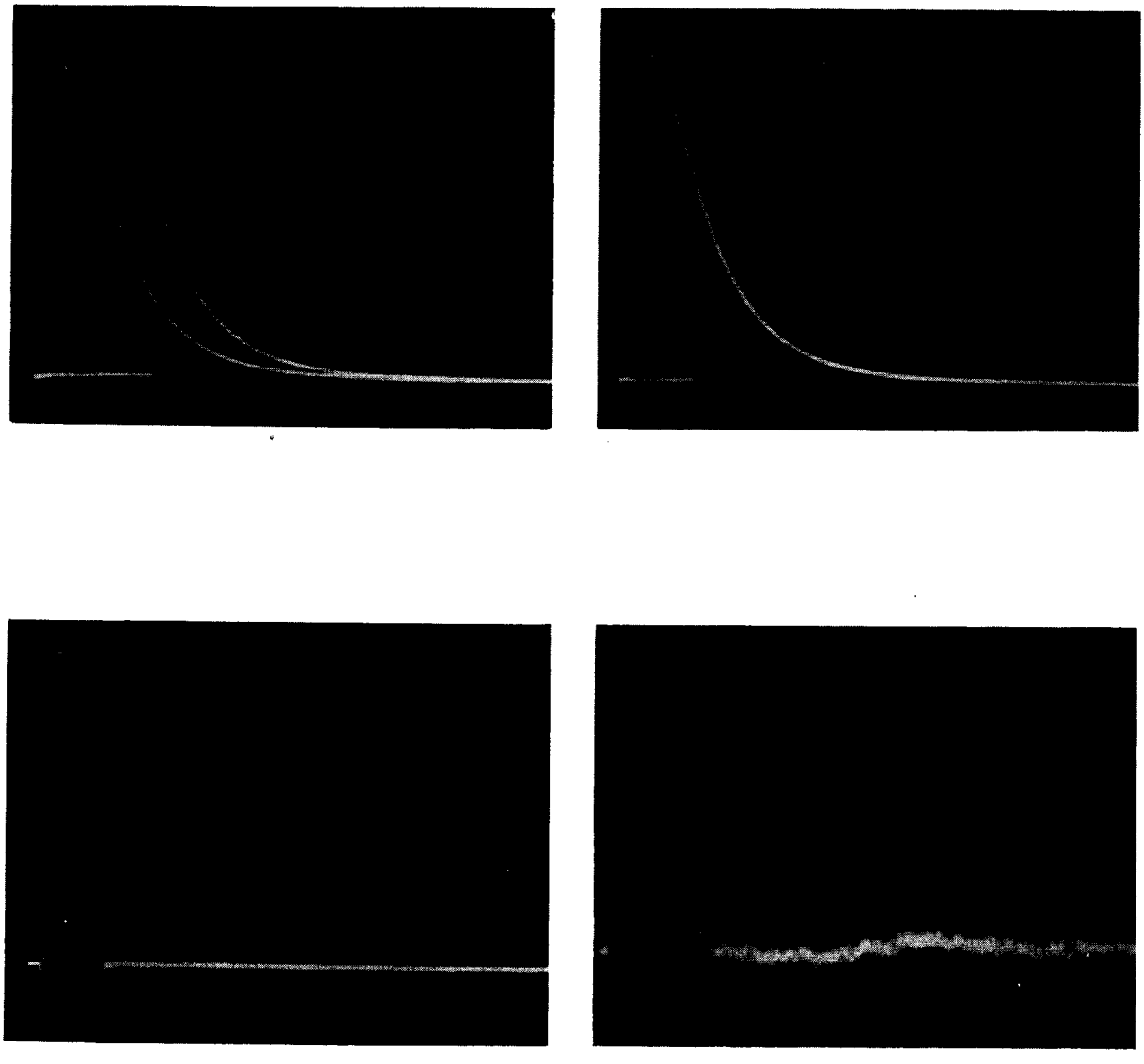

Figure 4.9. Procedure used to measure lifetime. The top photo shows the sample signal (the one on the left) and the exponential signal. The top right photo shows two matched signals. The lower left photo shows the subtracted signals and the lower right photo shows the subtracted signals amplified x 100

exponential generator is adjusted so that its maximum amplitude is at the 50% point on the photoconductive decay signal. Then the Helipot is adjusted until the exponential generator signal gives a best fit to photoconductive decay signal. During this operation, the horizontal positioning of the two signals is carried out using the variable delays in the pulse generators. This adjustment is mandatory in obtaining a good match between the signals. The matched traces are then examined more closely by first expanding the sweep time scale by a factor of five and varying the horizontal positioning of the oscilloscope. Then the signals are subtracted (which should yield a straight line if a perfect match exists) and the amplifier gain adjusted to its maximum value. The Helipot is readjusted if any mismatch occurs. Then, noting the potentiometer setting and the capacitance value, the lifetime is read from the graphs of Figure 4.8. The repeatability error of this measurement was found to be less than 5%. An oscilloscope containing a counter in the time base unit was obtained from the NASA labs at Langely Field, Virginia. This unit had been calibrated in the standards labs there, and when it was set up to count the lifetime, the difference between the lifetime read from the graph and the lifetime measured by the counter was always less than 5%, and generally agreement was found to be within 3%. This measurement was found to be accurate if the preceeding steps were carried out on every measurement, and if care was taken to perform the measurements in the same manner each time. While the disadvantage of this technique is that it requires

a great deal of human manipulation and judgement, it was felt that these disadvantages were minor in the light of the previously discussed tests for accuracy and repeatability.

In order to study the temperature dependence of the lifetimes measured, a Halfstrom-Thompson model HT-700W temperature chamber was used. Liquid CO_2 was used as the refrigerant, and a temperature range between 200°K - 400°K was readily obtainable. The temperature of the sample was measured using a chromel-alumel thermocouple, which had been calibrated in boiling water and at room temperature with a pyrometer provided on the temperature chamber. The thermocouple voltage was monitored with a Leeds and Northrup millivolt potentiometer. The temperature control unit was solid state and introduced little noise into the system. Access to the sample holder was obtained with fifty ohm teflon coated co-axial cable through ports provided on the temperature chamber.

4.3 Irradiation Facilities and Methods

Irradiations were carried out in a Gammacell 220 cobalt-60 radiation source manufactured by Atomic Energy of Canada,Ltd. Figure 4.10 shows a plot of the normalized output of the source as a function of the energy of the gamma rays, as supplied by the manufacturer. The manufacturer's specifications states that a cobalt source activity of 1,100 curies produces a mid point dose rate of 1×10^5 roentgens per hour of exposure time. Due to the half life of cobalt-60 (5.39 years), the dose rate varied during the period which the experiments were performed

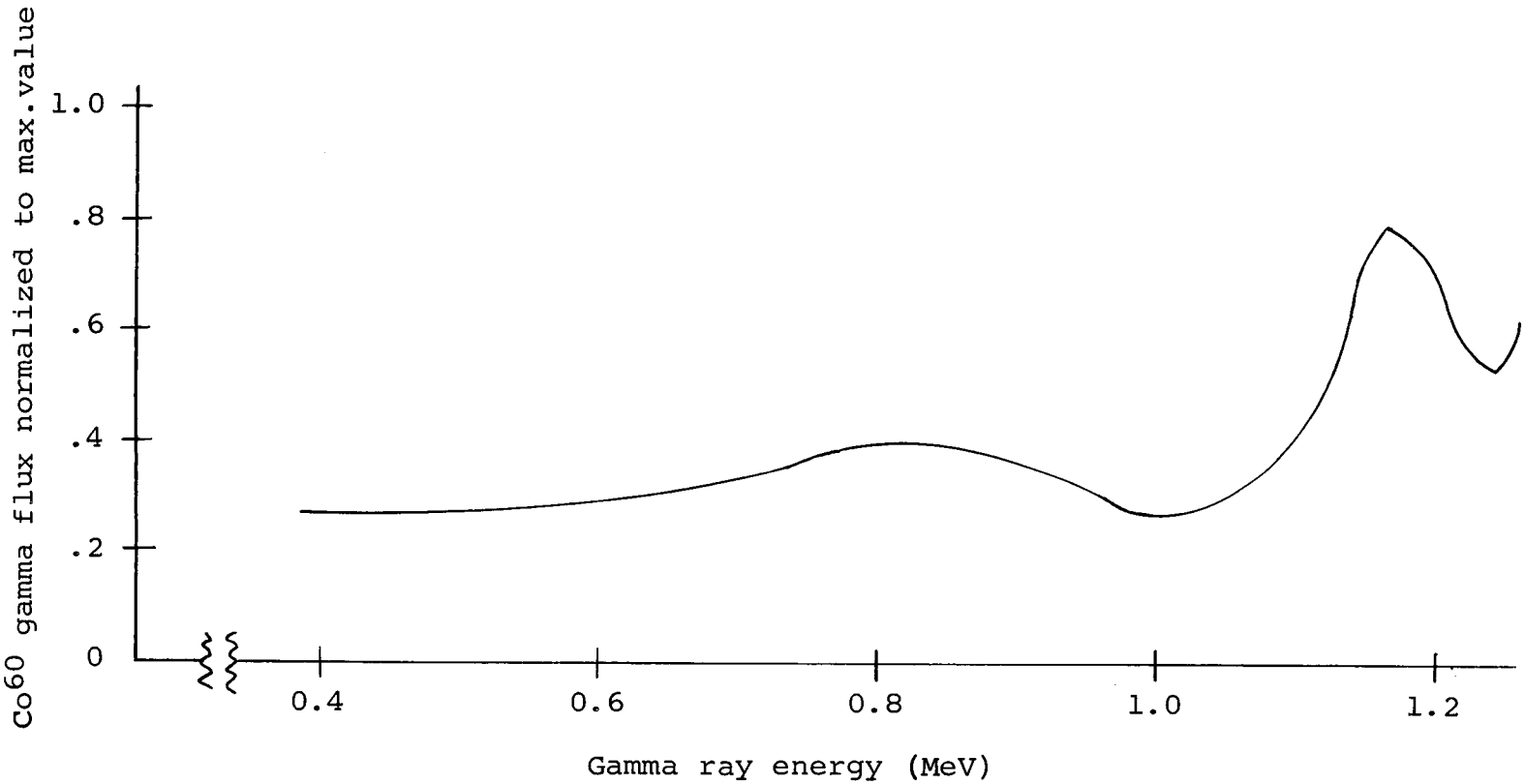

Figure 4.10. Normalized photon flux as a function of energy in the sample chamber of the Gamma cell 220 (Source: Atomic Energy of Canada, Ltd., Ottowa, Canada)

between 2.5×10^5 roentgens per hour and 1.89×10^5 roetgens per hour. Rough calculations showed that this corresponded to a gamma flux variation of approximately 1.4×10^{11} photons/cm^2 sec to 1.0×10^{11} protons/cm^2 sec.

To perform the irradiations each individual sample was stored in a plastic vial which had been flushed with argon. Then the samples were placed in a glass jar which was also flushed with argon and then tightly sealed. The inert argon atmosphere was used so that the ozone by-products which were produced in the irradiation chamber would not affect the surface properties of the thin filaments. Initial tests showed that ozone could drastically change measured lifetimes if the samples were irradiated in air. The irradiations were carried out at room temperature for carefully measured amounts of time, and the lifetimes were measured as soon after irradiation as possible. Measurements taken several days after irradiation showed that no room temperature annealing of the radiation damage had occurred.

CHAPTER V

5. THEORY OF BULK RECOMBINATION

5.1 Introduction

In a semiconductor crystal, excess charge carriers can recombine by three fundamentally different mechanisms: a) direct or band to band recombination, b) Auger, or three body recombination, c) recombination through defects with energies in the forbidden region. The recombination process is accomplished when an electron from the conduction band drops into an empty state in the valence band. The potential energy of the pair is transformed into some other kind of energy, and herein lies the difference between the various processes. For the band to band process, the energy is released in the form of photons and phonons, while for the Auger process the energy is given to a third carrier causing it to make a transition to an excited state. Now, when an electron goes from the conduction band to a localized state in the forbidden region, the energy is released in several forms. This energy can be in the form of photons or phonons, as well as transfer of energy to a third carrier. Thus it could be stated that there are only two processes by which carriers can recombine. They would be band to band or band to flaw recombination, with Auger recombination treated as a special case of either one. However, due to the basic difference in the energy mechanism, it is often advisable to consider the three body processes separately. Also, since only one of these

processes will be treated in detail in this thesis, it is a point of academic interest only.

It is quite understandable that a theoretical treatment of the recombination processes has led to several mathematical models for the various processes involved. A general treatment of all of them would indeed be extremely complex. Thus, one must examine both the physical situation and the mathematical model so that the relative importance of the various processes can be determined. Fortunately this has been accomplished for many elemental and compound semiconductors. Table 5.1 (Bemski, 1958) shows that recombination through localized states is the process which controls recombination in silicon. For this reason, only this recombination mechanism will be treated in detail here.

Table 5.1 Calculated values of lifetime for a band to band process compared with experimentally measured lifetimes

	Si	Ge
Eg (ev)	1.12	0.75
R (cm^{-3} sec^{-1})	2×10^{9}	3.7×10^{13}
τ rad (seconds)	3.5	0.30
τ obs (seconds)	$< 10^{-2}$	$< 10^{-2}$

Energy gap = Eg; radiative rate of recombination = R; calculated radiative lifetime = τ rad; and observed lifetime τ obs for Si and Ge at 300°K.

5.2 Derivation of Recombination Rates

The first theories of recombination processes in semiconductors which are dominated by a single defect with an energy in the forbidden region was developed by Hall (1951) and Shockley and Read (1952). Their treatments were limited by several assumptions and were valid for steady state conditions only. Sandiford, (1957) and Wertheim (1958) treated the transient case for a single level and showed that in the limit of small defect concentrations the net recombination rate is given by:

$$U = \sum_j U_j \qquad (5.1)$$

where U_j is the recombination rate due to the j^{th} defect. In the same paper, Wertheim (1958) treated trapping processes, whereby the probability of the completion of the recombination process is much smaller than the probability of re-excitation of the captured carrier from the flaw.

Sah and Shockley (1958) and Zhdanova et. al. (1959) have developed a theory for multivalent flaws which can capture more than one electron. For this multiple charge flaw, the position of the energy level in the forbidden region depends on the total charge of the defect, and a general treatment is very difficult. One of the problems is the derivation of the equilibrium and non-equilibrium distribution functions, which are quite different from those for a monovalent defect. It is also difficult, in general, to deduce from experimental data whether or not the defect is in fact multivalent, or whether there are

several monovalent flaws present. It is quite possible for both types of defects to be present. It should be noted that the developed theories for multivalent flaws only apply for steady state. No transient theories have been set forth, and thus application to photoconductive decay is impossible with the present theories.

After a careful gleaning of these theories, it was decided that, hopefully, the Shockley and Read (1952) and Wertheim (1958) theories would be applicable. These theories will now be derived.

The physical model to be employed is shown in Figure 5.1. Here E_c is the conduction band edge, E_r is the Shockely-Read recombination center in the forbidden region, and E_v is the valance band edge. Process 1 represents a free electron captured from the conduction band by the recombination center. Process 2 shows an electron being emitted from the recombination center into the conduction band. Process 3 shows a free hole being captured from the valence band by the recombination center and process 4 shows a hole emitted from the recombination center into the valence band. Processes 1 and 3 result in the annihilation of a hole-electron pair while processes 2 and 4 result in the generation of a hole-electron pair. It will be assumed that the rate limitation is due to the availability of electrons and holes to enter the recombination center. The readjustment time of the carrier in the center will be neglected. Thus, when an electron is captured by a recombination center, this center is in an excited state and there exists a time lag

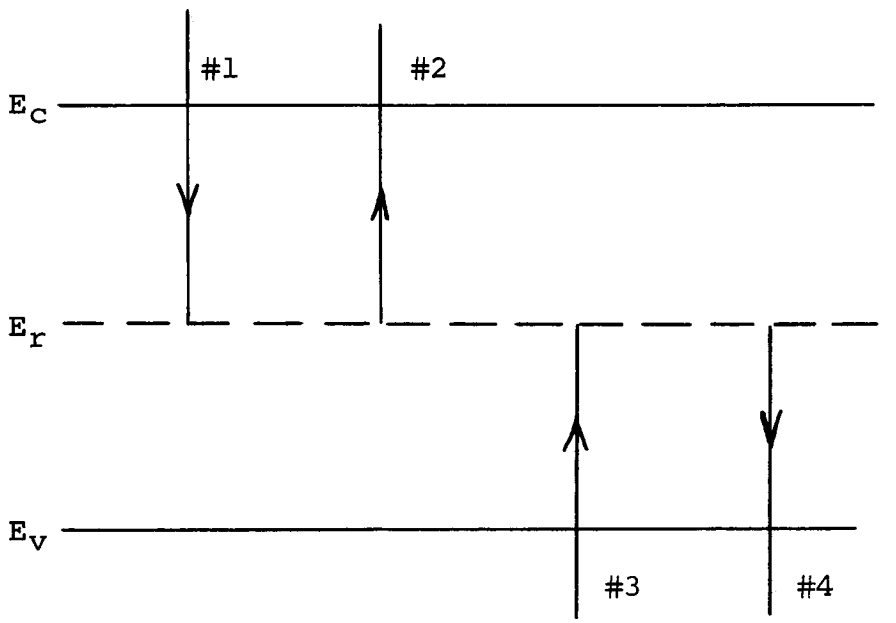

Figure 5.1. Transition diagram for the one level Shockley-Read model

before it can return to the ground state. This time is assumed to be negligibly small compared to the total time required to complete the recombination process.

The processes shown are assumed to be governed by Fermi-Dirac statistics. The probability that a state with energy E will be occupied by an electron is given by

$$f(E) = \left[1 + \exp\left(\frac{E - E_f}{kT}\right) \right]^{-1} \qquad (5.2)$$

Likewise, the probability that the same state be occupied by a hole is

$$f_p(E) = 1 - f(E) = f(E) \cdot \exp\left(\frac{E - E_f}{kT}\right) \qquad (5.3)$$

In Figure 5.1, the rate of electron capture in an energy range dE (above Ec) is

$$\text{Electron Capture} = f_{pr} N_r \, c_n(E) \, f(E) \, N(E) \, dE \qquad (5.4)$$

where $f_{pr} N_r$ represents the number of empty recombination centers that are able to capture electrons, $f(E)N(E)dE$ represents the total number of electrons in dE, and $c_n(E)$ is the probability per unit time that an electron in this energy range will be captured.

Similarly the rate of electron emission from the recombination center to a state in dE is

$$\text{Electron Emission} = f_r N_r \, e_n(E) \, f_p(E) N(E) dE \qquad (5.5)$$

where $e_n(E)$ is the emission constant corresponding to $c_n(E)$.

The net rate of electron capture from dE is given by the electron capture rate minus the electron emission rate.

$$dU_{cn} = \left[f_{pr}\, f(E) - \frac{e_n(E)}{c_n(E)}\, f_r f_p(E) \right] N_r N(E) c_n(E) dE \qquad (5.6)$$

Now, in thermal equilibrium the principle of detailed balance requires that equation 5.6 vanish, and thus the bracketed quantity must vanish. Thus in thermal equilibrium

$$\frac{e_n(E)}{c_n(E)} = \frac{f_{pr}\, f(E)}{f_r\, f_p(E)} = \exp\left(\frac{E_r - E}{kT}\right) \qquad (5.7)$$

Now, we assume that this ratio is a constant in non-thermal equilibrium, as well as thermal equilibrium. Substituting into equation 5.6 gives

$$dU_{cn} = \left[1 - \exp\left(\frac{E_{fr} - E_{fn}}{kT}\right) \right] f_{pr}\, f(E) N_r c_n(E) N(E) dE \qquad (5.8)$$

The total rate of electron capture is obtained by integrating equation 5.8 over all conduction band states.

$$U_{cn} = \left[1 - \exp\left(\frac{E_{fr} - E_{fn}}{kT}\right) \right] f_{pr}\, N_r \int_{E_c}^{\infty} f(E) N(E) c_n(E)\, dE \qquad (5.9)$$

Now, if we consider the case where the electron and hole distributions are non-degenerate, then

$$N_c \equiv \int_{E_c}^{\infty} \exp\left(\frac{E_c - E}{kT}\right) N(E)\, dE \qquad (5.10)$$

and

$$n = N_c \exp\left(\frac{E_{fn} - E_c}{kT}\right), \qquad (5.11)$$

where N_c is the effective density of states in the conduction band and n is the density of conduction band electrons. Substituting equations 5.10 and 5.11 into 5.9 gives

$$U_{cn} = \left[1 - \exp\left(\frac{E_{fr} - E_{fn}}{kT}\right) \right] f_{pr}\, nN_r \langle c_n \rangle \qquad (5.12)$$

where

$$\langle c_n \rangle \equiv \frac{\int_{E_c}^{\infty} \left[\exp\left(\frac{E_{fr} - E_{fn}}{kT}\right) \right] c_n(E) N(E)\, dE}{\int_{E_c}^{\infty} \left[\exp\left(\frac{E_c - E}{kT}\right) \right] N(E)\, dE} \qquad (5.13)$$

is defined to be the mean capture probability coefficient. Using equations 5.11, 5.3, and 5.2, 5.12 can be further reduced to

$$U_{cn} = C_n f_{pr} n - C_n f_r\, n_1 \qquad (5.14)$$

where

$$C_n \equiv \langle c_n \rangle N_r \quad \text{and}$$

$$n_1 \equiv N_c \exp\left(\frac{E_r - E_c}{kT}\right)$$

Note that n_1 represents the number of electrons in the conduction band when the Fermi level is at the recombination level, E_r.

The preceding treatment can be carried out for the processes 3 and 4 in Figure 5.1 to obtain the net rate of hole capture. Thus

$$U_{cp} = C_p f_r p - C_p f_{pr} p_1 \qquad (5.15)$$

Now consider the steady state non-thermal equilibrium situation. Since the readjustment time of the recombination

center has been assumed negligible, steady state requires that $U_{cp} = U_{cn}$. Then

$$C_p f_r p - C_p f_{pr} p_1 = C_n f_{pr} n - C_n f_r n_1 \tag{5.16}$$

Since $f_{pr} = 1 - f_r$, this equation can be solved for f_r, giving

$$f_r = \frac{C_n n_1 + C_p p_1}{C_p(p + p_1) + C_n(n + n_1)} \tag{5.17}$$

Also

$$f_{pr} = \frac{C_p p + C_n n_1}{C_p(p + p_1) + C_n(n + n_1)} \tag{5.18}$$

The net rate of recombination of holes and electrons is $U = U_{cn} = U_{cp}$. Substitution of equations 5.17 and 5.18 into either of equations 5.14 or 5.15 yields

$$U = \frac{C_n C_p \ (pn - n_i^2)}{C_p(p + p_1) + C_n(n + n_1)} \tag{5.19}$$

with

$$p_o n_o = p_1 n_1 = n_i^2 \ .$$

5.3 The concept of Lifetime

When non-equilibrium carriers exist in a semiconductor, there is a tendency for the carrier concentration to try to restore itself to its equilibrium density. Experiment has shown that while the strength of this tendency may not be exactly proportional to the excess density, it will not usually be far from linear in the excess density.

Now, when the excess holes and electrons are functions of time and the spatial co-ordinates, the rate of change of

each population can be expressed by a continuity equation (e.g. see Blakemore, 1962). This continuity equation for excess electrons, $\bar{n}(x,y,z,t)$ is

$$\frac{\partial \bar{n}}{\partial t} = g_E + (g - r) + 1/g \nabla \cdot \bar{J}_n \tag{5.20}$$

Here g_E is the net rate of transitions to the conduction band caused by externally applied sources (e.g., light of the proper frequency), (g - r) represents the sum of all generative processes by which electrons may be thermally excited to the conduction band from the valence band and from impurity states, and $\bar{J}_n$ is the electron current density. Because the tendency for restoration of excess carriers to equilibrium is linear in the excess carriers, we are encouraged to replace (g - r) in equation 5.20 by the equality

$$g - r = - \bar{n}/\tau_n \tag{5.21}$$

The quantity τ_n has the dimensions of time and is usually called the bulk electron lifetime. If we make this substitution and the decay to equilibrium is not linear in the excess carriers, then τ_n is not a constant but will be a function of the excess carriers. Now if we assume for simplicity that we have an infinite crystal, and that excess carriers are created uniformly throughout this crystal, then $\nabla \cdot \bar{J}_n = 0$. Then

$$\frac{d\bar{n}}{dt} = g_E - \frac{\bar{n}}{\tau_n} \tag{5.22}$$

This simple differential equation illustrates very well all the concepts of both steady-state and transient lifetime. For

example, when generation is maintained until a steady state is established, $d\bar{n}/d_t = 0$ and

$$\tau_{n_{s.s.}} = \bar{n}/g_E \tag{5.23}$$

This is the steady state bulk electron lifetime; simply the excess electron density divided by the excess generation required to maintain it. For the Shockley-Read model, the excess generation is just the quantity U derived in equation 5.19. If we assume that $\bar{n} = \bar{p}$, which requires that the charge due to the changing concentration of the recombination center is negligible, then U can be written as:

$$U = \frac{C_n C_p \, \bar{n} \, (p_o + n_o + \bar{n})}{C_p(p_o + p_1 + \bar{p}) + C_n(n_o + n_1 + \bar{n})} \tag{5.24}$$

From equation 5.23

$$\tau_{n_{s.s.}} = \tau_{p_{s.s.}} = \tau_{s.s.} = \frac{C_p(p_o + p_1 + \bar{n}) + C_n(n_o + n_1 + \bar{n})}{C_n C_p \, (n_o + p_o + \bar{n})} \tag{5.25}$$

Define

$$\tau_{po} = C_p^{-1}$$

$$\tau_{no} = C_n^{-1} \tag{5.26}$$

Then

$$\tau_{s.s.} = \tau_{no}\left(\frac{p_o + p_1 + \bar{n}}{p_o + n_o + \bar{n}}\right) + \tau_{po}\left(\frac{n_o + n_1 + \bar{n}}{p_o + n_o + \bar{n}}\right) \tag{5.27}$$

Note that in general this lifetime is a function of the excess carriers. However, note that

$$\lim_{n \to 0} \tau_{s.s.} = \tau_o = \tau_{no}\left(\frac{p_o + p_1}{p_o + n_o}\right) + \tau_{po}\left(\frac{n_o + n_1}{p_o + n_o}\right) \qquad (5.28)$$

Then for small excess densities the lifetime is independent of the excess carriers. This is the case that used exclusively throughout this thesis.

An examination of equation 5.28 shows that it is quite temperature dependent, mainly through the quantities p_1, p_o, n_1, and n_o. It will be instructive to examine this temperature dependence. First let us examine the temperature dependence of the various concentrations. Thus

$$n_1 = N_c \exp\left(\frac{E_r - E_c}{kT}\right)$$

$$p_1 = N_c \exp\left(\frac{E_v - E_r}{kT}\right) \qquad (5.29)$$

with $N_c \sim T^{3/2}$, $N_v \sim T^{3/2}$.

A simple model for the electron and hole concentrations is derived in Blakemore (1962) and will be considered here. Figure 5.2 shows the temperature variation of n_o and p_o as obtained from this model, as well as the variation of n_1 and p_1 from equation 5.29. The $T^{3/2}$ variation of N_c and N_v has been neglected. Using these results, Figure 5.3 shows the variation of equation 5.28 with inverse temperature for the case of a p-type semiconductor with a recombination center in the lower half of the gap, and with $\tau_{no} < \tau_{po}$. The following equation will also prove to be very useful during the temperature range where the majority carrier concentration is constant.

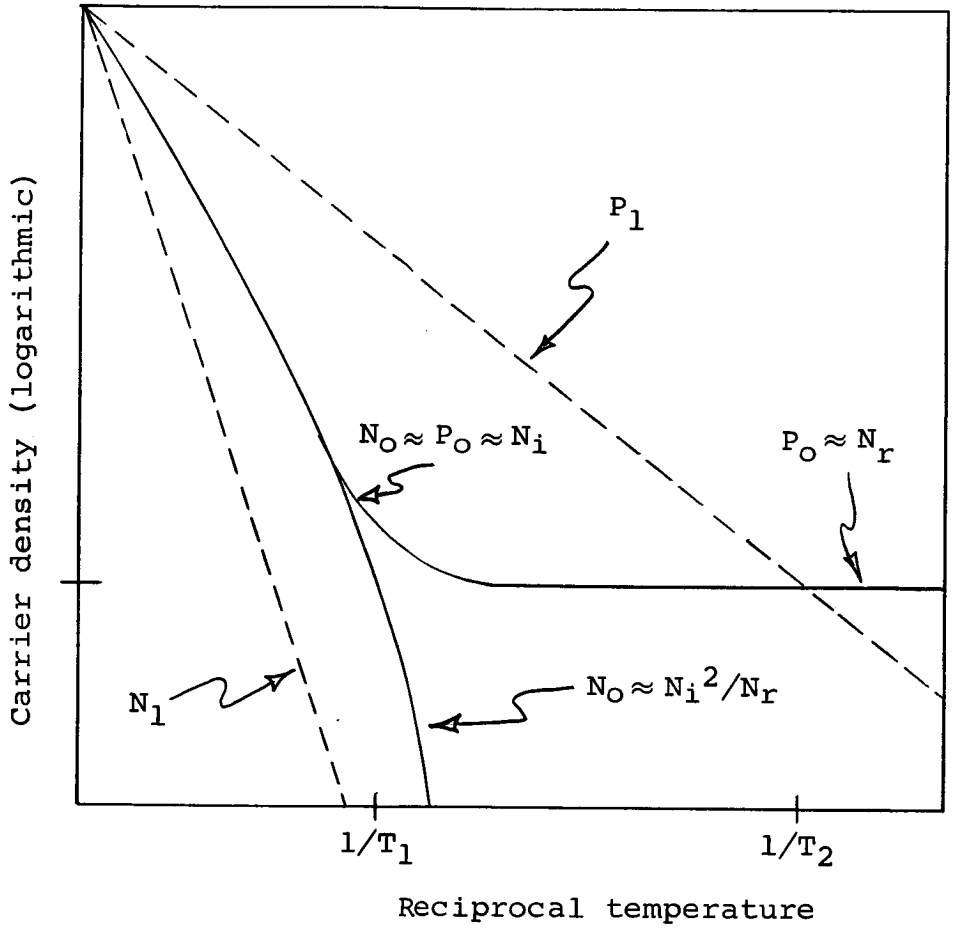

Figure 5.2. Temperature dependence of the carrier concentrations for a p-type semiconductor in which $N_r = N_o - P_o$

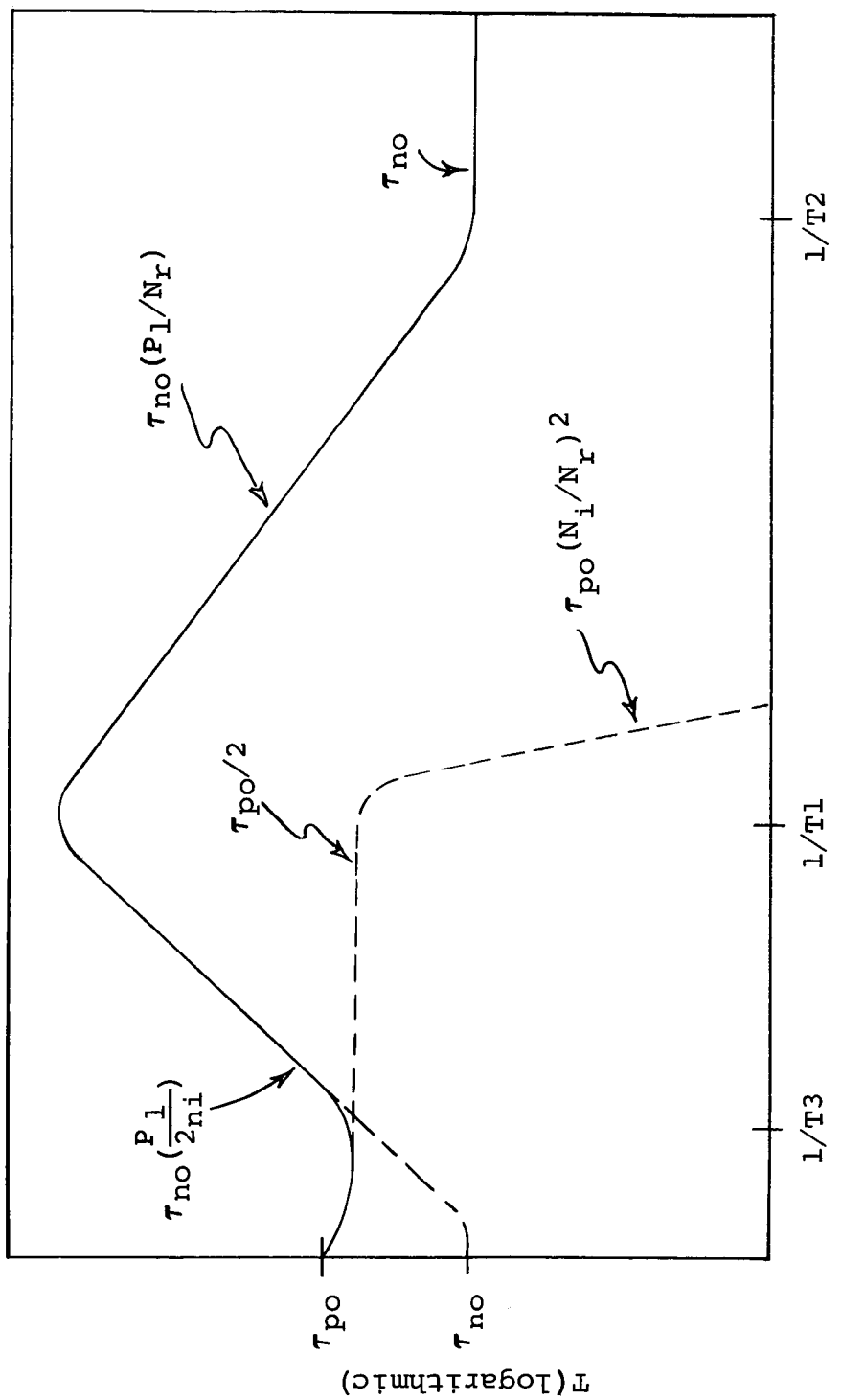

Figure 5.3. Temperature dependence of the lifetime in a p-type semiconductor with a recombination center in the lower half of the gap and $\tau_{no} > \tau_{po}$

Case I: $n_o \approx N_d >> p_o,\ n_1 >> p_1$

$$\tau_o \approx \tau_{po}\left(1 + \frac{n_1}{n_o}\right)$$

Case II: $n_o \approx N_d >> p_o,\ p_1 >> n_1$

$$\tau_o \approx \tau_{po} + \tau_{no} \cdot \frac{p_1}{n_o}$$

Case III: $p_o \approx N_a >> n_o,\ n_1 >> p_1$

$$\tau_o \approx \tau_{no} + \tau_{po} \cdot \frac{n_1}{p_o}$$

Case IV: $p_o \approx N_a >> n_o,\ p_1 >> n_1$

$$\tau_o \approx \tau_{no}\left(1 + \frac{p_1}{p_o}\right)$$

It thus appears that all these various cases should have a temperature dependence of the form

$$\tau_o = A + BT^{3/2} \exp(-C/T) \qquad (5.30)$$

If this equation can be fitted to the experimental data, information can be obtained about the position of the recombination center in the forbidden region.

5.4 Transient Lifetime

Because the experimental techniques utilized in this thesis are basically transient in nature, the steady state lifetime derived in section 5.3 does not, in general, apply here. However, it can be shown that under certain conditions, the transient lifetime is identically equal to the steady state lifetime of Shockley-Read.

Before proceeding, let us first define transient lifetime. In equation 5.22, the transient condition exists when $g_E = 0$. Then

$$\frac{d\bar{n}}{dt} = -\frac{\bar{n}}{\tau_n} \quad \text{(transient)} \tag{5.31}$$

and

$$\tau_{n(\text{transient})} = -\frac{\bar{n}(t)}{\frac{d\bar{n}(t)}{dt}} \tag{5.32}$$

Thus, the general instantaneous transient lifetime can be obtained from a solution of the excess carriers as a function of time.

Let us return to equations 5.14 and 5.15.

$$U_{cn} = C_n f_{pr}\, n - C_n f_r n_1$$

$$U_{cp} + C_p f_r p - C_p f_{pr} p_1 \tag{5.33}$$

Making the substitutions $c_p = C_p N_r$, $c_n = C_n N_r$, $N_r^o = f_{pr} N_r$, $N_{\bar{r}} = f_r N_r$ these equations become

$$U_{cn} = c_n n N_r^o - c_n n_1 N_{\bar{r}}$$

$$U_{cp} = c_p p N_{\bar{r}} - c_p p_1 N_r^o \tag{5.34}$$

Here N_r^o represents the number of recombination centers that are not occupied by electrons and $N_{\bar{r}}$ represents the number of centers that are occupied. If we now write these equations in terms of the equilibrium values and their instantaneous departures from equilibrium, we obtain

$$U_{cn} = c_n \left[(n_o + \bar{n})(N_r^o + \Delta N_r^o) - n_1(n_{\bar{r}} + \Delta N_{\bar{r}}) \right]$$

$$U_{cp} = c_p \left[(p_o + \bar{p})(N_{\bar{r}} + \Delta N_{\bar{r}}) - p_1(N_r^o + \Delta N_r^o) \right] \qquad (5.35)$$

Since the total number of recombination centers is a constant, $\Delta N_r = \Delta N_r^o + \Delta N_{\bar{r}} = 0$. Also the condition of charge neutrality requires that $\bar{n} = \bar{p} + \Delta N_r^o$. Making these substitutions and using the fact that

$$p_1 N_r^o = p_o N_{\bar{r}}$$

$$n_1 N_{\bar{r}} = n_o N_r^o \qquad (5.36)$$

equation 5.35 becomes

$$U_{cn} = c_n \left[(n_o + n_1 + N_r^o)\bar{n} - (n_o + n_1)\bar{p} - \bar{n}\bar{p} + \bar{n}^2 \right]$$

$$U_{cp} = c_p \left[(p_o + p_1 + N_{\bar{r}})\bar{p} - (p_o + p_1)\bar{n} - \bar{n}\bar{p} + \bar{p}^2 \right] \qquad (5.37)$$

Also we have that

$$U_{cn} = - d\bar{n}/dt$$

$$U_{cp} = - d\bar{p}/dt \qquad (5.38)$$

The differential equations that result are

$$- \frac{d\bar{n}}{dt} = c_n \left[(n_o + n_1 + N_r^o)\bar{n} - (n_o + n_1)\bar{p} - \bar{n}\bar{p} + \bar{n}^2 \right]$$

$$- \frac{d\bar{p}}{dt} = c_p \left[(p_o + p_1 + N_{\bar{r}})\bar{p} - (p_o + p_1)\bar{n} - \bar{n}\bar{p} + \bar{p}^2 \right]$$

Obviously these equations are highly non-linear. However, they

can be made linear for the case of low level injection, i.e., $\bar{n} << n_o + n_1$; $\bar{p} << p_o + p_1$. Then the differential equations that govern the decay of excess carriers become

$$- \frac{d\bar{n}}{dt} = c_n \left[(n_o + n_1 + N_r^o)\bar{n} - (n_o + n_1)\bar{p} \right]$$

$$- \frac{d\bar{p}}{dt} = c_p \left[(p_o + p_1 + N_r^-)\bar{p} - (p_o + p_1)\bar{n} \right] \qquad (5.39)$$

To get these equations into a pleasing mathematical form, make the following substitutions (Streetman, 1966). Let

$$y = \bar{n} \qquad x = \bar{p}$$

$$\alpha = c_p(p_o + p_1 + N_r^-) \qquad \beta = c_p(p_o + p_1)$$

$$\gamma = c_n(n_o + n_1 + N_r^o) \qquad \sigma = c_n(n_o + n_1)$$

Then we have

$$- \frac{dy}{dt} = \gamma y - \sigma x$$

$$- \frac{dx}{dt} = \alpha x - \beta y \qquad (5.40)$$

These equations can be solved by the use of Laplace Transforms with respect to time. Let

$$L \{ y(t) \} = Y(s)$$

$$L \{ x(t) \} = X(s) \qquad (5.41)$$

Then, the transformed equations become

$$(s + \gamma) Y(s) - \sigma X(s) = y(0+)$$

$$- \beta Y(s) + (s + \alpha) X(s) = x(0+) \qquad (5.42)$$

Solving simultaneously for X(s) obtain

$$X(s) = \frac{\beta y(0+) + (s + \gamma)X(0+)}{(s + \alpha)(s + \quad) - \sigma\beta} \tag{5.43}$$

or

$$X(s) = \frac{\beta y(0+) + (s + \gamma)\, X(0+)}{(s + s_1)(s + s_2)} \tag{5.44}$$

where s_1 and s_2 are found from the roots of the characteristic equation, $s^2 + (\alpha + \gamma)s + (\alpha\gamma - \sigma\beta) = 0$. X(s) can be written as

$$X(s) = \frac{A}{s + s_1} + \frac{B}{s + s_2} \tag{5.45}$$

where A and B are independent of s.

Then

$$X(t) = L^{-1}\left\{X(s)\right\}$$

$$X(t) = A_e^{-s_1 t} + B_e^{-s_2 t}$$

or

$$X(t) = A_e^{-t/\tau_1} + B_e^{-t/\tau_2} \tag{5.46}$$

Instead of the common quadractic formula let us use the equivalent form

$$s_{1,2} = \frac{1}{\tau_{1,2}} = -\left[\frac{-2C}{b \pm \sqrt{b^2 - 4ac}}\right] \tag{5.47}$$

Thus

$$\tau_{1,2} = \frac{b \pm \sqrt{b^2 - 4ac}}{2C} \tag{5.48}$$

or

$$\tau_{1,2} = \frac{(\alpha + \gamma) \pm \sqrt{(\alpha + \gamma)^2 - 4(\alpha\gamma - \sigma\beta)}}{2(\alpha\gamma - \sigma\beta)} \tag{5.49}$$

$$\tau_{1,2} = \frac{1}{2}\frac{(\alpha+\gamma)}{(\alpha\gamma-\sigma\beta)} \pm \frac{\alpha+\gamma}{2(\alpha\gamma-\sigma\beta)}\sqrt{1-\frac{4(\alpha\gamma-\sigma\beta)}{(\alpha+\gamma)^2}} \tag{5.50}$$

which can be written as

$$\tau_{1,2} = \tau_o\left(\frac{1 \pm \sqrt{1-R}}{2}\right) \tag{5.51}$$

where

$$\tau_o = \frac{\alpha+\gamma}{\alpha\gamma-\sigma\beta} \tag{5.52}$$

In order for the decay of excess carriers to be a single exponential requires that $R \ll 1$, which in turn requires that $\alpha\gamma - \sigma\beta \ll \alpha + \gamma$. With respect to the carrier densities, this requires that $N_r^- \ll p_o + p_1$ and $N_r^o \ll n_o + n_1$. This can be stated as a single condition that $N_r \ll n_o + p_o + p_1 + n_1$. For gamma ray induced recombination centers, this will in general be true, if the exposure rate is kept low. This condition will always be true in the experiments involved in this research. Thus

$$\tau_1 = \tau_o \qquad \text{and}$$

$$\bar{p}(t) = A_e^{-t/\tau_o} \tag{5.53}$$

Then

$$\tau_o = \frac{\frac{1}{c_n N_r}(N_r^- + p_o + p_1) + \frac{1}{c_p N_r}(N_r^o + n_o + n_1)}{n_o + p_o + \frac{N_r^o N_r^-}{N_r}} \tag{5.54}$$

and for the assumptions made

$$\tau_o \approx \frac{\tau_{no}(p_o + p_1) + \tau_{po}(n_o + n_1)}{n_o + p_o} \tag{5.55}$$

This is exactly the steady state lifetime as derived by Shockely and Read, and the fact that the transient and steady state lifetimes are equal (and thus the recombinations rates are equal) will prove very useful in the discussion and derivation of the surface recombination effects.

CHAPTER VI

6. THEORY OF SURFACE RECOMBINATION

6.1 Introduction

As mentioned in Chapter II, a crystal surface represents a termination of the periodicity of the lattice, and thus is a crystal defect. There are broken co-valent bonds for the surface atoms, and the surface of a crystal is highly susceptible to variations in the properties of the ambient to which it is exposed. In general, a semiconductor surface will be covered by several monolayers of foreign matter. In the case of silicon, this is usually silicon-dioxide (SiO_2). One might expect the study of semiconductor surfaces to be a study of interface phenomena, and this is indeed the case. One of the most important manifestations of the semiconductor-ambient interface is the variation of the electrostatic potential associated with the transition from one medium to the other. This is the controlling factor for many of the electronic properties of semiconductors surfaces, for the potential variation may extend a considerable distance into the bulk.

To say that the surface can be taken into account through boundary conditions when one is interested in studying bulk properties alone would be a gross simplification, both from the quantum-mechanical and the device viewpoint. However, this would indeed be desirable, and it is possible to do so if one is very careful in defining the term "boundary conditions". This point will be discussed later in this chapter.

There are two types of surfaces to be studied from an experimental viewpoint. One could purposely introduce a thick layer (thousands of angstroms) of foreign matter on a semiconductor surface, or one could examine a "free" surface which has been exposed only to some ambient. The former would be of interest because devices are subjected to various chemical and thermal processes during manufacture, and it is imperative to know how these processes effect a given device's performance. The latter is of interest when the effect of the free surface on the bulk properties is to be examined, or when the effect of the surface on a bulk device is to be taken into account (by the use of boundary conditions, for example). In this thesis the latter case is the one that will be examined and discussed, since it is the case that is experimentally tractable by photoconductive decay.

6.2 The Surface Space Charge Region

Because of the use of several terms and definitions later on in the chapter, it is advisable to discuss the mathematical theory of the variation of the electrostatic potential near the surface of a semiconductor which, through Poisson's equation, results in a space charge region.

The space charge region at the surface of a semiconductor can be produced by an external electric field, by placing the semiconductor in intimate contact with another solid of a different work function, or by the presence of localized states in the forbidden region near the surface.

Experimental results lead to the conclusion that the surface space charge region in silicon and germanium is influenced almost completely by the presence of surface states (Bardeen, 1947). However, the mathematics with respect to the semiconductor will be the same, irrespective of the method used to create the space charge region.

Figure 6.1 shows an energy band diagram in thermal equilibrium for the case of an n-type semiconductor with a depletion region near the surface (i.e. the electron concentration is smaller near the surface than in the bulk.) The quantities to be used are defined in this figure. The electron and hole concentrations can be written as

$$n_o = N_c \exp\left[\frac{-(E_c-E_f)}{kT}\right] = n_i \exp\left(\frac{E_f-E_i}{kT}\right) = n_i \exp\frac{q\phi(x)}{kT}$$

$$p_o = N_v \exp\left[\frac{E_v-E_f}{kT}\right] = n_i \exp\left[-\left(\frac{E_f-E_i}{kT}\right)\right] = n_i \exp\left(\frac{-q\phi(x)}{kT}\right) \tag{6.1}$$

where $q\phi(x) = E_f-E_i$ is the defining equation for the electrostatic potential, $\phi(x)$. Thus

$$n_{bo} = n_i \exp\left(\frac{q\phi_B}{kT}\right)$$

$$p_{bo} = n_i \exp\left(\frac{-q\phi_B}{kT}\right) \tag{6.2}$$

The electrostatic potential is obtained from a solution of Poisson's equation

$$\frac{d^2\phi(x)}{dx^2} = \frac{-\rho(x)}{\varepsilon} \tag{6.3}$$

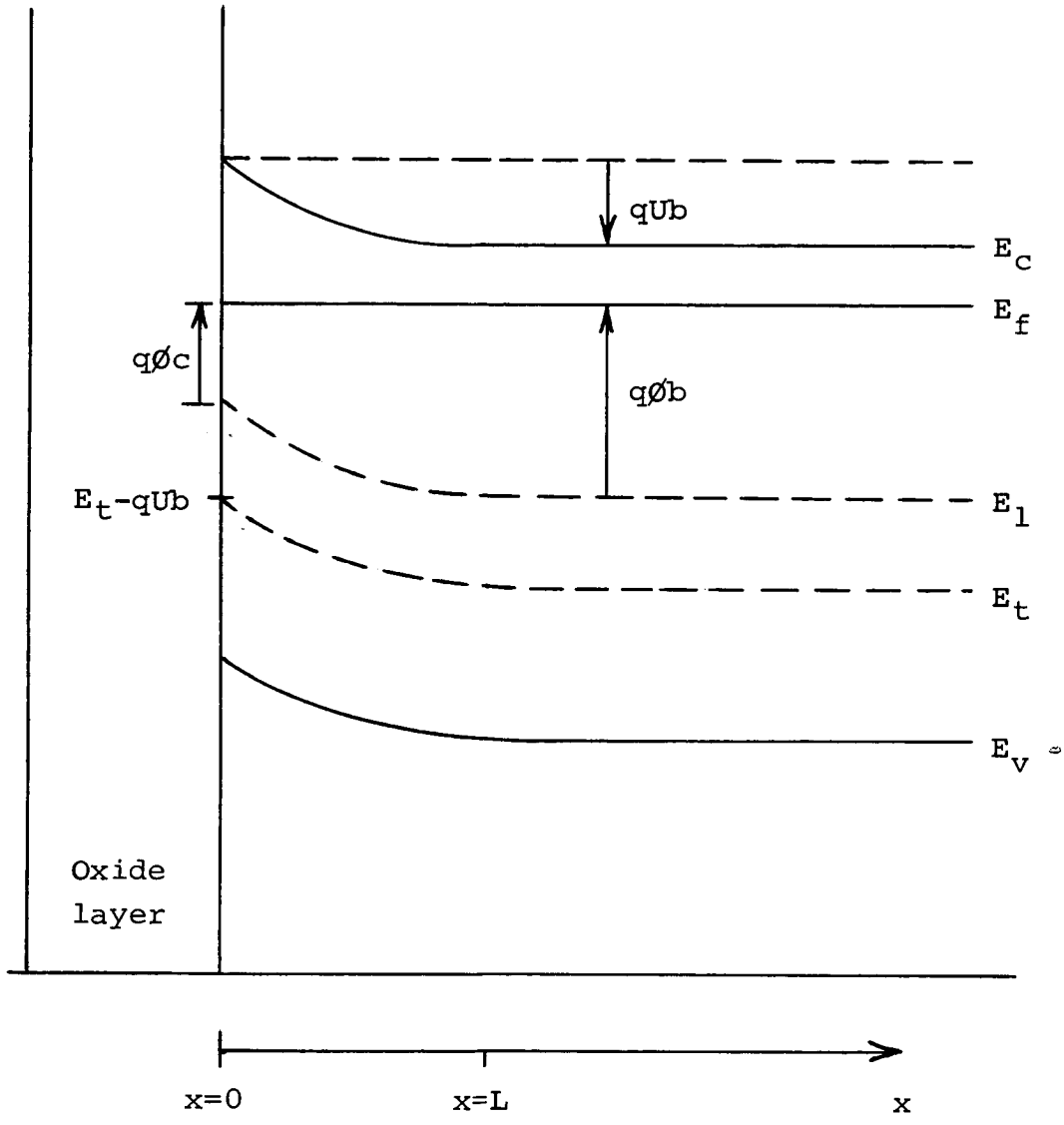

Figure 6.1. Energy band diagram at the surface of a semiconductor

where $\rho(x)$ is the total charge density. Here $\rho(x) = q(N_d - N_a + p_o - n_o)$ if we assume that the donor and acceptor atoms are completely ionized. Also, we know that in the bulk $\rho = o$ which implies $N_d - N_a = n_{bo} - p_{bo}$. Thus, $N_d - N_a = 2n_i \sinh U_b$ where U_b is defined as

$$U_b = \frac{q\phi_b}{kT} \quad (\text{or } u = \frac{q\phi}{kT}) \tag{6.4}$$

Since $n_o - p_o = 2n_i \sinh u$, Poisson's equation becomes

$$\frac{d^2u}{dx^2} = \frac{1}{L_i^2} (\sinh u - \sinh U_b) \tag{6.5}$$

where $L_i = (\epsilon kT/2q^2n_i)^{\frac{1}{2}}$ is called the intrinsic Debye length. If we make the substitution $y = du/dx$, then equation (6.5) becomes

$$y\frac{dy}{du} = \frac{1}{L_i^2} (\sinh u - \sinh U_b) \tag{6.6}$$

This equation can be integrated once. By noting that the electric field in the X direction is given by $E = - \frac{d\phi(x)}{dx}$, we can obtain the following expression for the field

$$E(x) = \pm \sqrt{2} \left(\frac{kT}{qL_i}\right) \left[(U_b - u)\sinh U_b - (\cosh U_b - \cosh u) \right]^{\frac{1}{2}} \tag{6.7}$$

The plus sign is used for $u<U_b$ and the minus sign for $u>U_b$. A concise representation for equation (6.7) is

$$E(x) = \pm \frac{kT}{qL_i} F\left[u(x), U_b\right] \tag{6.8}$$

$F(u,U_b)$ has been tabulated by Mattauch et. al., (1965) for various values of U_b. To obtain the electrostatic potential variation for the general case requires that equation (6.8) be integrated numerically. Thus the equation in normalized form

$$dx = \mp L_i \frac{du}{F(u,U_b)} \tag{6.9}$$

must be integrated numerically. This has been done (Many et. al., 1965) and some results are shown in Figure 6.2.

It should be noted that when free carriers are included in Poisson's equation, $\frac{du}{dx}$, approaches zero only as X approaches infinity, and thus the width of the space charge region is infinite. However, for all practical purposes, one can define the bulk of the semiconductor at the point where the rate of change with distance of the electric field is arbitrarily small, so that space charge neutrality holds. This can be done by defining the bulk to be that point where the change in the electrostatic potential over a distance ΔX becomes less than kT/q.

6.3 The Concept of Surface Recombination Velocity

When discussing experiments or devices employing semiconductor materials, it is customary to attribute to the surface of the material a surface recombination velocity. This is intended to represent a condition at the surface whereby it appears that excess carriers produced in the semiconductor flow into the surface with a velocity which is

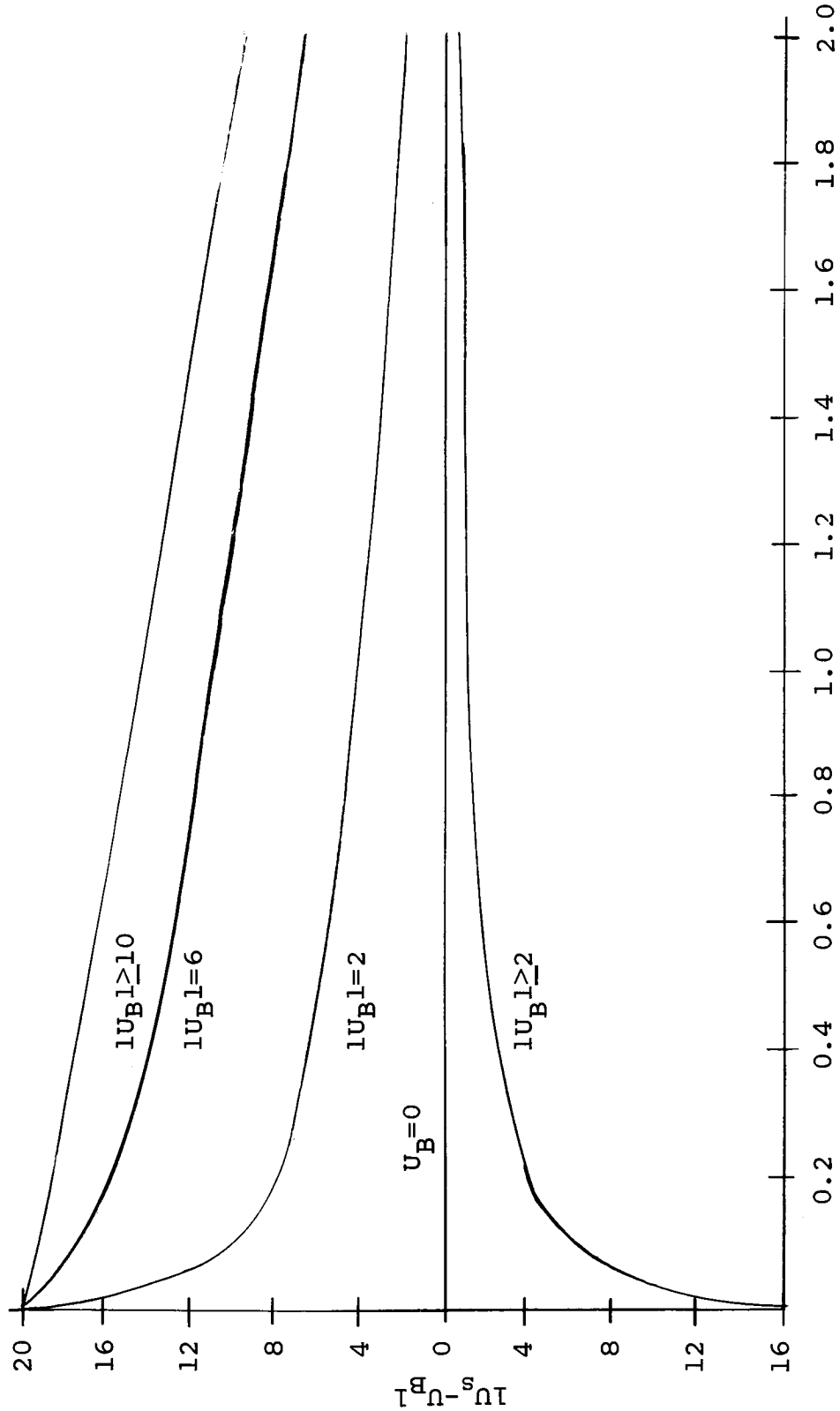

Figure 6.2. Electrostatic potential variation at the surface of a semiconductor

characteristic of the surface. Thus, for electrons flowing into a surface at X = O, this condition could be written

$$J_n(O) = + q\bar{n}(o)S \tag{6.10}$$

where S is the surface recombination velocity. In essence this says that the effects of the surface on the carrier distributions can be replaced by a boundary condition. For this situation where there exist diffusion currents only, equation (6.10) becomes

$$-qD_n \frac{d\bar{n}}{dx}\Big|_{x=o} = -q\bar{n}(o)S \tag{6.11}$$

or

$$S/D_n = \frac{\frac{d\bar{n}}{dx}\Big|_{x=o}}{\bar{n}(o)} \tag{6.12}$$

This should be compared to the definition for transient lifetime.

The true meaning of surface recombination is more far reaching than the above simple definition. However, using this definition allows the solution of a large class of device problems in a very general manner by providing sufficient boundary conditions.

One should again realize that excess carriers created in the material recombine in the bulk, at the surface, and in the space charge region near the surface. Experiment shows that this recombination takes place through defects in the forbidden gap. Thus one could say that surface recombination encompasses both the true recombination at the surface and the

recombination in the space charge region as viewed from the bulk. Consider the continuity equation for electrons in the space charge region.

$$\frac{\partial \bar{n}}{\partial t} = q_e - U_{cn}(x) + \frac{1}{q}\frac{dJ_n(x)}{dx} \tag{6.13}$$

If we assume steady state and $q_e = 0$, then

$$\int_o^L dJ_n(x) = q\int_o^L U_{cn}(x)dx = q\int_o^L U(x)dx \tag{6.14}$$

where $X = 0$ and $X = L$ are the limits of the space charge region. Integrating we have

$$J_n(L) - J_n(o) = q\int_o^L U(x)dx \tag{6.15}$$

This equation can be written in terms of the surface recombination velocity as

$$q\bar{n}(L)S = J_n(o) + q\int_o^L U(x)dx \tag{6.16}$$

In the presently accepted theories of surface recombination velocity, it is generally assumed that $J_n(o)\approx 0$ and thus equation (6.16) becomes

$$S = \frac{1}{\bar{n}_b}\int_o^L U(x)dx \tag{6.17}$$

or by the use of the Mean Value Theroem:

$$S = \frac{U(\xi)}{\bar{n}_b}, \quad 0 \leq \xi \leq L \tag{6.18}$$

In the limit, as the space charge region width becomes small equation (6.18) becomes

$$S = \frac{U(o)}{\bar{n}_b} \tag{6.19}$$

This is used as the defining equation for the surface recombination velocity. For germanium, this model yields good agreement with experimental results (Many et.al., 1965). For silicon the results are not quite as satisfactory and very few experimental results have been obtained. Later in the chapter, refinements of the theory of surface recombination velocity will be made. It will be instructive at that time to be familiar with the present theories, and these will be derived now.

Let us go back to the rate equations derived in Chapter V. At the surface these equations become

$$\begin{aligned} U_{cn} &= c_n \left[n_s (N_{rs} - n_{rs}) - n_1 n_{rs} \right] \\ U_{cp} &= c_p \left[p_s n_{rs} - p_1 (N_{rs} - n_{rs}) \right] \end{aligned} \tag{6.20}$$

where now the quantities N_{rs} and n_{rs} represent the total number of <u>surface</u> recombination centers (cm^{-2}) and the number of recombination centers filled with electrons (cm^{-2}), respectively. Again, in steady state $U_{cn} = U_{cp}$, and solving for n_{rs} gives

$$n_{rs} = \frac{c_n n_s + c_p p_1}{c_n (n_s + n_1) + c_p (p_s + p_1)} \cdot N_{rs} \tag{6.21}$$

Substitution of this result back into equation (6.20) gives

$$U_{cn} = U_{cp} = U = \frac{c_n c_p (n_s p_s - n_{bo} p_{bo}) \cdot N_{rs}}{c_n (n_s + n_1) + c_p (p_s + p_1)} \tag{6.22}$$

If the quasi-Fermi levels are continuous throughout the space charge region, then $n_s p_s = n_b p_b$ (Lade, 1962). Equation (6.20) becomes

$$U = \frac{c_n c_p \bar{n}_b (n_{bo} + p_{bo} + \bar{n}_b)}{c_n (n_s + n_1) + c_p (p_s + p_1)} \cdot N_{rs} \tag{6.23}$$

Then from equation (6.19)

$$S = \frac{U}{\bar{n}} = \frac{c_n c_p (n_{bo} + p_{bo} + \bar{n}_b) \cdot N_{rs}}{c_n (n_{so} + n_1 + \bar{n}_s) + c_p (p_{so} + p_1 + \bar{p}_s)} \tag{6.24}$$

is the expression for the surface recombination velocity for a single recombination center in the forbidden region. In general $\bar{n}_b \ll p_{bo} + n_{bo}$ so that

$$\frac{1}{S} = \frac{c_n (n_{so} + n_1) + c_p (p_{so} + p_1)}{c_n c_p (n_{bo} + p_{bo}) \cdot N_{rs}} + \frac{c_n \bar{n}_s + c_p \bar{p}_s}{c_n c_p (n_{bo} + p_{bo}) \cdot N_{rs}}$$

or

$$\frac{1}{S} = \frac{1}{S_o} + f(\bar{n}_s, \bar{p}_s) \tag{6.25}$$

For low level injection $S \approx S_o$. Thus

$$S = S_o = \frac{c_n c_p (n_{bo} + p_{bo}) \cdot N_{rs}}{c_n (n_{so} + n_1) + c_p (p_{so} + p_1)} \tag{6.26}$$

If we now make the following substitutions

$$n_{so} = n_i \exp(u_s) \qquad n_1 = n_i \exp\left[\frac{E_r - E_i}{kT}\right]$$

$$p_{so} = n_i \exp(-u_s)$$

$$u_o = \ln(c_p/c_n)^{\frac{1}{2}} \qquad p_1 = n_i \exp\left[-\left(\frac{E_r - E_i}{kT}\right)\right]$$

the surface recombination velocity becomes

$$S_o = \frac{\sqrt{c_n c_p}\ (n_{bo} + p_{bo})\ N_{rs}}{2n_i \left[\cosh(u_s - u_o) + \cosh(\frac{E_r - E_i}{kT} - u_o)\right]} \qquad (6.27)$$

It should be noted that this is a bell-shaped curve centered about a maximum when $u_s = u_o$, or

$$S_{max} = \frac{\sqrt{c_n c_p}\ (n_{bo} + p_{bo})\ N_{rs}}{2n_i \left[\cosh(\frac{E_r - E_i}{kT} - u_o) + 1\right]} \qquad (6.28)$$

Then normalizing S to S_{max} gives

$$S/S_{max} = \frac{\cosh(\frac{E_r - E_i}{kT} - u_o) + 1}{\cosh(u_s - u_o) + \cosh(\frac{E_r - E_i}{kT} - u_o)} \qquad (6.29)$$

Figure 6.3 shows a plot of S/S_{max} vs. u_s for various values of the parameter $(\frac{E_r - E_i}{kT} - u_o) = u_t - u_o$.

6.4 A Complete Model for Surface Recombination Velocity

In this section a complete model for surface recombination velocity will be derived which includes recombination in the space charge region.

Consider an energy band diagram near the surface of a semiconductor, such as shown in Figure 6.1. The surface is at X = O and at X = L the electrostatic potential variation is less than kT/q from the bulk value. The continuity equation is valid in the space charge region, and in one dimension is

$$\frac{\partial \bar{n}}{\partial t} = g_e + (g - r) + \frac{1}{q}\frac{dJ_n}{dx} \qquad (6.30)$$

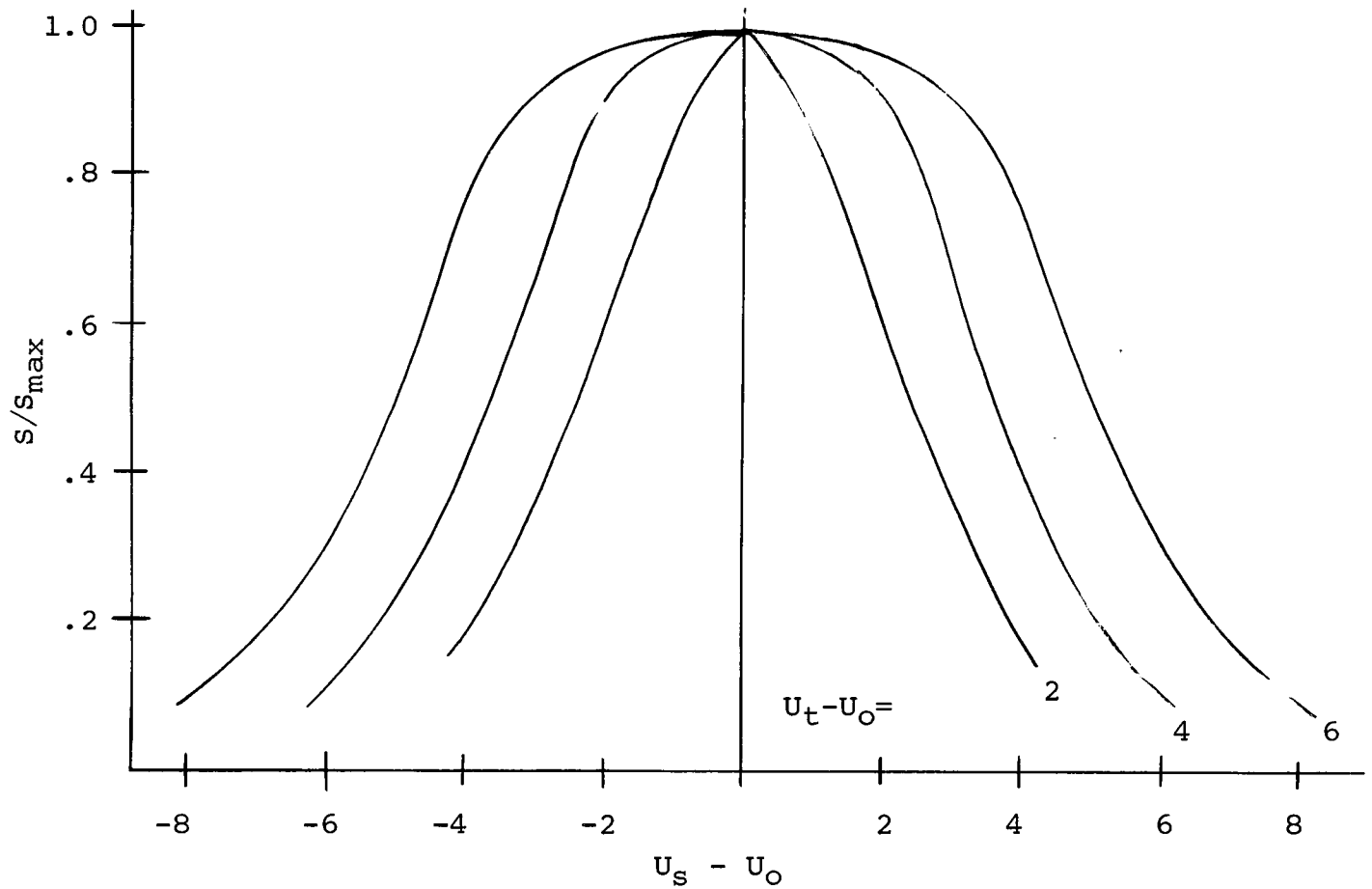

Figure 6.3. Surface recombination velocity vs. surface potential neglecting recombination in the space charge region

We will assume steady state and no external generation so that $g_e = 0$. Then

$$\frac{dJ_n}{dx} = q\ (g-r) = q\ U_{cn}(x) \tag{6.31}$$

where U_{cn} is the net rate of recombination of electrons from the conduction band to the recombination center. But as shown in Chapter V, $U_{cn} = U_{cp} = U$ in steady state. Integrating equation (6.31) over the space charge region yields

$$J_n(L) = J_n(o) + q \int_o^L U(x)dx \tag{6.32}$$

which in terms of the true surface recombination velocity for electrons at X = O, and the effective surface recombination velocity for electrons at X = L is

$$q\bar{n}(L)Sn_{eff} = q\bar{n}(o)\ S_n(o) + q \int_o^L U(x)dx \tag{6.33}$$

Solving for Sn_{eff} gives

$$Sn_{eff} = \frac{\bar{n}(o)}{\bar{n}(L)}\ S_n(o) + \frac{1}{\bar{n}(L)} \int_o^L U(x)dx \tag{6.34}$$

An expression for $S_n(o)$ can be derived from the rate equations of the Shockley-Read model. At the surface X = O, these equations are

$$\begin{aligned} U_{ps} &= c_{ps}p_s\bar{N}_{rs} - c_{ps}p_{1s}N^{\circ}_{rs} \\ U_{ns} &= c_{ns}n_sN^{\circ}_{rs} - c_{ns}n_{1s}\bar{N}_{rs} \end{aligned} \tag{6.35}$$

Now, we define the following surface recombination velocities at the surface (these velocities are the true surface

recombination velocities).

$$U_{ps} = S_p(o)\bar{p}(o)$$
$$U_{ns} = S_n(o)\bar{n}(o) \qquad (6.36)$$

Then

$$S_p(o)\bar{p}(o) = c_{ps}N_{rs}^{-}p_s - c_{ps}p_{1s}N_{rs}^{o}$$

$$S_n(o)\bar{n}(o) = -c_{ns}n_{1s}N_{rs}^{-} + c_{ns}n_sN_{rs}^{o} \qquad (6.37)$$

Since a recombination center with a discrete energy in the forbidden region has been assumed, we have the condition that

$$N_{rs} = N_{rs}^{-} + N_{rs}^{o} \qquad (6.38)$$

Equation (6.37) can then be solved for N_{rs} in terms of $S_n(o)$ and $S_p(o)$. This result is

$$N_{rs} = \frac{S_p(o)c_{ns}\bar{p}(o)(n_s+n_{1s}) + S_n(o)c_{ps}\bar{n}(o)(p_s+p_{1s})}{c_{ps}c_{ns}(n_sp_s - n_i^2)} \qquad (6.39)$$

Also, since in steady state $U_{ns} = U_{ps}$, then $S_p\bar{p}(o) = S_n\bar{n}(o)$. Thus

$$N_{rs} = \frac{S_n(o)\bar{n}(o)\left[c_{ns}(n_s+n_{1s}) + c_{ps}(p_s+p_{1s})\right]}{c_{ps}c_{ns}(n_sp_s - n_i^2)} \qquad (6.40)$$

and

$$S_n(\rho) \doteq \frac{c_{ps}c_{ns}N_{rs}(n_bp_b-n_i^2)}{\bar{n}(o)\left[c_{ns}(n_s + n_{1s}) + c_{ps}(p_s + p_{1s})\right]} \qquad (6.41)$$

where we have assumed $p_sn_s = p_bn_b$. This is the quasi-equilibrium approximation mentioned previously in section 6.3. By expanding the expression in parenthesis in the numerator of equation (6.41), and invoking mass action ($n_op_o = n_i^2$) and

assuming low level injection, we have

$$\frac{\bar{n}(o)}{\bar{n}(L)}\, s_n(o) = \frac{c_{ps} c_{ns} N_{rs} (p_{bo} + n_{bo})}{c_{ns}(n_{so} + n_{1s}) + c_{ps}(p_{so} + p_{1s})} \qquad (6.42)$$

This is precisely the result for surface recombination velocity obtained in equation (6.26) by neglecting recombination in the space charge region and using the definition of equation (6.19). It can now be stated that the effective surface recombination velocity given by equation (6.34) is the sum of two components; one due to recombination at the true surface, and the other due to recombination in the space charge region near the surface of the semiconductor. This is a very enlightening and useful result; especially considering the fact that the technique used to derive this result is general, and a minimum of assumptions has been made.

6.5 Evaluation of the Integral for Recombination in the Space Charge Region

In general, the integral of equation (6.34) must be evaluated numerically. However, an approximation to this integral when the surface is in depletion and slight inversion as derived by Hauser (1965), lends itself to useful analytical examination. Hauser has shown that

$$\int_o^L U(x)dx \approx \frac{(p_b n_b - n_i^2)\, L}{\tau_{po} n_1 + \tau_{no} p_1 + (\tau_{po} + \tau_{no})\sqrt{p_b n_b}} \qquad (6.43)$$

Using the fact that $\tau_{po} = (c_p N_r)^{-1}$ and $\tau_{no} = (c_n N_r)^{-1}$, and assuming low level injection, then

$$\frac{1}{\bar{n}(L)} \int_{o}^{L} U(x)\, dx \approx \frac{\sqrt{c_{ps}c_{ns}}\, N_r\, (p_{bo} + n_{bo})\, L}{2n_i[\cosh\,(u_{rs} - u_{os}) + \cosh\, u_{os}]} \qquad (6.44)$$

where $u_{rs} = (E_{rs}-E_{is})/kT$ and $u_{os} = 1/2 \ln c_{ps}/c_{ns}$. This expression is a function of surface potential through L, the width of the space charge region. An expression for L can be derived for the conditions of depletion and slight inversion at the surface. In this situation, $p-n << N_d - N_a$ for n-type material. Then, Poisson's equation becomes

$$\frac{d^2\phi}{dx^2} = \frac{qN_d}{\epsilon_r\epsilon_o}\,, \quad 0 \le x \le L \qquad (6.45)$$

subject to the boundary conditions

$$\phi(L) = \phi_b$$

$$\left.\frac{d\phi}{dx}\right|_{x=L} = 0 \qquad (6.46)$$

The solution of this equation is

$$\phi(x) = \frac{-qN_d}{2\epsilon_r\epsilon_o}\,(x - L)^2 + \phi_b \qquad (6.47)$$

This equation defines the electrostatic potential as the surface X = 0. For then

$$\frac{qN_d}{2\epsilon_r\epsilon_o}\,L^2 = \phi_b - \phi_s,\ \phi_s \le \phi_b \qquad (6.48)$$

which in the notation of section 6.2 becomes

$$L = \left(\frac{2kT\epsilon_r\epsilon_o}{q^2\, N_d}\right)^{\frac{1}{2}}\,(u_b - u_s)^{\frac{1}{2}},\ u_s \le u_b \qquad (6.49)$$

The quantity $(\frac{2kT\epsilon_r\epsilon_o}{q^2N_d})^{\frac{1}{2}}$ has the units of length and is called the extrinsic Debye length, L_d. Figure 6.4 shows a plot of L_d as a function of carrier concentration for silicon at 300°K. Thus

$$S_r = \frac{1}{\bar{n}(L)} \int_o^L U(x)dx = \frac{\sqrt{c_{ps}c_{ns}}\, N_r(p_{bo} + n_{bo})L_D(u_b - u_s)^{\frac{1}{2}}}{2n_i\,[\cosh\,(u_r - u_{os}) + \cosh\, u_{os}]} \tag{6.50}$$

for $u_s \leq u_b$. Then, the complete model for surface recombination at low injection levels can be stated as

$$S_{eff} = S_o + S_r \tag{6.51}$$

where S_o is defined by equation 6.27 and S_r is defined by equation 6.50. Figure 6.5 shows the effects of recombination in the space charge region for several combinations of parameters. In these figures the parameter

$$K = \sqrt{\frac{c_{nr}c_{pr}}{c_{ns}c_{ps}}}\quad \frac{N_r}{N_{rs}} \quad .$$

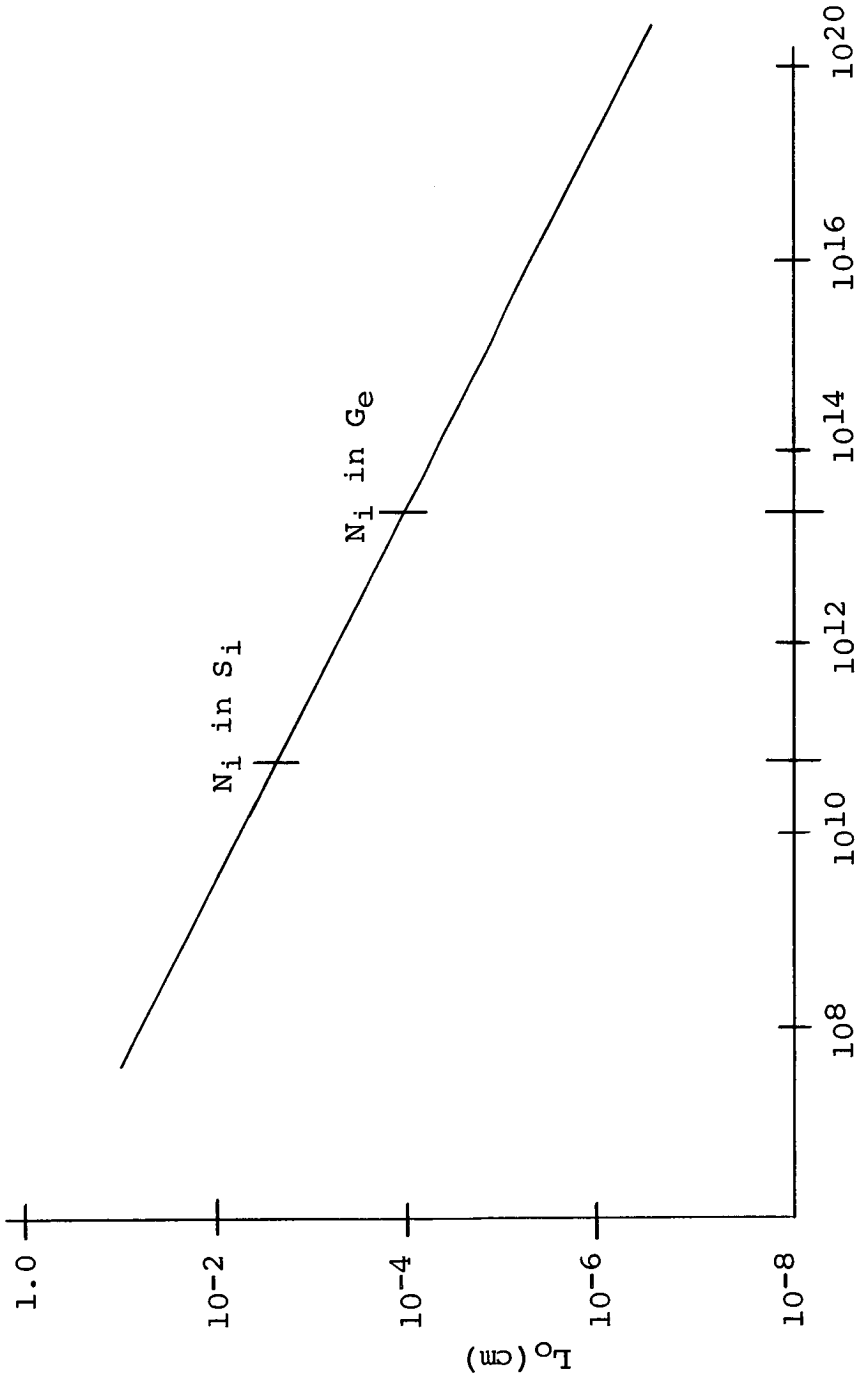

Figure 6.4. Plot of extrinsic Debye length vs. impurity concentration

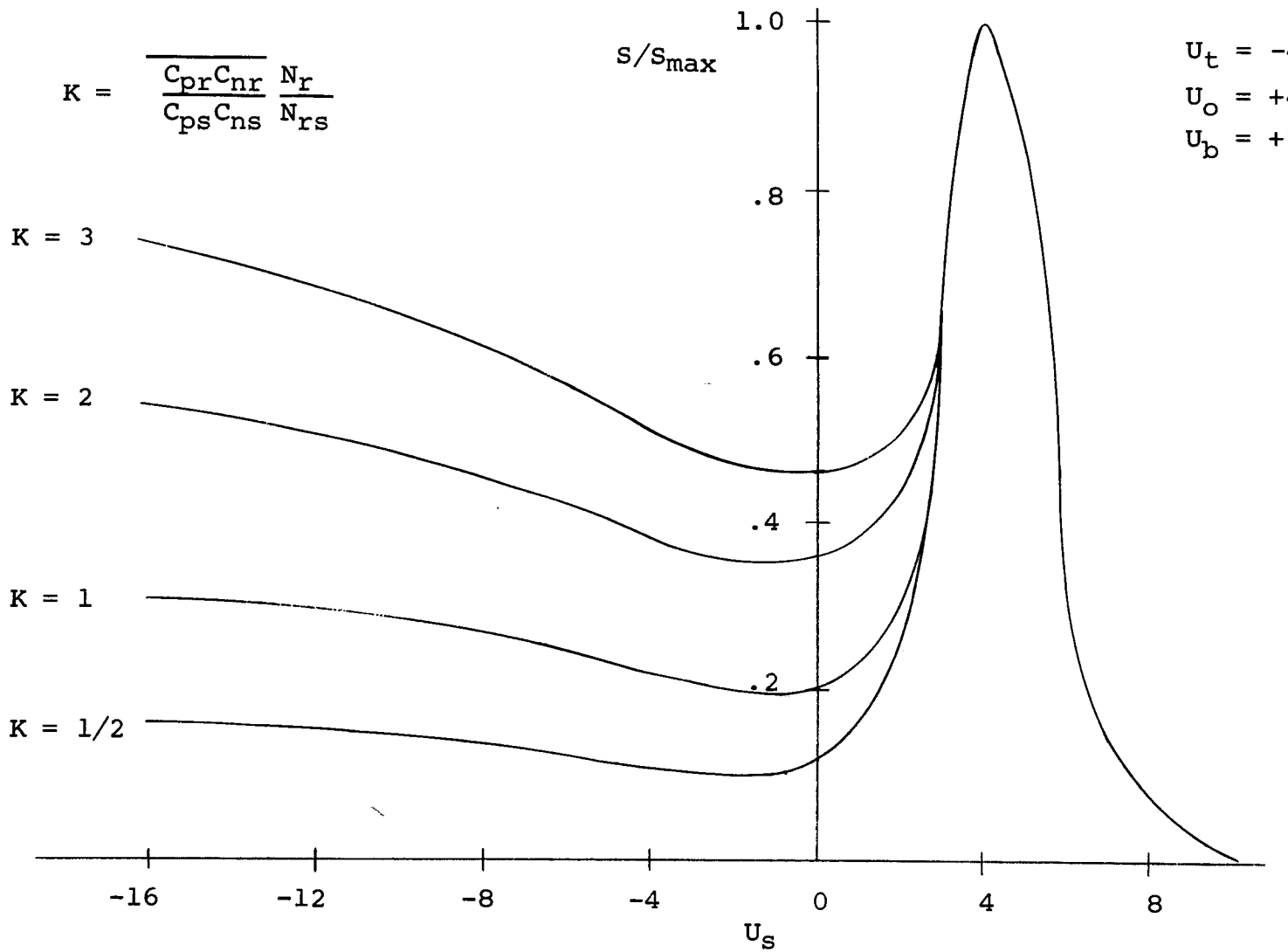

Figure 6.5. Surface recombination velocity vs. surface potential including recombination in the space charge region

CHAPTER VII

7. EXPERIMENTAL RESULTS

7.1 Introduction

During the course of the experiments, a total of forty-five samples were used in the measurements. The results were consistant from sample to sample, and correlation of the data was good. To reduce the amount of graphs presented, this thesis will describe data taken on a representative number of samples: six n-type and six p-type. The resistivity of these samples was nominally one hundred ohm cm as specified by the manufacturer. In all cases the material was received in ingot form and had been prepared by the manufacturer using the floating zone technique.

The data that is not presented in graphical form here can be obtained elsewhere (see Littlejohn and Lade, 1965).

All gamma irradiations were carried out in a Co^{60} Gamma Cell in Nelson Hall on the N. C. State University campus. Pre- and post-irradiation measurements were made in the Solid State Device Laboratory located in Daniels Hall.

7.2 Preliminary Experiments

In order to first determine the variations in bulk lifetime and surface recombination velocity, two bulk samples and five thin filaments were prepared. The standard preparation technique previously described in Chapter IV was not adhered to. All the thin filaments were lapped with #100 grit, and

two of them were etched in a 95% HNO_3 and 5% HF solution for fifteen minutes. The ambient was also changed during each irradiation.

The first irradiation was carried out in a forming gas atmosphere (95% N_2, 5% H_2). There was a marked reduction in the value of bulk lifetime for both samples, the change being at least two orders of magnitude in each case. There was likewise a reduction in the surface recombination velocity for the five thin filaments, the percentage changes being greater for the filaments that were not etched. Also, the pre-irradiation values of S for these samples were at least a factor of two greater than those for the etched filaments.

The second irradiation was carried out in an argon atmosphere, and again the bulk lifetime decreased. However, the percentage change was much less, being on the order of 25% for both samples. An examination of the values of surface recombination showed that S continued to decrease for the etched samples, but increased with semi-blasted surfaces.

The third irradiation was carried out in air and the bulk lifetime continued to decrease. The percentage change from the second irradiation was greater than 50% for both samples. Also, the value of surface recombination velocity decreased for each of the thin filaments, the total change being greater than 75% in each case. This illustrates the adverse effect on the surface velocity for irradiations carried out in an oxidizing atmosphere.

Due to the fact that three samples showed a marked increase in surface recombination velocity between the first and second irradiations, and the fact that the data taken when the samples were irradiated in air deviated drastically from the rest of the data, an extrapolation procedure was carried out in hopes of predicting results if the third irradiation had been carried out in a non-oxidizing atmosphere. First the bulk lifetime data was plotted and a smooth curve drawn through the points corresponding to the first and second irradiations. This yielded a predicted value for the bulk lifetime in an non-oxidizing atmosphere, and this value was used to correct the measured values of S for the third irradiation. The corrected values showed an increase over the values for the second irradiation in every case. For these measurements, it was decided to carry out all further irradiations in an argon atmosphere.

Next, a set of three bulk samples and nine thin filaments were prepared from n-type material. The standard surface preparation procedure was followed and bulk lifetime and surface recombination velocity measured as a function of irradiation dosage. Figure 7.1 shows the results for bulk lifetime variations and Figure 7.2 shows the variation of surface recombination velocity for a typical set of samples.

In each case the bulk lifetime decreased drastically upon initial irradiation and then continued to decrease slowly with additional irradiation. This is explained by using the Shockley

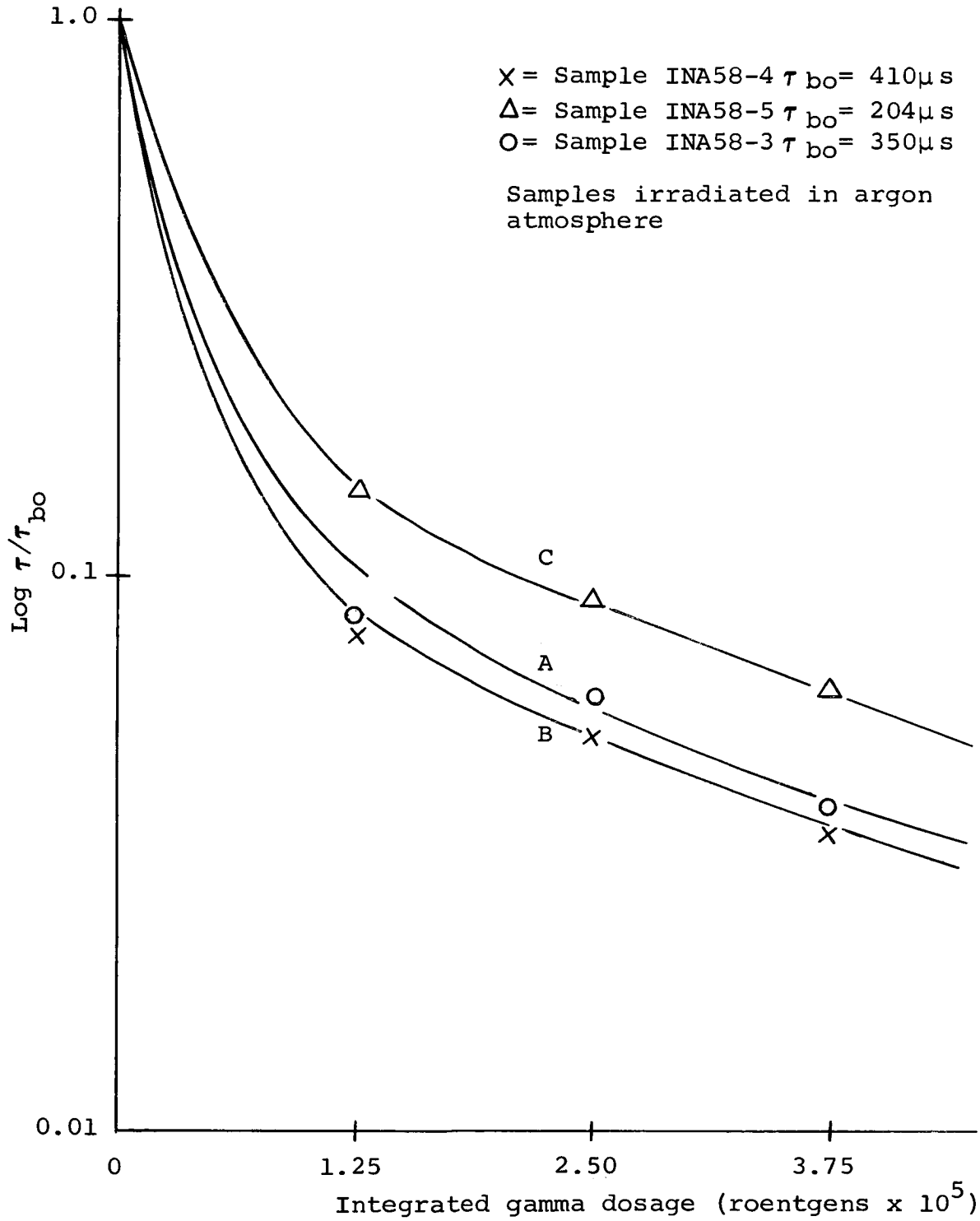

Figure 7.1. Bulk lifetime vs. integrated gamma dosage for n-type material

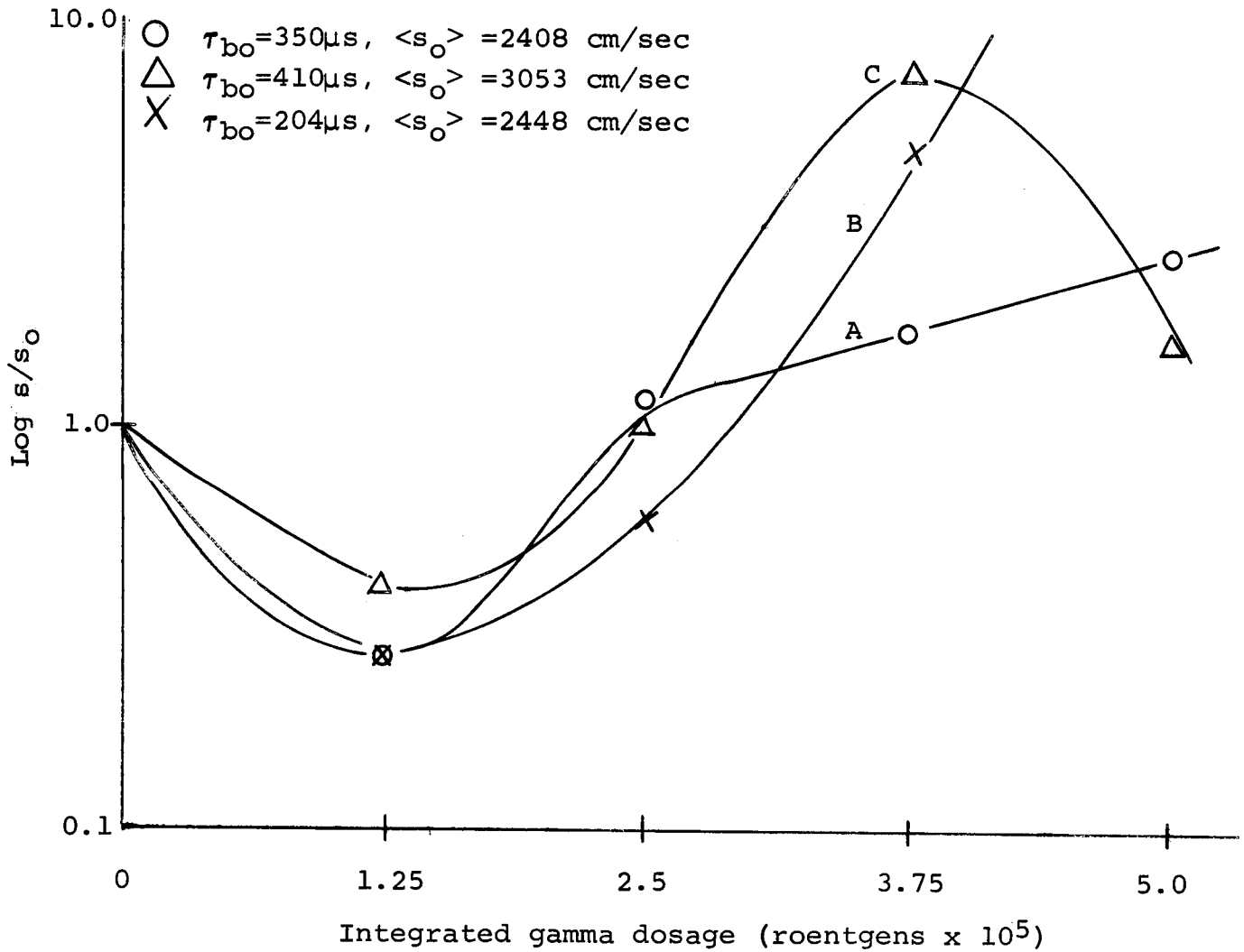

Figure 7.2. Surface recombination velocity vs. integrated gamma dosage for n-type material

Read model and assuming that the number of irradiation induced defects vary linearly with irradiation dosage.

Surface recombination velocity is seen to exhibit a relative minimum as the irradiations are carried out. Figure 7.2 shows one exception, in which S decreased after a fourth irradiation. However, it should be pointed out that the injection level had to be reduced in order to eliminate a characteristic "hump" that appeared in the decay curve after several irradiations. The decrease is due to a change in experimental conditions, and the effect was eliminated in further experiments by carrying our all measurements at lower injection levels.

In computing the values of bulk lifetime and surface recombination velocity, it was assumed that the minority carrier diffusion constant did not vary with irradiations. The Hall Effect measurements which were reported by Littlejohn and Lade (1965) verified this assumption.

Next, three bulk samples and nine thin filaments were prepared from p-type material and irradiations carried out in the same manner as before. Some typical results are shown in Figures 7.3 and 7.4 for bulk lifetime and surface recombination velocity variations. The bulk lifetime in p-type silicon decreased upon initial irradiation, the percentage decrease being approximately 20-40% for the various samples. This should be compared with the initial two orders of magnitude decrease for n-type material.

After the initial irradiation, the bulk lifetime for p-type silicon continued its gradual decrease and approached

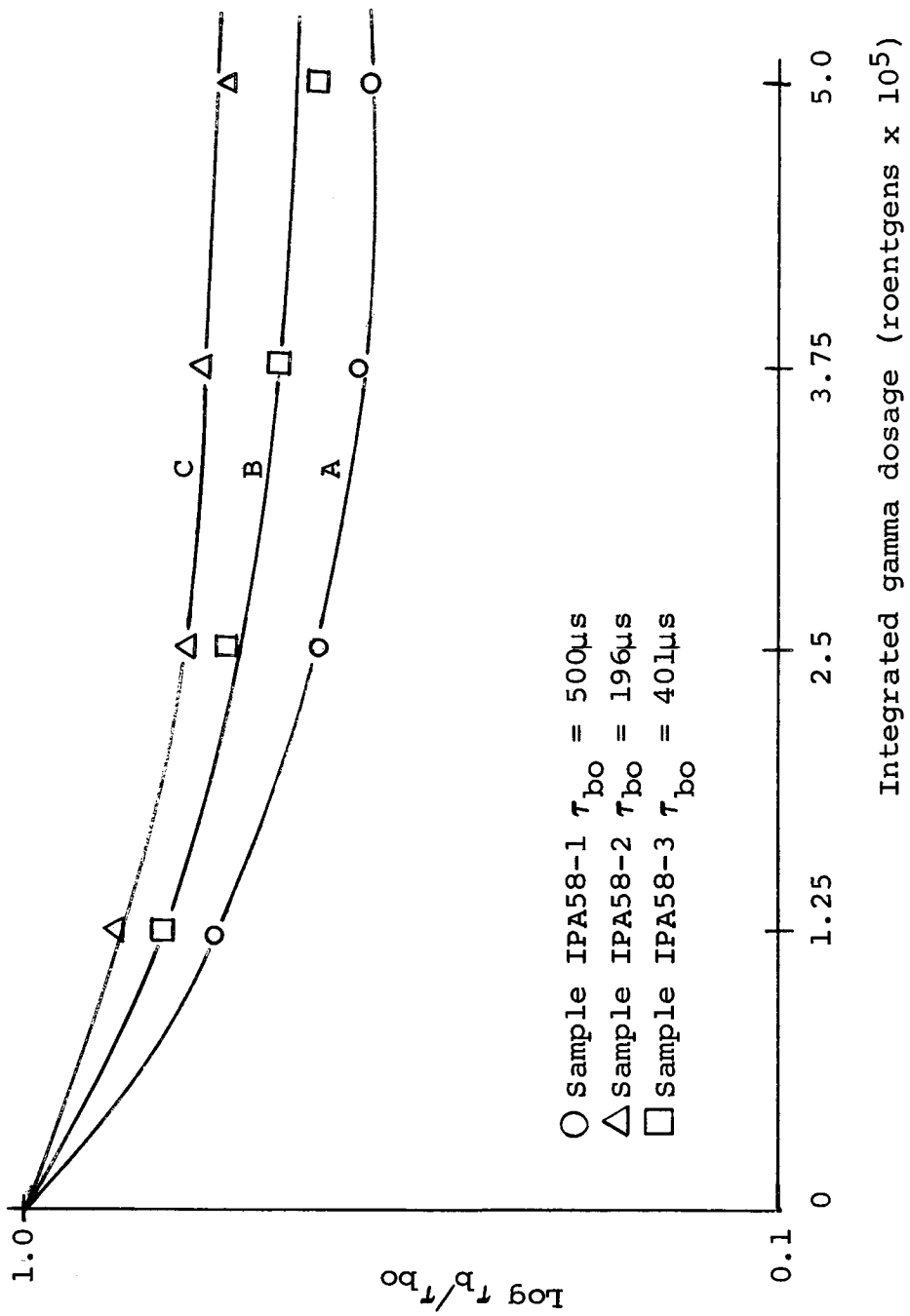

Figure 7.3. Bulk lifetime vs. integrated gamma dosage for p-type material

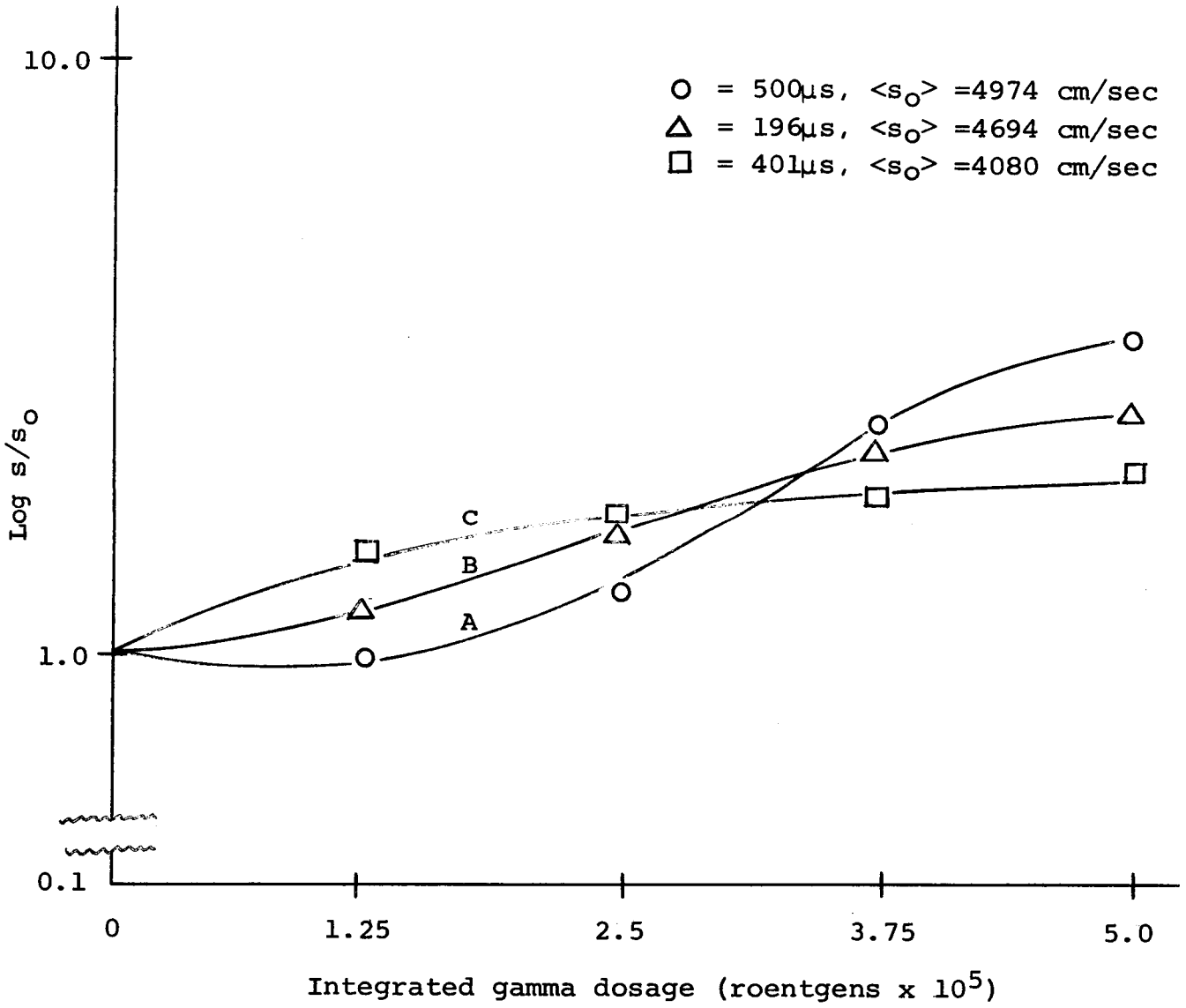

Figure 7.4. Surface recombination velocity vs. integrated gamma dosage for p-type material

a constant value which was never more than one-half of its pre-irradiated value.

The surface recombination velocity was also a slowly varying function of irradiation; its value increased monotonically with increasing irradiation for all samples.

Some problems did arise when making ohmic contacts to p-type material by the electroless nickel plating technique described in Chapter IV. Samples with non-ohmic contacts exhibited a slight decrease in surface recombination velocity upon initial irradiation. As a result, the technique described for applying ohmic contacts given in Chapter IV was optimized, and no further problems with contacts resulted.

With these preliminary room temperature measurements made, the temperature dependence of the bulk and surface lifetimes was examined. The techniques and equipment which were utilized were described in Chapter IV.

Before irradiations were made, the annealing properties of gamma induced defects in n- and p-type silicon were examined to obtain an upper bound on the temperature variations after the samples had been irradiated. Several samples which had been previously irradiated to a total exposure of 1.0×10^6 roentgens were annealed at various temperatures for between five and fifteen minutes, and then cooled back to room temperature. The pre- and post anneal lifetimes gave an indication of the fraction of defects that had been annealed from the lattice. These tests showed that gamma induced defects in n-type silicon

started to anneal at approximately 130°C while those in p-type silicon annealed at between 110°C and 125°C.

Measurements were taken on one bulk sample and one thin filament between room temperature and 300°C for various irradiation exposures. This data has been presented in NASA report NsG-588-4. The results indicated that the gamma rays introduced into the bulk a defect approximately 0.4 eV below the conduction band edge. This defect position in the forbidden region did not vary, within experimental error, for various irradiation doses.

However, at the surface, the defect appeared at 0.25 eV above the valence band edge upon initial irradiation, and this position varied as the irradiations proceeded. The level seemed to approach the valence band edge as the irradiation dose increased. This effect was unexpected. It could be postulated that the gamma irradiation changes the surface potential but has no effect on the bulk electrostatic potential. Also, some of the parameters in the equations could have temperature dependences that have not been accounted for. This phenomena will be discussed further in section 7.4.

7.3 Final Measurements - Bulk Lifetime

Armed with this information, six n-type and six p-type (two bulk samples and four thin filaments each) samples were prepared and bulk and surface lifetimes were measured as a function of temperature for several values of gamma ray dosage. Surface recombination velocity measurements were calculated at room temperature for the various irradiation exposures.

Table 7.1 shows the data obtained from computer curve fits to the experimentally determined values of bulk and surface lifetimes versus temperature for various values of gamma dosage.

Figures 7.5 through 7.14 show the data taken on the n-type bulk samples for the various irradiations. The results of the computer curve fit indicates that a deep level with an energy separation of about 0.4 eV below the conduction band edge is created by the gamma irradiation. Contrary to results reported by others (Glaenzer and Wolf, 1965 and Hewes, 1966), there did not appear to be a second level which had any influence on the lifetime measurements in the 100 ohm cm n-type material. Glaenzer and Wolf did not examine material with resistivity quite this high. They used 30 and 70 ohm cm material and located another defect with an energy level at .17 eV below the conduction band edge. They identified this level to be the so called "A center" which is associated with a substitutional oxygen atom in the lattice (Watkins and Corbett, 1961 and Sonder and Templeton, 1960). Hewes also saw the effects of this level in material with resistivity less than 70 ohm cm, but in material with resistivity greater than this value the effects of this level were of second order. He came to the conclusion that it was very likely that only one type of defect was present in the crystal, this being the level at Ec-0.40 eV. Also, he stated that the parameters of the level at Ec-0.17 eV appeared to be determined more by the original estimate required

Table 7.1 Energy levels obtained from computer curve fits to experimentally determined values of bulk and surface lifetimes vs. reciprocal temperature

Sample	Irradiation	Position of defect in forbidden region	τ_{po} (μsec)	τ_{no} (μsec)
1NA58-7	Pre	Ev + .190	81.2	(.571)
	1st	Ec - .335	41.8	-
	2nd	Ec - .465	27.6	-
	3rd	Ec - .404	22.4	-
	4th	Ec - .427	21.7	-
	5th	Ec - .372	19.1	-
	6th	Ec - .409	16.0	-
1NA58-8	Pre	Ev + .068	13.5	1.68×10^{-8}sec.
	1st	Ec - .417	49.5	-
	2nd	Ec - .423	31.2	-
	3rd	Ec - .404	23.0	-
	4th	Ec - .407	21.9	-
	5th	Ec - .426	20.0	-
	6th	Ec - .406	15.8	-
1NA 3/4 5-1	Pre	Ev + .104	21.9	3.45×10^{-9}sec.
	1st	Ev + .240	38.3	.155
	2nd	Ev + .107	29.7	3.59×10^{-9}sec.
	3rd	Ev + .074	37.3	1.64×10^{-9}sec.
	4th	Ev + .163	29.9	27.2×10^{-9}sec.
	5th	Ev + .302	20.1	1.55
	6th	Ev + .291	20.3	1.05
1NA 3/4 5-2	Pre	Ev + .132	27.7	6.89×10^{-9}sec.
	1st	Ev + .281	44.1	.561
	2nd	Ev + .161	52.4	1.47×10^{-8}sec.
	3rd	Ev + .135	56.6	1.12×10^{-8}sec.
	4th	Ev + .073	20.2	2.81×10^{-9}sec.
	5th	Ev + .287	31.1	1.69×10^{-6}sec.
	6th	Ev + 284	20.1	1.57×10^{-6}sec.
1 NA 3/4 5-3	Pre	Ev + .162	27.4	2.04×10^{-8}sec.
	1st	Ev + .158	40.3	1.11×10^{-8}sec.
	2nd	Ev + .096	38.0	2.26×10^{-9}sec.
	3rd	Ev + .027	29.8	3.93×10^{-10}sec.
	4th	Ev + .296	56.4	8.2×10^{-7}sec.
	5th	Ev + .247	35.8	.296
	6th	Ev + .265	22.5	.592

Continued

Table 7.1. Continued

Sample	Irradiation	Position of defect in forbidden region	τ_{po} (μsec)	τ_{no} (μsec)
1NA 3/4 5-4	Pre	Ev + .152	34.9	1.5×10^{-8}sec.
	1st	Ev + .256	54.3	.146
	2nd	Ev + .143	51.0	1.34×10^{-8}sec.
	3rd	Ev + .052	46.1	$.904 \times 10^{-10}$sec.
	4th	Ev + .099	30.0	4.92×10^{-9}sec.
	5th	Ev + .246	36.3	.301
	6th	Ev + .247	23.1	.406
1PA58-5	Pre	Ev + .064	.507	-
	1st	Ev + .117	133	-
	2nd	Ev + .188	191	-
	3rd	Ev + .190	177	-
	4th	Ev + .178	166	-
	5th	Ev + .200	173	-
	6th	Ev + .193	145	-
1PA58-6	Pre	Ev + .097	44.8	-
	1st	Ev + .129	133	-
	2nd	Ev + .162	151	-
	3rd	Ev + .179	148	-
	4th	Ev + .192	147	-
	5th	Ev + .161	138	-
	6th	Ev + .182	122	-
1PA 3/4 5-1	Pre	Ec - .067	8.45	9.82×10^{-10}sec.
	1st	Ec - .235	13.5	.110
	2nd	Ec - .230	14.7	8.8×10^{-8}sec.
	3rd	Ec - .198	14.3	2.98×10^{-8}sec.
	4th	Ec - .184	14.0	4.71×10^{-8}sec.
	5th	Ec - .161	13.8	1.57×10^{-8}sec.
	6th	Ec - .229	13.0	1.23×10^{-7}sec.
1PA 3/4 5-2	Pre	Ec - .142	10.3	5.5×10^{-9}sec.
	1st	Ec - .318	11.1	.202
	2nd	Ec - .272	11.8	.799
	3rd	Ec - .186	10.2	1.82×10^{-8}sec.
	4th	Ec - .168	9.92	1.21×10^{-8}sec.
	5th	Ec - .189	9.58	2.51×10^{-8}sec.
	6th	Ec - .123	8.74	3.60×10^{-9}sec.

Continued

Table 7.1. Continued

Sample	Irradiation	Position of defect in forbidden region	τ_{po} (μsec)	τ_{no} (μsec)
1PA 3/4 5-3	Pre	Ec - .083	15.5	2.18×10^{-9}sec.
	1st	Ec - .237	20.2	.166
	2nd	Ec - .170	18.0	1.17×10^{-8}sec.
	3rd	Ec - .142	19.1	3.42×10^{-8}sec.
	4th	Ec - .118	16.5	7.47×10^{-9}sec.
	5th	Ec - .126	16.1	8.69×10^{-9}sec.
	6th	Ec - .123	16.8	8.38×10^{-9}sec.
1PA 3/4 5-4	Pre	Ec - .087	13.7	2.41×10^{-9}sec.
	1st	Ec - .220	19.5	9.99×10^{-8}sec.
	2nd	Ec - .149	18.1	1.48×10^{-8}sec.
	3rd	Ec - .172	17.9	4.04×10^{-8}sec.
	4th	Ec - .120	17.5	6.74×10^{-8}sec.
	5th	Ec - .099	14.8	3.88×10^{-9}sec.
	6th	Ec - .186	20.7	4.46×10^{-8}sec.

Figure 7.5. Bulk lifetime vs. reciprocal temperature for sample INA58-7 for pre-irradiation and after 4.82×10^4 roentgens and 9.64×10^4 roentgens of Co^{60} gamma ray exposure

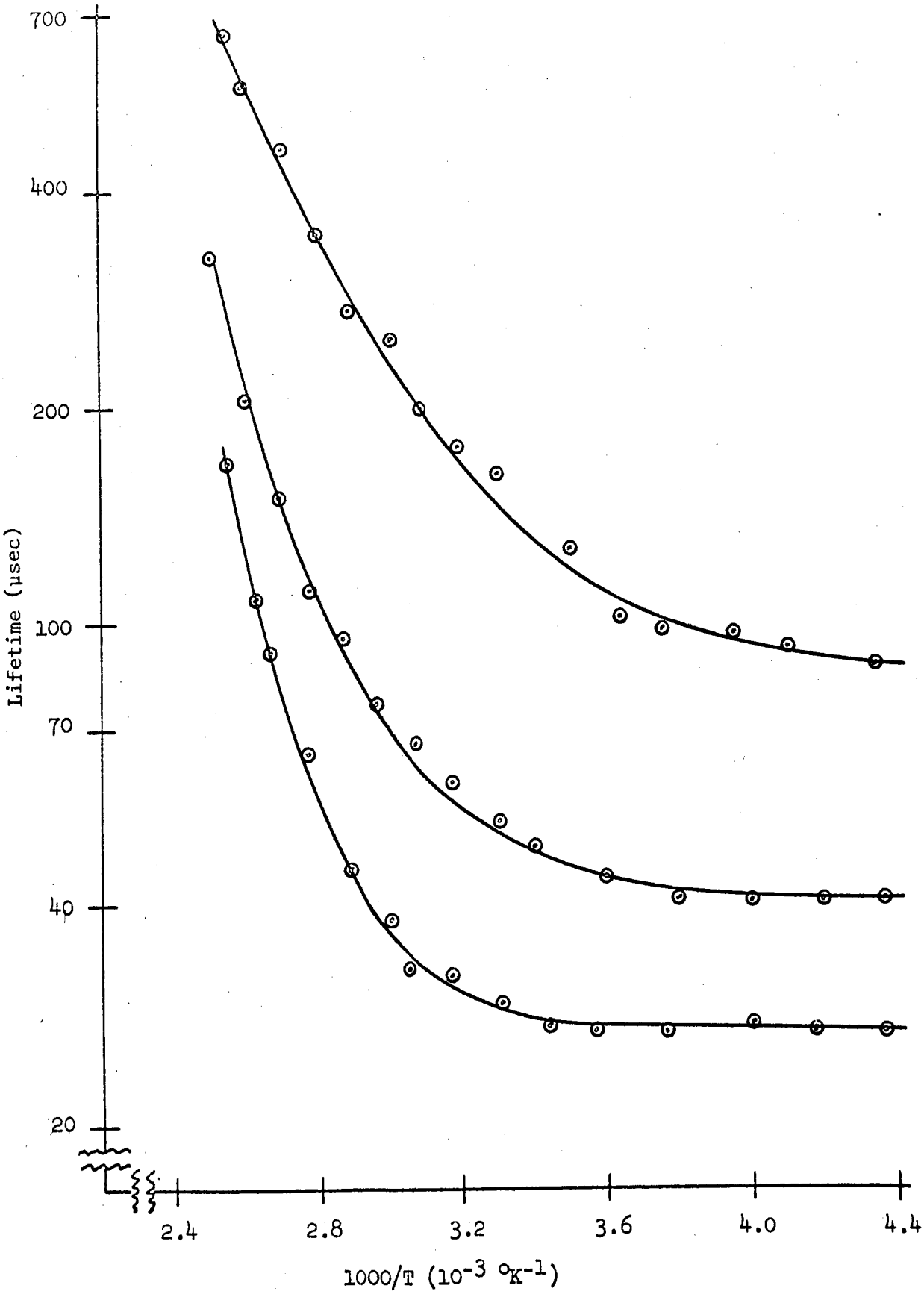
700
400
200
100
70
40
20
Lifetime (μsec)
2.4
2.8
3.2
3.6
4.0
4.4
1000/T (10-3 °K-1)

Figure 7.6. Bulk lifetime vs. reciprocal temperature for sample INA58-7 after 1.45×10^5 roentgens of Co^{60} gamma ray exposure

Figure 7.7. Bulk lifetime vs. reciprocal temperature for sample INA58-7 after 1.93×10^5 roentgens of Co^{60} gamma ray exposure

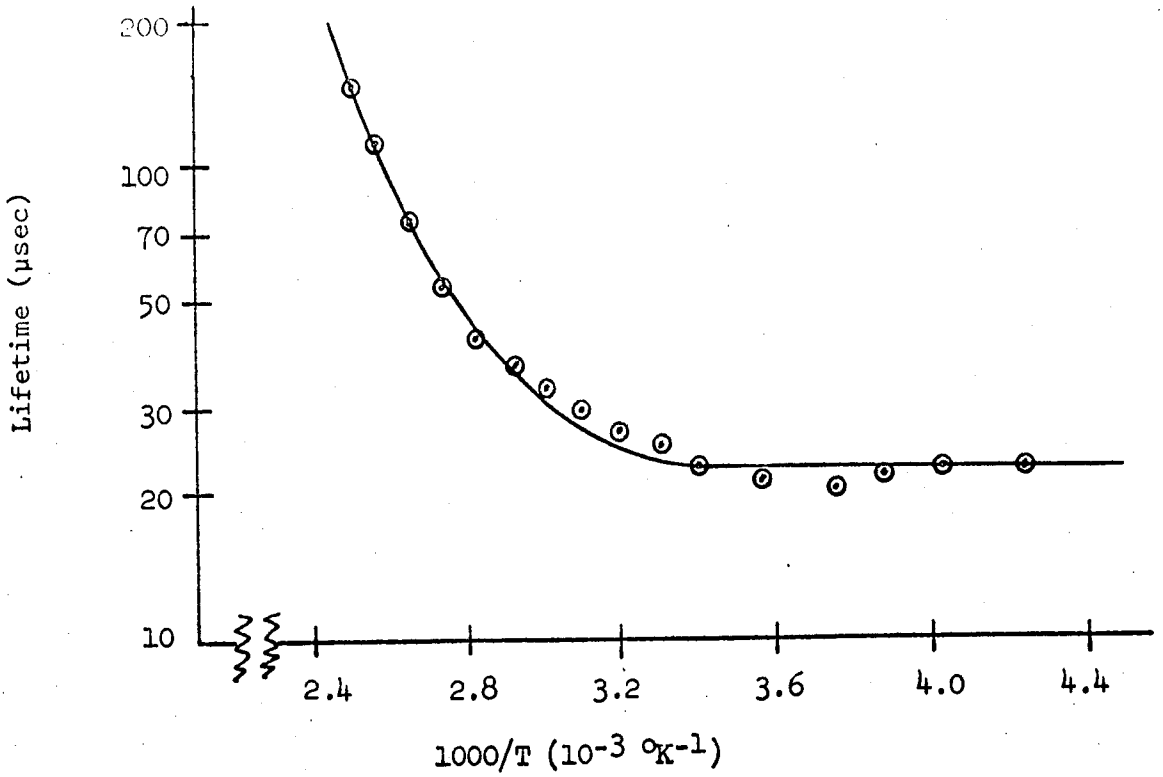
Lifetime (μsec)
200
100
70
50
30
20
10
2.4
2.8
3.2
3.6
4.0
4.4
1000/T (10-3 °K-1)

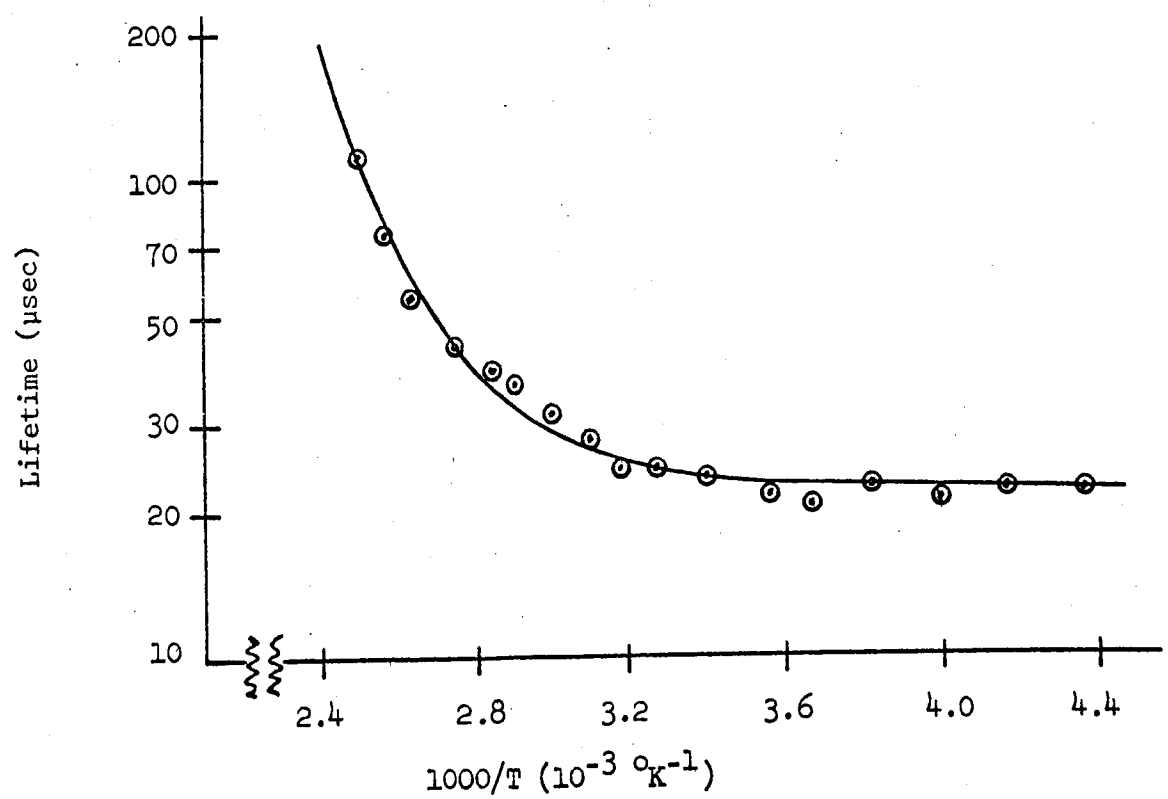
Lifetime (μsec)
200
100
70
50
30
20
10
2.4
2.8
3.2
3.6
4.0
4.4
1000/T (10-3 °K-1)

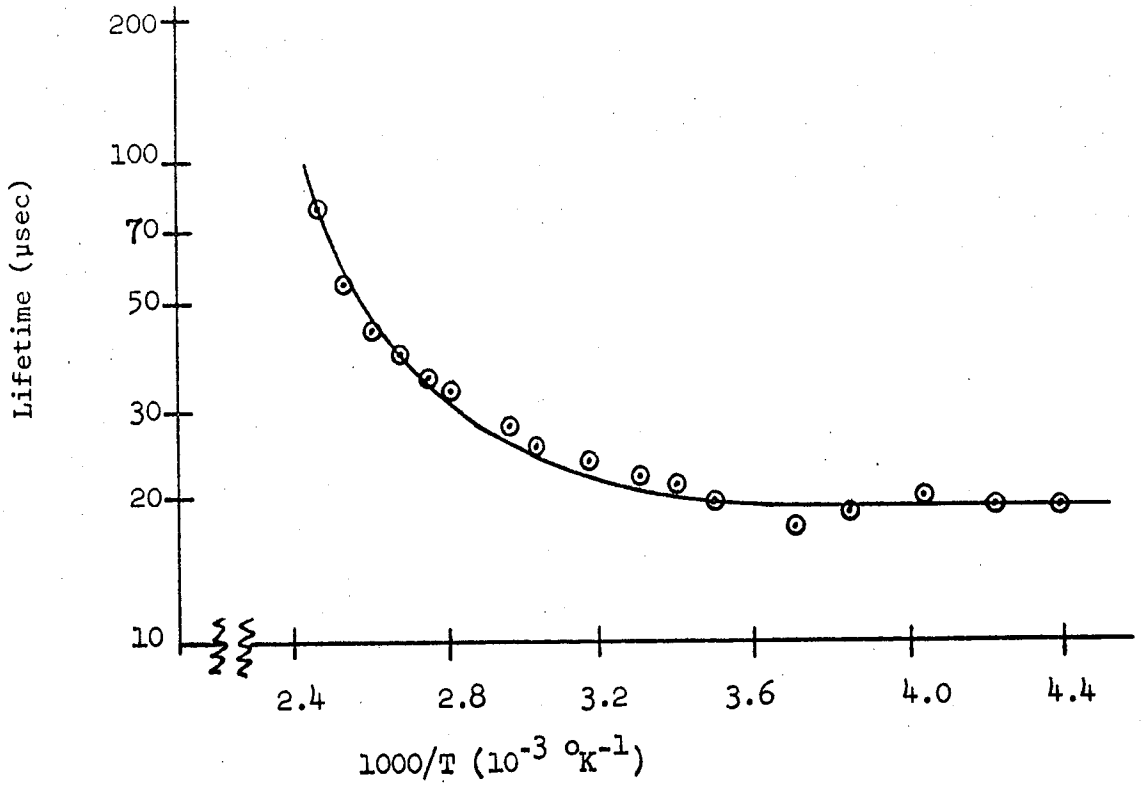
Lifetime (μsec)
200
100
70
50
30
20
10
2.4
2.8
3.2
3.6
4.0
4.4
1000/T (10-3 °K-1)

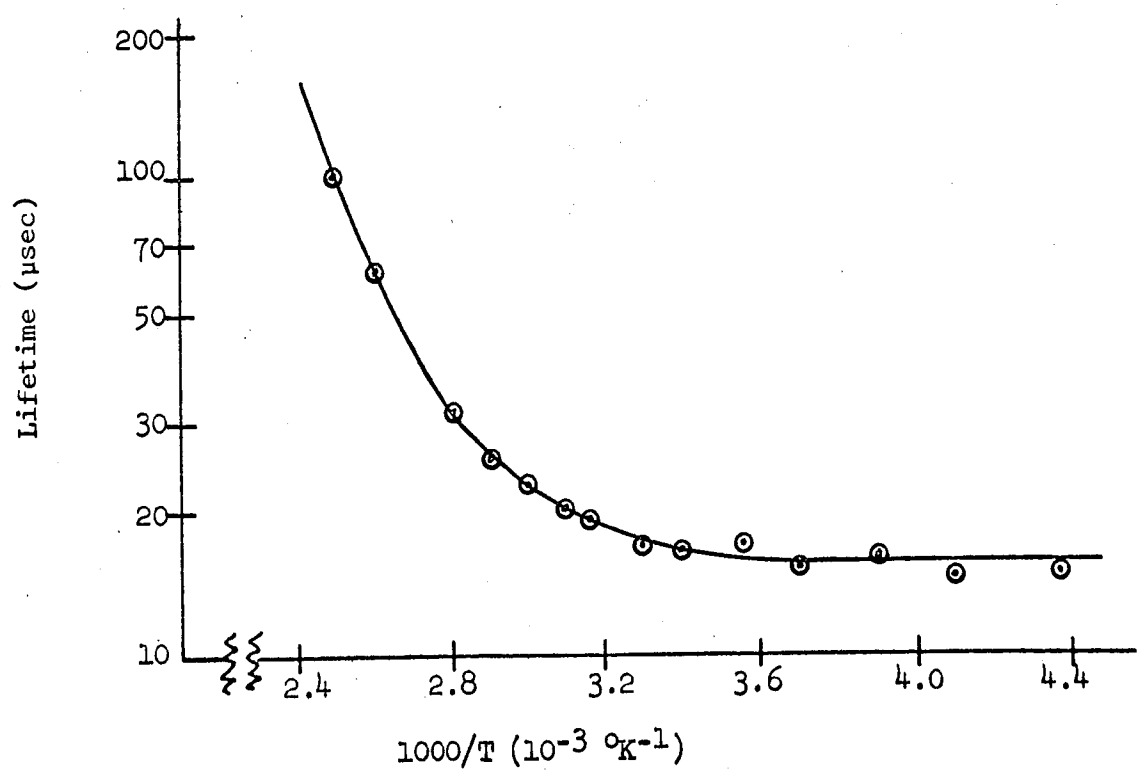
Lifetime (μsec)
200
100
70
50
30
20
10
2.4
2.8
3.2
3.6
4.0
4.4
1000/T (10-3 °K-1)

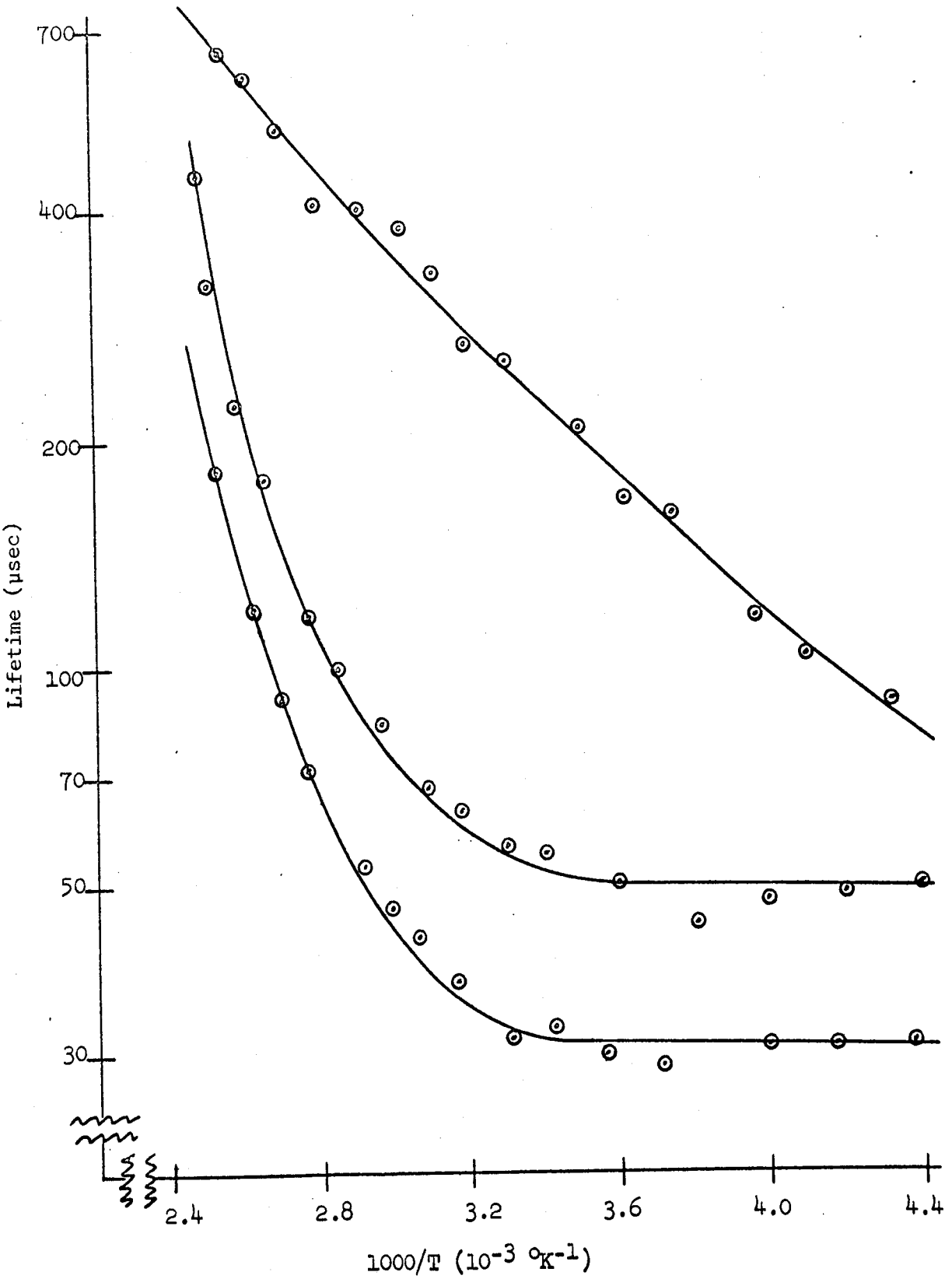
700
400
200
100
70
50
30
Lifetime (μsec)
2.4
2.8
3.2
3.6
4.0
4.4
1000/T (10-3 °K-1)

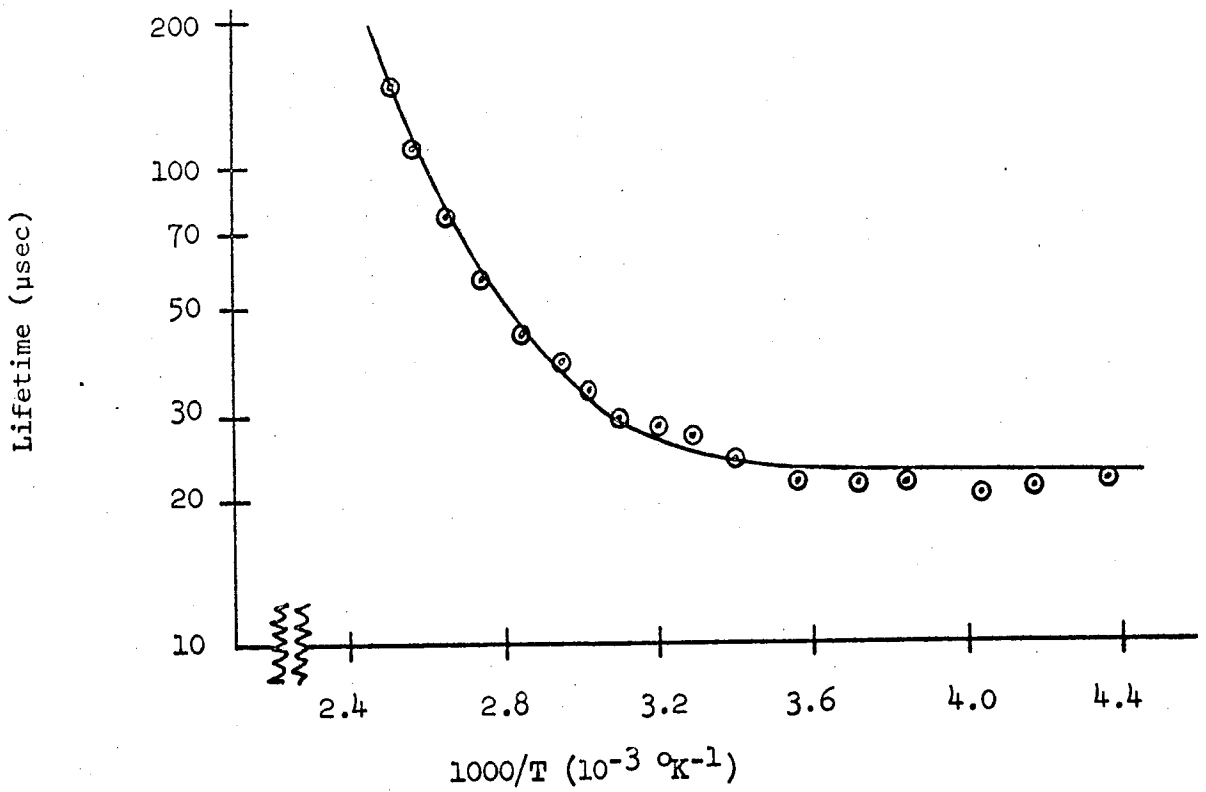
Lifetime (μsec)
200
100
70
50
30
20
10
2.4
2.8
3.2
3.6
4.0
4.4
1000/T (10-3 °K-1)

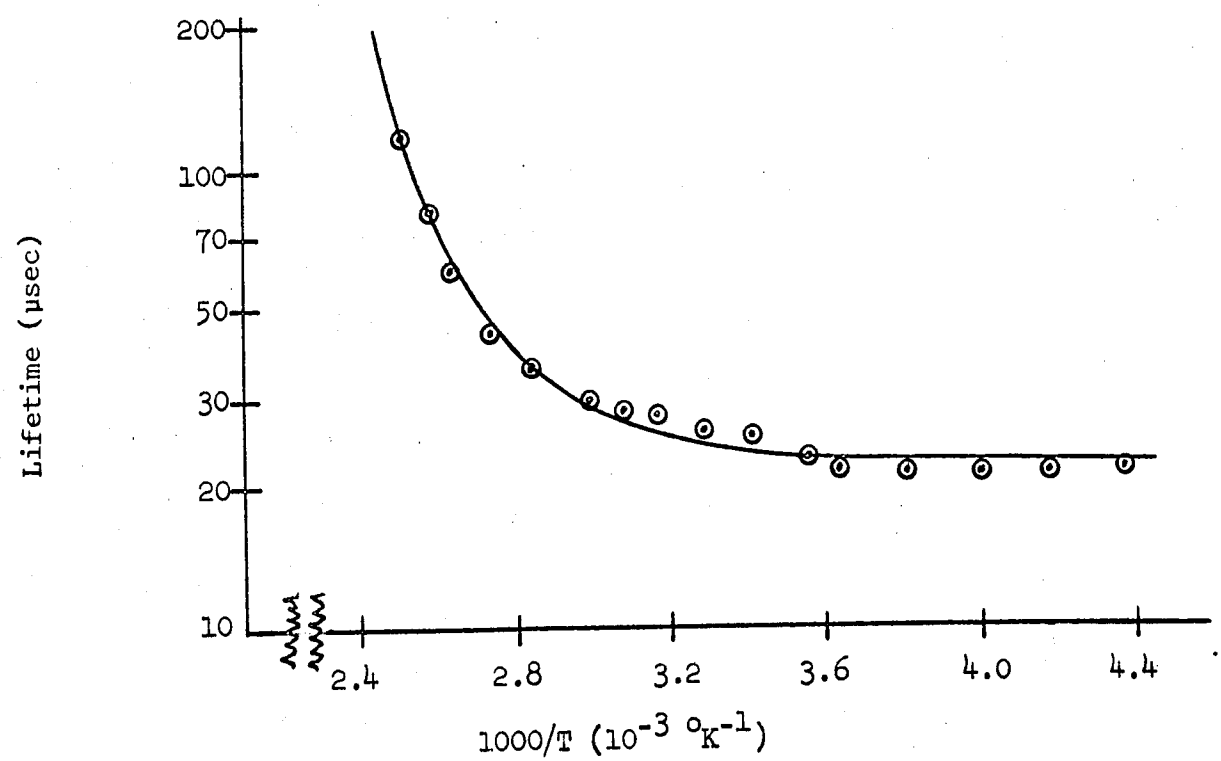
Lifetime (μsec)
200
100
70
50
30
20
10
2.4
2.8
3.2
3.6
4.0
4.4
1000/T (10-3 °K-1)

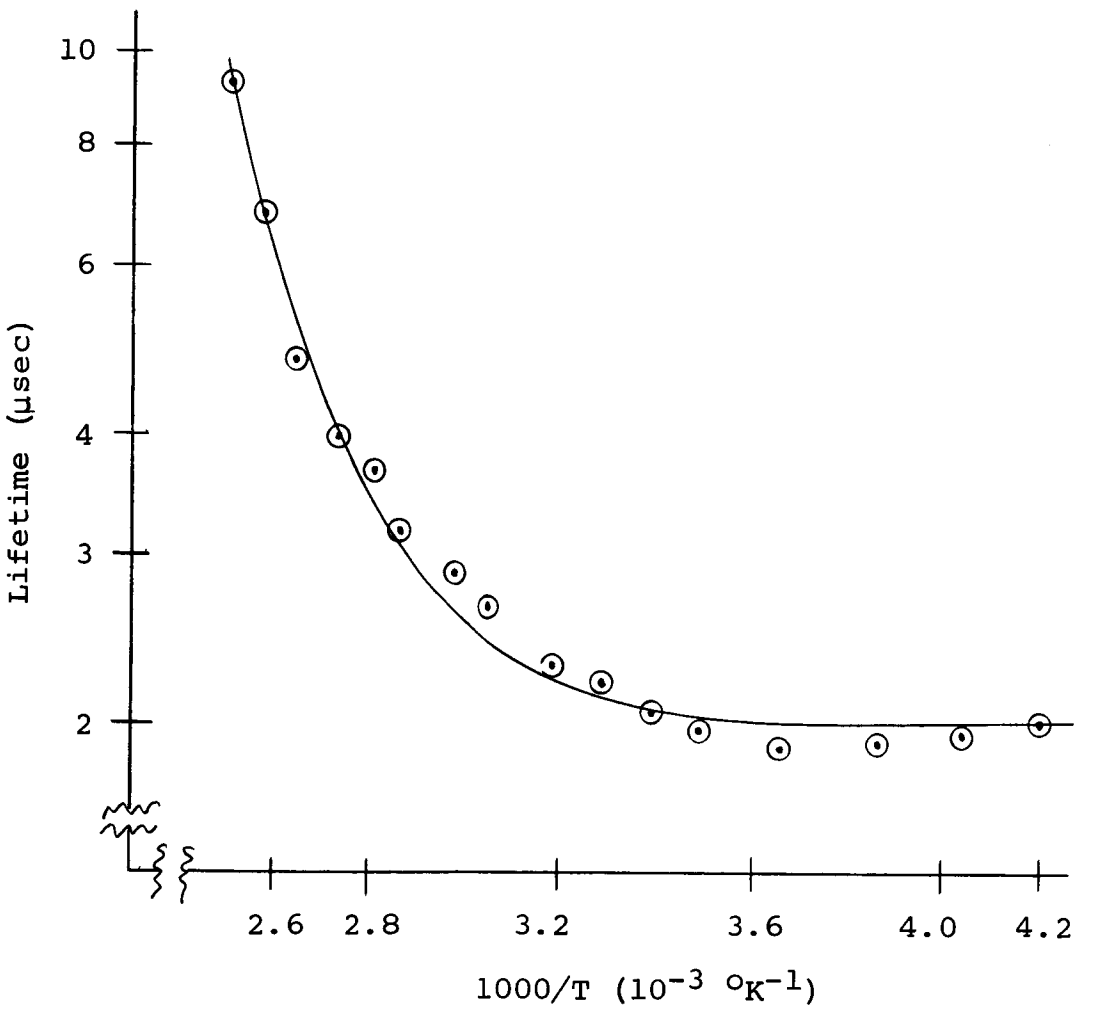

Figure 7.13. Bulk lifetime vs. reciprocal temperature for sample INA58-8 after 2.89 x 10^5 roentgens of Co^{60} gamma ray exposure

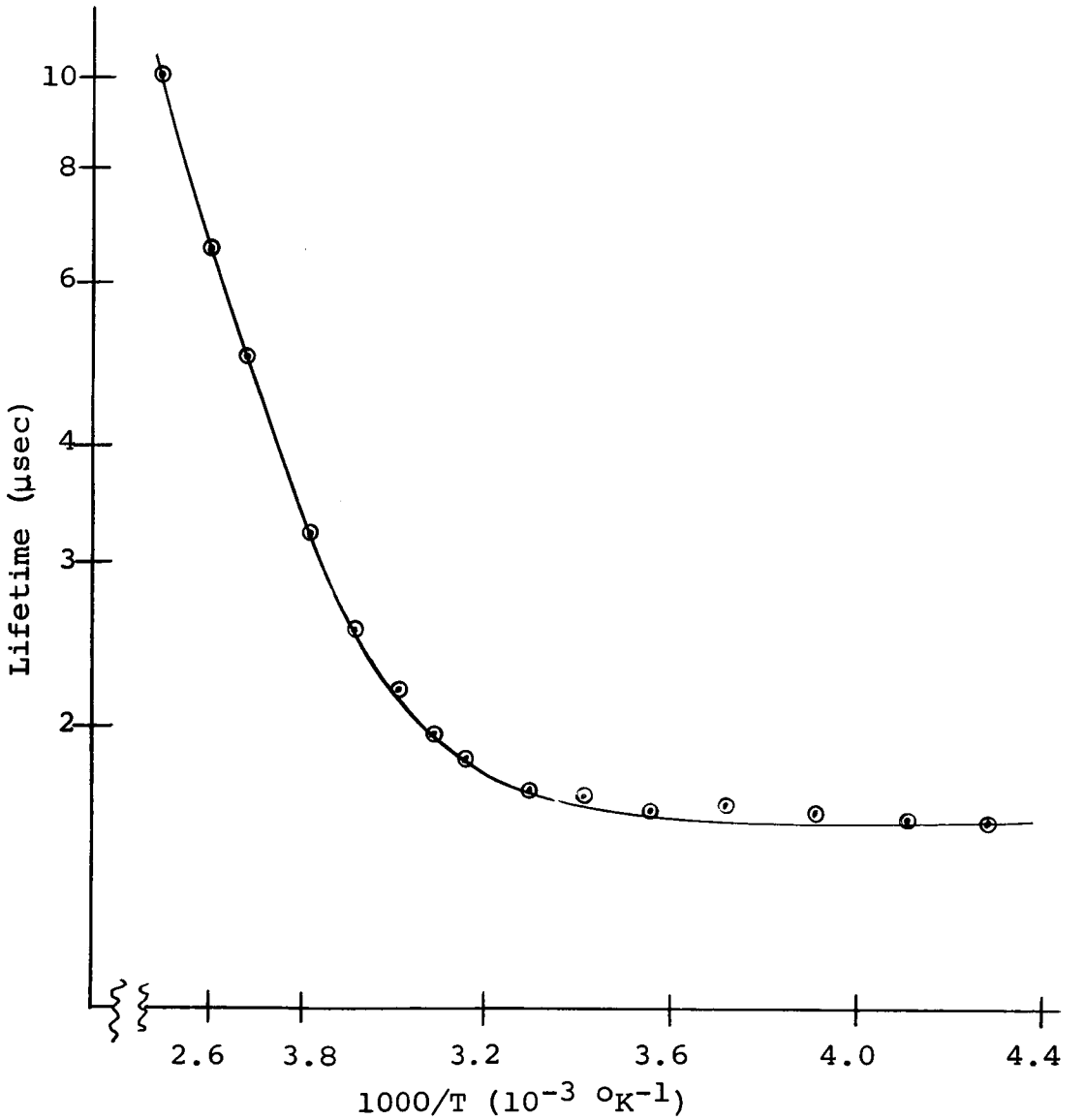

Figure 7.14. Bulk lifetime vs. reciprocal temperature for sample INA58-8 after 3.85 roentgens of Co^{60} gamma ray exposure

by his computer program than by anything else, and he could not reach any definite conclusions about this level.

Since the oxygen content in material prepared by the floating zone technique generally is quite small, then the conclusion reached on the basis of these experiments is that the dominant defect in 100 ohm cm n-type material prepared by the floating zone technique is one with an energy of Ec-o.40 eV. This center is identified with the E-center (Watkins and Corbett, 1964) which is a phosphorous-vacancy complex, i.e., a phosphorous atom with a vacancy as its nearest neighbor.

Figures 7.15 through 7.28 show the lifetime versus temperature variations for the p-type bulk samples for several values of gamma ray exposure. Table 7.1 shows that a level is created by the gamma irradiation which is located at approximately 0.18 eV above the valence band edge. Again there did not appear to be any influence from any other levels for p-type material of this resistivity. In his experiments Hewes (1966) did see another level influencing the lifetime in p-type material. However, the position of this second level in the energy gap varied from sample to sample and ingot to ingot. Sometimes its presence could not be detected at all, and sometimes this level was the dominant one in his lifetime-temperature characteristics. Also, it was obvious that in the higher resistivity material (except for one sample) his data could have been described using only one level.

From the data presented here the conclusion is reached that in these experiments gamma irradiation introduced a level at Ev + .18 eV in p-type material.

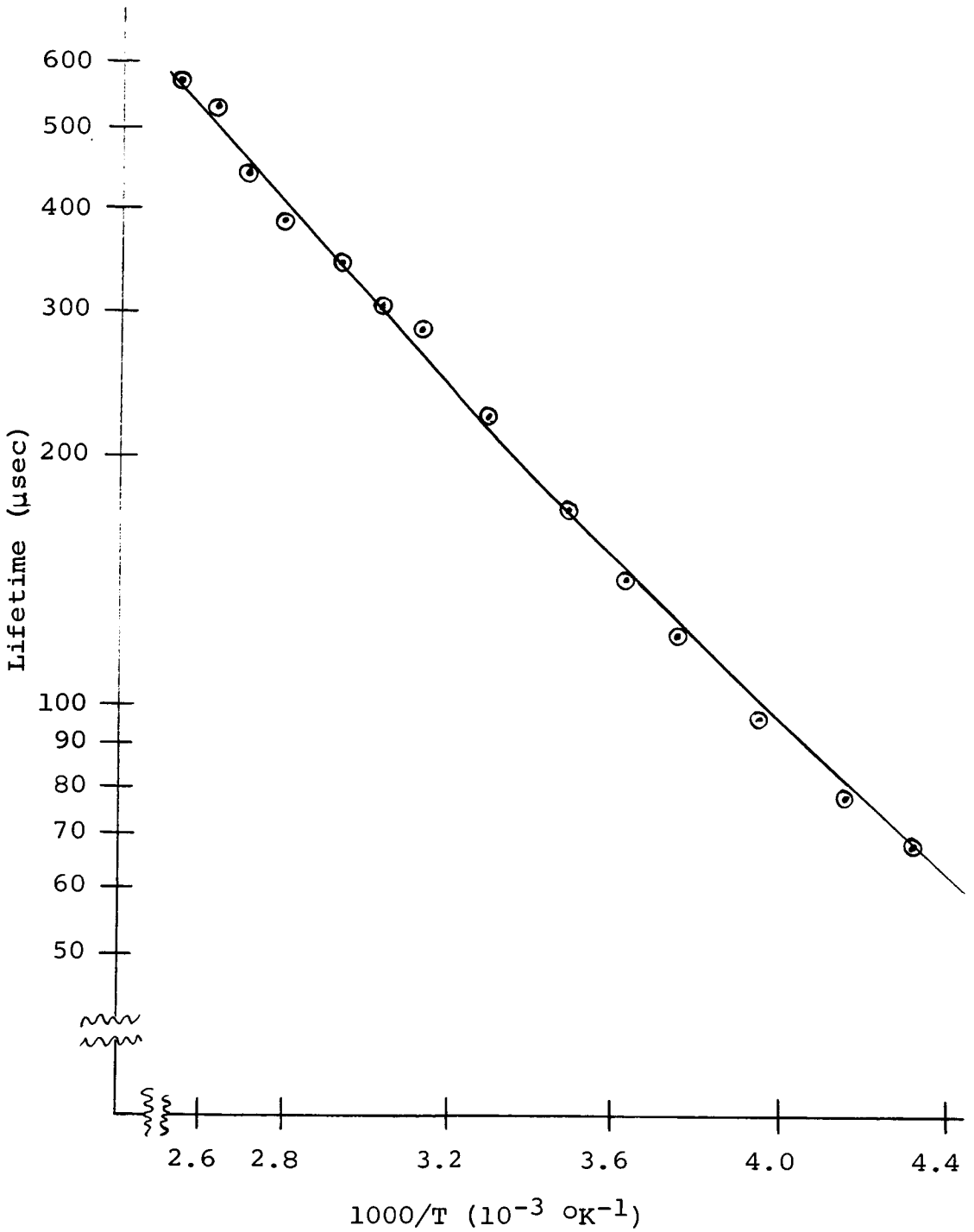

Figure 7.15. Bulk lifetime vs. reciprocal temperature for sample IPA58-5 before irradiation

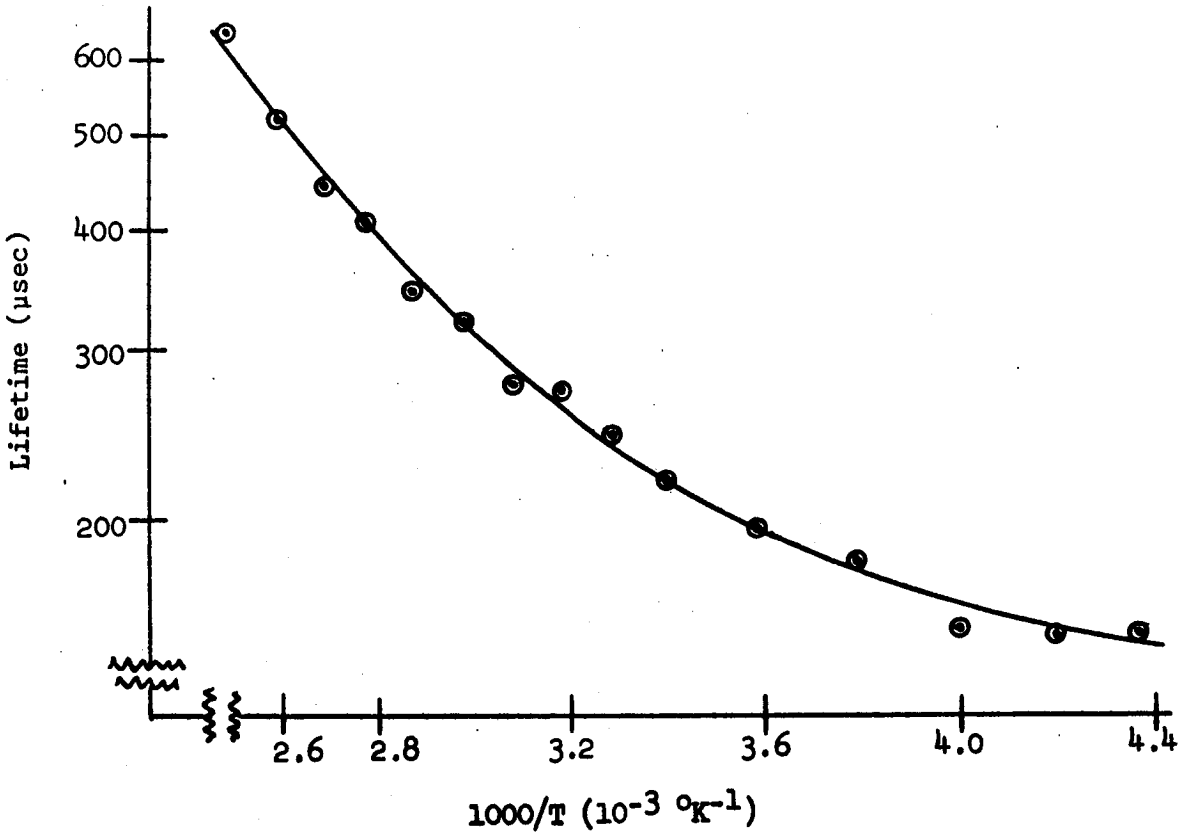
600
500
400
300
200
Lifetime (μsec)
2.6
2.8
3.2
3.6
4.0
4.4
1000/T (10-3 °K-1)

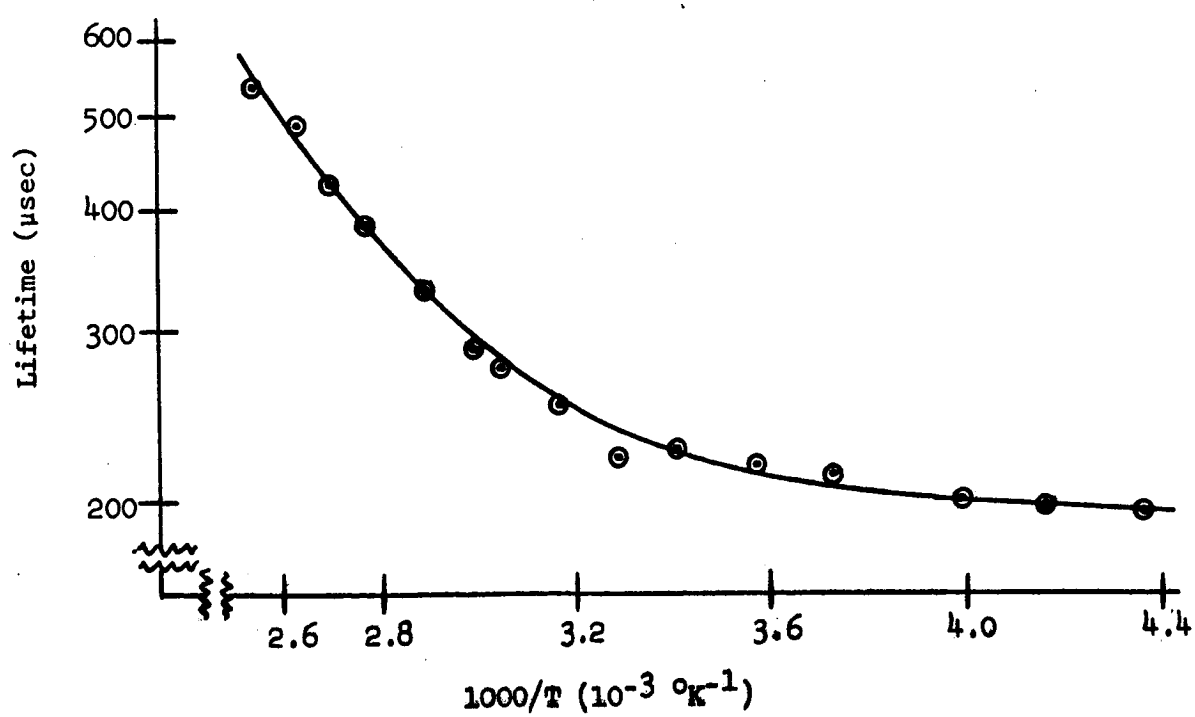
600
500
400
300
200
Lifetime (μsec)
2.6
2.8
3.2
3.6
4.0
4.4
1000/T (10-3 °K-1)

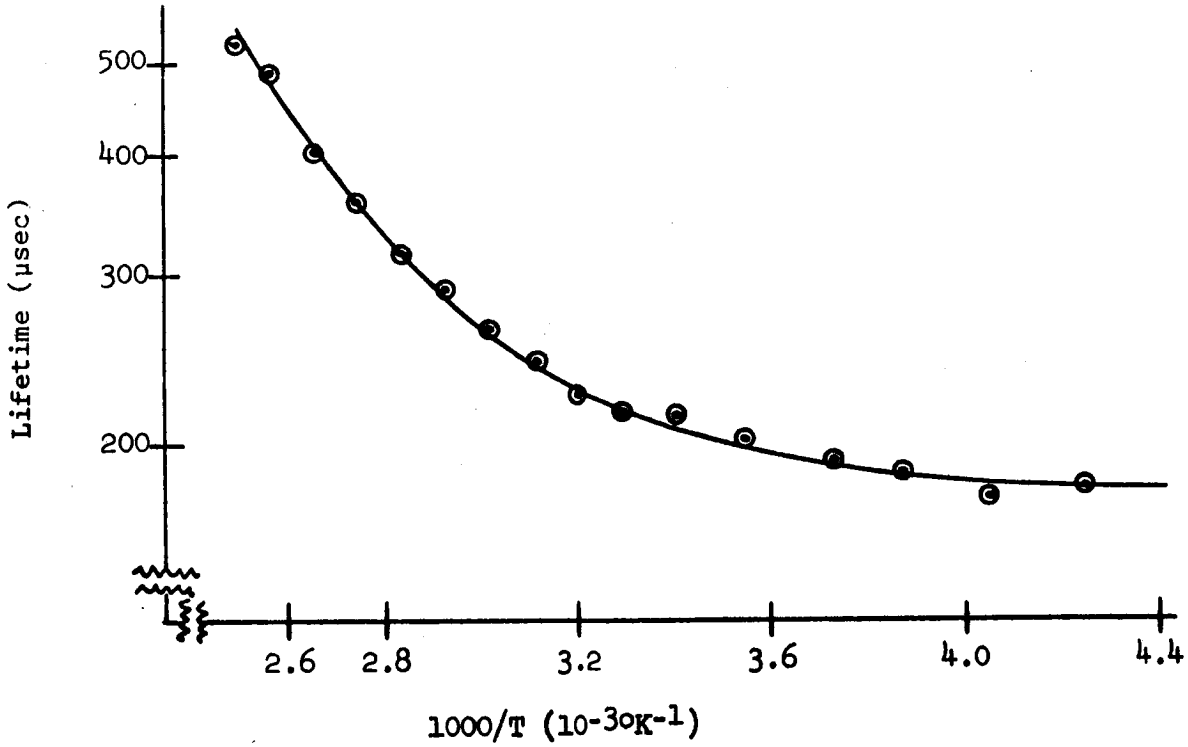
Lifetime (μsec)
500
400
300
200
2.6
2.8
3.2
3.6
4.0
4.4
1000/T (10-3oK-1)

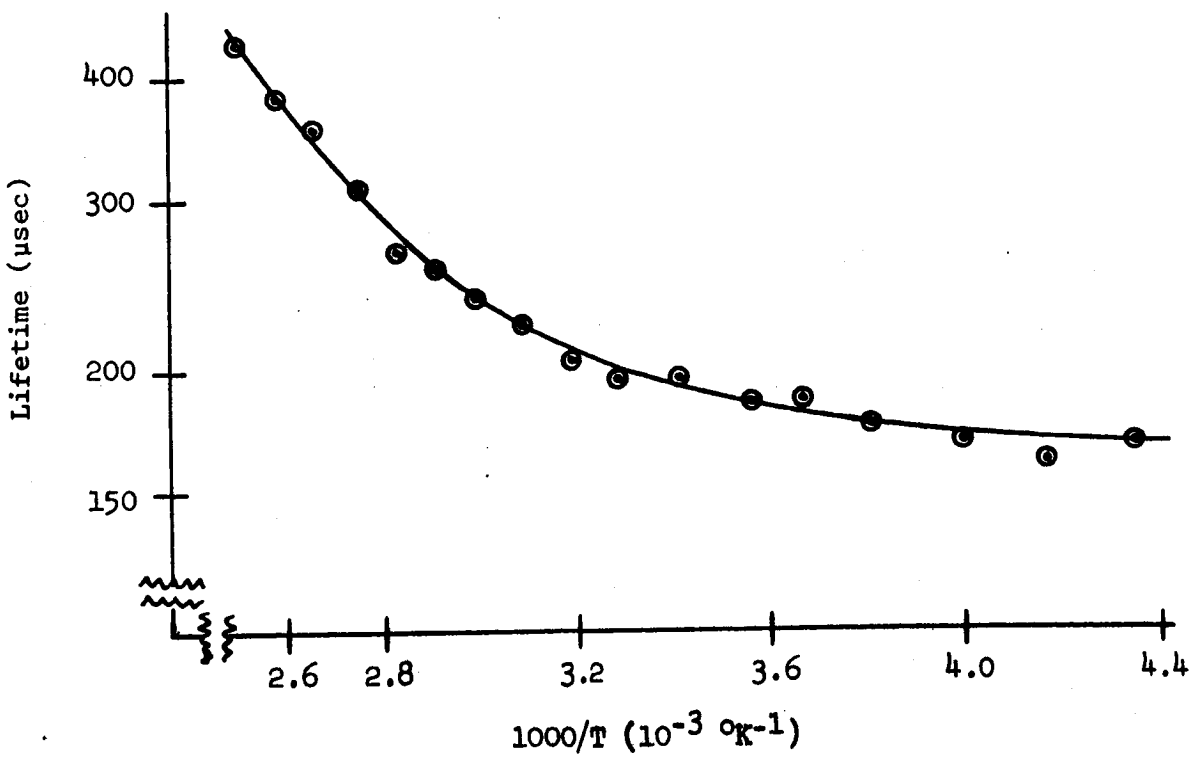
Lifetime (μsec)
400
300
200
150
2.6
2.8
3.2
3.6
4.0
4.4
1000/T (10-3 oK-1)

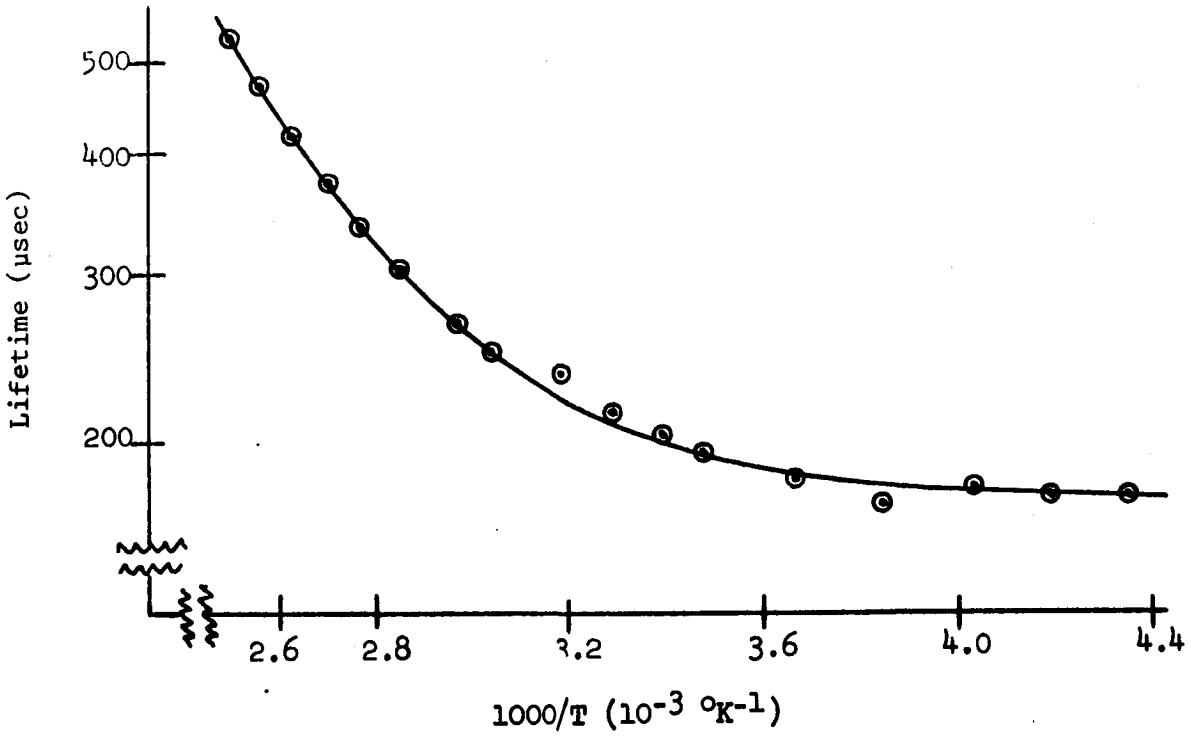
500
400
300
200
Lifetime (μsec)
2.6
2.8
3.2
3.6
4.0
4.4
1000/T (10-3 °K-1)

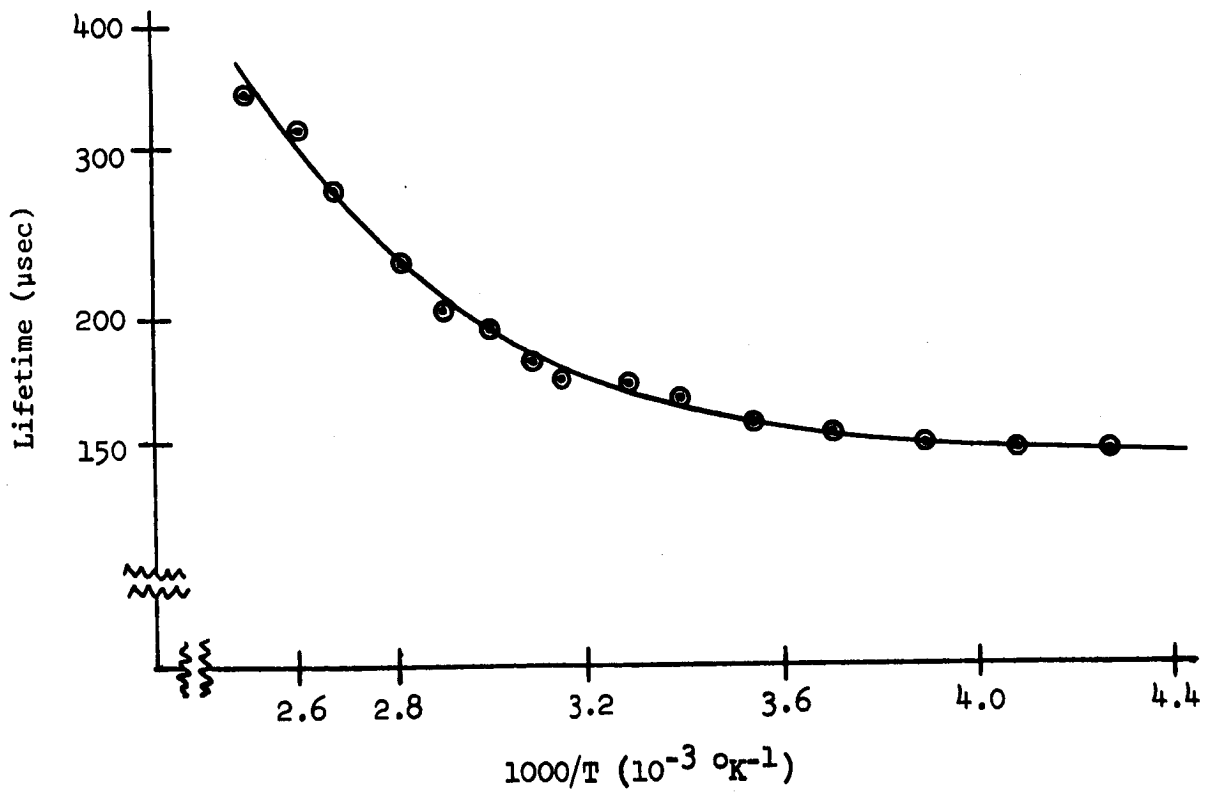
400
300
200
150
Lifetime (μsec)
2.6
2.8
3.2
3.6
4.0
4.4
1000/T (10-3 °K-1)

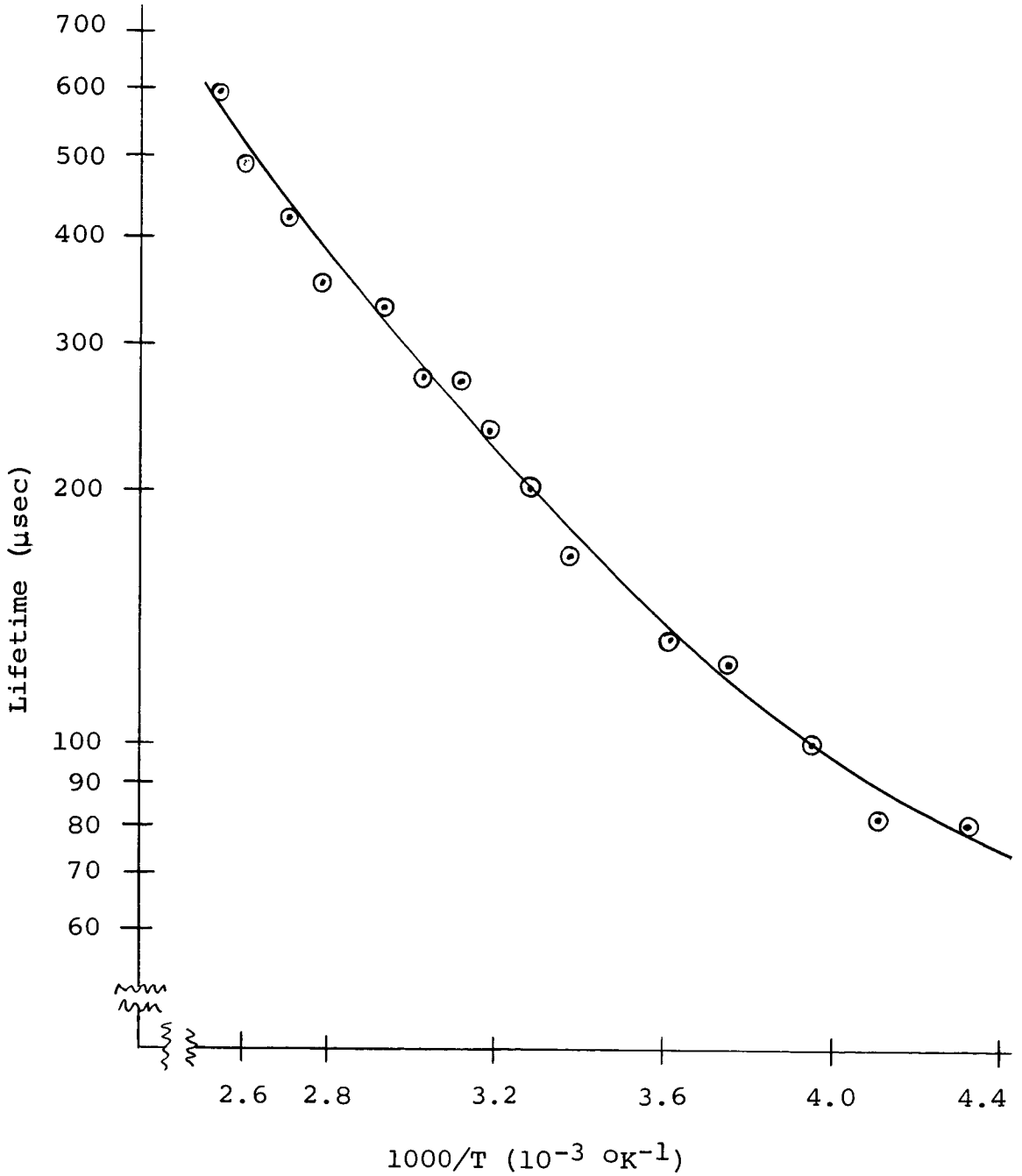

Figure 7.22. Bulk lifetime vs. reciprocal temperature for sample IPA58-6 before irradiation

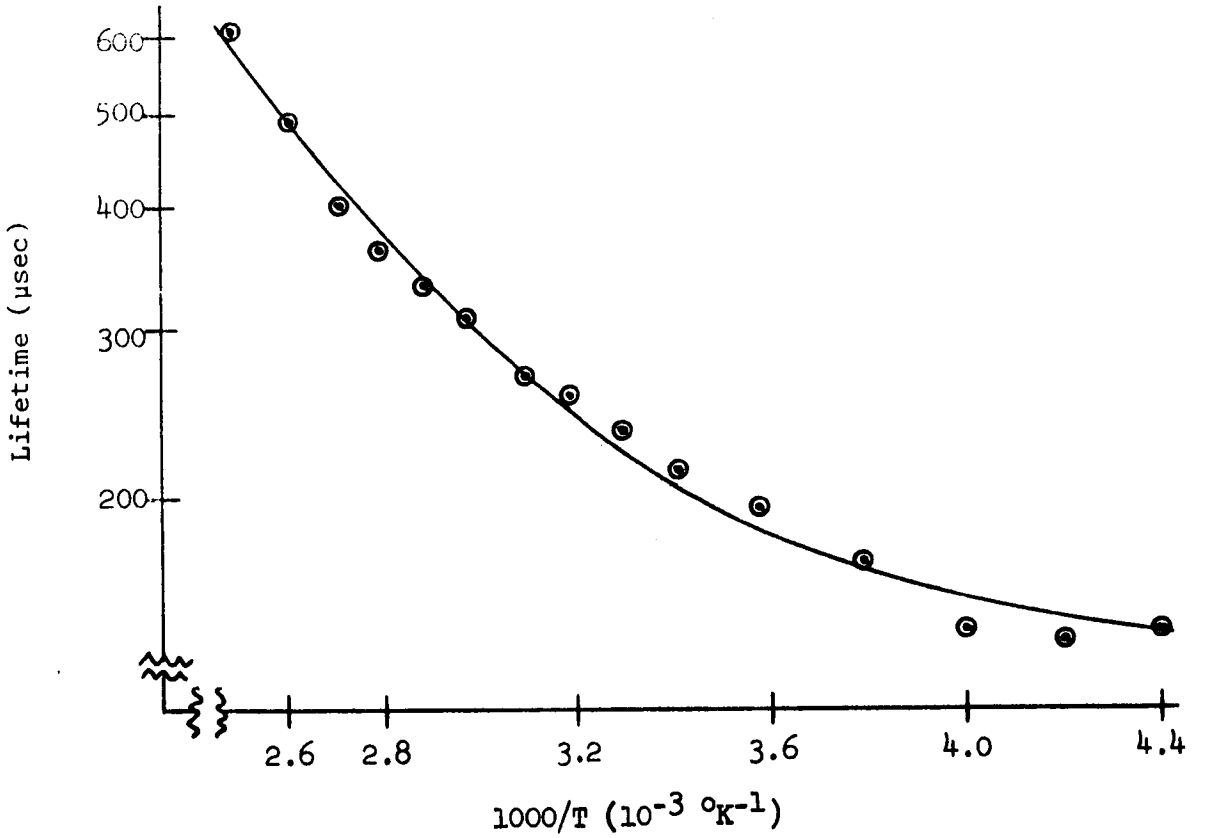
600
500
400
300
200
Lifetime (μsec)
2.6
2.8
3.2
3.6
4.0
4.4
1000/T (10-3 °K-1)

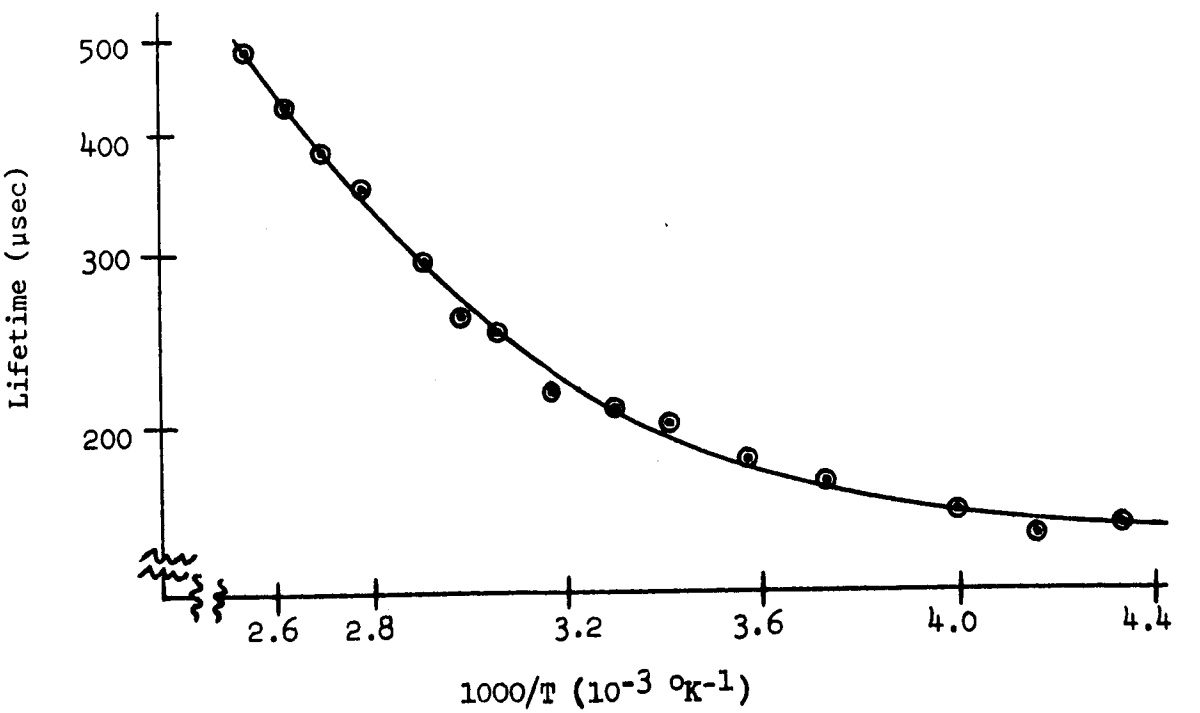
500
400
300
200
Lifetime (μsec)
2.6
2.8
3.2
3.6
4.0
4.4
1000/T (10-3 °K-1)

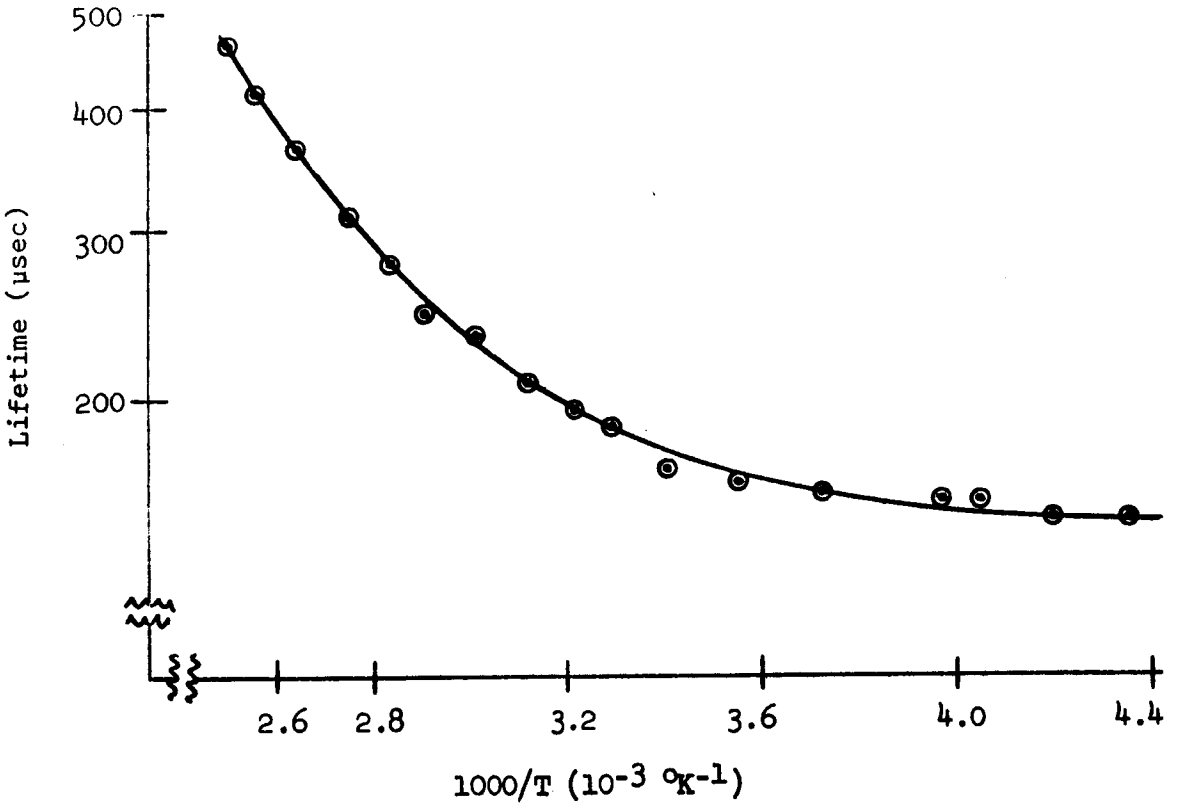
500
400
300
200
Lifetime (μsec)
2.6
2.8
3.2
3.6
4.0
4.4
1000/T (10-3 °K-1)

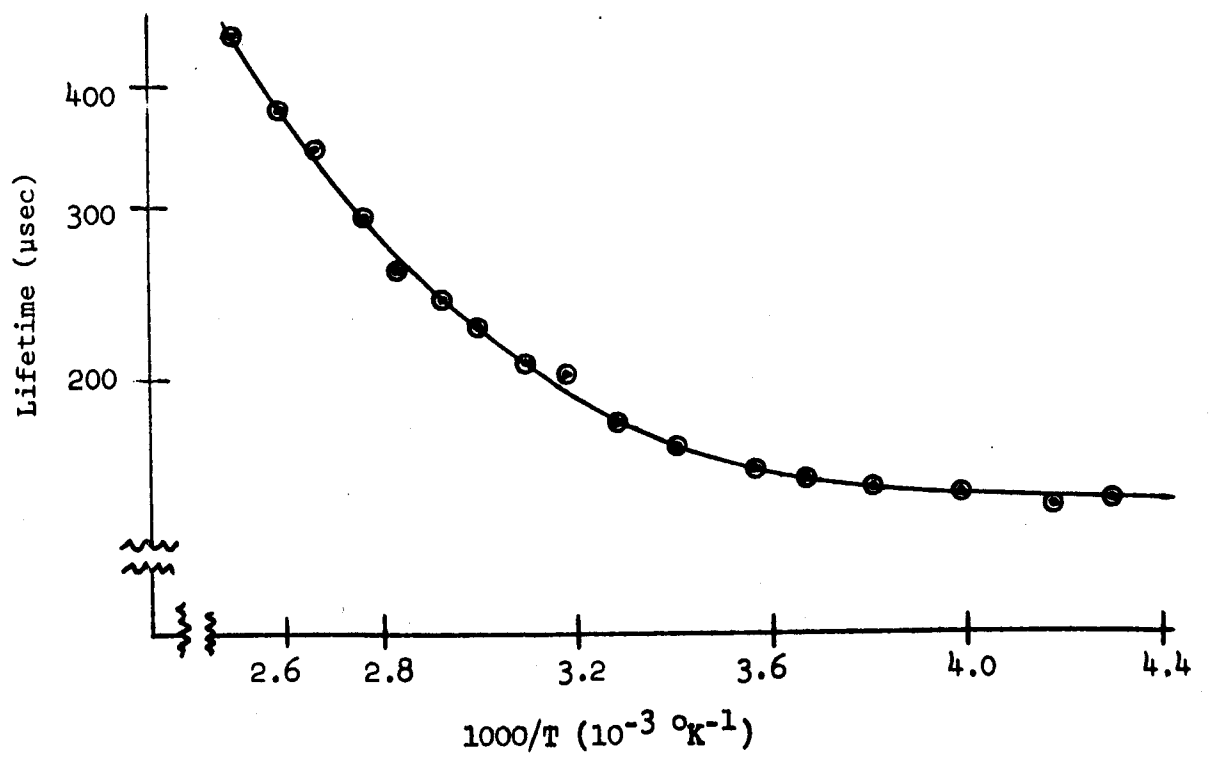
400
300
200
Lifetime (μsec)
2.6
2.8
3.2
3.6
4.0
4.4
1000/T (10-3 °K-1)

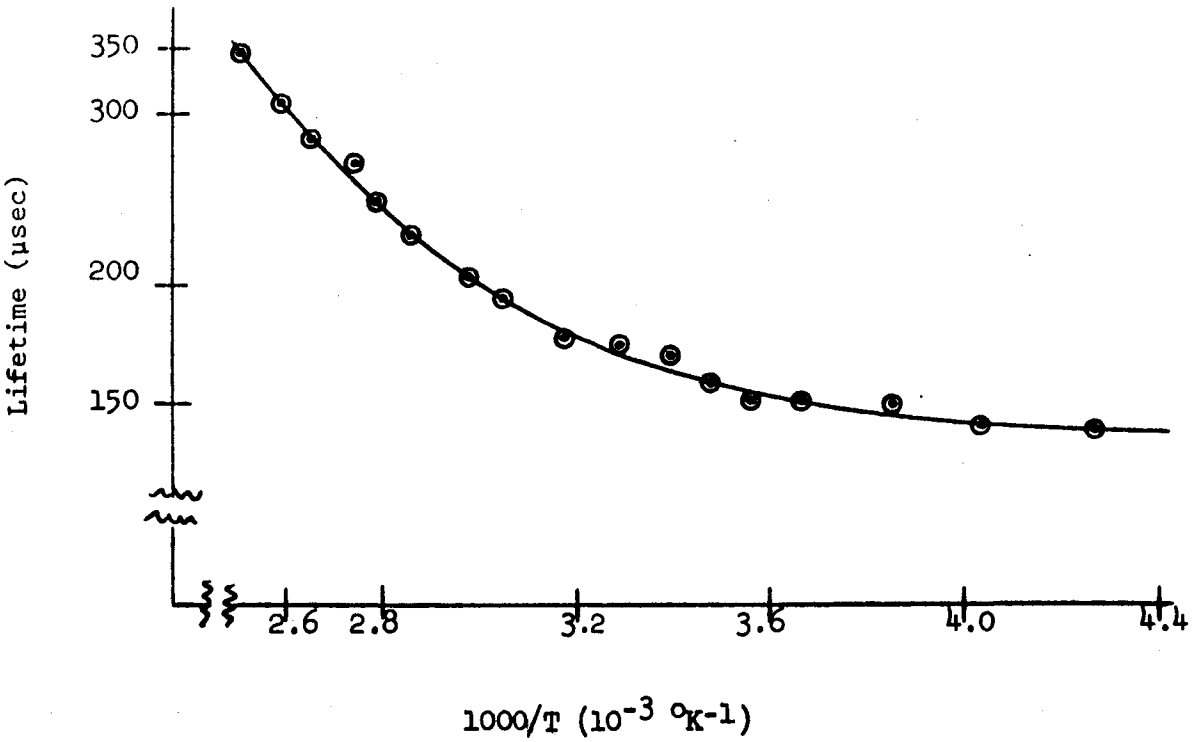
350
300
200
150
Lifetime (μsec)
2.6
2.8
3.2
3.6
4.0
4.4
1000/T (10-3 °K-1)

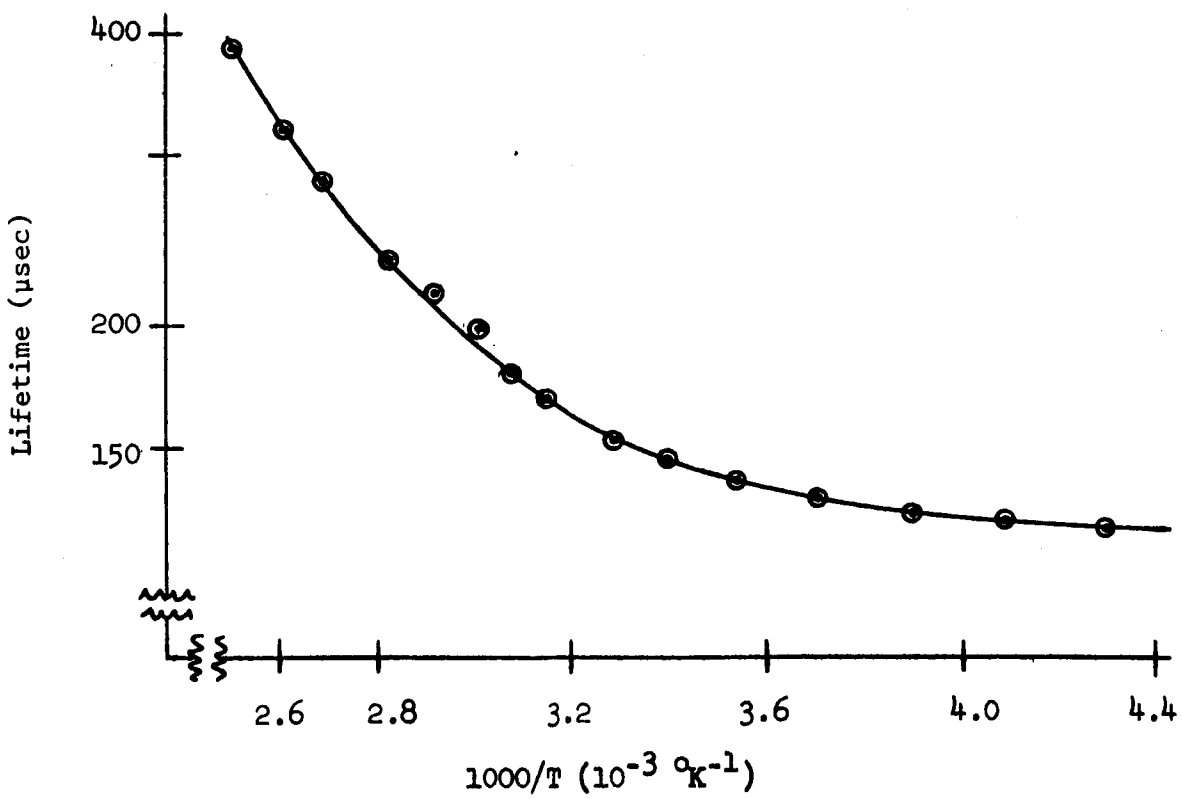
400
200
150
Lifetime (μsec)
2.6
2.8
3.2
3.6
4.0
4.4
1000/T (10-3 °K-1)

The question of multiple energy level defects in semiconductors might be considered a moot point. It could be argued that there will always be multiple energy levels even in so-called "near perfect crystals". One could go even further in saying that not only are there many defects with levels in the forbidden region, but that one should in general expect defects to be either "quasi-continuous" (that is existing in impurity bands) or else be distributed continuously in energy over the forbidden region. Our mathematical model predicts (if theory and experiment can be coorelated) that a discrete energy level exists. If the states are really distributed continuously in energy, our experiment has given us the "average energy" or else the "energy moment" of this distribution. The quantities in the equations will be integrals over the distribution; but to calculate the integrals we must know the distribution function. We are thus in an unfortunate situation, because in general the distribution function is unknown and almost impossible to calculate. We then resort to using practical assumptions in the equations.

One could theoretically write a computer program for n levels in the forbidden region. The complexity of the problem would be compounded n-fold, and the uncertainty in determining the parameters involved would also be similiarly compounded. It is the author's feeling that one should resort to the more complex problems if and only if a simpler analysis shows that this is warrented.

7.4 Final Measurements - Surface Lifetimes and Surface Recombination Velocity

The surface lifetime was also measured by the technique shown in Appendix III. Figures 7.29 through 7.56 show surface lifetime plotted as a function of reciprocal temperature for four n-type samples and several values of gamma ray exposure. The data shows that as irradiation proceeds the position of the defect is in the lower half of the energy gap and its location with respect to the valence band edge is changing. The level approaches the valence band and then begins to approach the center of the gap again. Its position seems to stabilize at approximately 0.25 eV to 0.30 eV above the valence band edge. This behavior was not expected.

At this point it should be stated that it has been assumed that the surface lifetime obeys the Shockley-Read model, without any a priori knowledge that this assumption would be true. The experimental evidence seems to point out that this assumption is in fact true, if the results are properly interpreted.

From Appendix III it is seen that the surface lifetime is intimately related to the surface recombination velocity. However, there are certain temperature variations contained explicitly in the expression for surface recombination velocity. It is possible that the quantities τ_{no} or τ_{po} given in Table 7.1 are not really meaningful for the surface lifetime due to the fact that in these expressions the number of conduction band electrons (valence band holes) near the surface has been

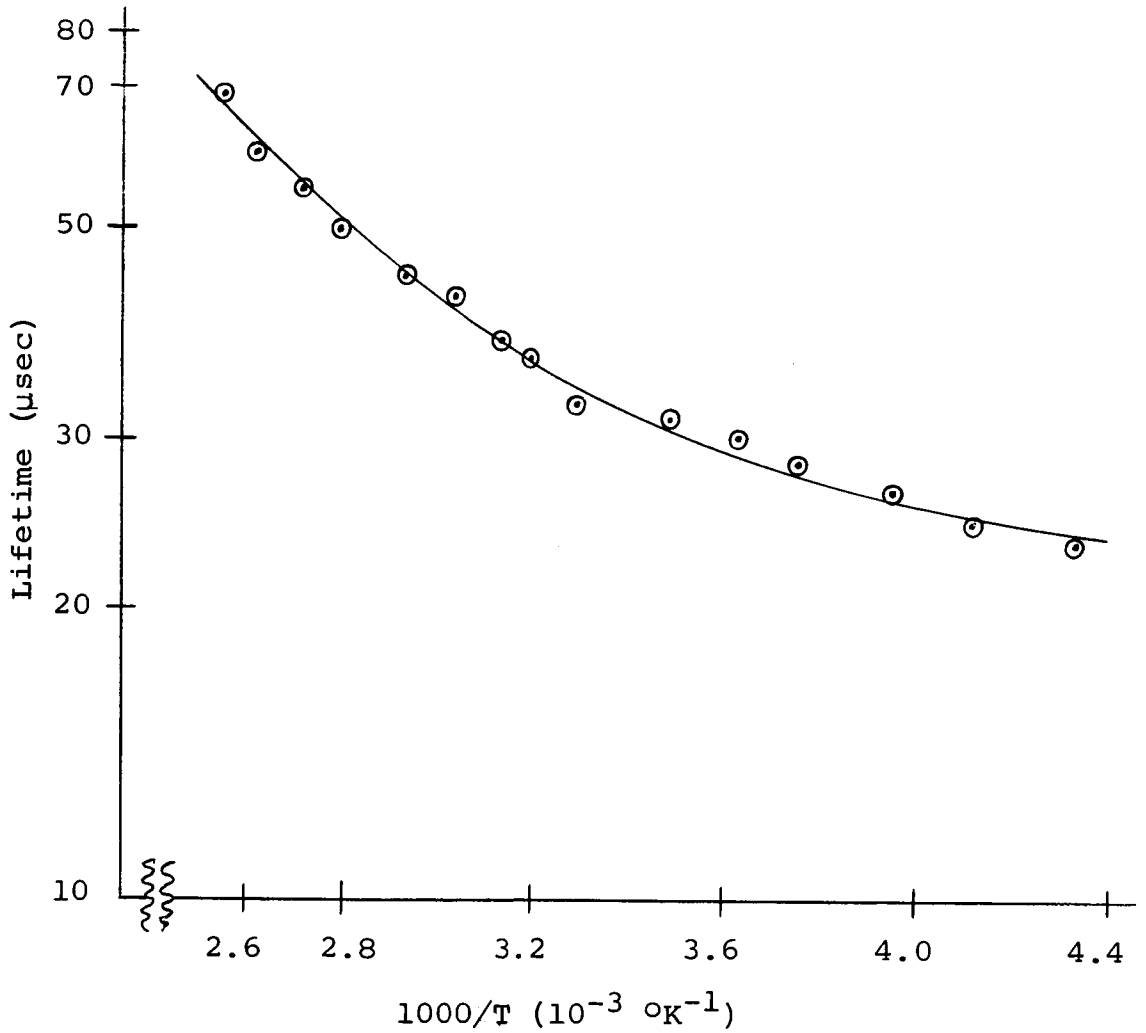

Figure 7.29. Surface lifetime vs. reciprocal temperature for sample INA3/4 5-1 before irradiation

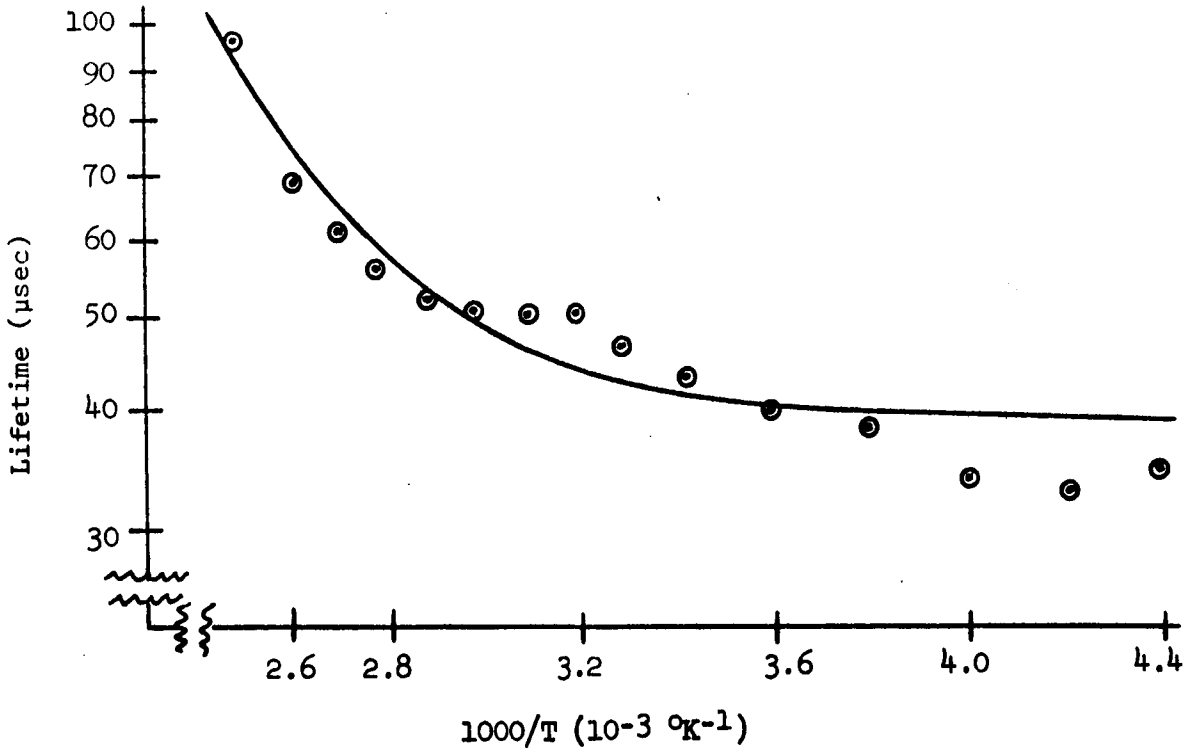
Lifetime (μsec)
100
90
80
70
60
50
40
30
2.6
2.8
3.2
3.6
4.0
4.4
1000/T (10-3 °K-1)

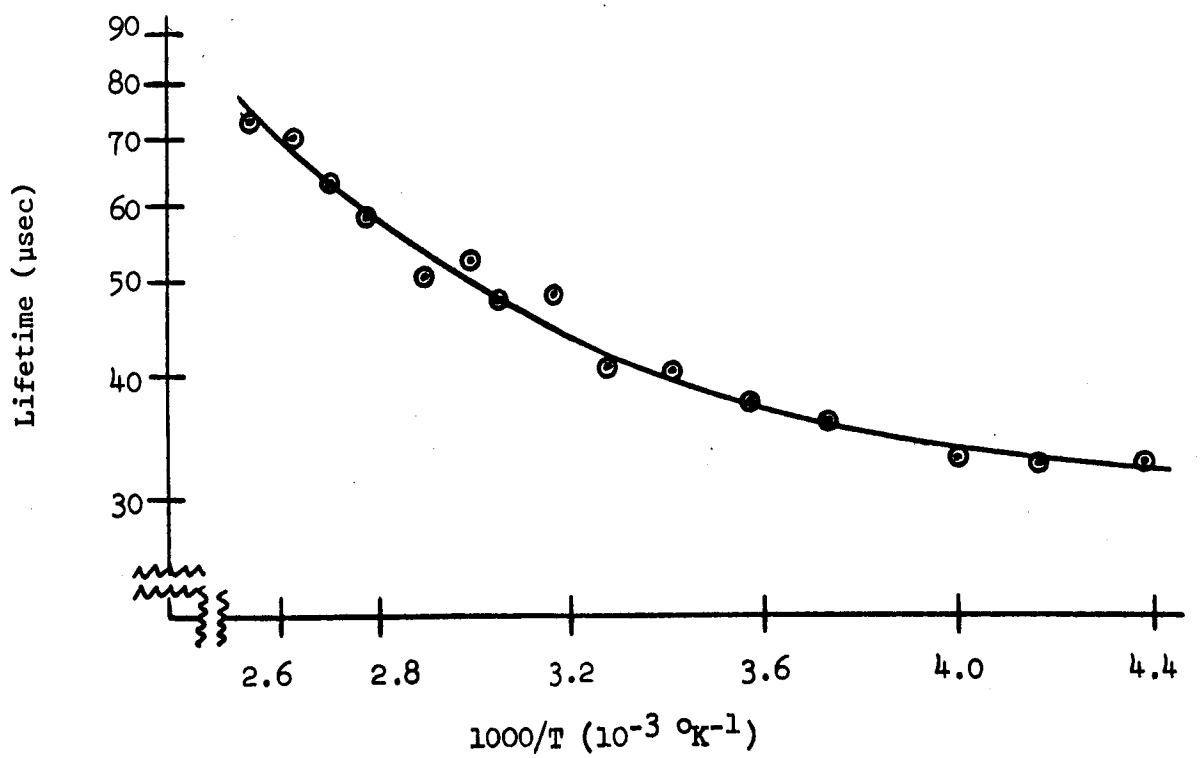
Lifetime (μsec)
90
80
70
60
50
40
30
2.6
2.8
3.2
3.6
4.0
4.4
1000/T (10-3 °K-1)

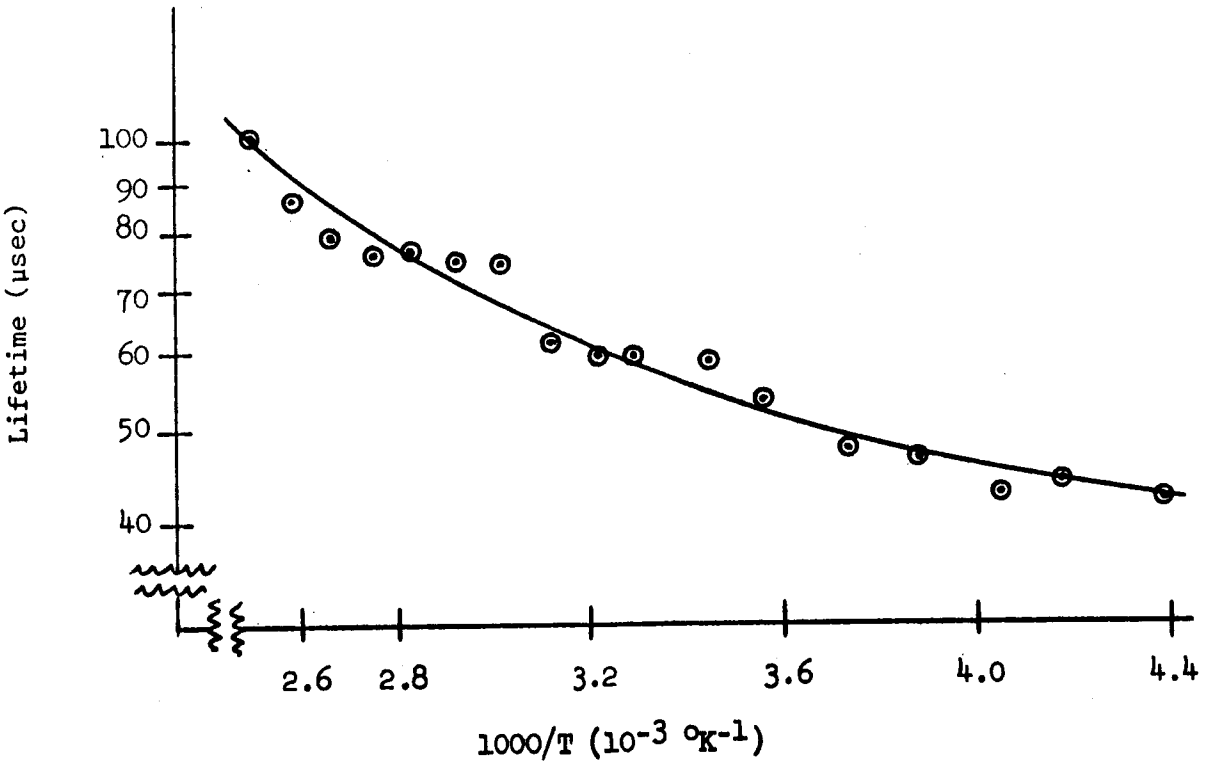
Lifetime (μsec)
100
90
80
70
60
50
40
2.6
2.8
3.2
3.6
4.0
4.4
1000/T (10-3 °K-1)

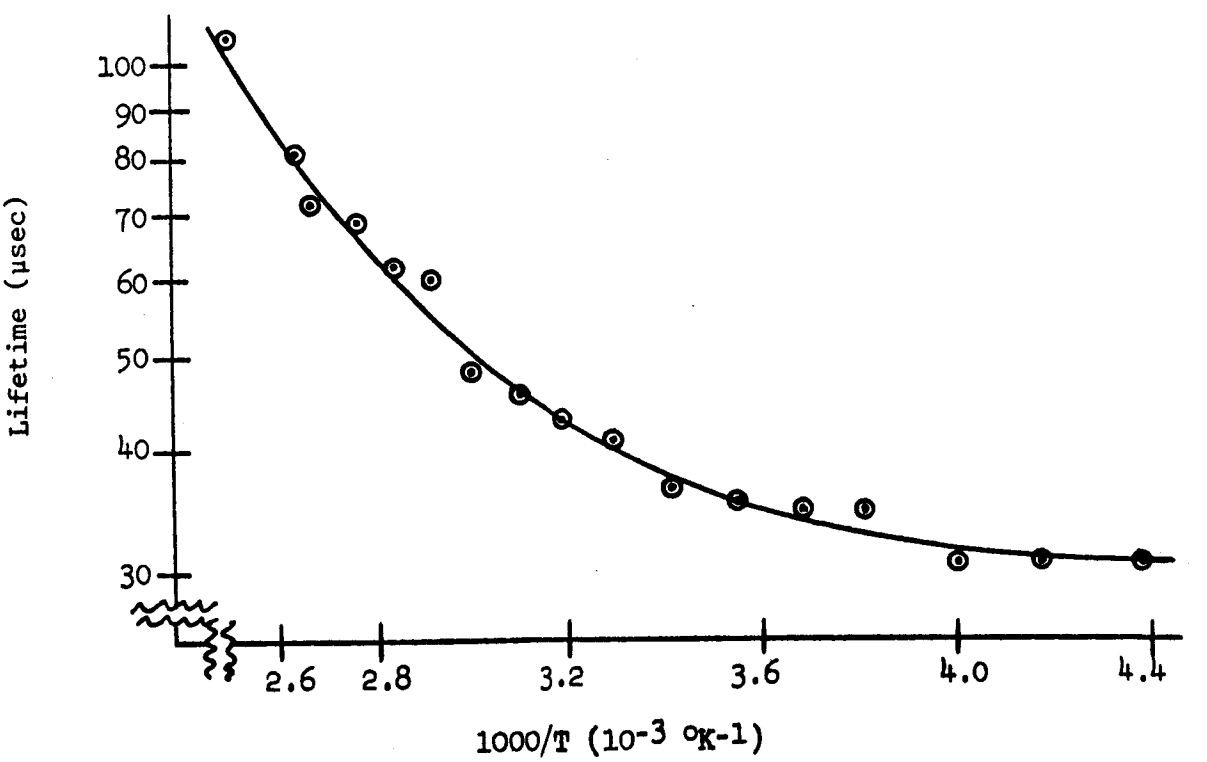
Lifetime (μsec)
100
90
80
70
60
50
40
30
2.6
2.8
3.2
3.6
4.0
4.4
1000/T (10-3 °K-1)

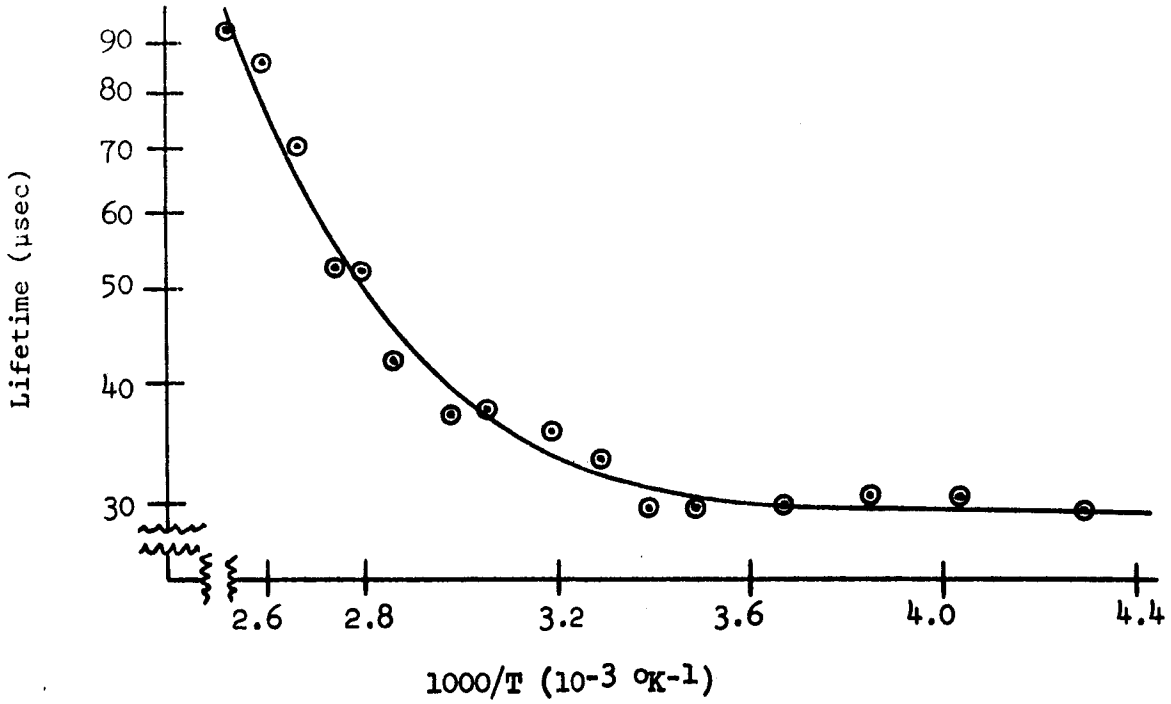
Lifetime (μsec)
90
80
70
60
50
40
30
2.6
2.8
3.2
3.6
4.0
4.4
1000/T (10-3 °K-1)

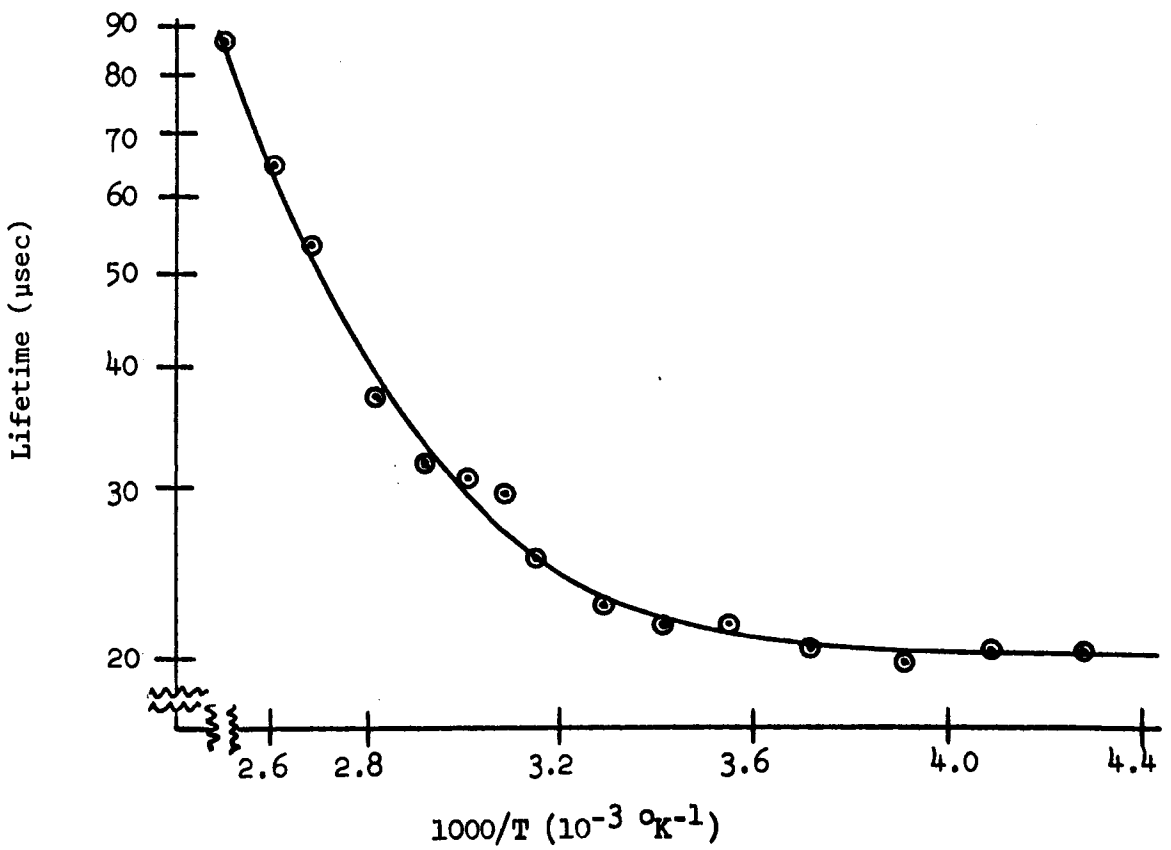
Lifetime (μsec)
90
80
70
60
50
40
30
20
2.6
2.8
3.2
3.6
4.0
4.4
1000/T (10-3 °K-1)

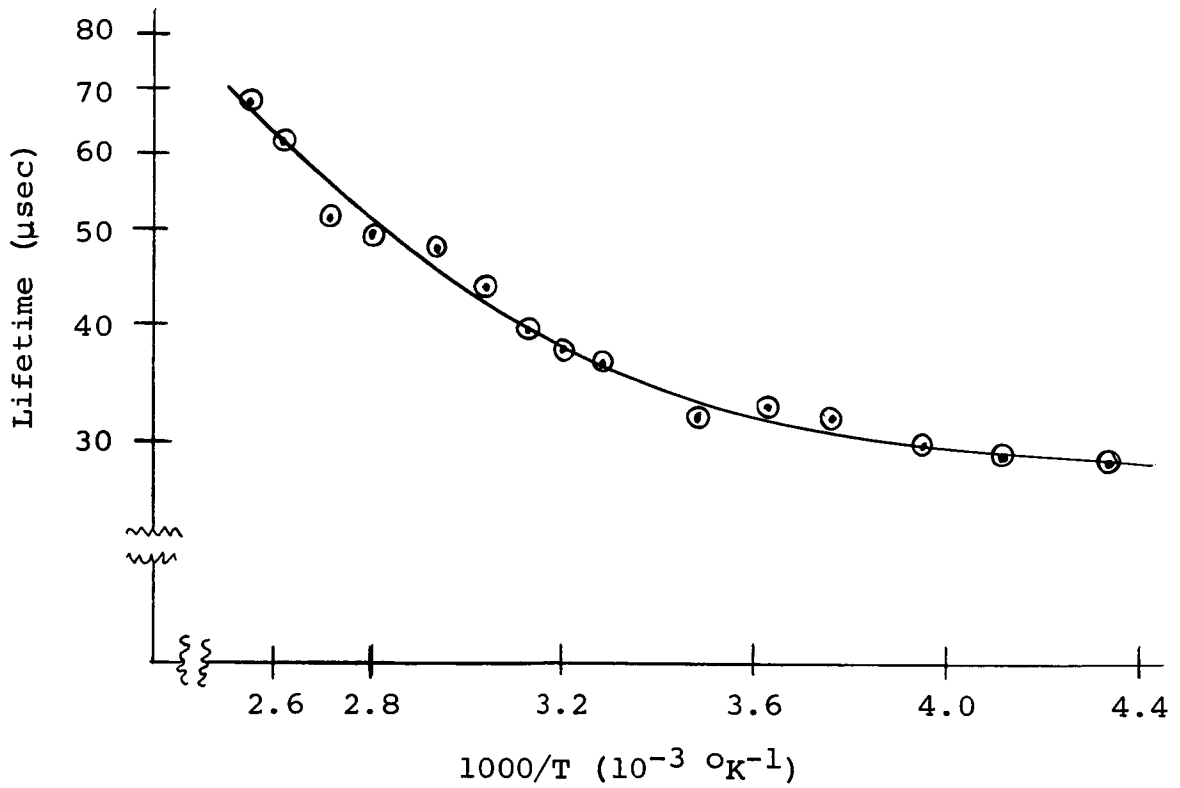

Figure 7.36. Surface lifetime vs. reciprocal temperature for sample INA3/4 5-2 before irradiation

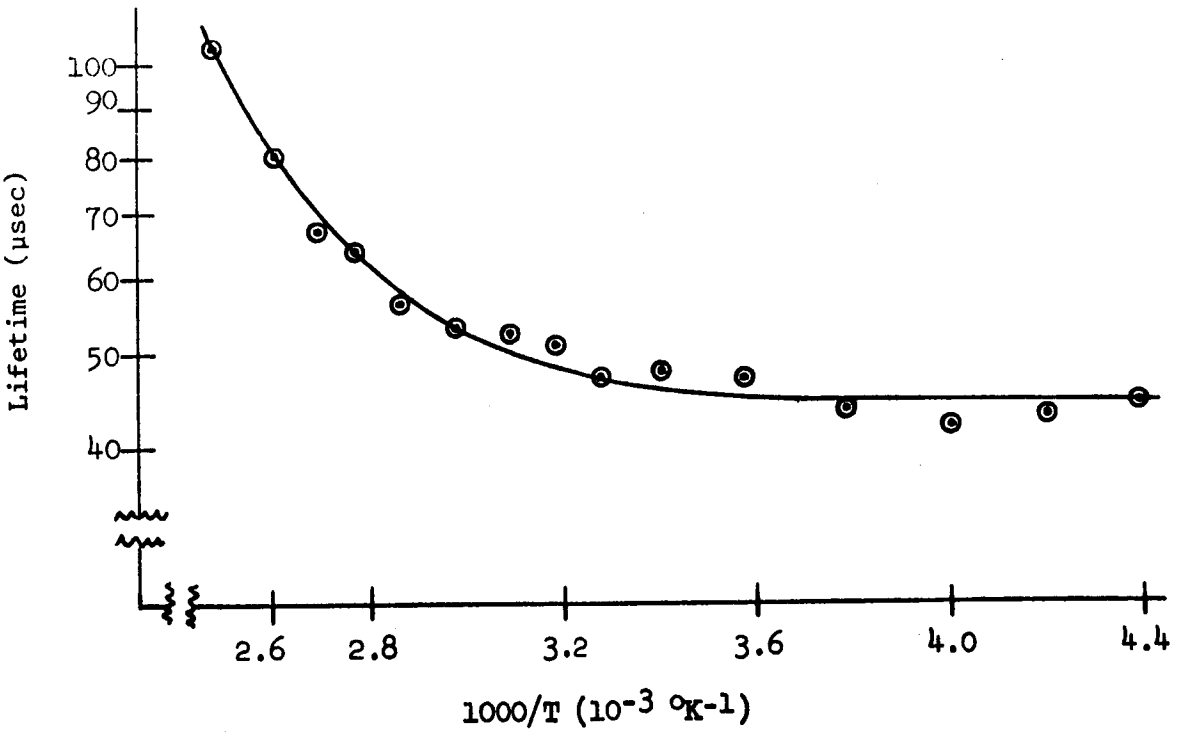
Lifetime (μsec)
100
90
80
70
60
50
40
2.6
2.8
3.2
3.6
4.0
4.4
1000/T (10-3 °K-1)

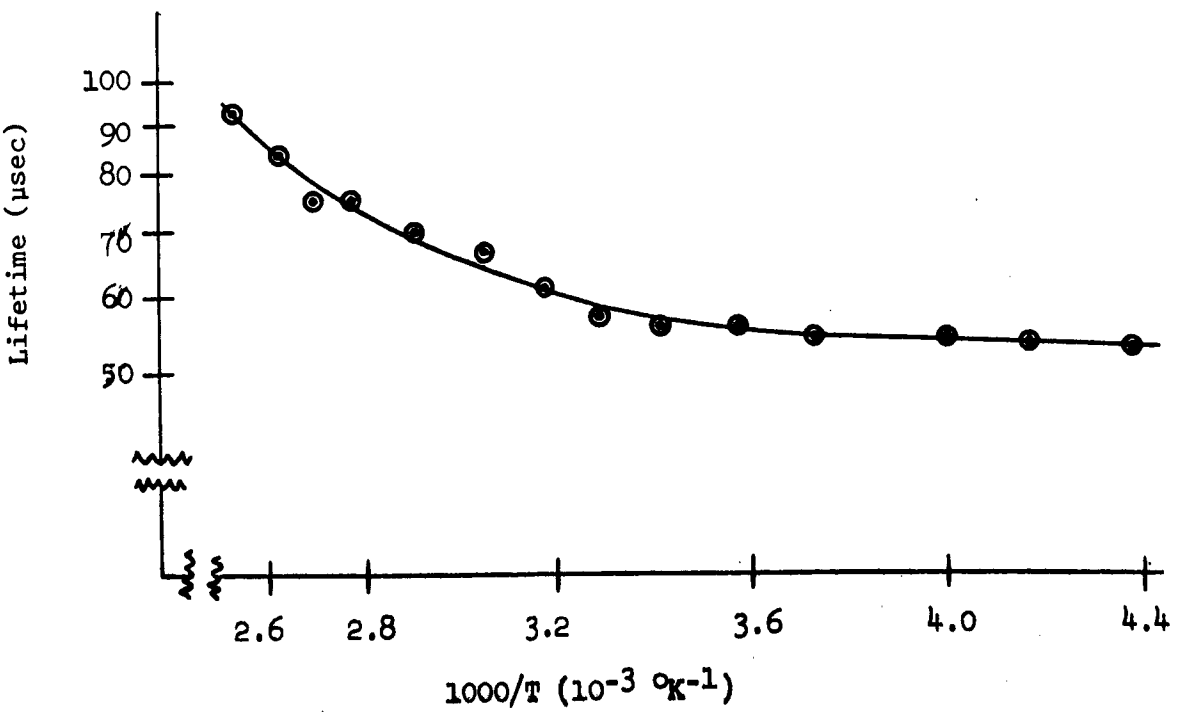
Lifetime (μsec)
100
90
80
70
60
50
2.6
2.8
3.2
3.6
4.0
4.4
1000/T (10-3 °K-1)

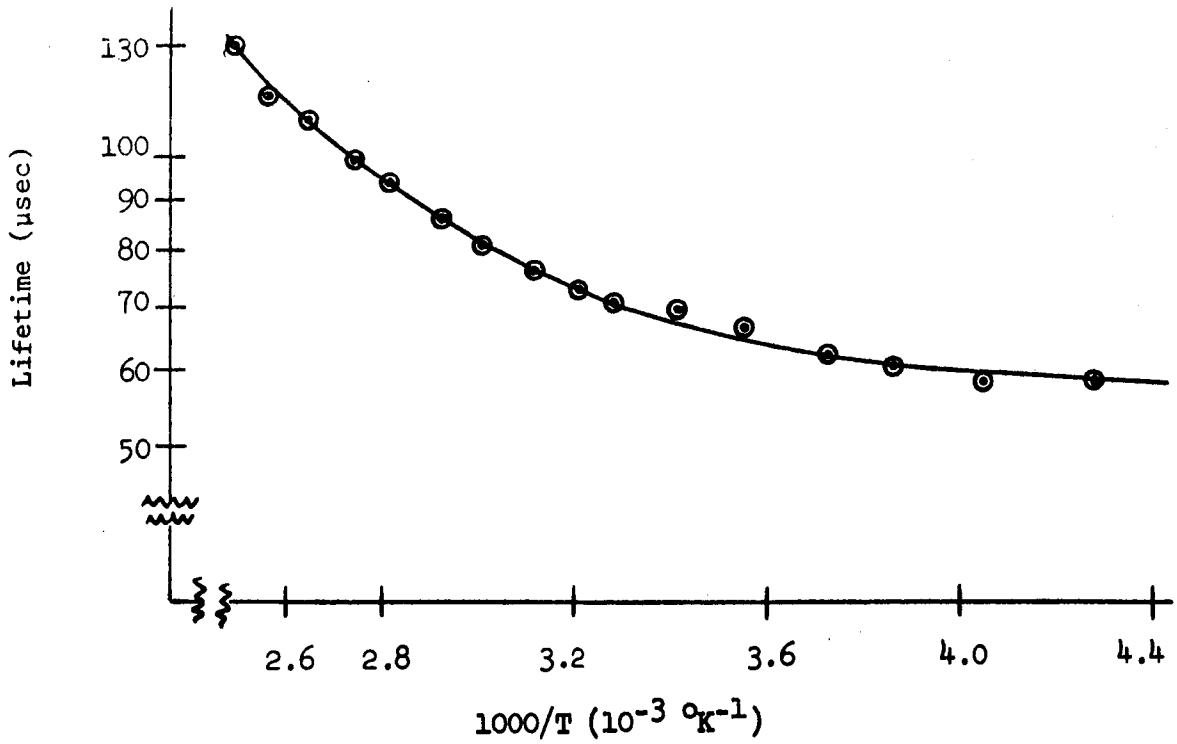
Lifetime (μsec)
130
100
90
80
70
60
50
2.6
2.8
3.2
3.6
4.0
4.4
1000/T (10^{-3} $^{o}K^{-1}$)

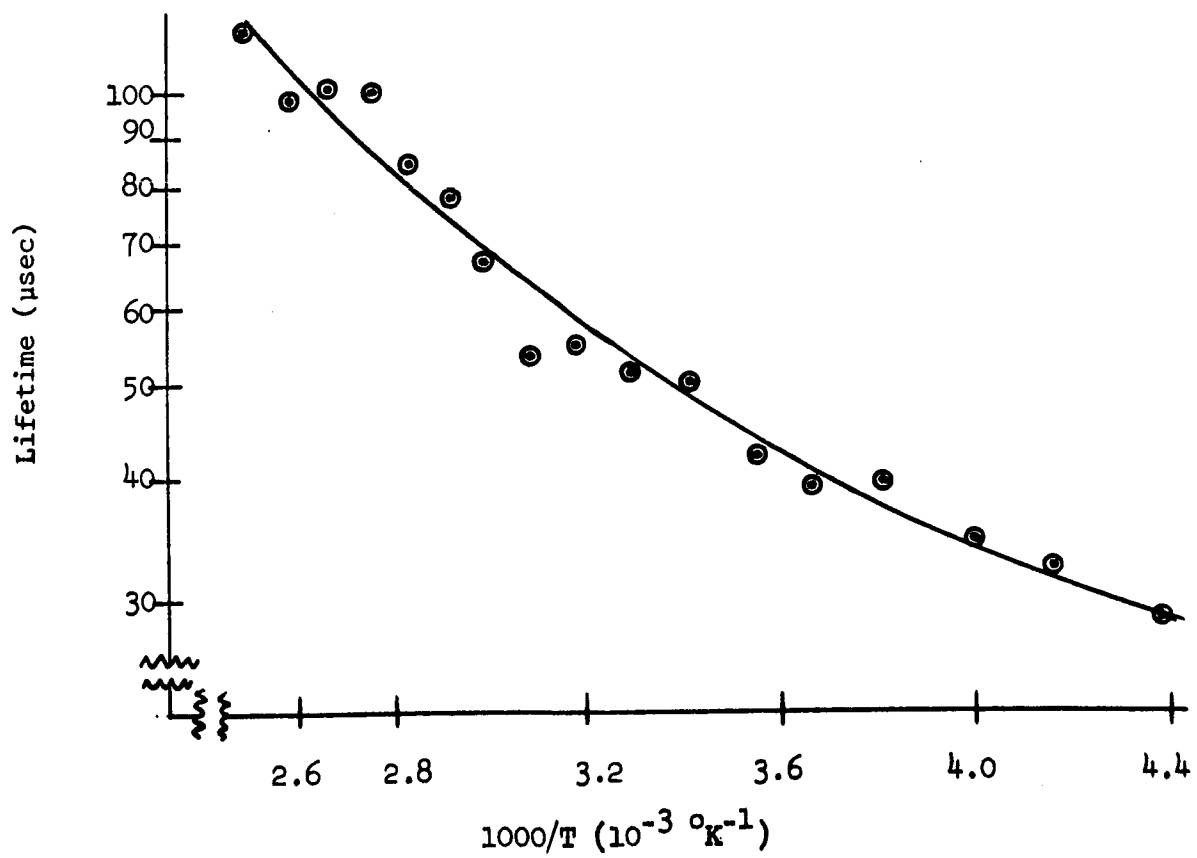
Lifetime (μsec)
100
90
80
70
60
50
40
30
2.6
2.8
3.2
3.6
4.0
4.4
1000/T (10^{-3} $^{o}K^{-1}$)

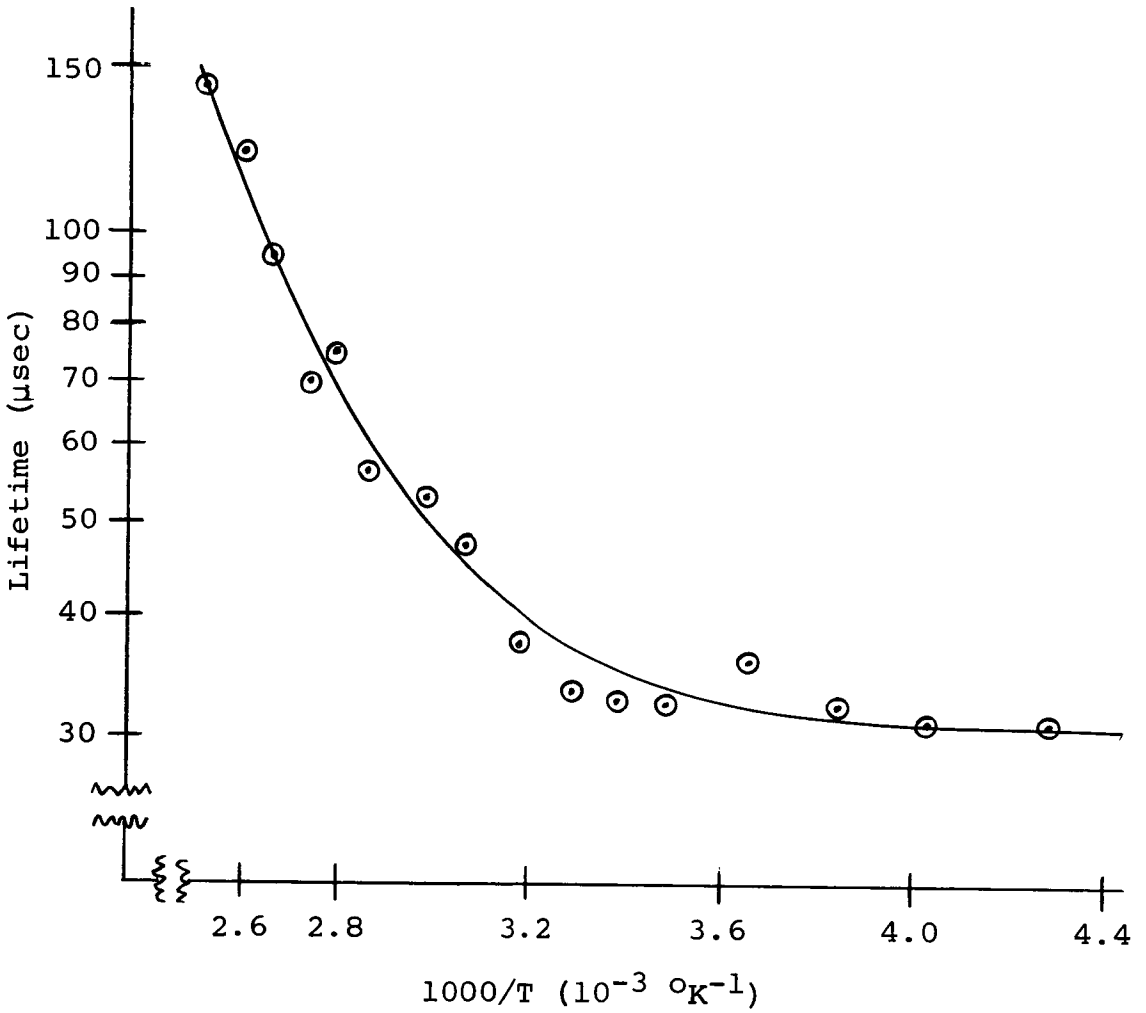

Figure 7.41. Surface lifetime vs. reciprocal temperature for sample INA 3/4 5-2 after 2.89 x 10^5 roentgens of Co^{60} gamma ray exposure

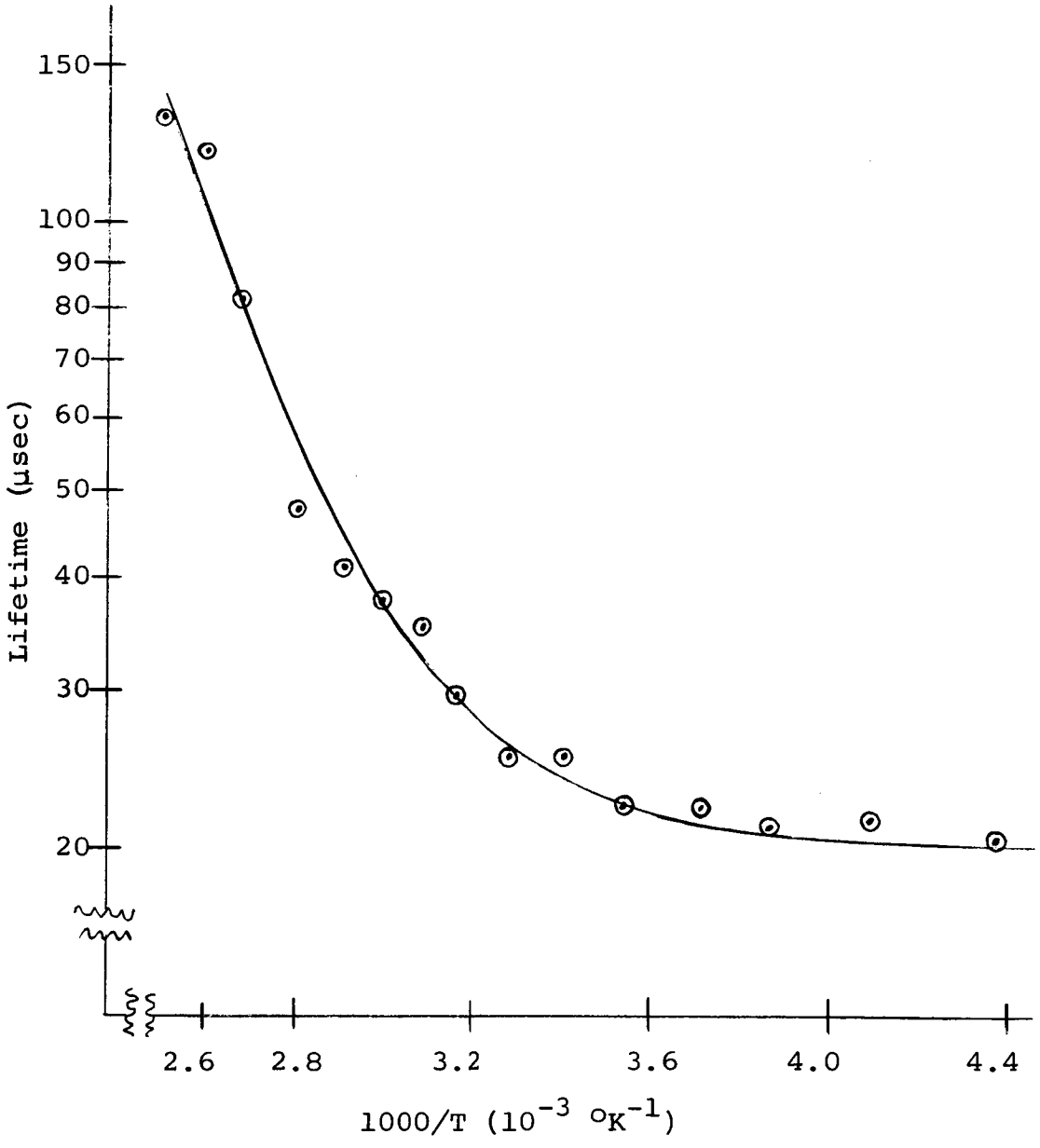

Figure 7.42. Surface lifetime vs. reciprocal temperature for sample INA3/4 5-2 after 3.85×10^5 roentgens of Co^{60} gamma ray exposure

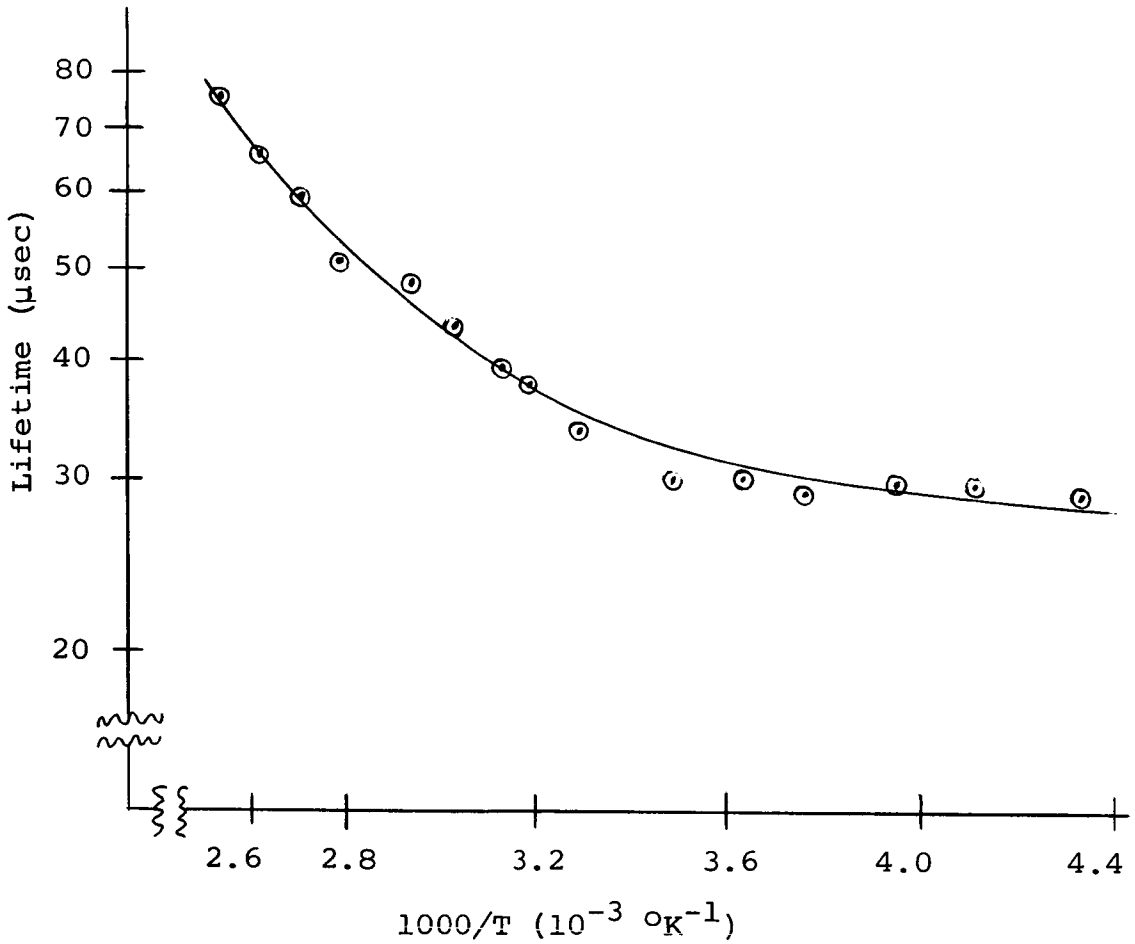

Figure 7.43. Surface lifetime vs. reciprocal temperature for sample INA3/4 5-3 before irradiation

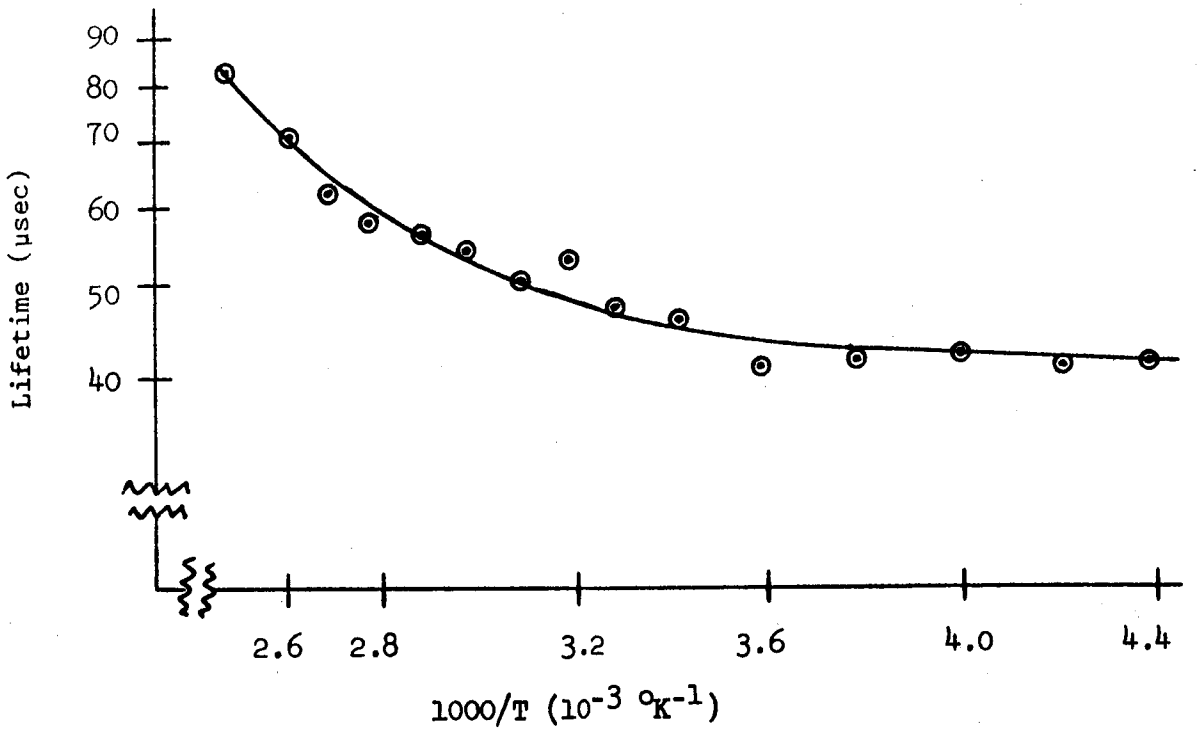
Lifetime (μsec)
90
80
70
60
50
40
2.6
2.8
3.2
3.6
4.0
4.4
1000/T (10-3 °K-1)

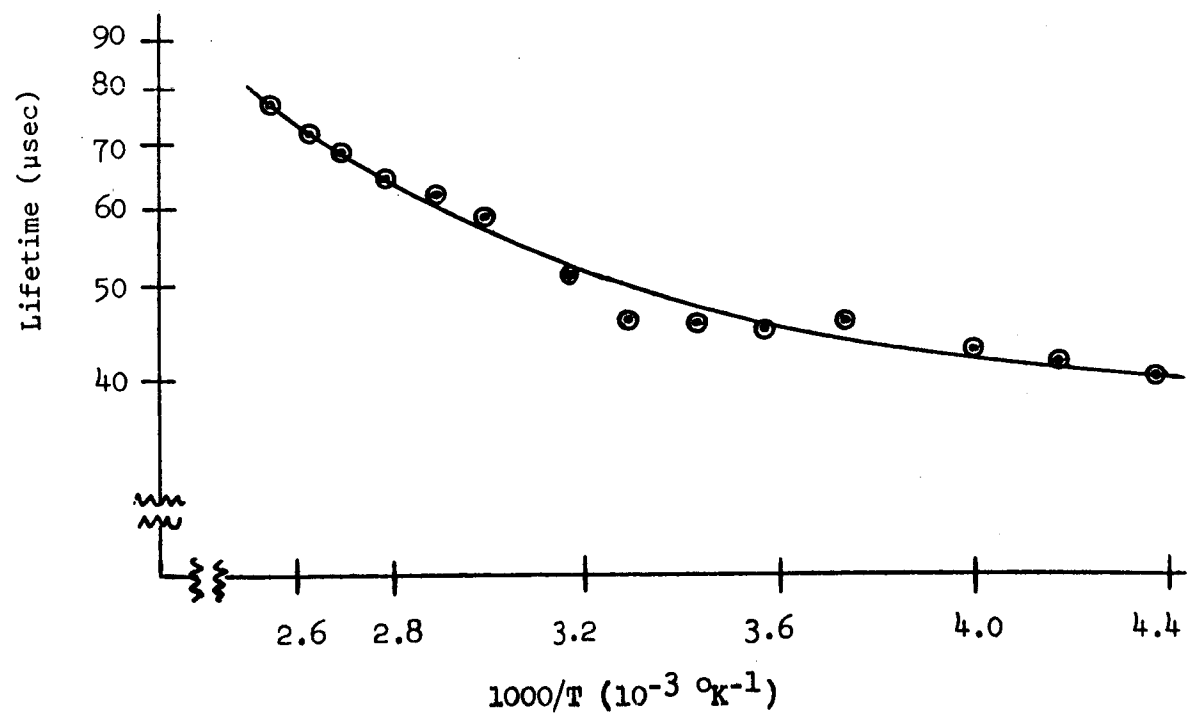
Lifetime (μsec)
90
80
70
60
50
40
2.6
2.8
3.2
3.6
4.0
4.4
1000/T (10-3 °K-1)

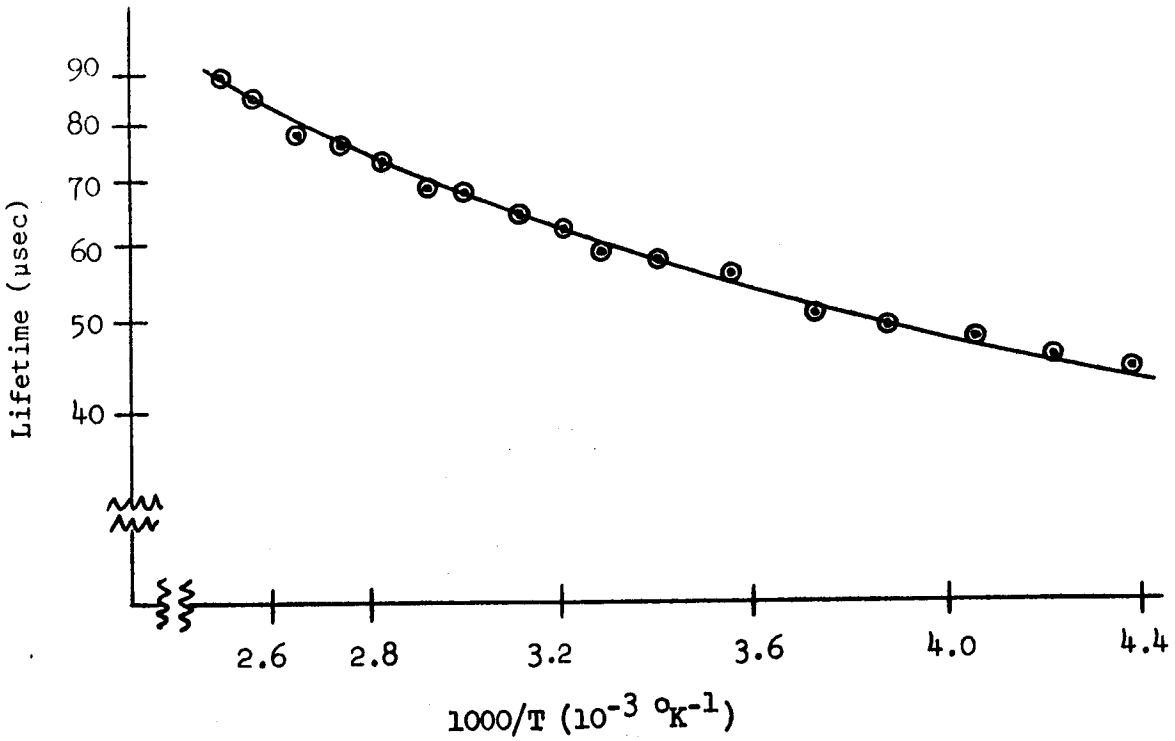
Lifetime (μsec)
90
80
70
60
50
40
2.6
2.8
3.2
3.6
4.0
4.4
1000/T (10^{-3} $^{o}K^{-1}$)

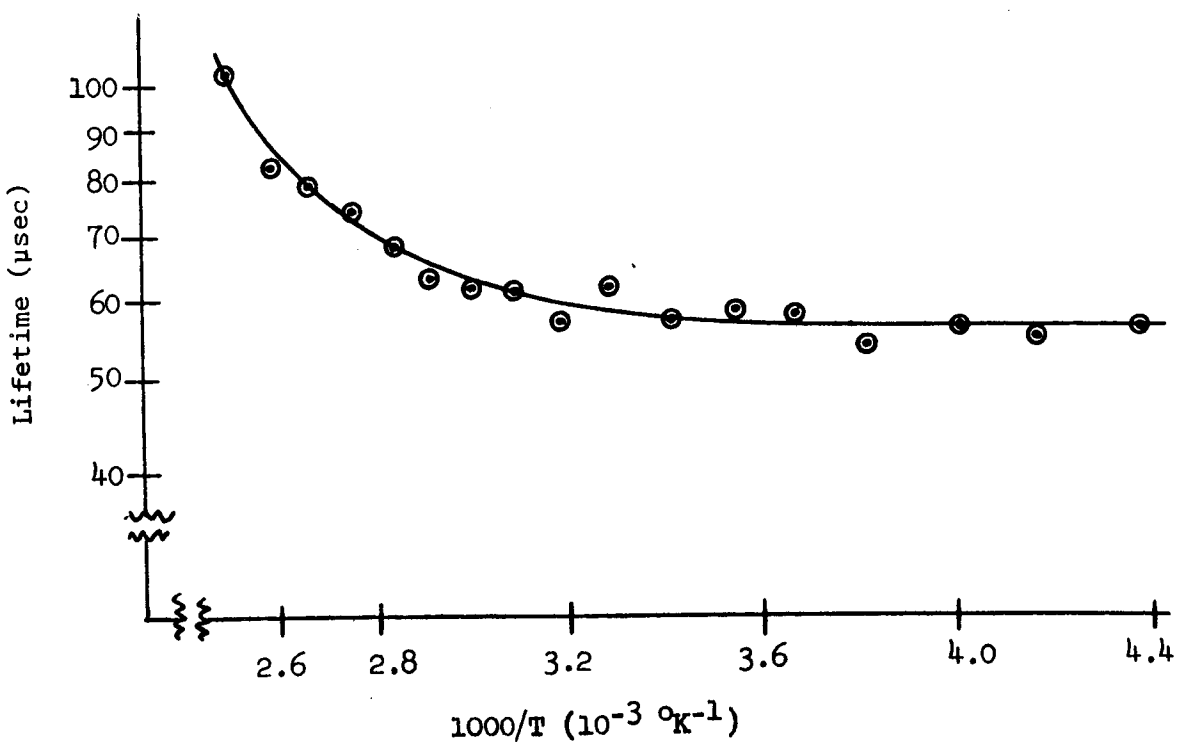
Lifetime (μsec)
100
90
80
70
60
50
40
2.6
2.8
3.2
3.6
4.0
4.4
1000/T (10^{-3} $^{o}K^{-1}$)

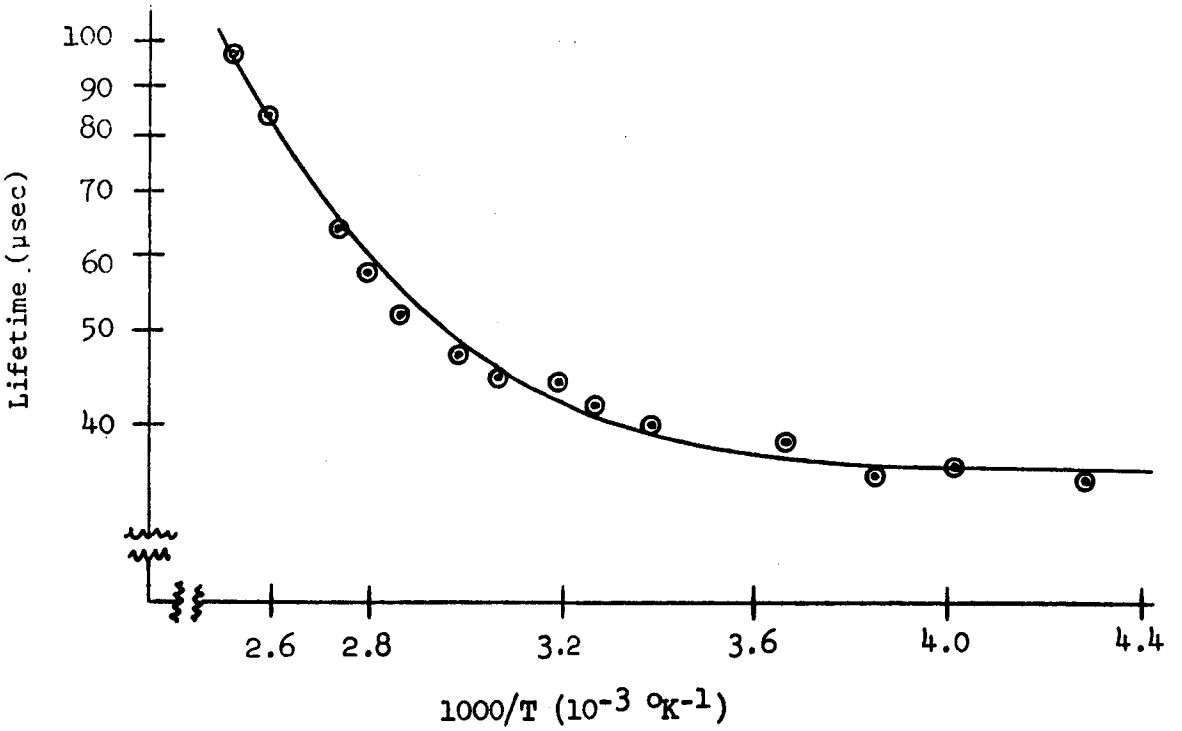
100
90
80
70
60
50
40
Lifetime (μsec)
2.6
2.8
3.2
3.6
4.0
4.4
1000/T (10-3 °K-1)

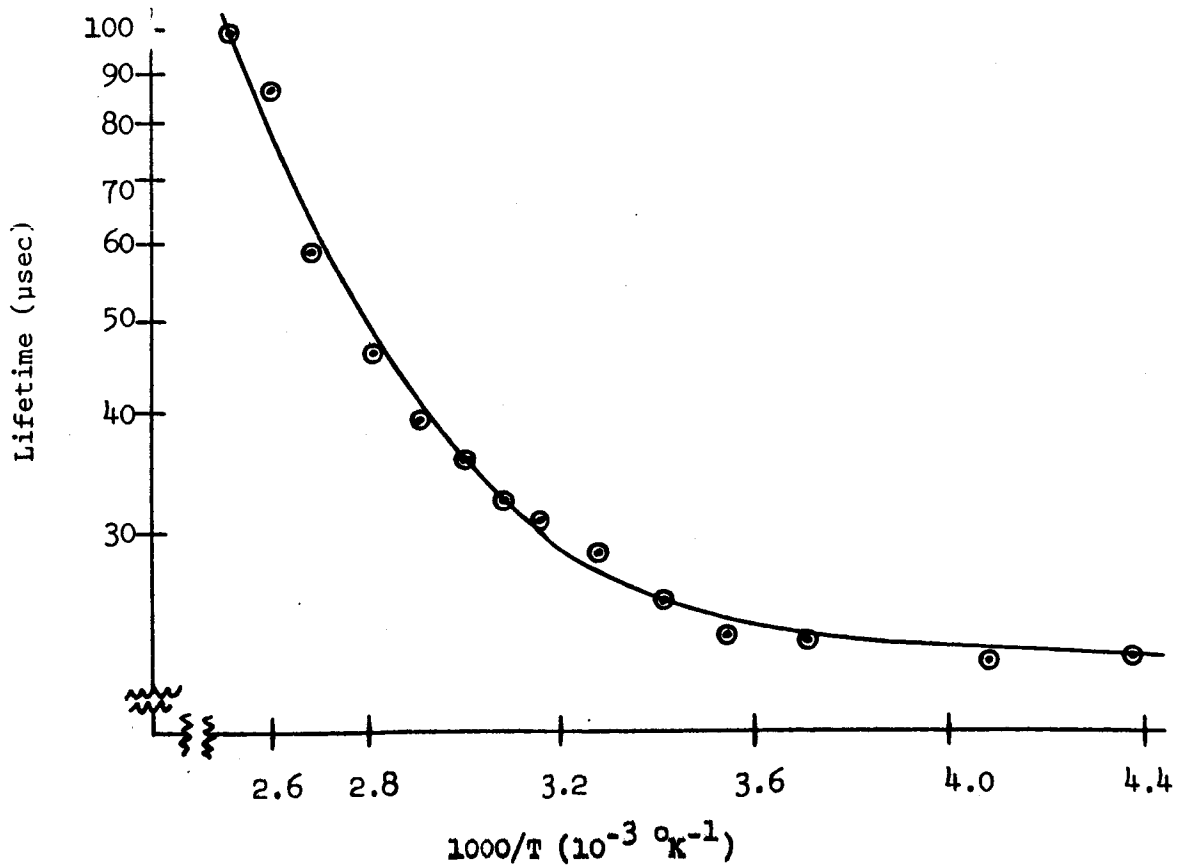
100
90
80
70
60
50
40
30
Lifetime (μsec)
2.6
2.8
3.2
3.6
4.0
4.4
1000/T (10-3 °K-1)

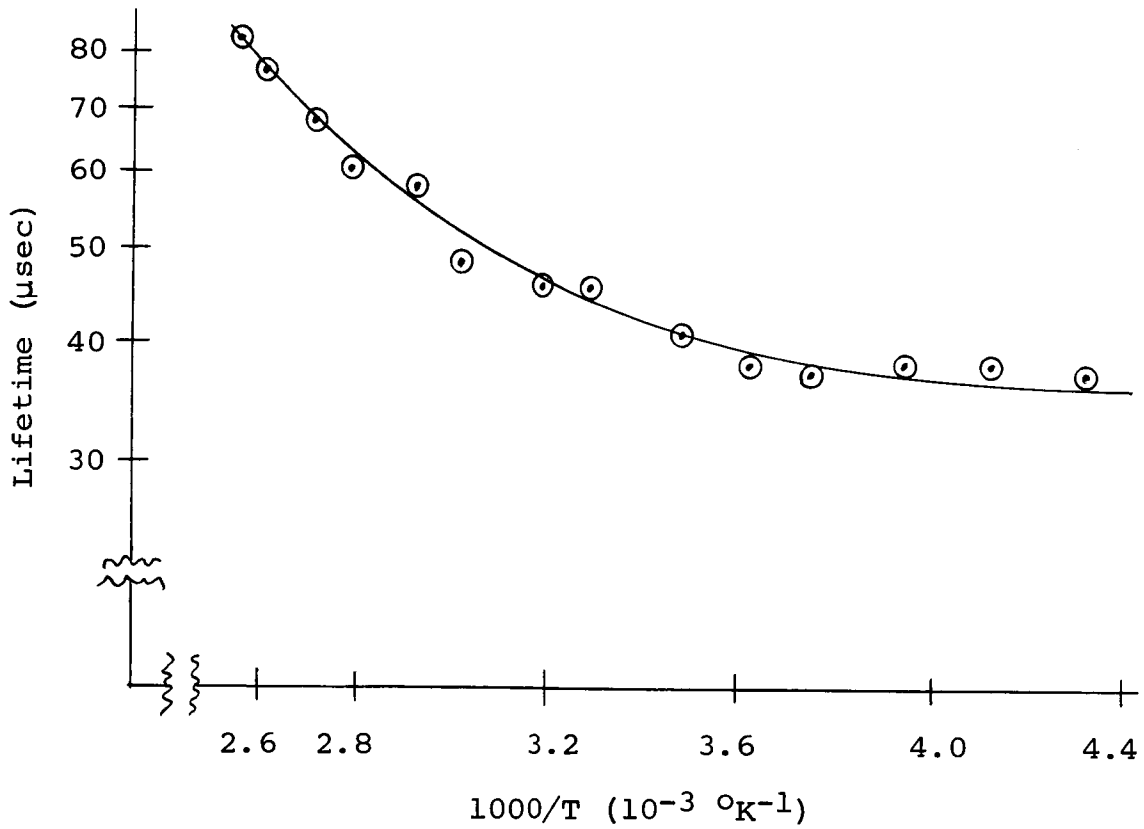

Figure 7.50. Surface lifetime vs. reciprocal temperature for sample INA3/4 5-4 before irradiation

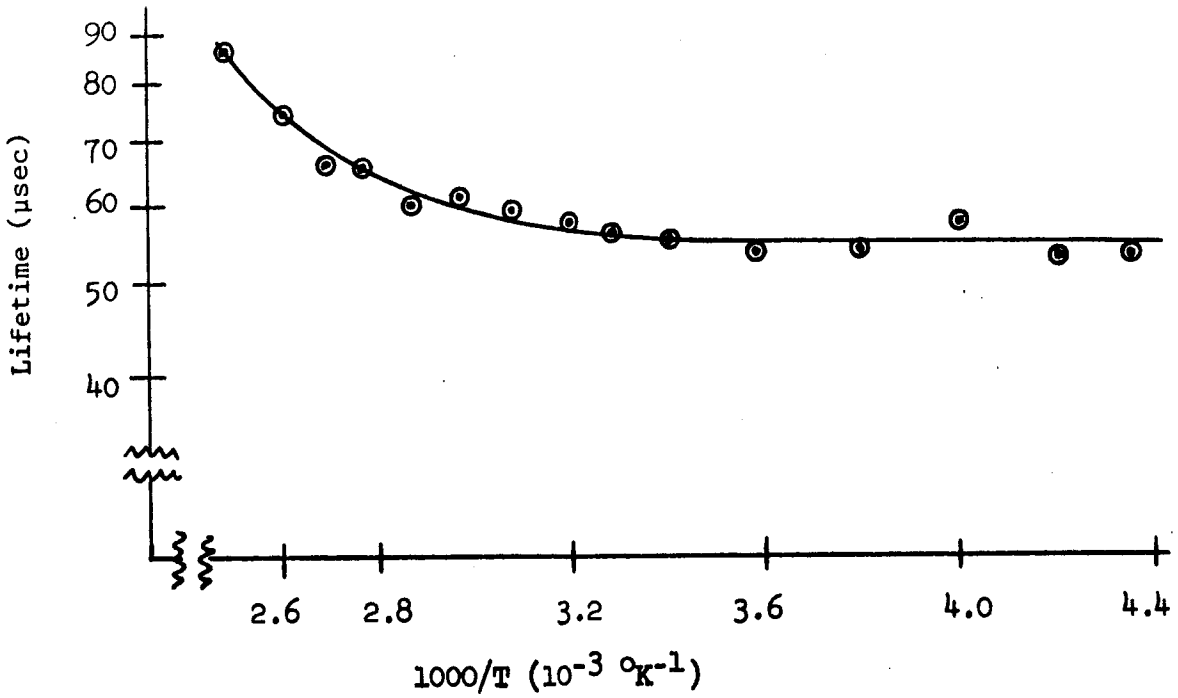
Lifetime (μsec)
90
80
70
60
50
40
2.6
2.8
3.2
3.6
4.0
4.4
1000/T (10-3 °K-1)

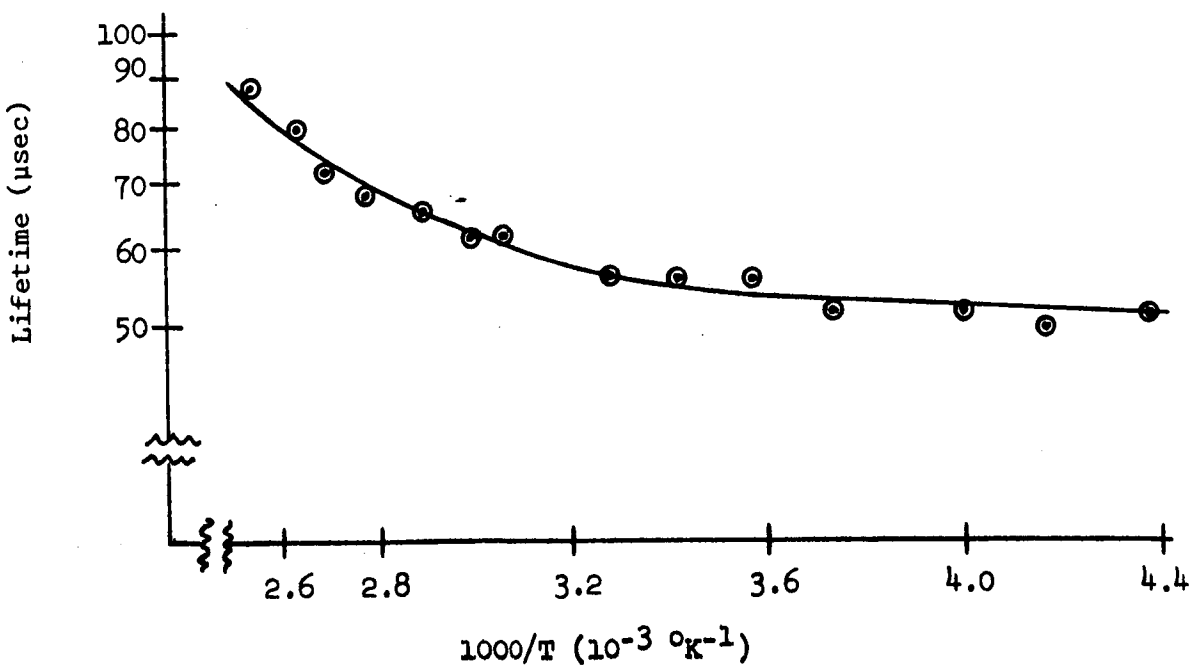
Lifetime (μsec)
100
90
80
70
60
50
2.6
2.8
3.2
3.6
4.0
4.4
1000/T (10-3 °K-1)

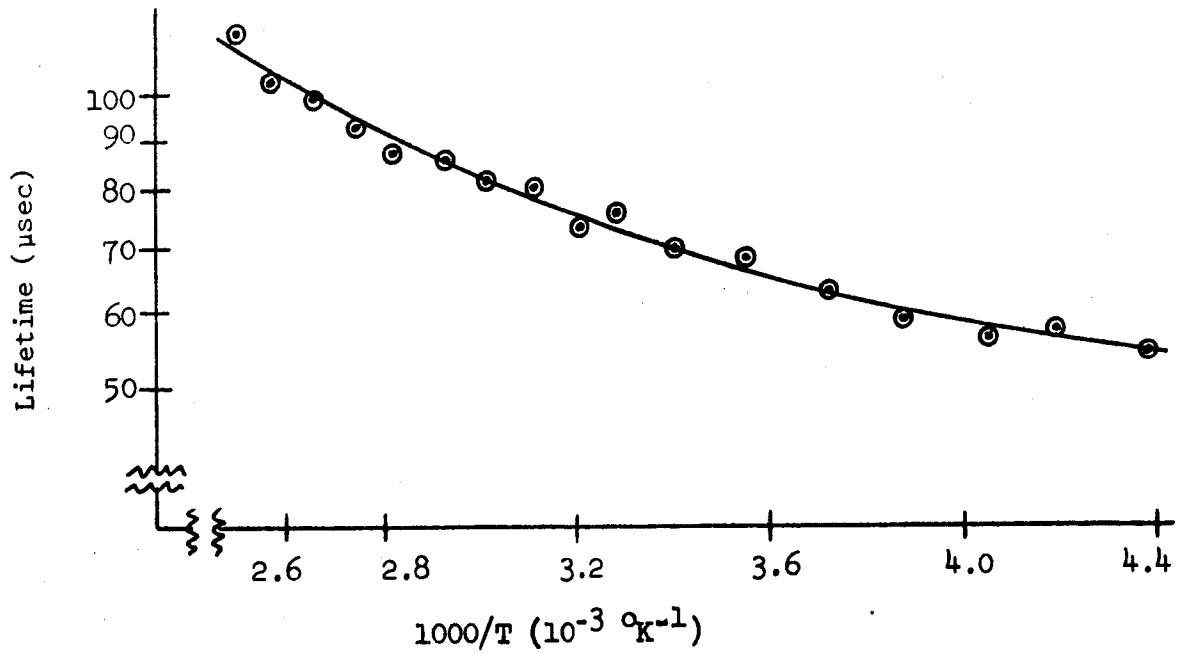
Lifetime (μsec)
100
90
80
70
60
50
2.6
2.8
3.2
3.6
4.0
4.4
1000/T (10^{-3} $^{o}K^{-1}$)

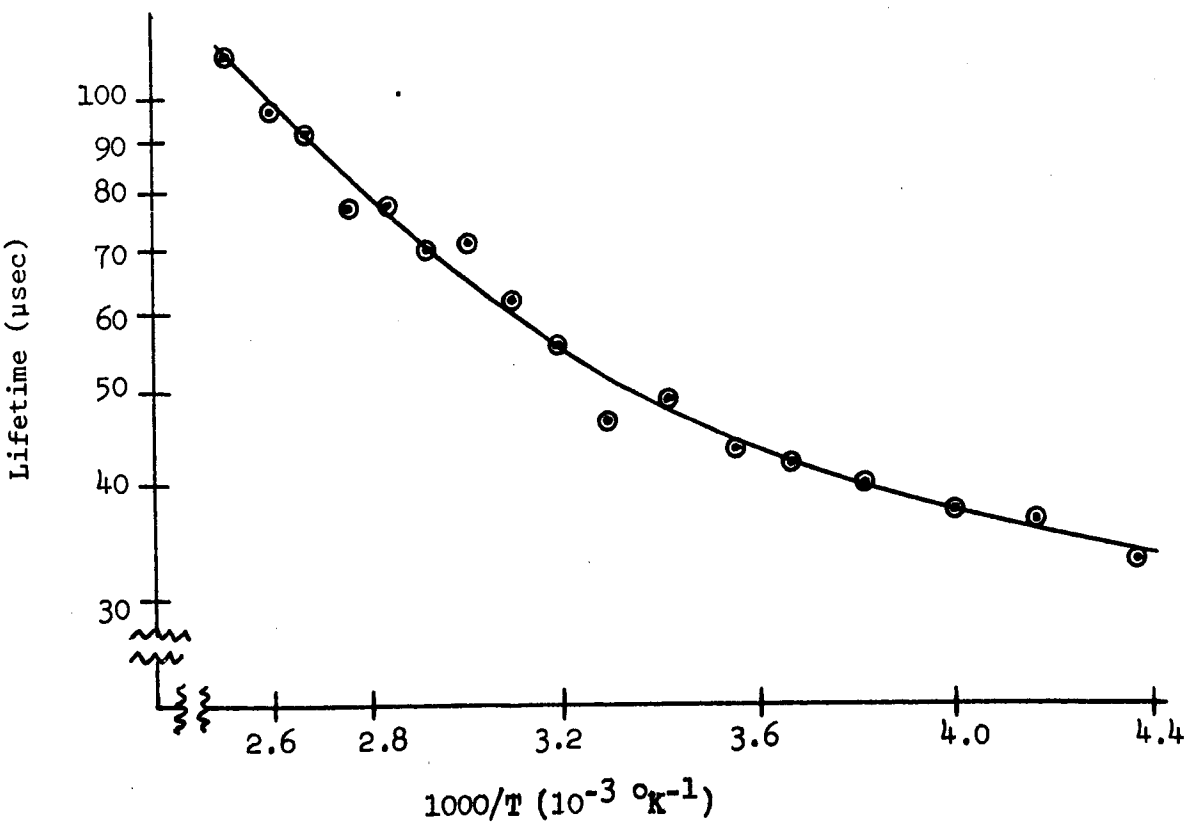
Lifetime (μsec)
100
90
80
70
60
50
40
30
2.6
2.8
3.2
3.6
4.0
4.4
1000/T (10^{-3} $^{o}K^{-1}$)

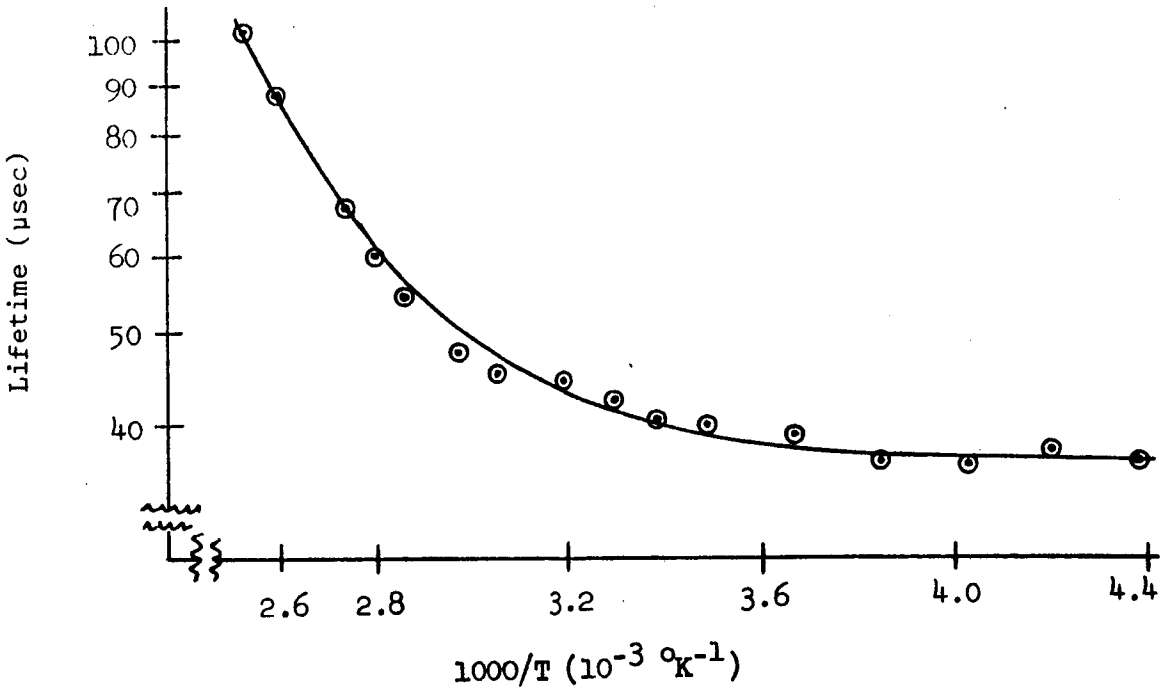
Lifetime (μsec)
100
90
80
70
60
50
40
2.6
2.8
3.2
3.6
4.0
4.4
1000/T (10^{-3} $^{o}K^{-1}$)

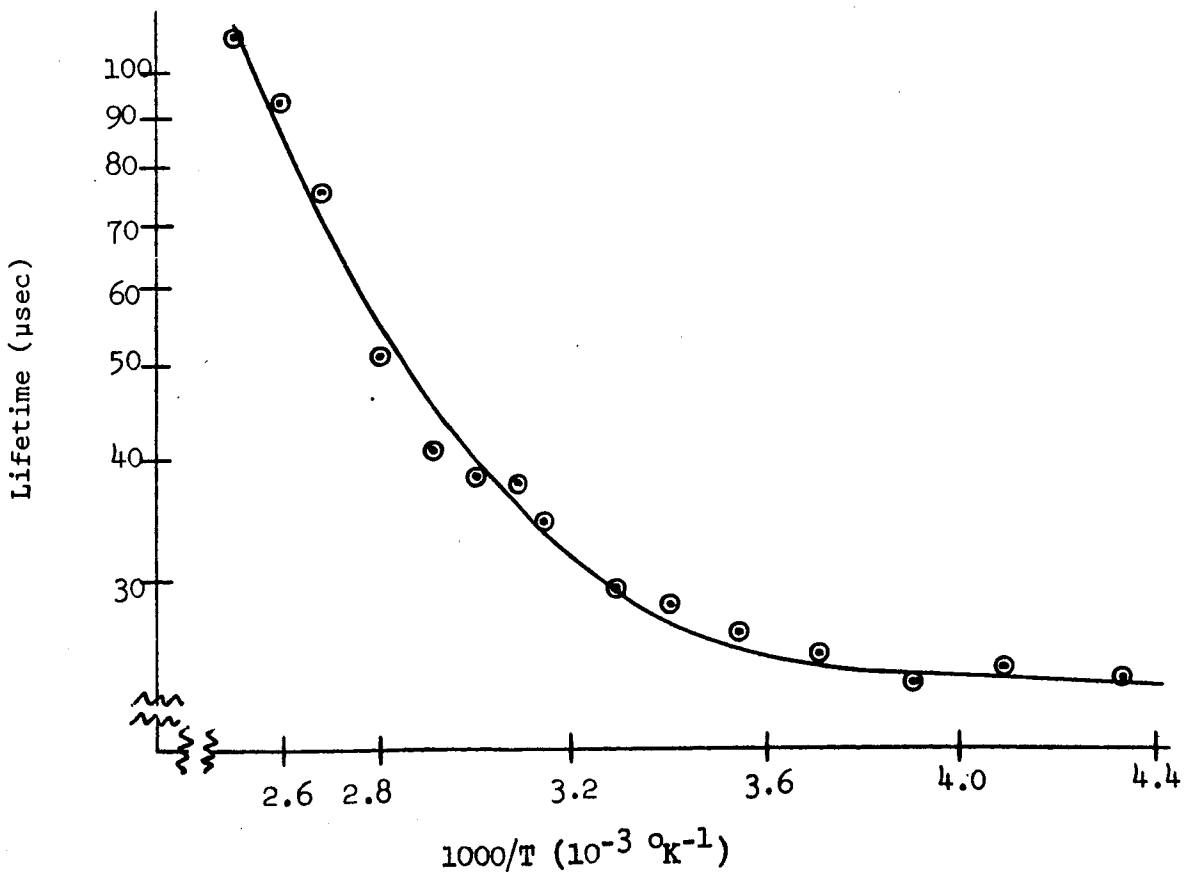
Lifetime (μsec)
100
90
80
70
60
50
40
30
2.6
2.8
3.2
3.6
4.0
4.4
1000/T (10^{-3} $^{o}K^{-1}$)

assumed to be constant potential with temperature. This may not be true due to the variation of the surface potential with temperature. However, one would expect this variation to be small in the temperature range used, and the approximation is essentially valid.

Figures 7.57 through 7.84 shows the surface lifetime as a function of reciprocal temperature for four p-type samples with several values of gamma ray exposure. The states that govern the lifetime in p-type material are located in the upper half of the forbidden region. As the irradiation proceeds the energy level of the defect moves slightly towards the conduction band edge and then returns gradually nearer the center of the gap. The variation of the energy level with irradiation in p-type material is not quite as large as that for n-type material. The energy levels for the surface defects in n- and p-type material are not the same, being located at approximately the same position, but in opposite halves of the forbidden region.

From the data taken on surface lifetime, room temperature values of surface recombination velocity were calculated for the various gamma ray dosages. Figures 7.85 and 7.86 show how the gamma irradiation effects the surface recombination velocity in n-type material, and Figures 7.87 and 7.88 give the surface recombination velocity in p-type material as a function of gamma ray exposure. In n-type material the velocity exhibits a relative minimum as irradiation progresses, while the gamma rays do not have a large influence on this parameter for the p-type material.

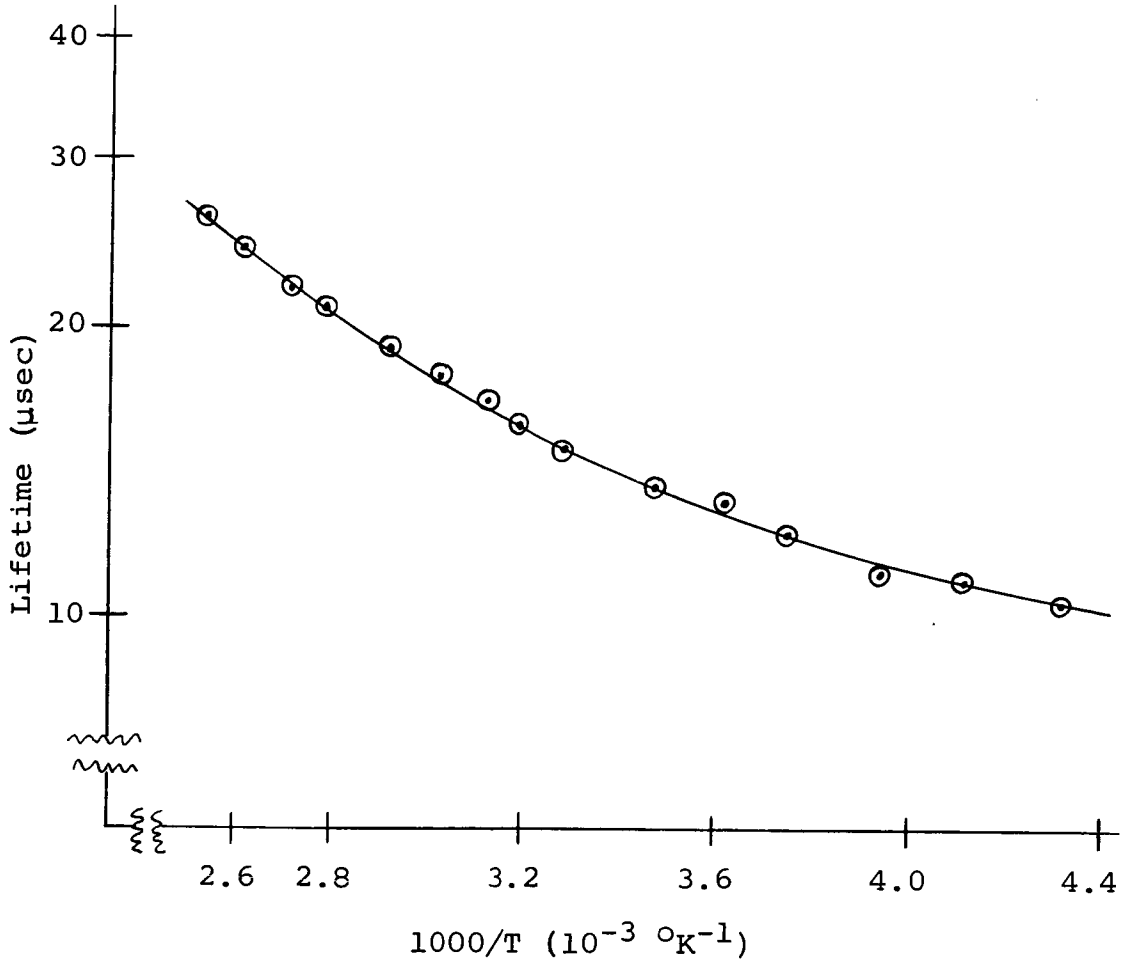

Figure 7.57. Surface lifetime vs. reciprocal temperature for sample IPA3/4 5-1 before irradiation

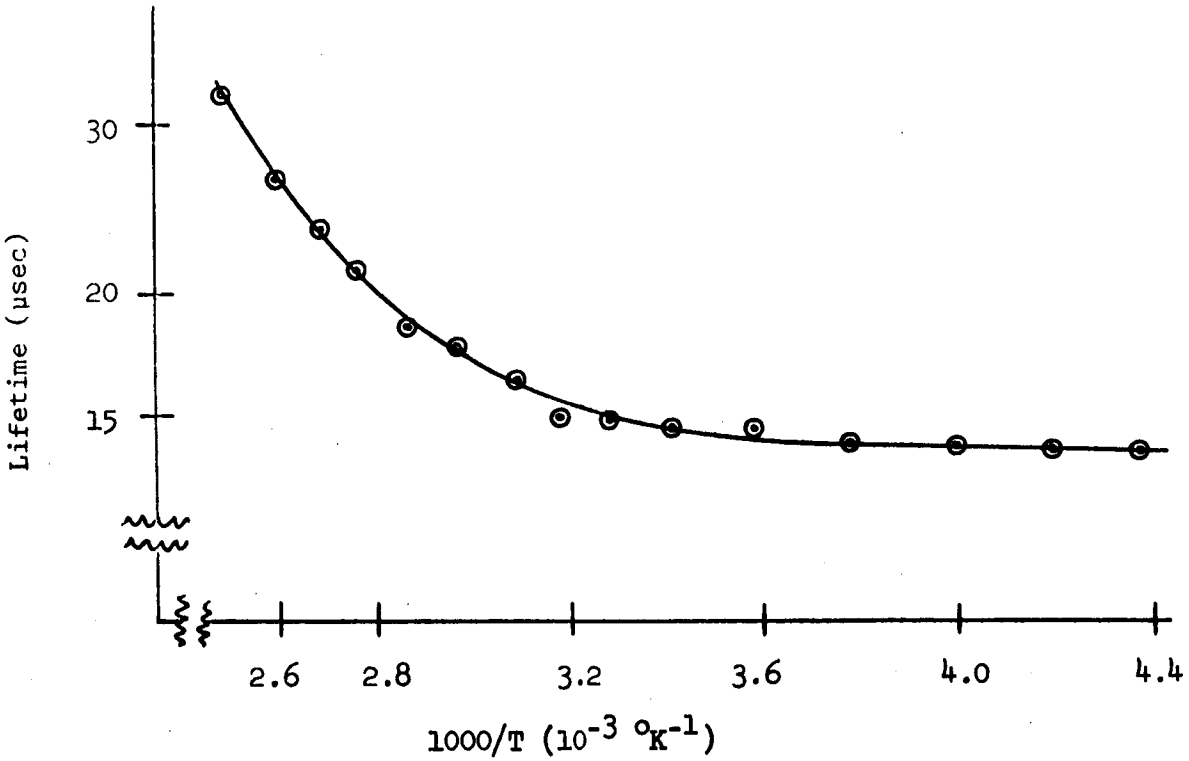
30
20
15
Lifetime (μsec)
2.6
2.8
3.2
3.6
4.0
4.4
1000/T (10^{-3} $^{o}K^{-1}$)

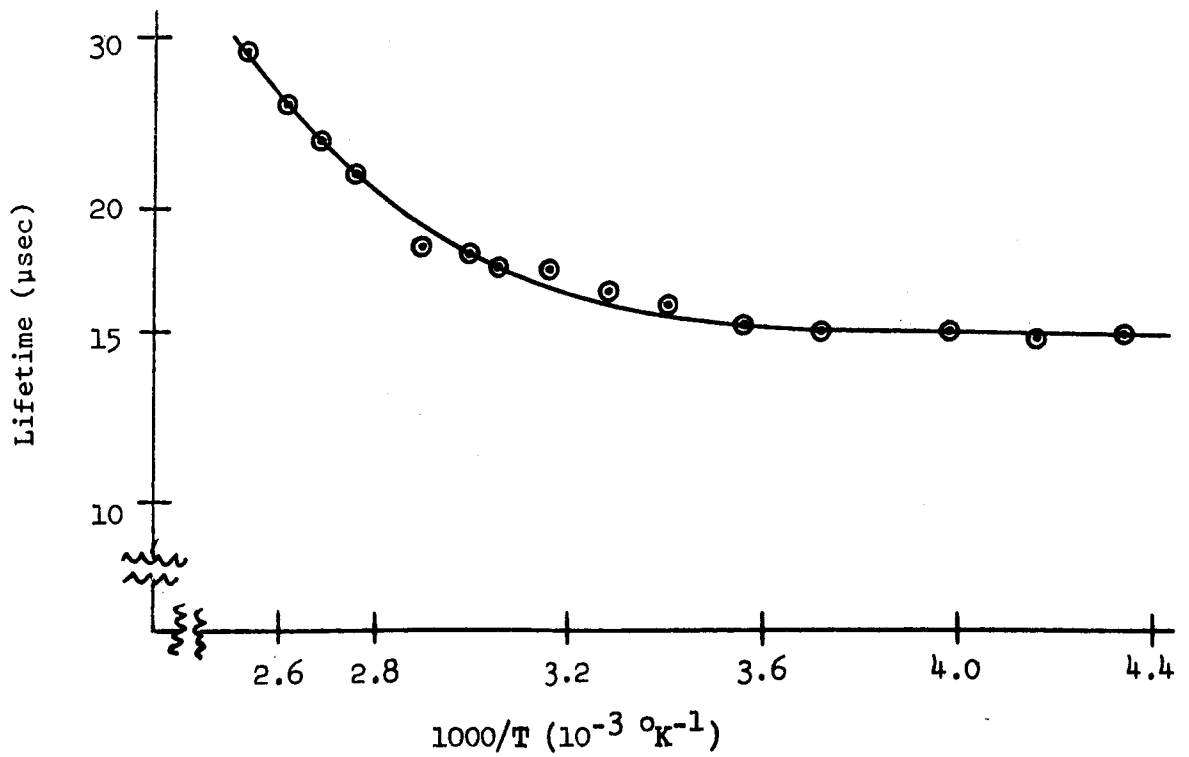
30
20
15
10
Lifetime (μsec)
2.6
2.8
3.2
3.6
4.0
4.4
1000/T (10^{-3} $^{o}K^{-1}$)

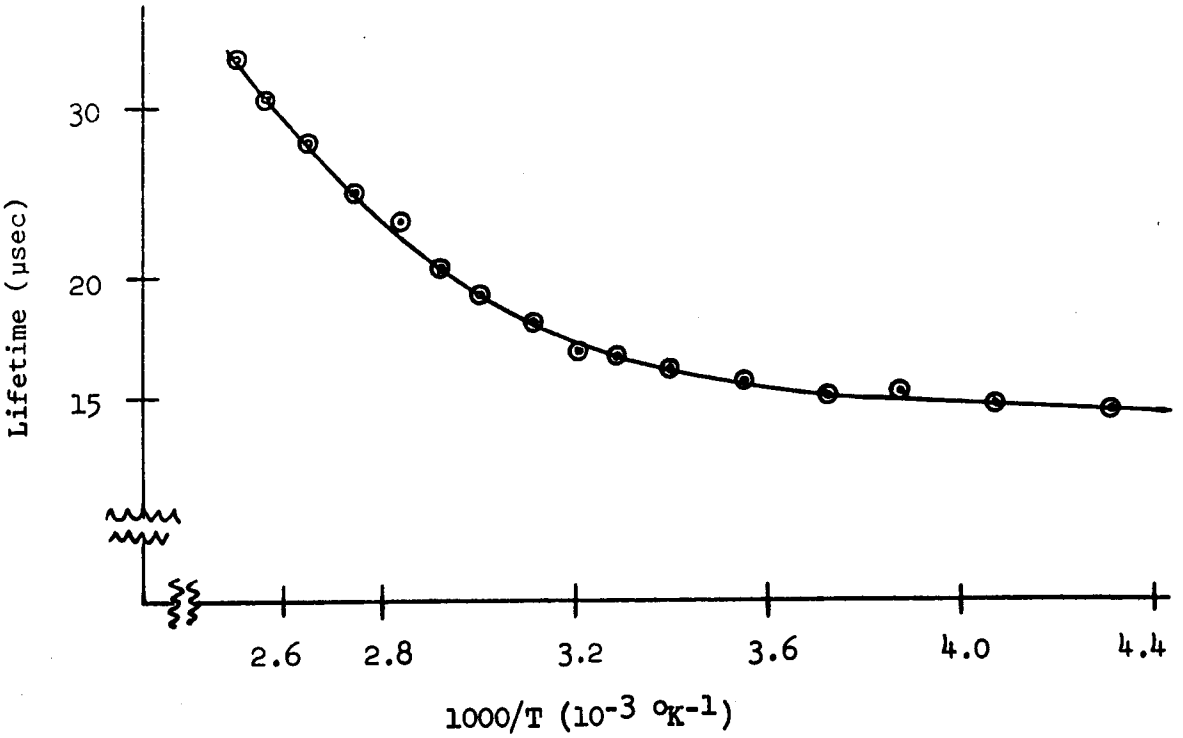
Lifetime (μsec)
30
20
15
2.6
2.8
3.2
3.6
4.0
4.4
1000/T (10-3 °K-1)

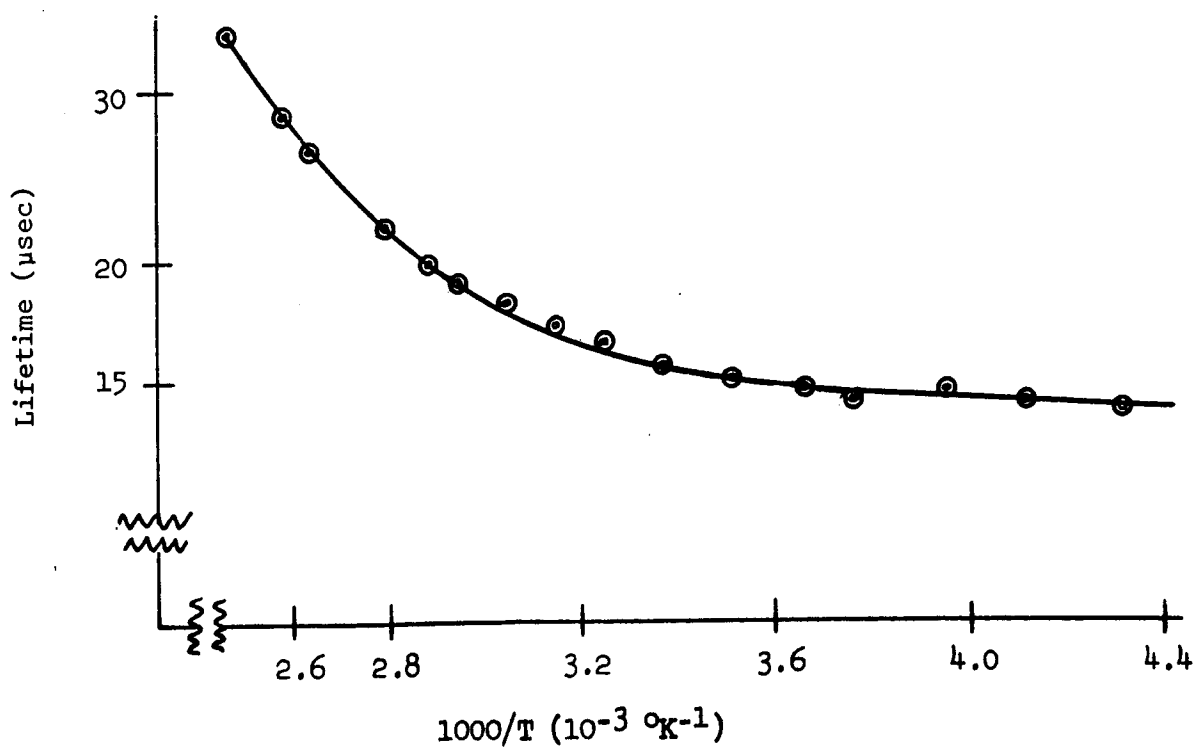
Lifetime (μsec)
30
20
15
2.6
2.8
3.2
3.6
4.0
4.4
1000/T (10-3 °K-1)

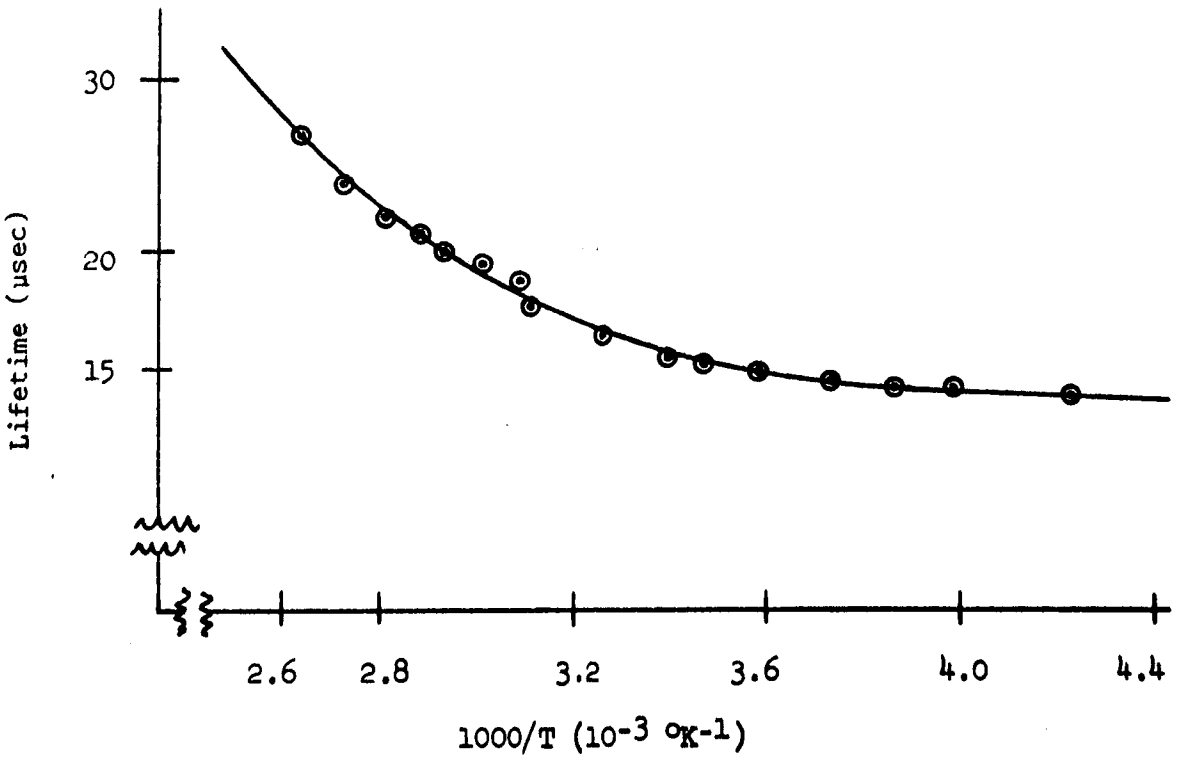
30
20
15
Lifetime (μsec)
2.6
2.8
3.2
3.6
4.0
4.4
1000/T (10-3 °K-1)

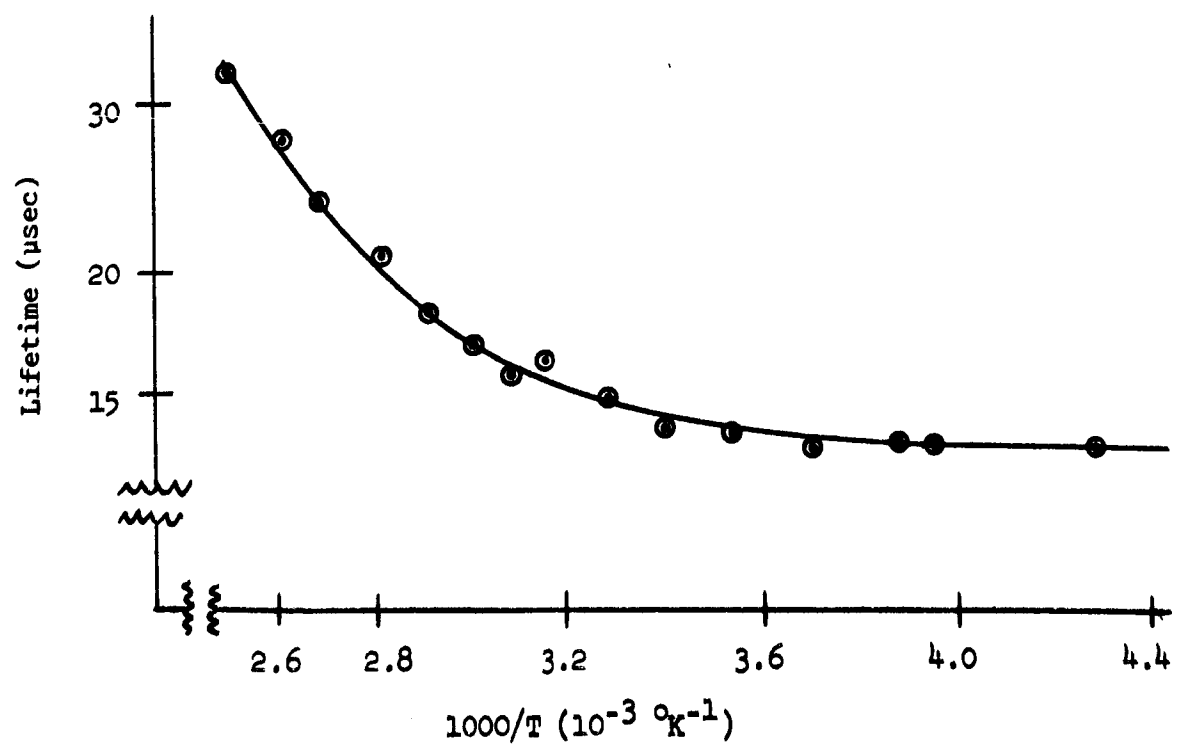
30
20
15
Lifetime (μsec)
2.6
2.8
3.2
3.6
4.0
4.4
1000/T (10-3 °K-1)

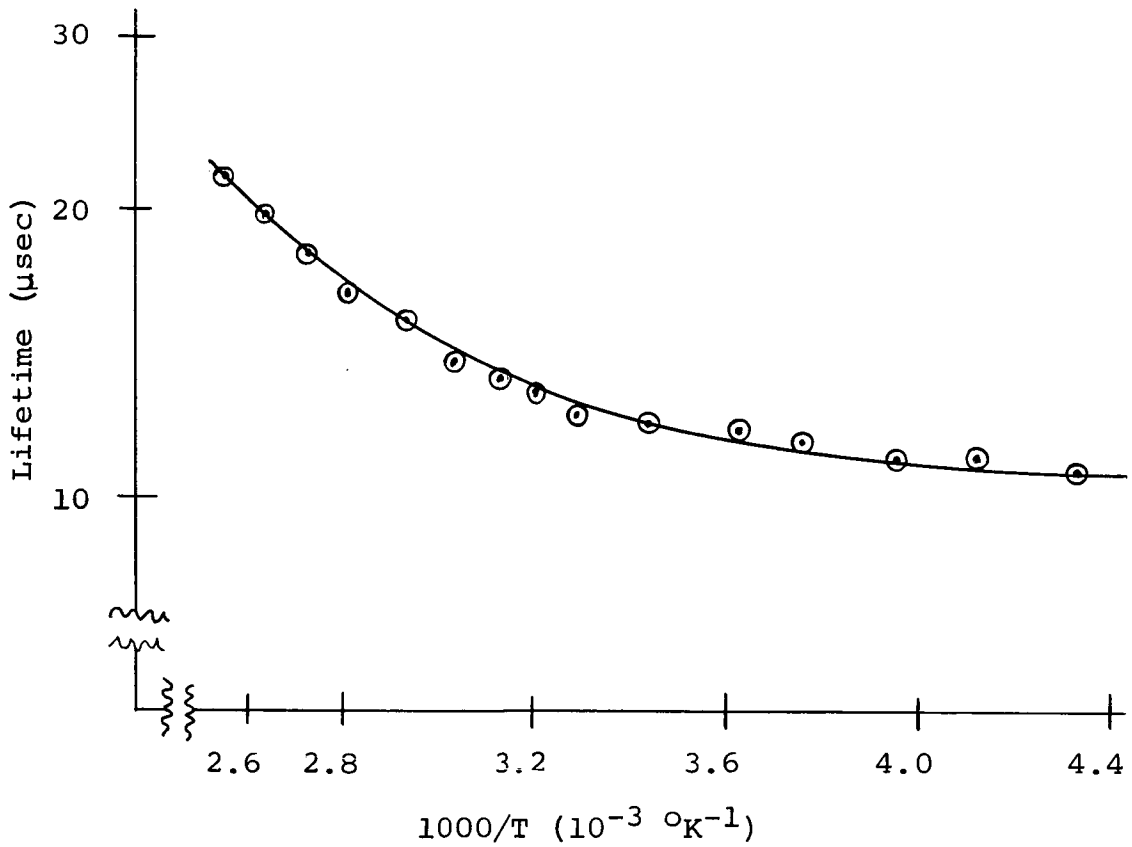

Figure 7.64. Surface lifetime vs. reciprocal temperature for sample IPA3/4 5-2 before irradiation

Figure 7.65. Surface lifetime vs. reciprocal temperature for sample IPA3/4 5-2 after 4.82×10^4 roentgens of Co^{60} gamma ray exposure

Figure 7.66. Surface lifetime vs. reciprocal temperature for sample IPA3/4 5-2 after 9.64×10^4 roentgens of Co^{60} gamma ray exposure

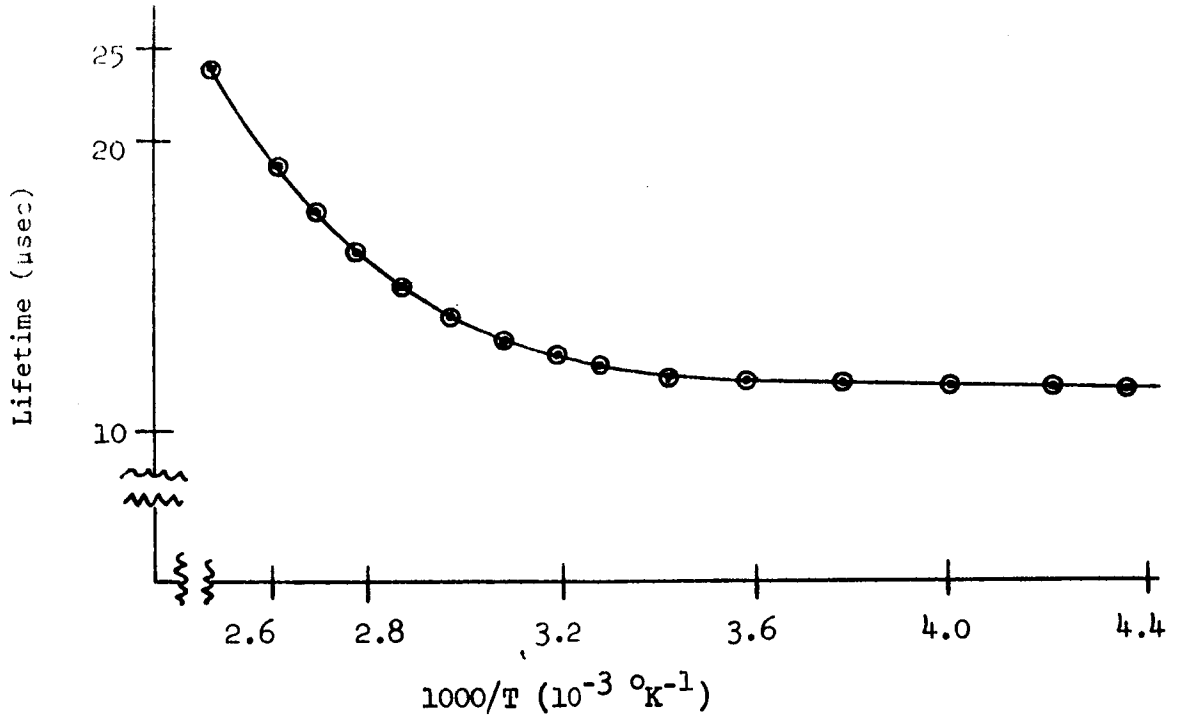
25
20
10
Lifetime (μsec)
2.6
2.8
3.2
3.6
4.0
4.4
1000/T (10^{-3} $^{o}K^{-1}$)

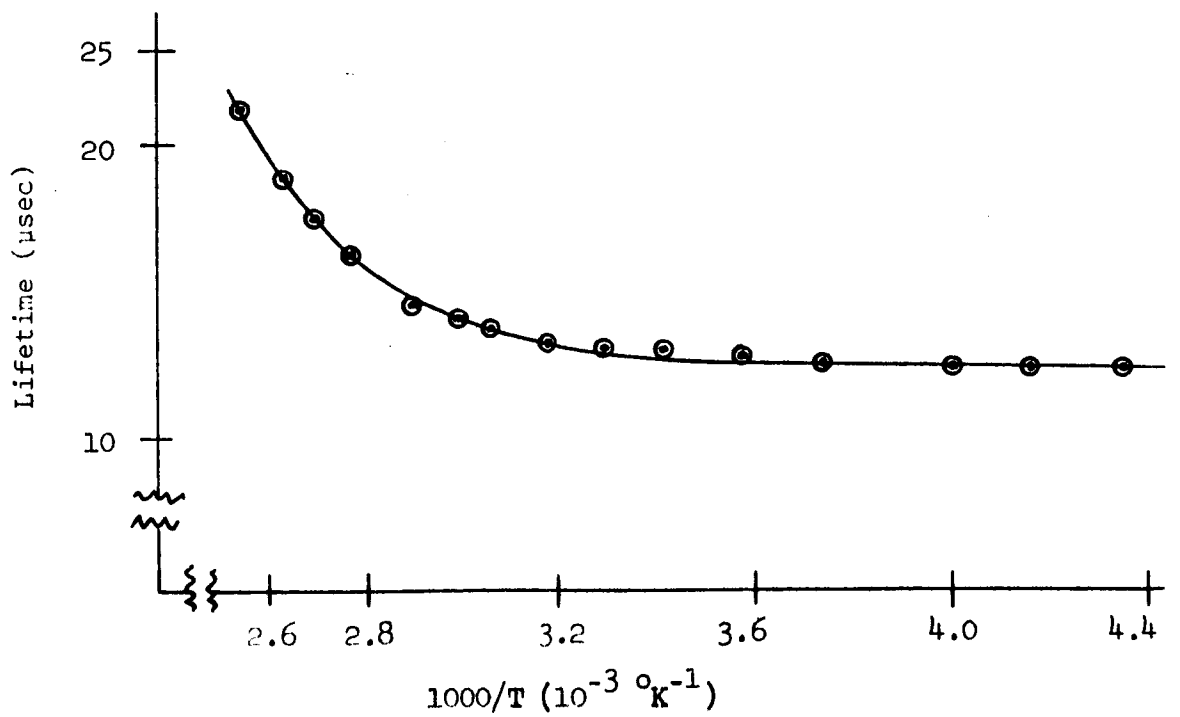
25
20
10
Lifetime (μsec)
2.6
2.8
3.2
3.6
4.0
4.4
1000/T (10^{-3} $^{o}K^{-1}$)

Figure 7.67. Surface lifetime vs. reciprocal temperature for sample IPA3/4 5-2 after 1.45×10^5 roentgens of Co^{60} gamma ray exposure

Figure 7.68. Surface lifetime vs. reciprocal temperature for sample IPA3/4 5-2 after 1.93×10^5 roentgens of Co^{60} gamma ray exposure

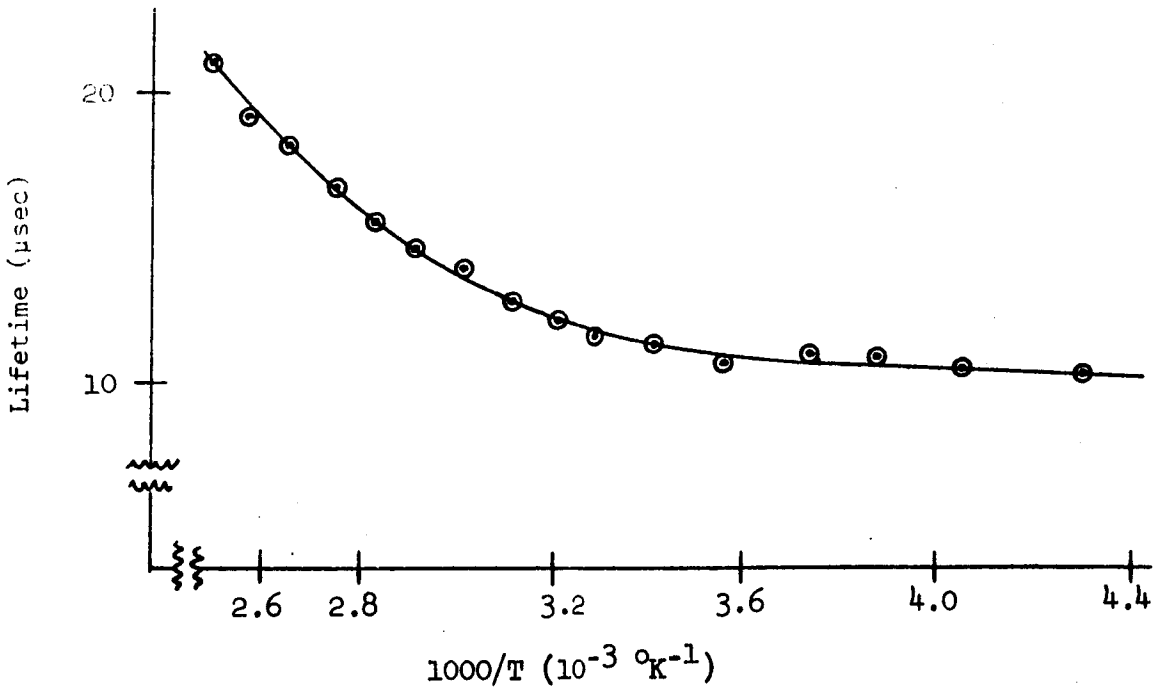
Lifetime (μsec)
20
10
2.6
2.8
3.2
3.6
4.0
4.4
1000/T (10^{-3} $^{o}K^{-1}$)

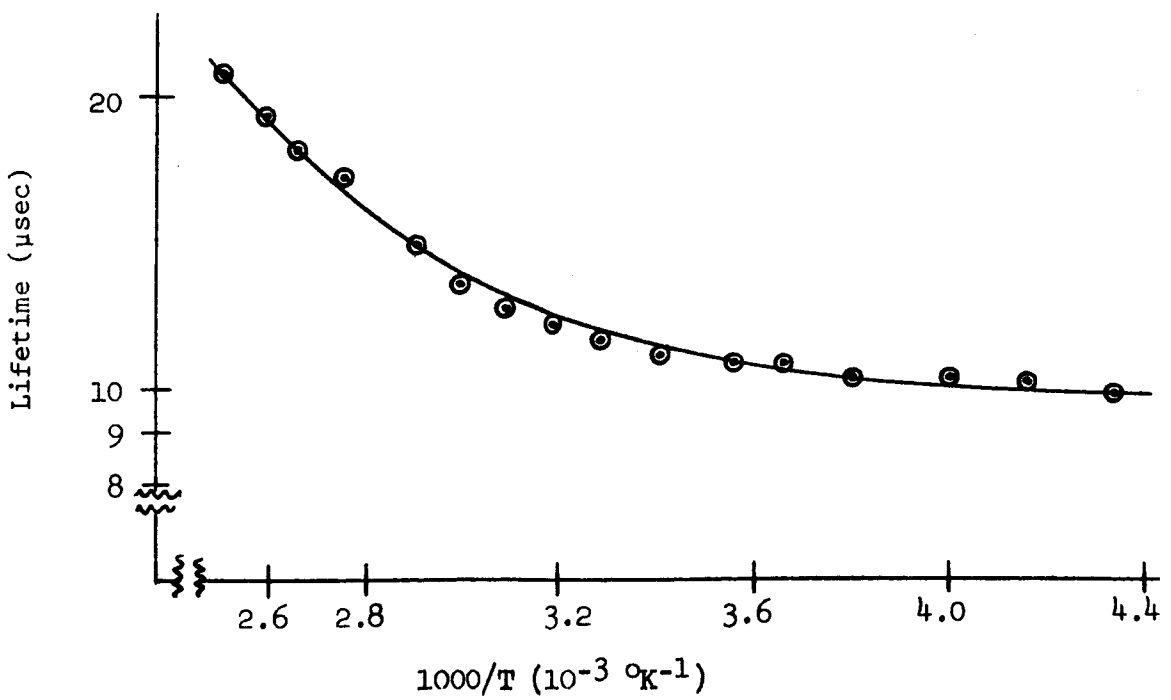
Lifetime (μsec)
20
10
9
8
2.6
2.8
3.2
3.6
4.0
4.4
1000/T (10^{-3} $^{o}K^{-1}$)

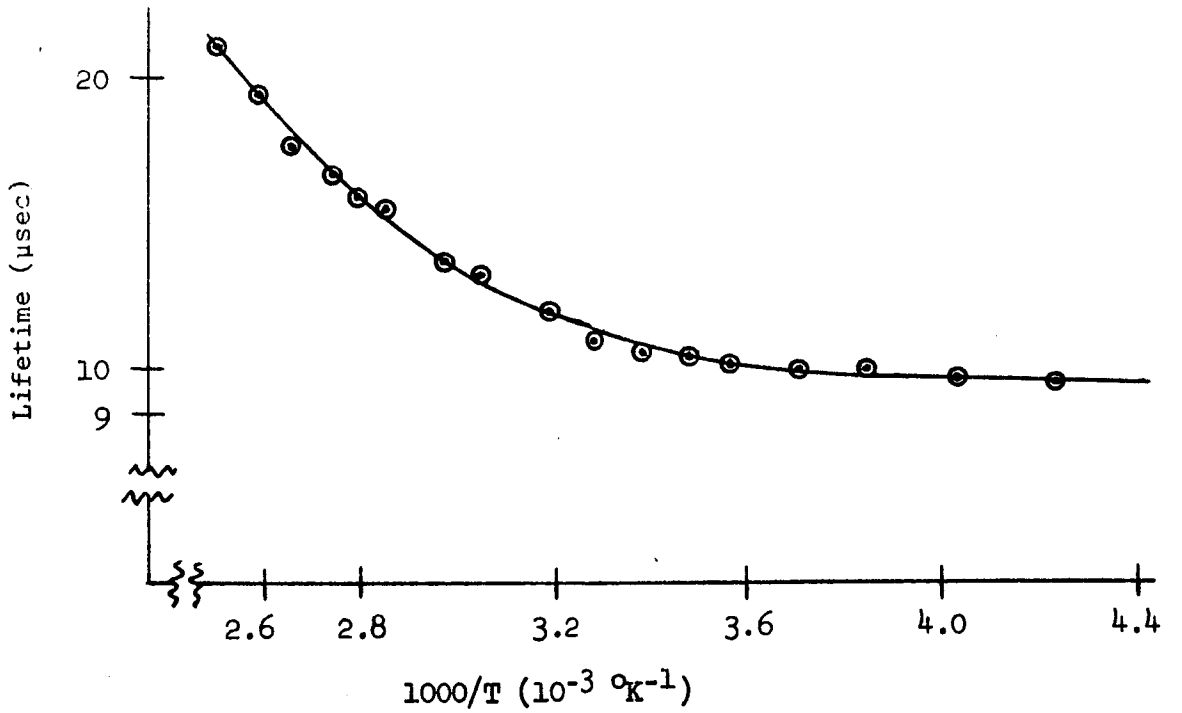
20
10
9
Lifetime (μsec)
2.6
2.8
3.2
3.6
4.0
4.4
1000/T (10-3 °K-1)

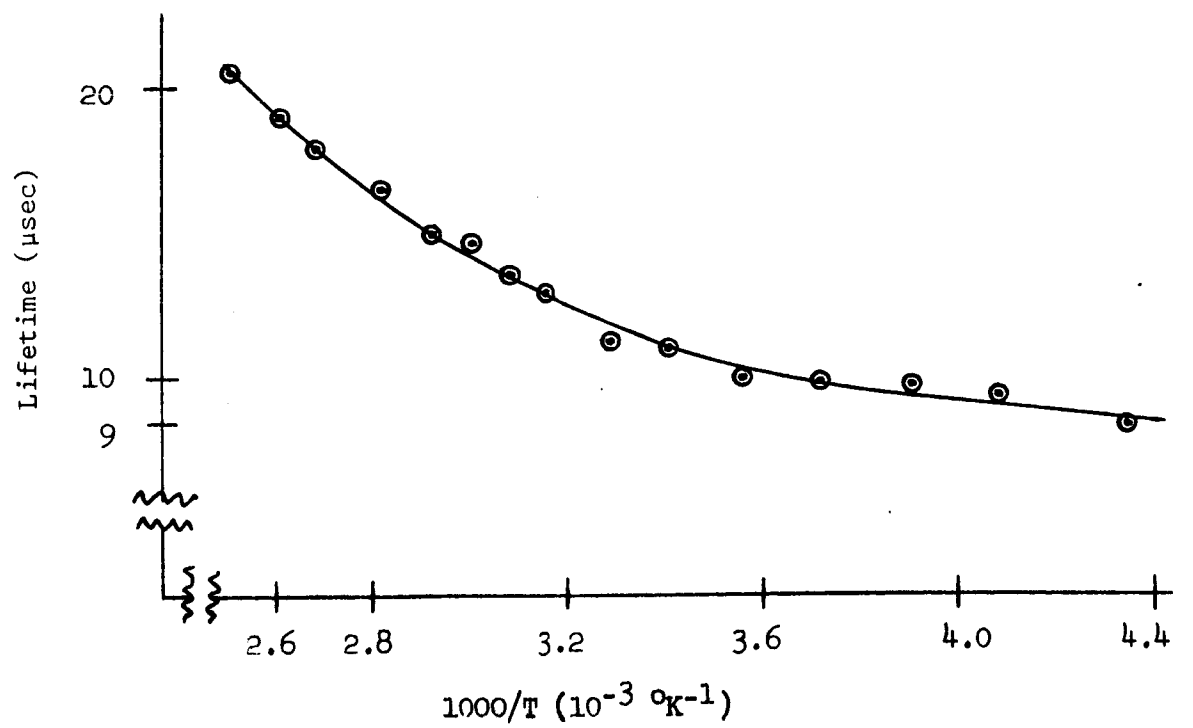
20
10
9
Lifetime (μsec)
2.6
2.8
3.2
3.6
4.0
4.4
1000/T (10-3 °K-1)

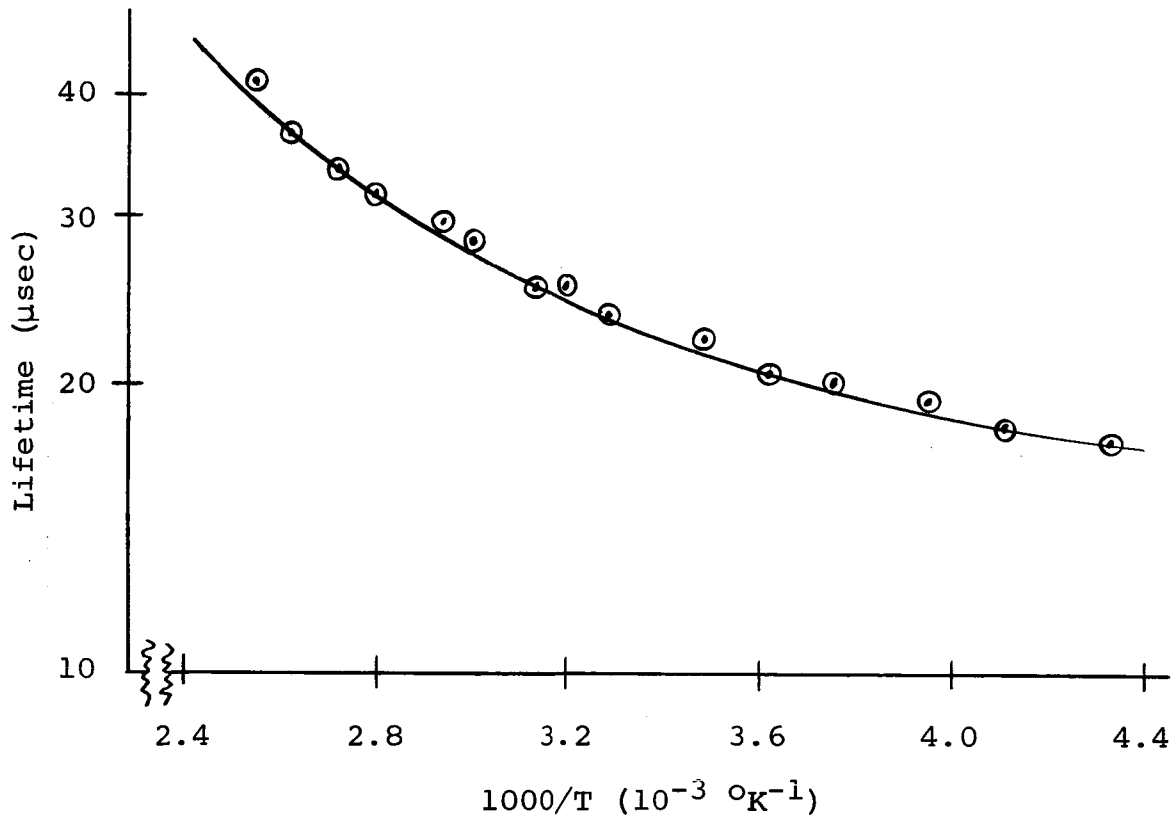

Figure 7.71. Surface lifetime vs. reciprocal temperature for sample IPA3/4 5-3 before irradiation

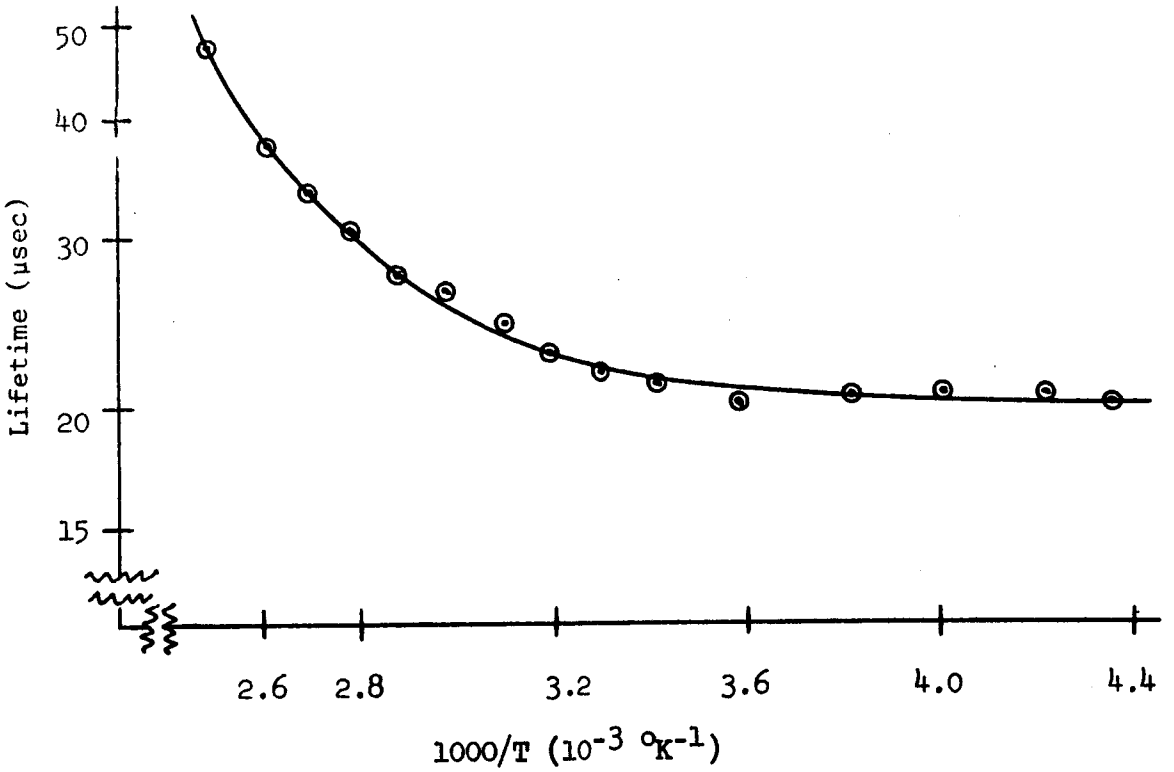
50
40
30
20
15
Lifetime (μsec)
2.6
2.8
3.2
3.6
4.0
4.4
1000/T (10-3 °K-1)

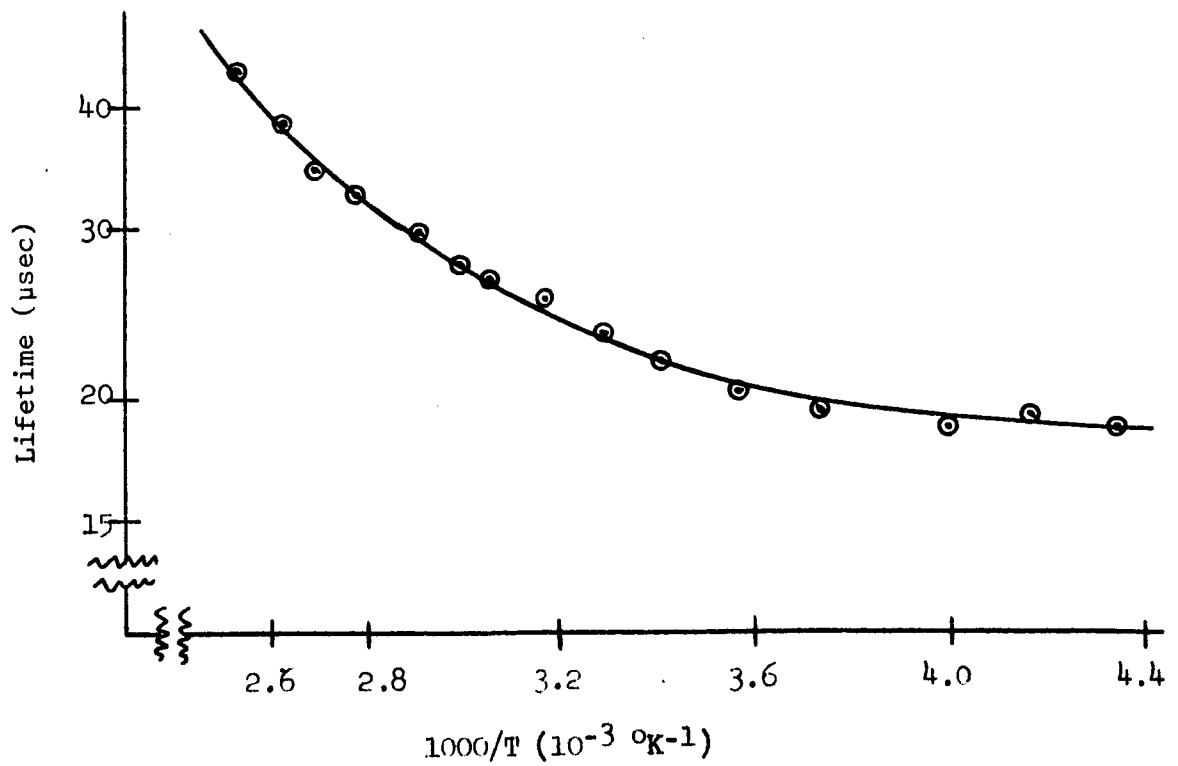
40
30
20
15
Lifetime (μsec)
2.6
2.8
3.2
3.6
4.0
4.4
1000/T (10-3 °K-1)

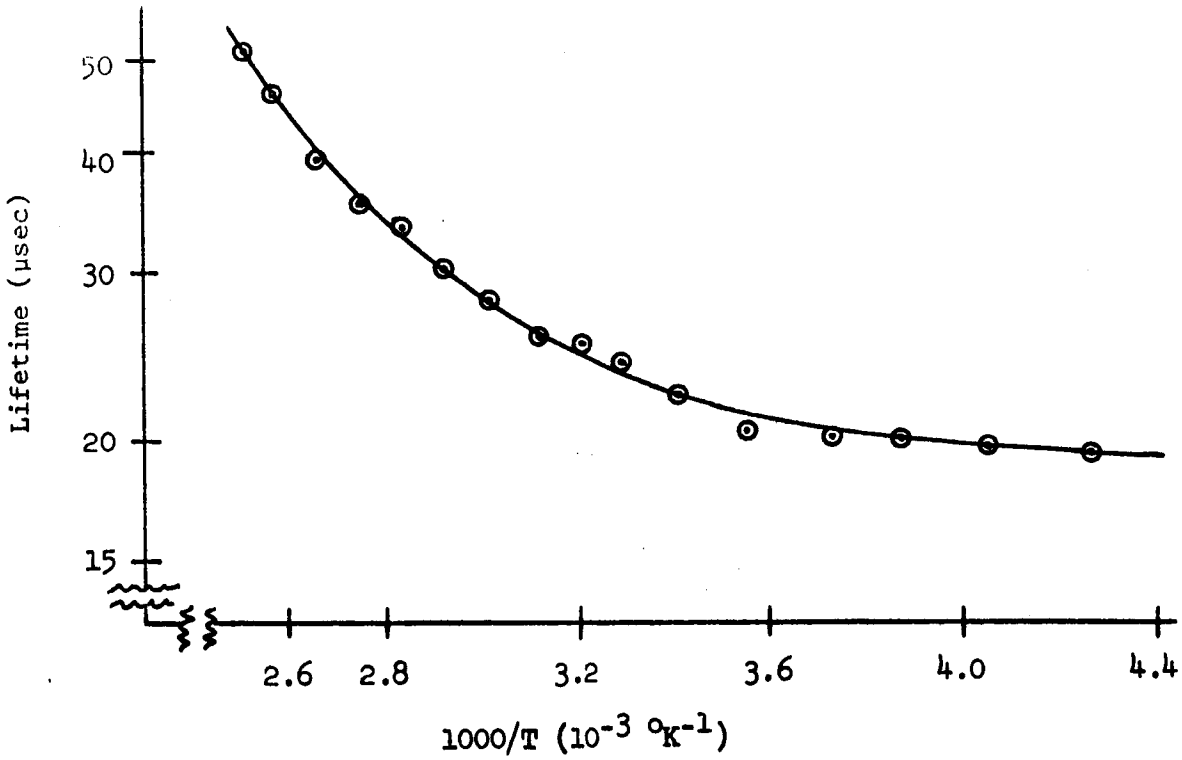
Lifetime (μsec)
50
40
30
20
15
2.6
2.8
3.2
3.6
4.0
4.4
1000/T (10-3 °K-1)

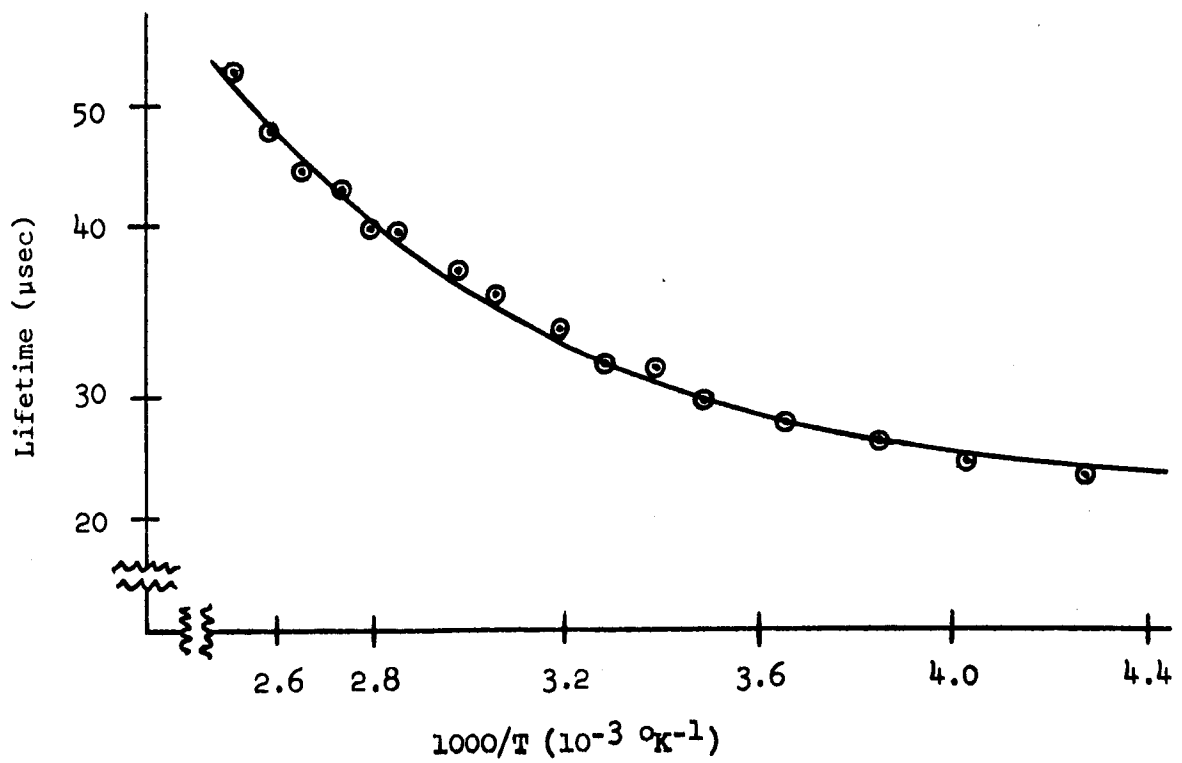
Lifetime (μsec)
50
40
30
20
2.6
2.8
3.2
3.6
4.0
4.4
1000/T (10-3 °K-1)

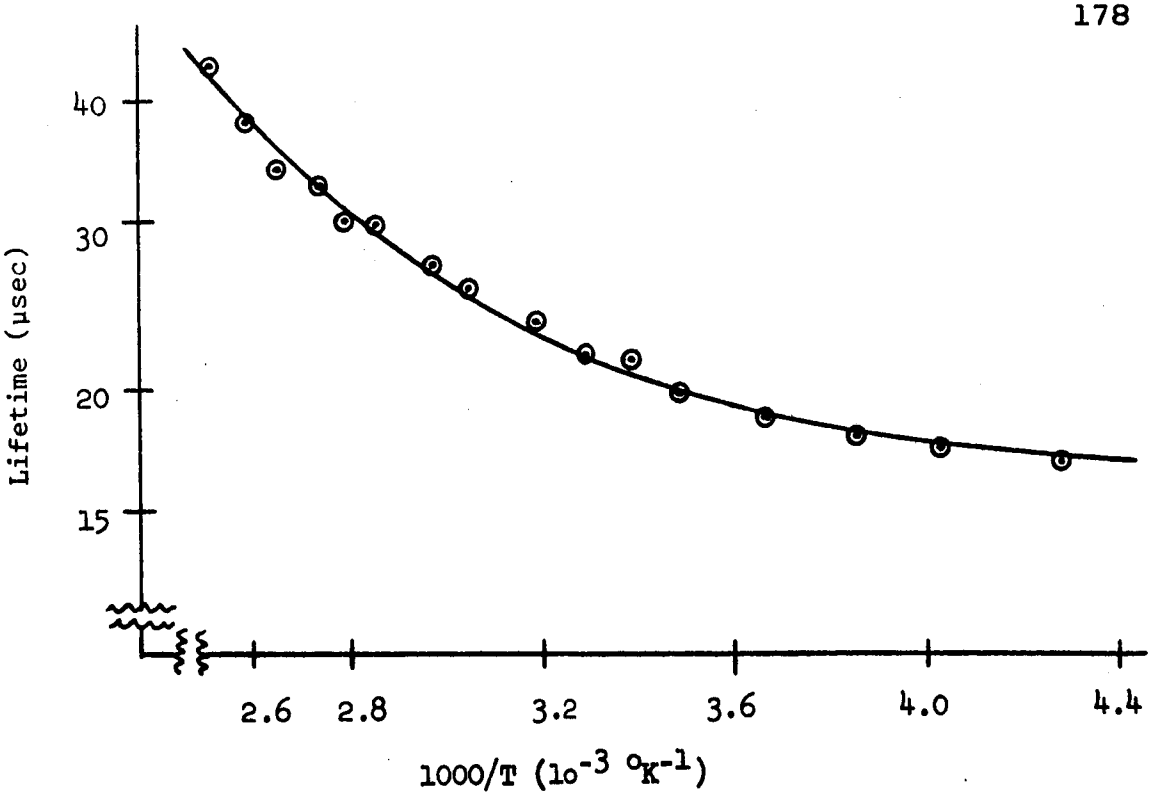
Lifetime (μsec)
40
30
20
15
2.6
2.8
3.2
3.6
4.0
4.4
1000/T (10-3 °K-1)

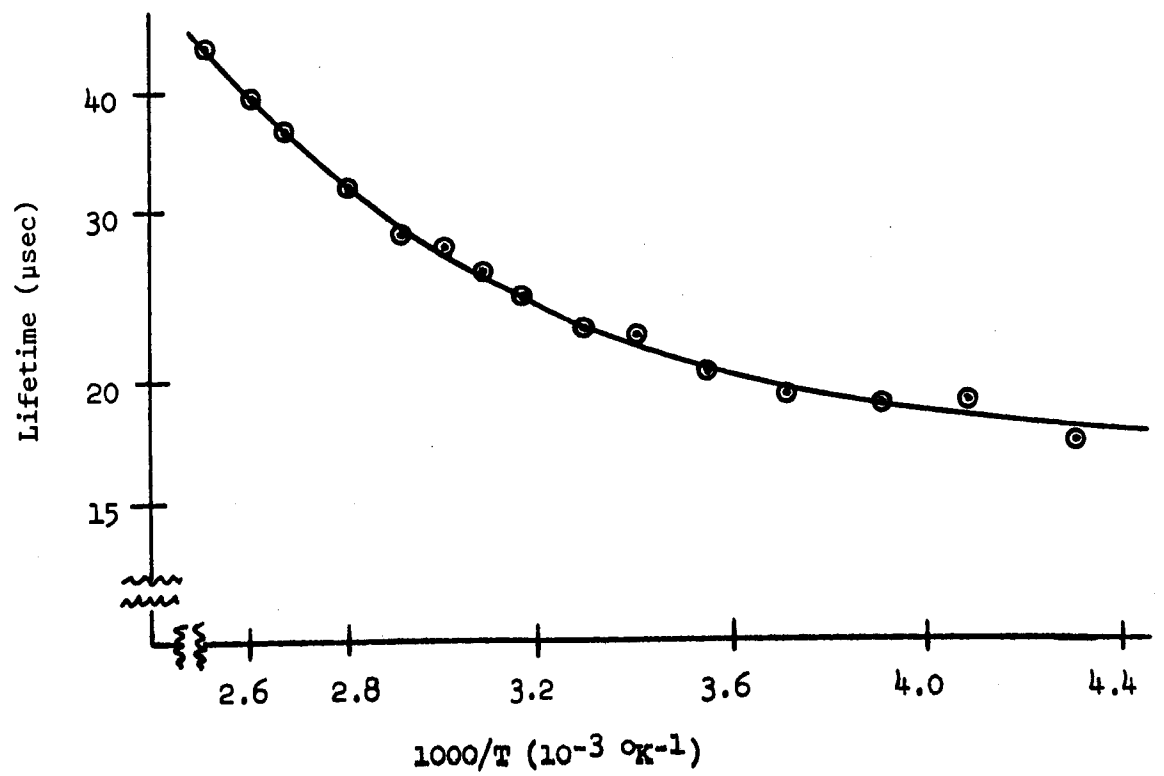
Lifetime (μsec)
40
30
20
15
2.6
2.8
3.2
3.6
4.0
4.4
1000/T (10-3 °K-1)

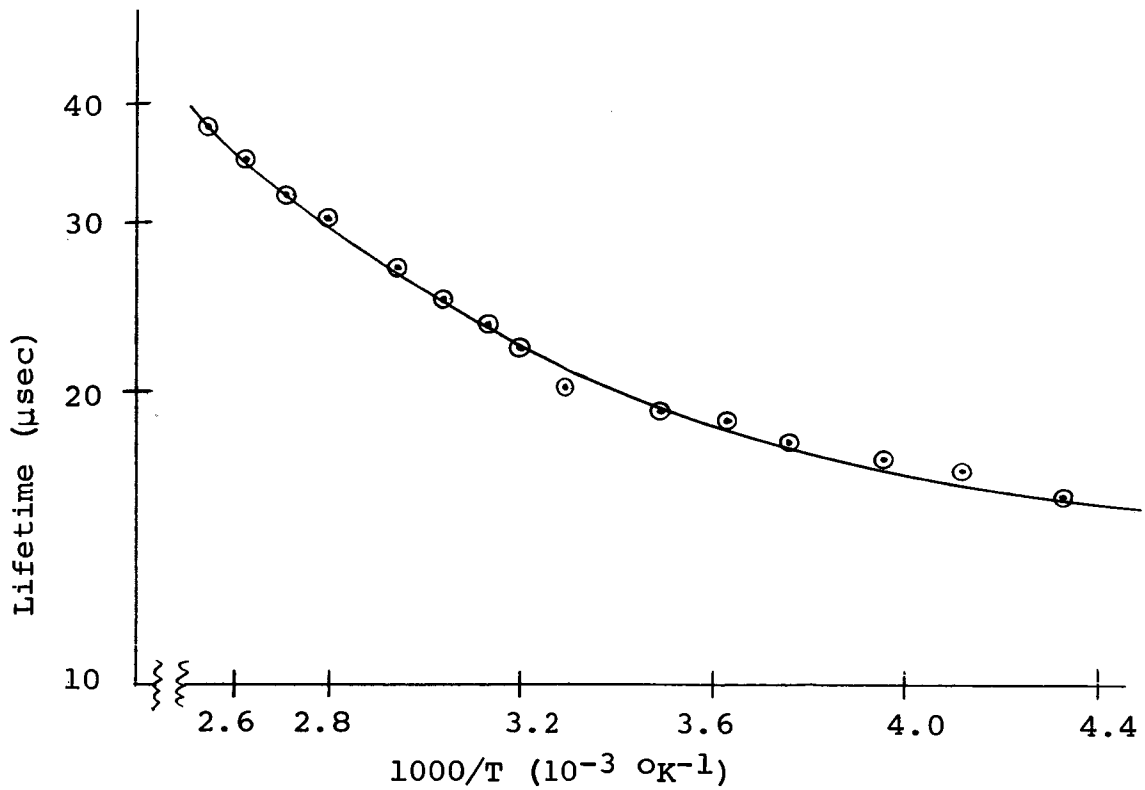

Figure 7.78. Surface lifetime vs. reciprocal temperature for sample IPA3/4 5-4 before irradiation

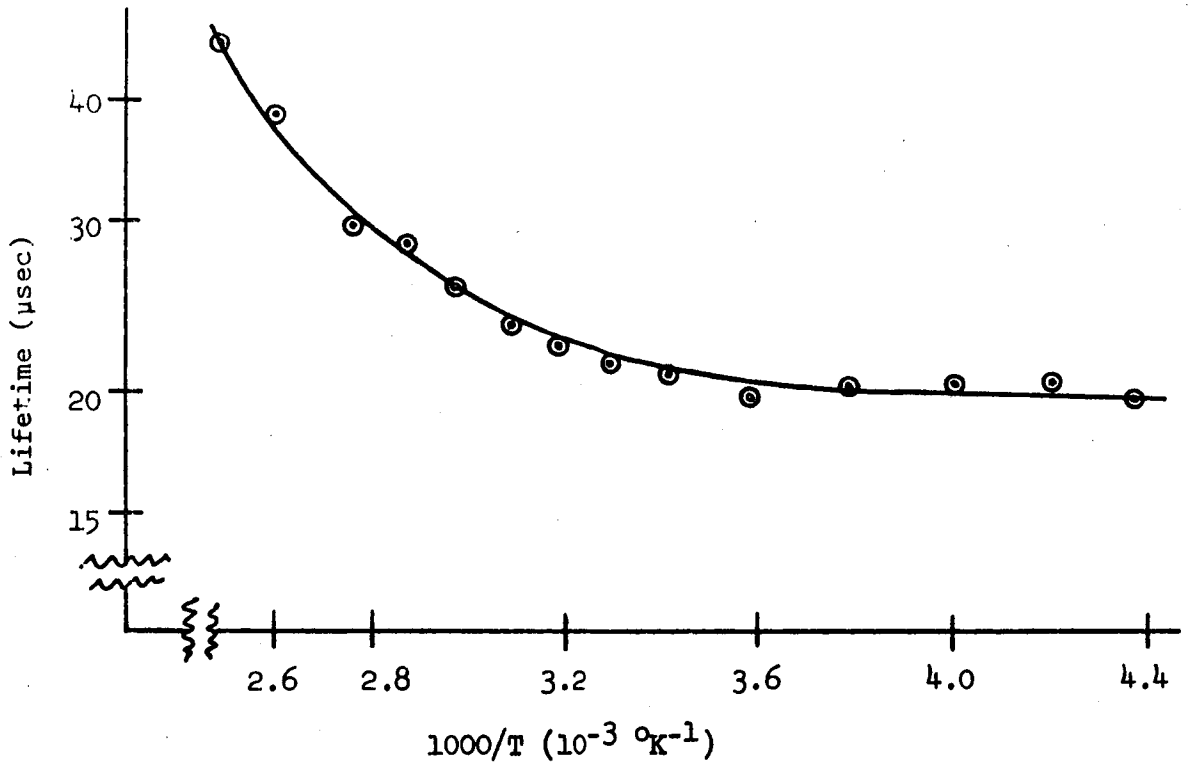
Lifetime (μsec)
40
30
20
15
2.6
2.8
3.2
3.6
4.0
4.4
1000/T (10-3 °K-1)

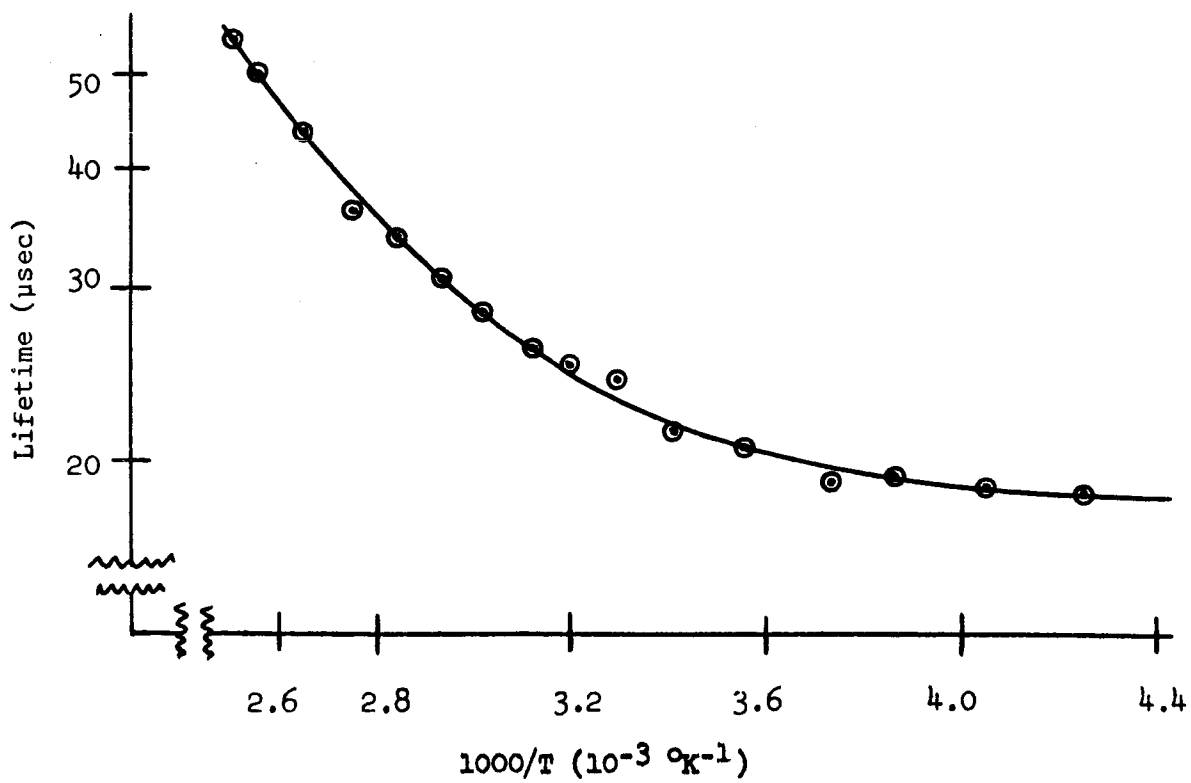
Lifetime (μsec)
50
40
30
20
2.6
2.8
3.2
3.6
4.0
4.4
1000/T (10-3 °K-1)

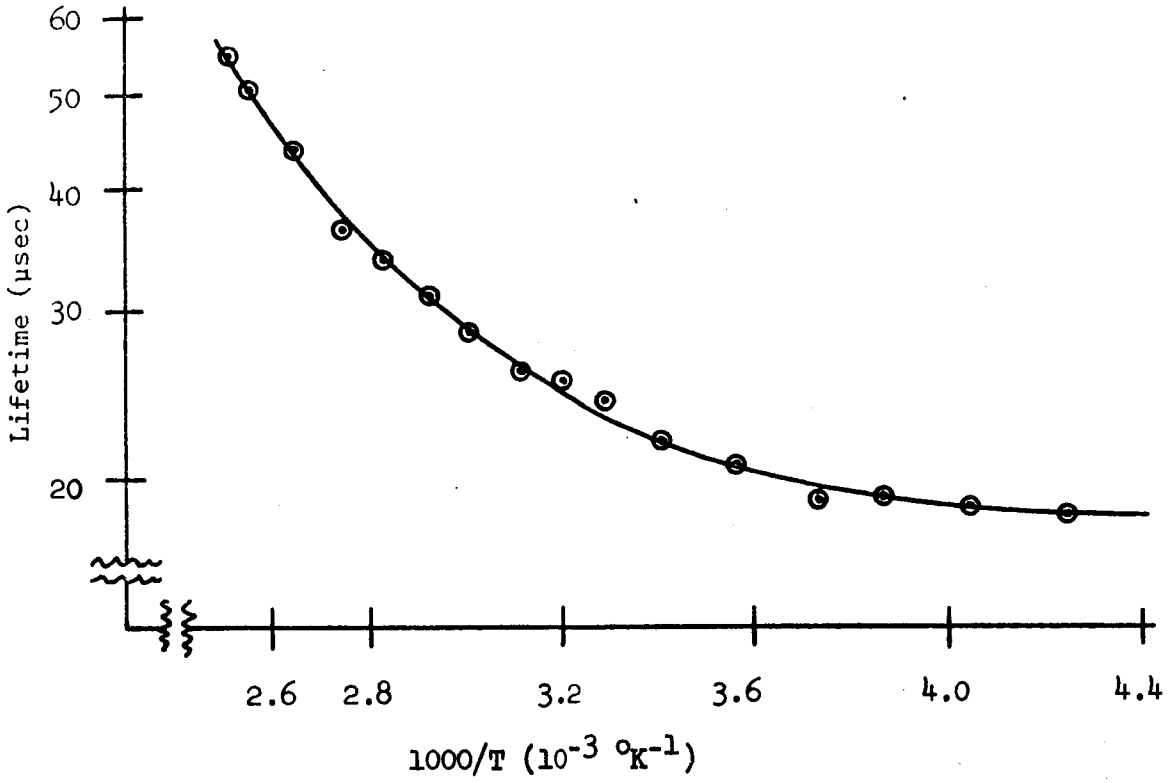
60
50
40
30
20
Lifetime (μsec)
2.6
2.8
3.2
3.6
4.0
4.4
1000/T (10-3 °K-1)

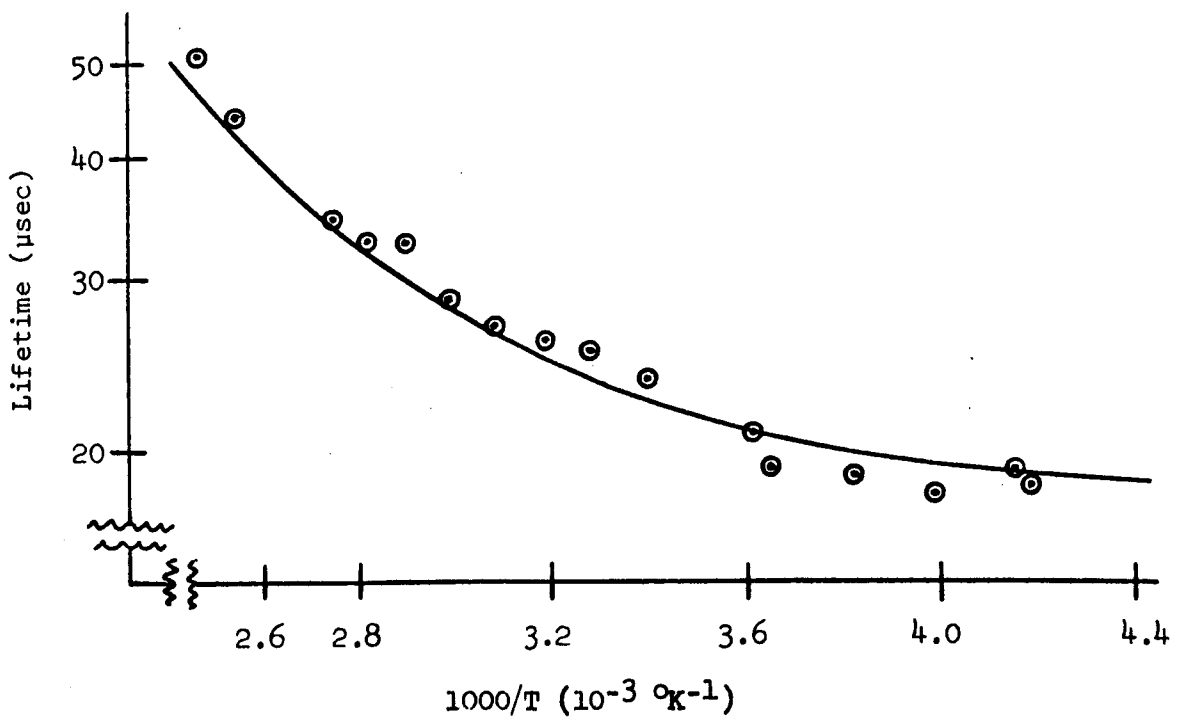
50
40
30
20
Lifetime (μsec)
2.6
2.8
3.2
3.6
4.0
4.4
1000/T (10-3 °K-1)

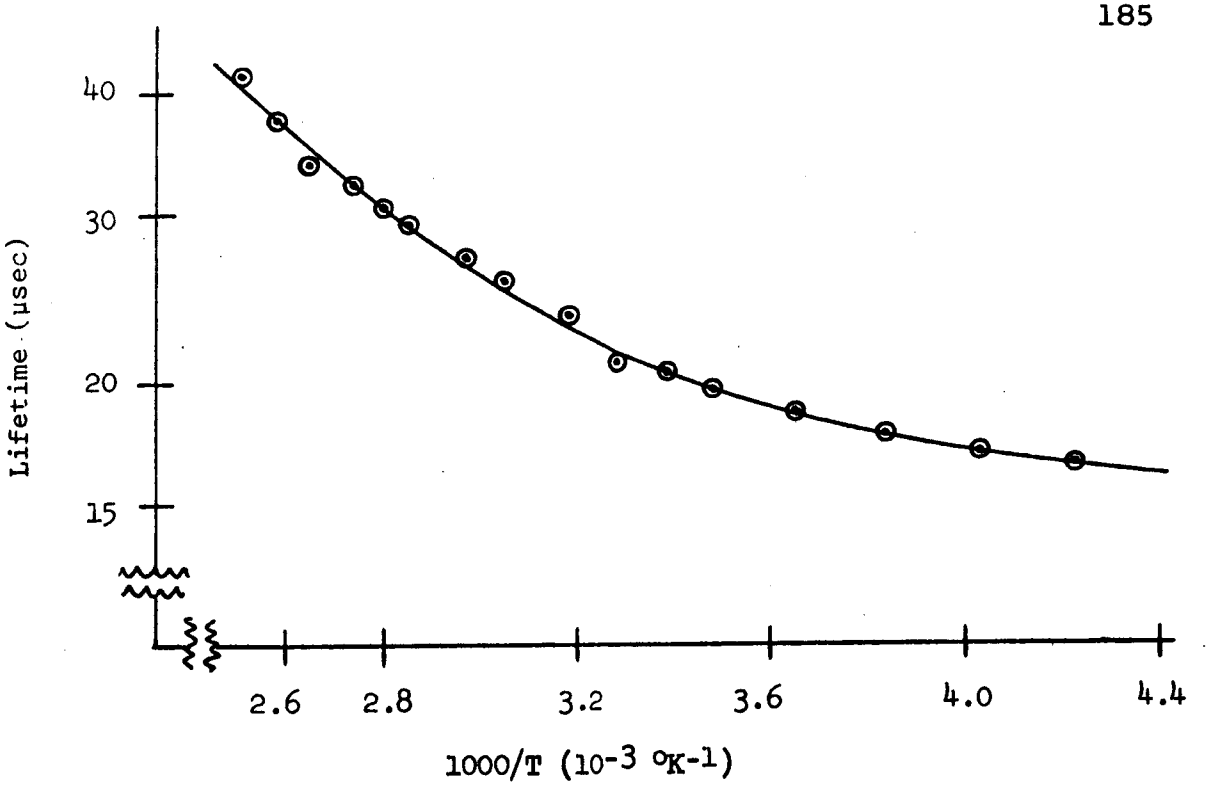
Lifetime (μsec)
40
30
20
15
2.6
2.8
3.2
3.6
4.0
4.4
1000/T (10-3 °K-1)

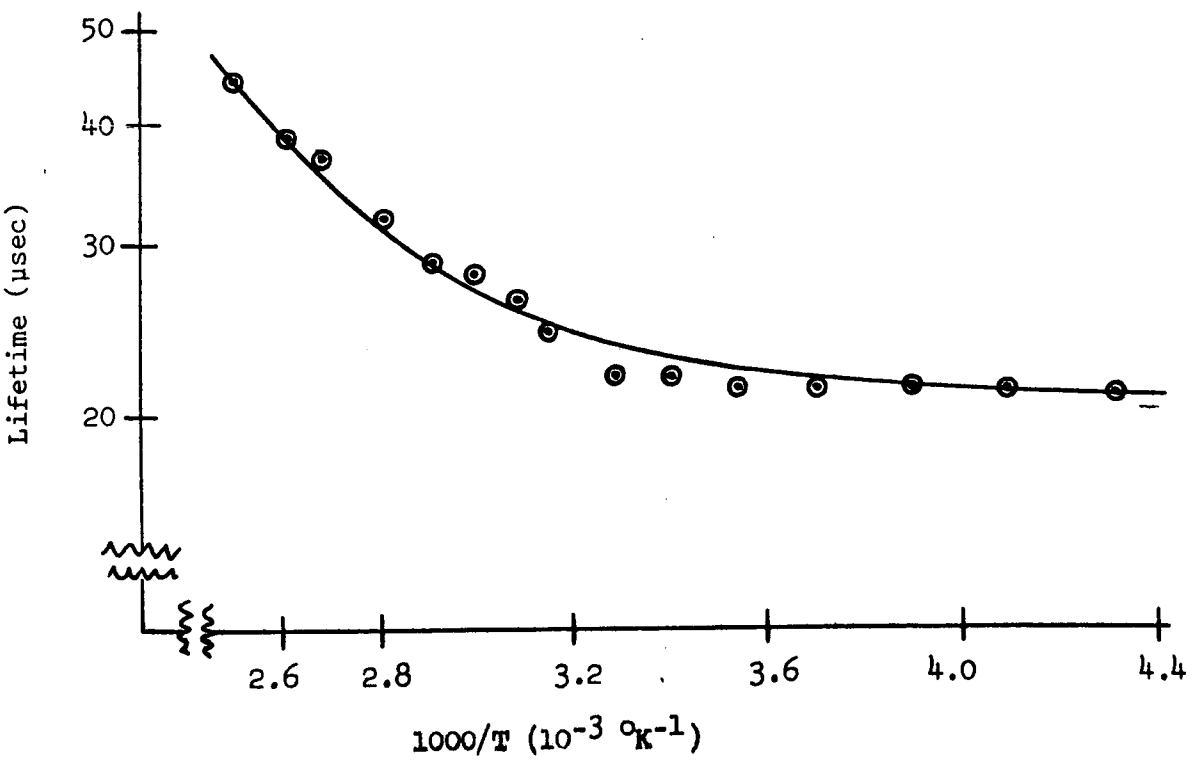
Lifetime (μsec)
50
40
30
20
2.6
2.8
3.2
3.6
4.0
4.4
1000/T (10-3 °K-1)

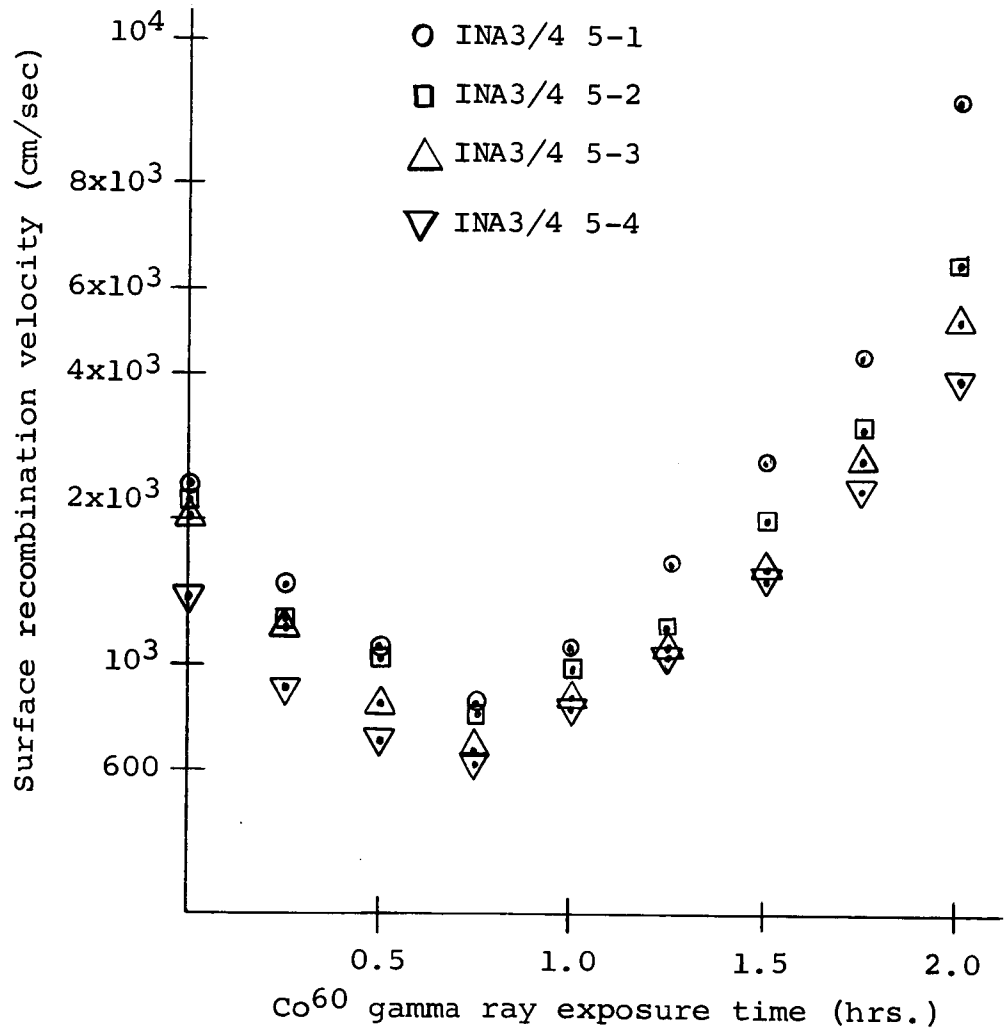

Figure 7.85. Surface recombination velocity vs. gamma ray exposure time. The exposure rate is 1.94×10^5 roentgens per hour

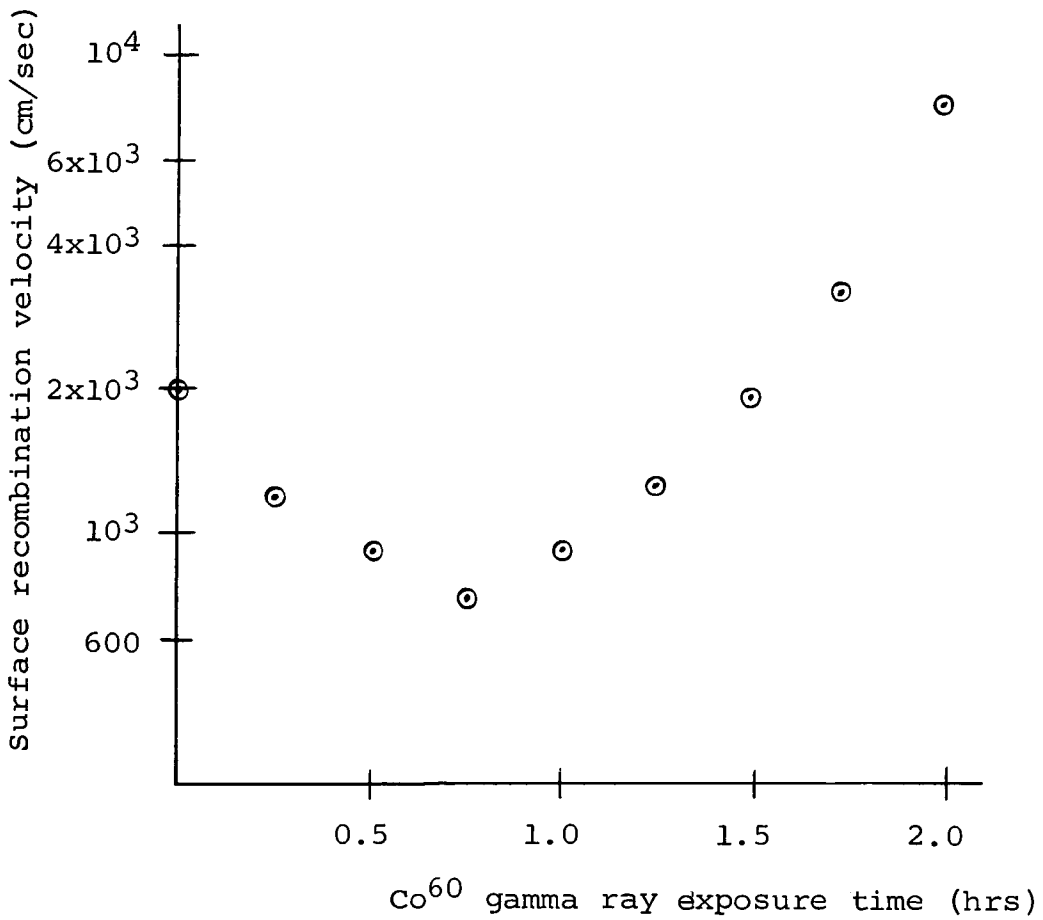

Figure 7.86. Average surface recombination velocity for the four samples of Figure 7.85 vs. gamma ray exposure time at the same exposure rate

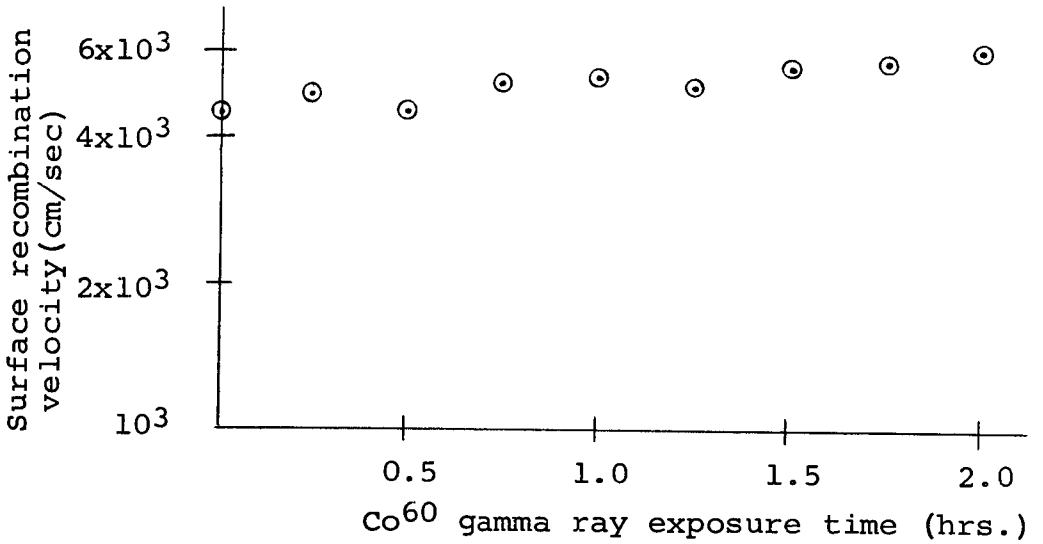
Surface recombination velocity (cm/sec)
6x10^3
4x10^3
2x10^3
10^3
0.5
1.0
1.5
2.0
Co^60 gamma ray exposure time (hrs.)

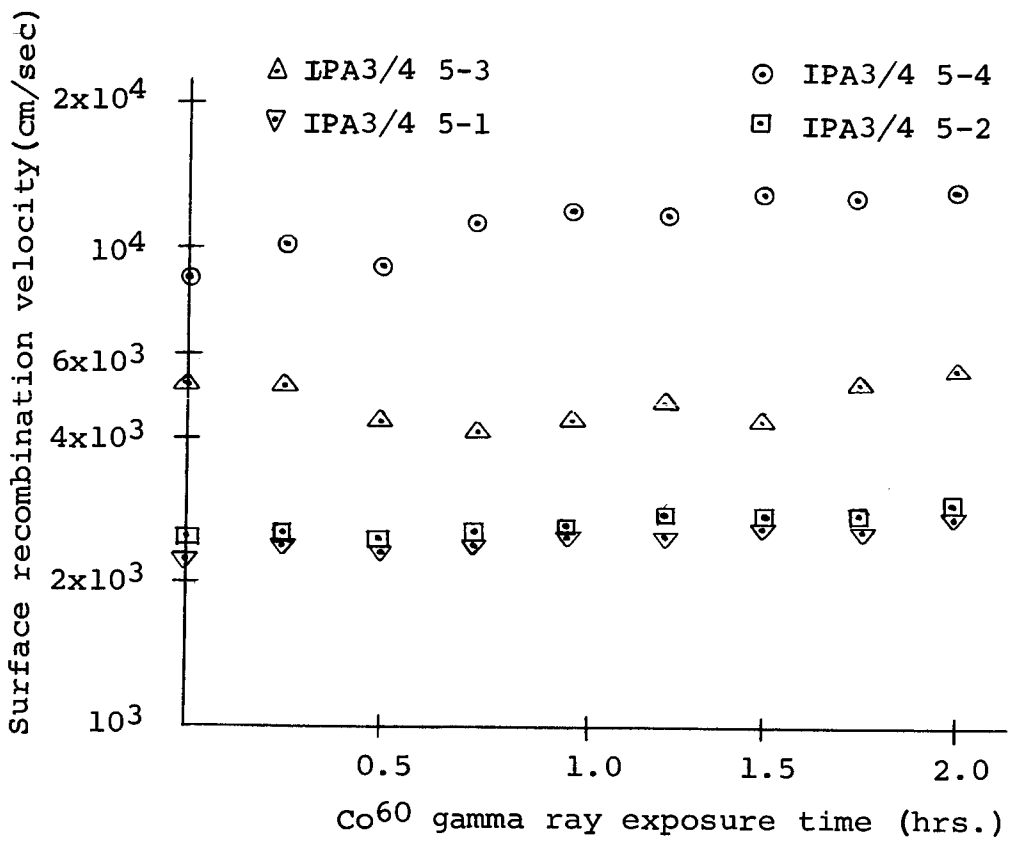
Surface recombination velocity (cm/sec)
IPA3/4 5-3
IPA3/4 5-4
IPA3/4 5-1
IPA3/4 5-2
2x10^4
10^4
6x10^3
4x10^3
2x10^3
10^3
0.5
1.0
1.5
2.0
Co^60 gamma ray exposure time (hrs.)

To explain the variations of surface recombination velocity with gamma ray exposure requires the use of the model derived in Chapter VI, which includes effects due to the space change region, and one-well founded assumption. It will be assumed that the gamma irradiation causes the energy bands to always bend upwards near the surface. Thus, an n-type surface will tend to first become depleted of majority electrons and then to invert to a p-type surface (i.e. Pos $< n_i < n_{os}$). A p-type surface will instead tend to become more p-type as the bands bend upward.

Consider the case of n-type material. It would be difficult to say exactly what condition the surface would be in initially, but since there is a very thin silicon oxide layer on the surface, one would expect it to still remain n-type. However, the presence of ozone in the Gamma Cell could tend to make the surface p-type (Staz et. al., 1965). Since the bands have been assumed to bend upwards, the surface recombination velocity would be greatly influenced by recombination in the space charge region, and the complete model of Chapter VI must be included. Figure 7.89 shows a pictorial sketch of this model along with the predicted variation of surface recombination velocity. If one assumes typical values of the parameters (Kinston, 1956) such as $C_{ps} = C_{ns} = 10^{-8}$ cm^3 sec^{-1}, $N_{ts} = 10^{12}$cm^{-2} , $N_{bo} = 10^{14}$ cm^{-3}, $N_i = 10^{10}$ cm^{-3}, and $U_t - U_o = 10$, then $s_{max} = 2500$ cm/sec. The minimum value of surface recombination velocity could occur from $.2s_{max}$ to $.5s_{max}$ as from 500 cm/sec to 1225 cm/sec. (See Figure 6.5). These values

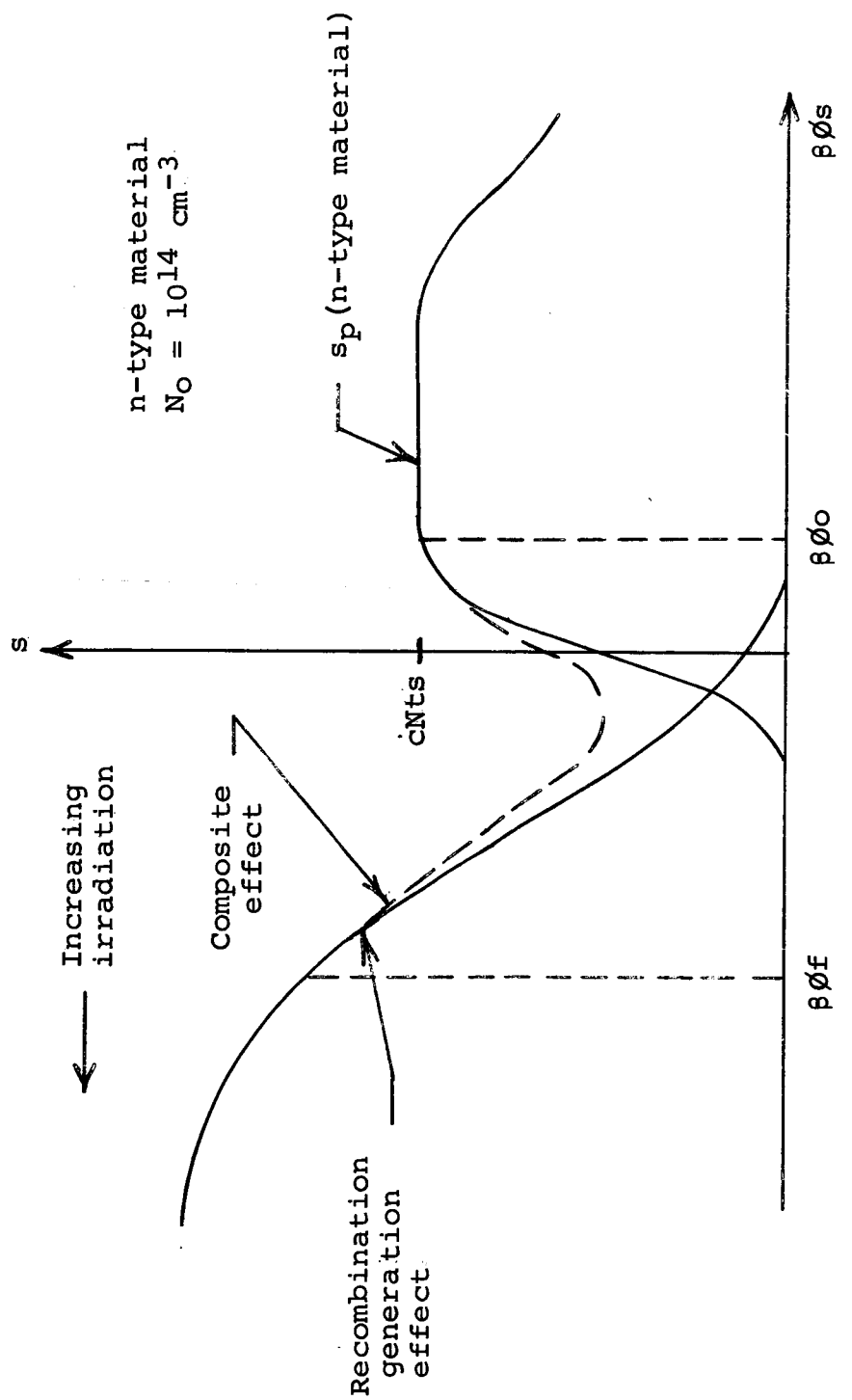

Figure 7.89. Predicted variation of surface recombination velocity in n-type material

from the theoretical model compare very favorably to values measured experimentally as well as the range on the values measured experimentally as irradiation is increased.

Now, in p-type material the change in electrostatic potential at the surface (the amount of band bending) is limited due to the fact that the initial condition of the surface is p-type and irradiation causes it to become more so. The amount of irradiation is not sufficient to increase the majority carrier concentration appreciably, and thus the variation of surface potential in p-type material due to gamma irradiation is small. For this reason, the variation in surface recombination velocity is small. Figure 7.90 shows the expected variation of surface recombination velocity for p-type material. Using the same typical values as before, it is seen that the values calculated from the theoretical model compare very favorably with those measured experimentally.

One point remains, and that is the question of why the energy level at the surface changes its position in the energy gap as the irradiation increases. As mentioned previously, this should not be expected. For example, in a non-degenerate semiconductor at reasonable temperatures, a donor atom in the crystal has an ionization energy that does not change even if the semiconductor is non-homogeneous (i.e. if the bands vary with position in our energy band scheme). While the analogy between a donor atom and a defect caused by a gamma photon is not complete, one can still argue that the ionization energy

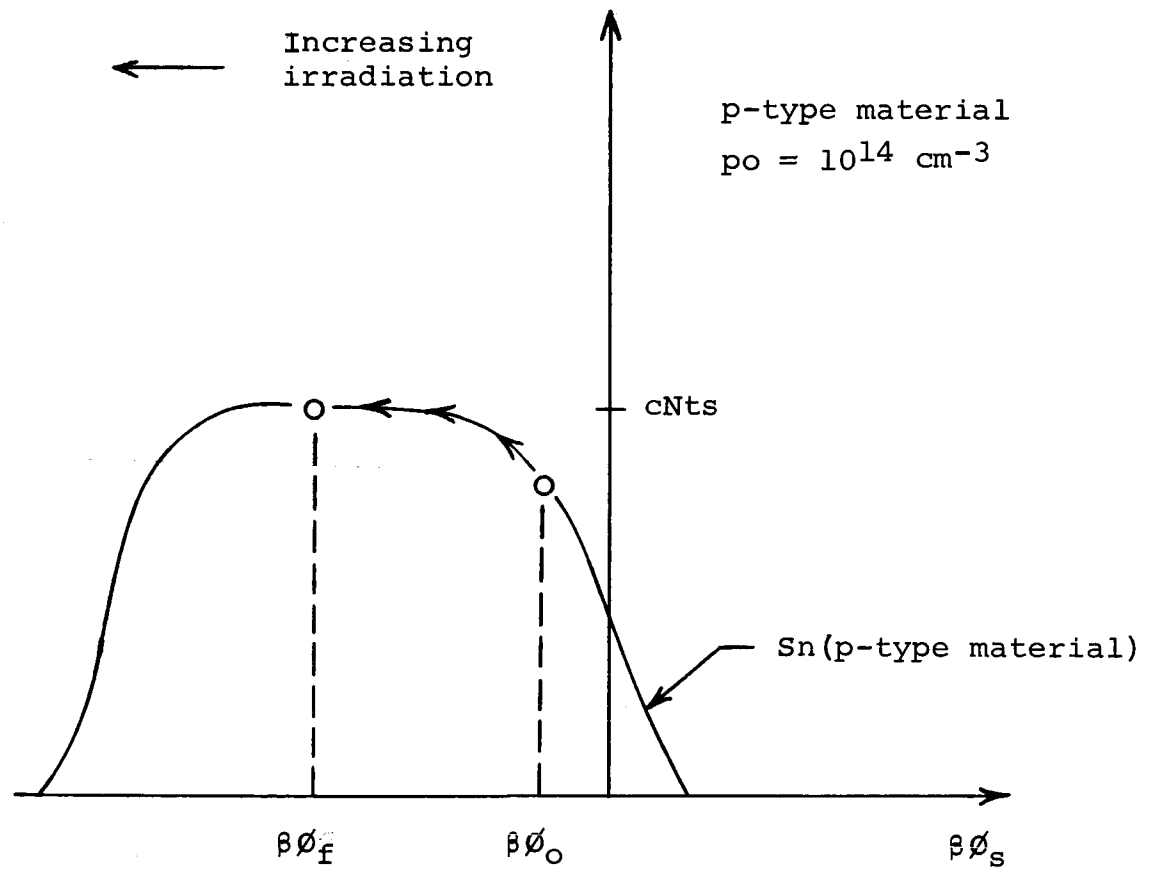

Figure 7.90. Predicted variation of surface recombination velocity in p-type material

of the defect should not change even though their density is being changed by additional gamma photons. Several possibilities exist to account for this variation of energy level position with irradiation. The energy level position could vary with temperature. The capture cross sections could also have a marked temperature dependence. (Hewes, 1966). The carrier concentration at the surface could change with temperature. While these possibilities exist, the temperature dependencies can not be determined and thus can not be accounted for.

Another argument might be that the states at the surface are distributed in energy. Such is often the case on surfaces which have been subjected to fabrication treatments. Then, the energy level might be some average energy over the distribution of surface states in energy. That is

$$\langle E \rangle = \frac{\int E N_S(E,\phi)\ dE}{\int N_S(E,\phi)\ dE} \qquad (7.1)$$

Thus $\langle E \rangle$ would be changing with irradiation flux ϕ, because the surface state density is changing with flux. However, whether or not this was true, could not be determined in this thesis because there was no way to determine $N_S(E,\phi)$.

While these possibilities exist for the explanation of the reason for the apparent change in the energy level position with irradiation, no attempt was made to formulate a model because of the limitations in obtaining useful information concerning this phenomenon with the measurement techniques used.

CHAPTER VIII

8. CONCLUSIONS AND FURTHER RECOMMENDATIONS

Based on the experimental results presented in the previous chapters, several conclusions can be reached concerning the effects of gamma irradiation on the bulk and surface recombination rates in silicon.

First of all, the bulk recombination center which dominates the lifetime of minority carriers in n-type material is not the same as the one which controls this lifetime in p-type material. However, for each type of material with a resistivity of approximately 100 ohm cm, the recombination process could be described mathematically using a one recombination center Shockley-Read model. No effects which would be attributed to more than one recombination center were observed in these experiments.

The defect controlling the bulk lifetime in n-type material was found to be located at 0.4 eV below the conduction band edge. This level has been observed by others and has been denoted as the E center, or the phosphorous-vacancy complex (Watkins and Corbett, 1961).

In p-type material the dominant recombination center was located at 0.18 eV above the valence band edge. While this level has been observed before in p-type pulled crucible material (which has an inherently large oxygen concentration) irradiated by electrons and gamma rays, this is the first time

it has appeared in p-type float zone material irradiated by gamma rays. As of yet, no positive identification has been made. It does not appear to depend upon whether or not oxygen is in the crystal since it has been found to be the dominant recombination center in both pulled crucible and float zone refined material, and its dependence on the type of dopant in the crystal is not known.

Gamma irradiation has a very large effect on the bulk lifetime of holes in n-type material, causing gross changes in the lifetime. In p-type material the changes in lifetime due to irradiation are small. This implies that the introduction rate (the number of defects created per incident gamma photon) for the defect in n-type material is much larger than that for the defect in p-type material. This has been proven experimentally (Nakano and Iniusho, 1964). However, it could also point out that the level at Ev + 0.18 eV in p-type material is not due to an interaction between the gamma rays and the impurity atom in the crystal.

No single energy level can be identified at the surface for either p-type or n-type material. As the samples are irradiated the position of the level, as determined by computer curve fits of surface lifetime versus reciprocal temperature to the Shockley-Read model changes its position in the forbidden region. For both types of material the locations of the level are nearly the same with respect to band edge. In n-type material the levels in the lower half of the forbidden

region at approximately 0.25 eV above the valence band while in p-type material the levels in the upper half of the forbidden region at approximately 0.2 eV below the conduction band edge. The variation of the level with the radiation is nearly the same in both types of materials. This behavior is very unusual, and cannot be explained with data and models used in these experiments. A closer look at the microscopic nature of the energy level will be required in order to explain this phenomena.

Gamma irradiation has a very large effect on the surface recombination velocity in n-type material whereas in p-type material there is a relatively small influence caused by the irradiation (This should be compared to the similiar variations of the bulk lifetime). This has been attributed to the influence of recombination in the space charge region near the surface of the semiconductor. A complete mathematical model has been derived which explains this effect, and shows that quantitatively one should expect the observed variations of surface recombination velocity.

Several recommendations can be made for extension of the work carried out here. First of all, a study of the introduction rates should be carried out to see what effect the resistivity and dopant in the pre-irradiated crystals have on the presence of the levels observed in this research. This study has already begun, and is presently being carried out in the Solid State Device Laboratory.

Also, a technique should be developed for directly measuring surface recombination velocity as a function of surface potential, to directly verify the theory presented here. This should be done for passivated surfaces as well as for free surfaces of silicon.

This theory could be utilized in a device analysis of the solar cell to completely explain why p/n solar cells are less radiation resistant than n/p solar cells. The results of this thesis illustrate the well-known results that the p-type bulk is less sensitive to irradiation, but the results for surface recombination have not been previously reported.

The effects of other types of irradiation such as electrons and neutrons should be examined, since these particles are known to have a drastic effect on the recombination processes in silicon.

Finally, the reason for the variation of the position of the energy level at the surface should be investigated and thoroughly explained.

9. LIST OF REFERENCES

Bardeen, John. 1947. Surface states and rectification at a metal-semiconductor contact. Phys. Rev., 71: 717-727.

Bemski, G. 1958. Recombination in semiconductors. Proc. Inst. Elec. Electron. Engrs. 46: 990-1004.

Blakemore, J. S. 1962. Semiconductor Statistics. Pergammon Press, New York.

Crawford, J. H. 1964. Radiation Effects and Defect Structures in Diamond Structure Semiconductors. pp. 421-470. In R. Strumane, J. Nihoul, R. Gevers, and S. Amelinckx (editors), The Interaction of Radiation with Solids. North Holland Publishing Co., Amsterdam.

Glaenzer, R. H., and C. J. Wolf. 1965. Recombination in gamma-irradiated silicon. J. Appl. Phys., 36: 2197-2201.

Hall, R. N. 1952. Electron-hole recombination in germanium. Phys. Rev., 87: 387.

Hauser, J. R. 1965. An approximation for generation-recombination current in p-n junctions. Proc. Inst. Elect. Electron. Engrs., 53: 743.

Haynes, J. R., and W. Shockley. 1951. The mobility and life of injected holes and electrons in germanium. Phys. Rev., 81: 835-843.

Heitler, W. 1956. Elementary Wave Mechanics With Applications to Quantum Chemistry. Oxford University Press, London.

Hewes, R. A. 1966. Recombination lifetimes in Gamma irradiated silicon. Unpublished Ph.D. thesis, Department of Physics, University of Illinois. University Microfilm, Urbana, Illinois.

Inuishi, Y., and K. Matsuura. 1963. The interaction of radiation with solids. J. Phys. Soc. Japan, Supplement III, 18: 240-246.

Johnson, W. E., and K. Lark-Horovitz. 1949. Neutron irradiated semiconductors. Phys. Rev., 76: 442-443.

Kingston, R. H. 1954. Switching time in junction diodes and junction transistors. Proc. Inst. Elec. Electron. Engrs. 42: 829-834.

Lade, R. W. 1962. A study of high-low junctions and high-low junction semiconductor devices. Unpublished Ph.D. thesis, Department of Electrical Engineering, Carnegie Institute of Technology. University Microfilm, Pittsburgh, Pennsylvania.

Lark-Horovitz, K, E. Bleuler, R. David, and D. Tendam. 1948. Deuteron bombarded semiconductors. Phys. Rev., 73: 1256.

Littlejohn, M. A., and R. W. Lade. 1965. Silicon surface damage due to gamma irradiation. Proc. Nat. Electron. Conf. 21: 67-72.

Littlejohn, M. A., and R. W. Lade. 1966. Surface recombination velocity investigations. Semi-annual Progress Report No. 4. NASA Grant NsG-588: 1-16.

Many, A., Y. Goldstein, and N. B. Grover. 1965. Semiconductor Surfaces. John Wiley and Sons, Inc., New York.

Mattauch, R. J., R. W. Lade, and G. B. Hoadley. 1965. Tables of $F(U_s, U_b)$ and $G(U_s, U_b)$ functions for semiconductor surface calculations. Bulletin 80. North Carolina State University, Department of Engineering Research. Raleigh, N. C.

Mattauch, R. J., and R. W. Lade. 1965. Surface state density variations on MOS structures due to gamma irradiation. Proc. Inst. Elect. Electron. Engrs., 53 (11): 1748.

Nakano, T., and Y. Inuishi. 1964. Effects of dosage and impurities on radiation damage of carrier lifetime in silicon. J. Phys. Soc. Japan, 19: 851-858.

Nakano, T., and Y. Inuishi. 1964. Hall effect measurement of radiation damage and annealing in silicon. J. Phys. Soc. Japan, 19: 167-174.

Nakano, T., K. Nakasima, and Y. Inuishi. 1965. Radiation damage of carrier lifetime in p-type silicon. J. Phys. Soc. Japan, 20: 2140-2146.

Nussbaum, Allen. 1962. Semiconductor Device Physics. Prentice Hall, Inc., Englewood Cliffs, N. J.

Price, W. J. 1964. Nuclear Radiation Detection. McGraw Hill Book Company, Inc., New York.

Rhodes, R. G. 1964. Imperfections and Active Centers in Semiconductors. The MacMillan Company, New York.

Sah, C. T., and W. Shockley. 1958. Electron-hole recombination statistics in semiconductors through flaws with many charge conditions. Phys. Rev., 109: 1103-1115.

Saito, H., M. Hirata, and T. Horuichi. 1963. The interaction of radiation with solids. J. Phys. Soc. Japan, Supplement III, 18: 246-251.

Sandiford, D. J. 1957. Carrier lifetimes in semiconductors for transient conditions. Phys. Rev., 105: 524.

Shockley, W., and W. Read. 1952. Statistics of the recombination of holes and electrons. Phys. Rev., 87: 835-842.

Sonder, E., and L. C. Templeton. 1960. Gamma irradiation of silicon. I. Levels in n-type pulled crucible material. J. Appl. Phys., 31: 1279-1286.

Sonder, E., and L. C. Templeton. 1963. Gamma irradiation of silicon. II. Levels in n-type-float zone material.

Sonder, E., and L. C. Templeton. 1965. Gamma irradiation of silicon. III. Levels in p-type material. J. Appl. Phys., 36: 1811-1815.

Statz, H., G. A. DeMars, L. Davis, Jr., and A. Adams, Jr. 1956. Measurements of inversion layers on silicon and germanium and their interpretation. pp. 139-168. In R. H. Kingston (ed.) Semiconductor Surface Physics. University of Pennsylvania Press, Philadelphia.

Streetman, B. G. 1966. Carrier recombination and trapping effects in transient photoconductive decay measurements. J. Appl. Phys., 37: 3137-3144.

Sullivan, M. V., and J. H. Eigler. 1957. Electroleso nickel plating for making ohmic contacts to silicon. J. Electrochem. Soc., 104(4): 226-229.

Tanaka, T., and Y. Inuishi. 1965. Hall effect measurement of radiation effect on p-type silicon. Japan. J. Appl. Phys., 4(10): 725-730.

Watkins, G. D., and J. W. Corbett. 1961. Defects in irradiated silicon. Phys. Rev., 101: 1001-1022.

Watkins, G. D., and J. W. Corbett. 1964. Defects in irradiated silicon: electron paramagnetic resonance and electron-nuclear double resonance of the silicon-E center. Phys. Rev., 134: A1359-A1377.

Wertheim, G. K. 1958. Transient recombination of excess carriers in semiconductors. Phys. Rev., 109: 1086-1091.

Zhdanova, N. G., S. G. Kalashnikov, and A. I. Morozov. 1959. The effect of temperature on the recombination rate of electrons and holes at copper atoms in germanium. Soviet Physics - Solid State, 1: 481-490.

10. APPENDICES

10.1 Appendix I. Discussion of the IRE Standards on Photoconductive Decay Measurements

In the August, 1961 issue of the Proceedings of the Institute of Radio Engineers the Standards Committee on Semiconductor Electronics set up the IRE standards on the measurement of minority carrier lifetime in germanium and silicon by the method of photoconductive decay. These standards set forth a set of generally accepted rules which should be followed when using this technique.

These standards have been followed throughout the experiments, and the techniques specified are summarized in the following paragraphs.

10.1.1 Life Time Measurements

1. Turn all components of system on and allow time for warm-up.
2. Put sample in sample holder. Make sure light source is perpendicular to sample and filter. Filter should be parallel with sample.
3. Adjust the calibrated dial on the exponential generator until the curve from the exponential generator matches the curve from the sample. The match should be made between the 15% and 50% values of the sample signal (preferably between 40% and 15%). This can be done by adjusting the vertical gain until the signal covers at least 5 cm. and matching the two signals between .75 cm and 2 cm. Make sure the initial base lines at both signals are matched before and

after measurement. Read the dial on the exponential generator, noting the switch position, and read the tentative life time from the curve for that respective switch position from Figure 4.8.

4. After the life time (τ) has been determined, note the reading V_o on the 610R (d-c voltage across sample) and compare with value on Figure 10.1 for respective material types. For a given τ measured, the value of V_o from the 610R should be less than the value from the graph. If not, reduce V_o and redetermine τ.
5. If the above condition is satisfied, use this value of V_o and find the gain-V_o product. From Figure 10.2 determine the macimum $\Delta V'$. The value of $\Delta V'$ observed on the scope should be less than this maximum $\Delta V'$ from Figure 10.2. The gain and aplitude limitations of the pre-amp. should be known before any measurements are made.
6. Check the life time measurement again as described in 3 and record the value.
7. If there is suspected error in the value of τ; check the value of ΔV without V_o and with V_o across the sample. ΔV without V_o should be less than 1% of ΔV with V_o.
8. Life time measurements as outlined above should be made at different values of I_{cc} (both positive and negative). The value of τ should not vary beyond the accuracy of measurement for a different magnitude and current direction.

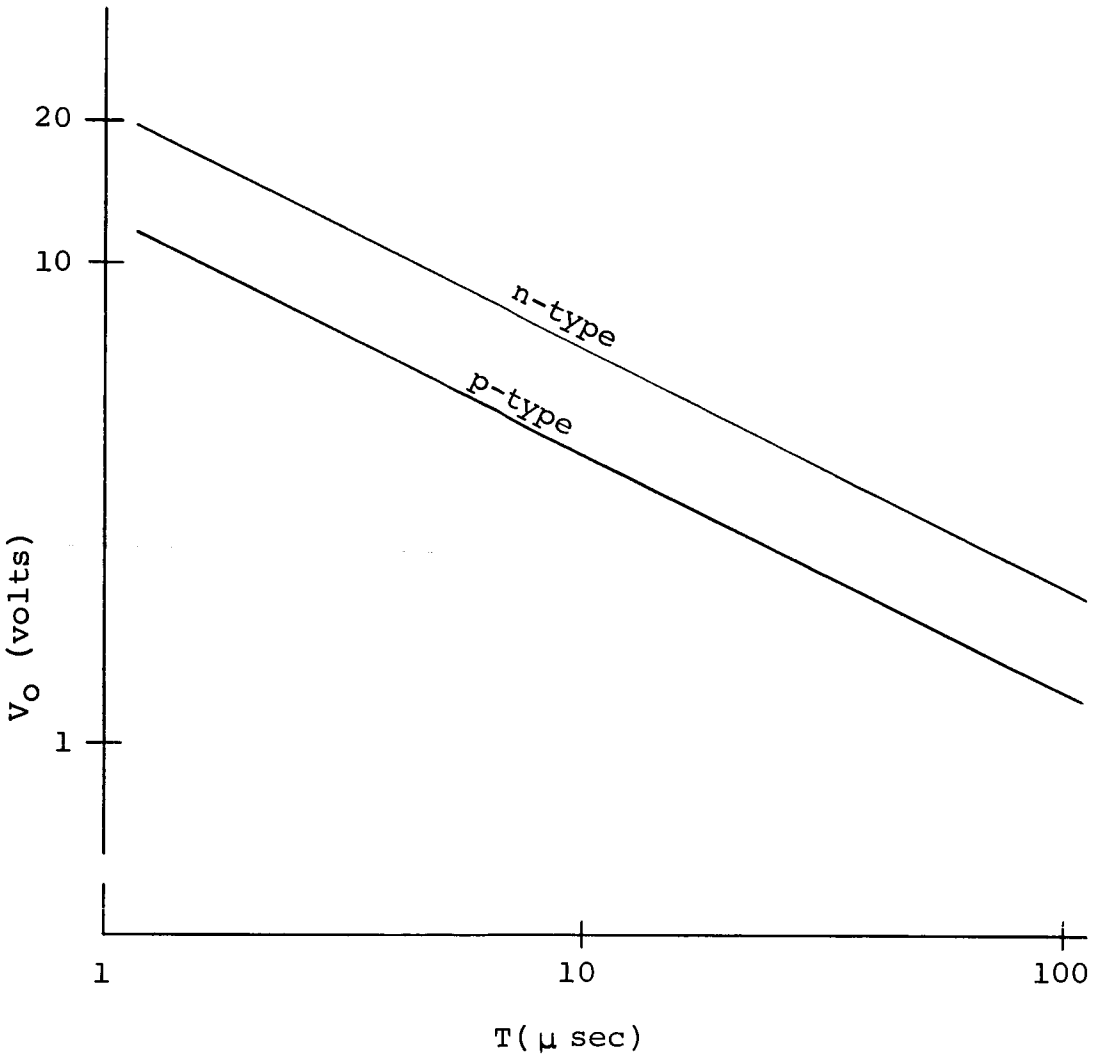

Figure 10.1. Maximum voltage across the sample vs. filament lifetime

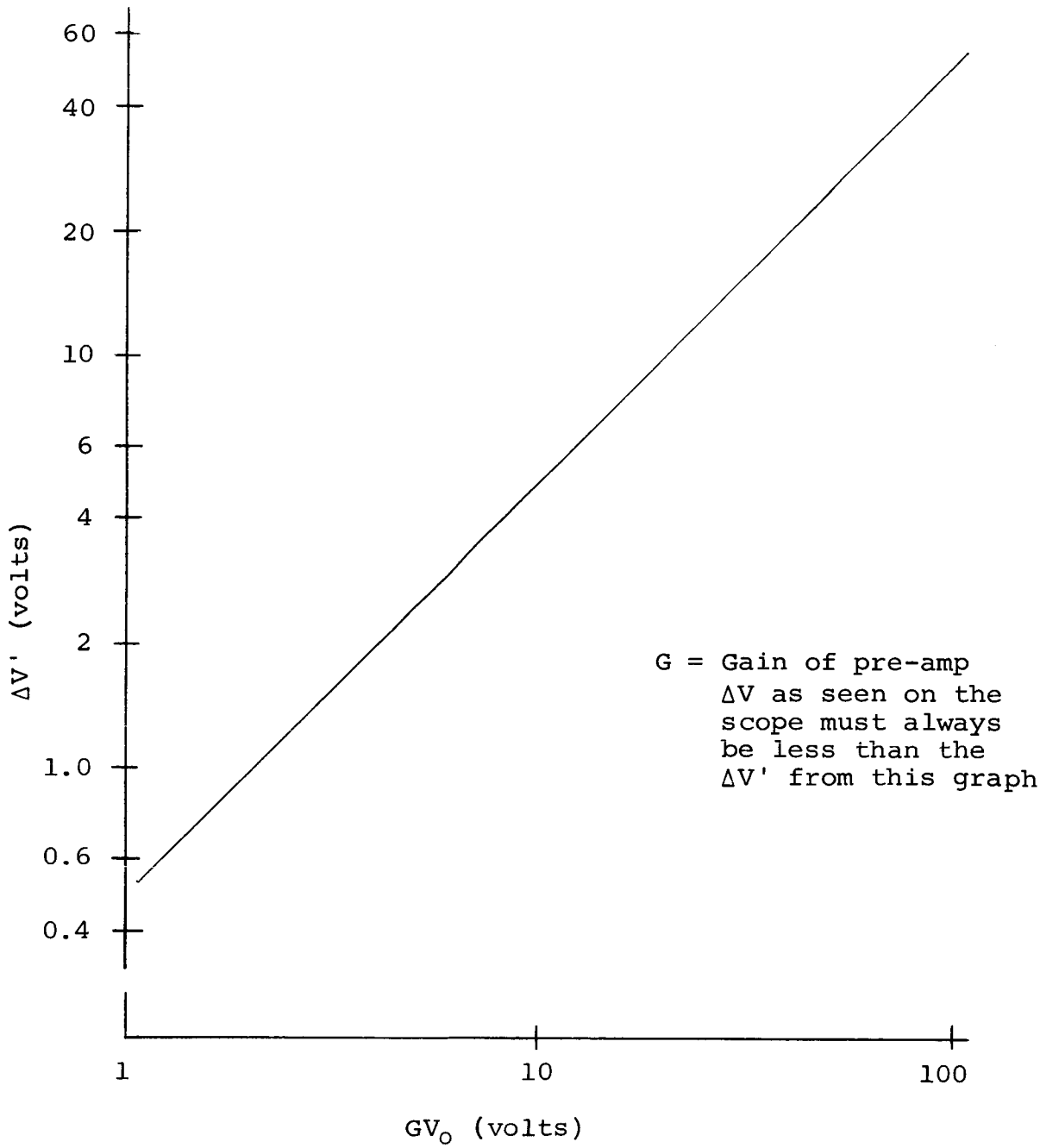

Figure 10.2. Maximum change in voltage across the sample vs. voltage across the sample before illumination

10.2 Appendix II. Curve Fitting

In Chapter V, it is seen that if the experimentally measured values of lifetime versus reciprocal temperature can be fitted to the Shockley-Read model, then the location of the recombination center in the forbidden region can be determined. In this work, a technique described by Matthews (1964) is used to adjust the parameters in the Shockley-Read model, until a best fit of the experimental data to this model is obtained.

To discuss this curve fitting technique, the following quantities are defined:

- N - total number of parameters in the fitting function
- M - total number of data points
- G_i - assumed value for the ith parameter
- G_i^b - value of the ith parameter which provides the best fit
- g_i - best change of its parameter, with $G_i^b - G_i = g_i$
- f_m - $f(T_m, G_1, G_2, \ldots, G_n)$, value of the fitting function at the temperature, T_m.
- f_m^b - $f(T_m, G_1^b, G_2^b, \ldots, G_n^b)$, value of the fitting function which provides the best fit at T_m.
- F_m - value of the measured quantity at the temperature, T_m.

Now, if the derivatives of the fitting function exist near a point T_m, then a Taylor series expansion around this point gives

$$f(T, G_1, \ldots, G_n) = f_m + \left.\frac{\partial f}{\partial T}\right|_{T=T_m} \Delta T + \sum_{L=1}^{N} \left.\frac{\partial f}{\partial G_i}\right|_{T=T_m} \Delta G_i \qquad (10.1)$$

$$+ \ldots$$

If it is assumed that the parameters are close to those which yield a best fit, then equation 10.1) becomes

$$f_m^b \approx f_m + \sum_{i=1}^{N} \frac{\partial f_m}{\partial G_i} dG_i \tag{10.2}$$

where $\Delta T = 0$. This can be written as

$$f_m^b \approx f_m + \sum_{i=1}^{N} \frac{\partial f_m}{\partial G_i} g_i \tag{10.3}$$

The error at $T = T_m$, between the measured quantity and the function of best fit is

$$\epsilon_m = F_m - f_m^b \tag{10.4}$$

or

$$\epsilon_m \approx F_m - f_m^b - \sum_{i=1}^{N} \frac{\partial f_m}{\partial G_i} g_i \tag{10.5}$$

The square of the error summed over the M data points is

$$\sum_{m=1}^{M} \epsilon_m \epsilon_m = \langle \epsilon^2 \rangle = \sum_{m=1}^{M} [F_m - f_m - \sum_{i=1}^{N} \frac{\partial f_m}{\partial G_i} g_i]^2 \tag{10.6}$$

Note that $\langle \epsilon^2 \rangle$ is a function only of the g_i's. The total differential of $\langle \epsilon^2 \rangle$ is

$$d\langle \epsilon^2 \rangle = -2 \sum_{m=1}^{M} \left\{ [F_m - f_m - \sum_{i=1}^{N} \frac{\partial f_m}{\partial G_i} g_i] \, [\sum_{j=1}^{N} \frac{\partial f_m}{\partial G_j} dg_j] \right\} \tag{10.7}$$

By setting the co-efficients of the dg_j's equal to zero for $j = 1, 2, \ldots, N$ insures that the mean square error is a minimum. Thus

$$\sum_{m=1}^{M} \left\{ [F_m - f_m - \sum_{j=1}^{N} \frac{\partial f_m}{\partial G_i} g_i][\frac{\partial f_m}{\partial G_j}] \right\} = 0 \qquad (10.8)$$

for $j = 1, 2, \ldots, N$. This can be written as

$$\sum_{m=1}^{M} (F_m - f_m)(\frac{\partial f_m}{\partial G_j}) = \sum_{m=1}^{M} \sum_{j=1}^{N} \frac{\partial f_m}{\partial G_i} \frac{\partial f_m}{\partial G_j} g_i \qquad (10.9)$$

for $j = 1, 2, \ldots, N$. Equation 10.9 represents a set of N equations (one for each value of j) in the N unknowns $g_1, g_2, \ldots, g_n$.

The procedure used to find the best fit of a set of experimental data to the Shockley-Read model is to first arbitrarily choose initial values for the G_i parameters. A computer is programmed to solve the set of equation 10.9 by Matrix inversion. Once the g_i's are known then a new set of parameters G_i can be calculated from the relation $G_i = G_i + g_i$. In reality, the initial arbitraty choice of the G_i's is not sufficiently accurate to permit the g_i's to yield the best fit. However, the g_i's provide a means for making a better estimate of the G_i's so that an iterative procedure may lead to their convergence to the G_i^b's. In general, this procedure will lead to convergence if no parameter is allowed to change by more than 20% - 75%, in each iteration. Also all parameters change in proportion to their g_i's and in proportion to a scaling factor which is determined by max (g_i/G_i). (See Matthews, 1964).

This method has been used to obtain the energy levels of the recombination centers, and as seen by the graphs in Chapter VII, good agreement is obtained between experiment and theory.

10.3 Appendix III. Photoconductive Decay in a Rectangular Semiconductor Bar

A complete analysis of this problem has been presented in Blakemore (1962). The following treatment indicates how the method of photoconductive decay is used to measure bulk and surface lifetime. Figure 10.3 shows the geometry used in the analysis. The sample is a rectangular semiconductor bar with cross sectional dimensions 2A and 2B. The sample is assumed to be very long in the X direction so that any end effects are negligible. A constant current I is assumed to pass through the bar, and a protion of the bar is illuminated. This illumination modulates the conductivity of the bar, and the conductivity of the bar, and the conductivity is given by

$$G = \frac{4AB}{L}\sigma = \frac{4AB}{L}(\sigma_o + \Delta\sigma) \tag{10.10}$$

Here σ_o is the equilibrium (no illumination) conductivity, and $\Delta\sigma$ is the change in conductivity due to illumination. Thus

$$\begin{aligned} \sigma_o &= q\mu_p p_o + q\mu_n n_o \\ \Delta\sigma &= q\mu_p \bar{p} + q\mu_n \bar{n} \end{aligned} \tag{10.11}$$

Defining $\mu_n/\mu_p = b$ and assuming $\bar{p} = \bar{n}$

$$\begin{aligned} \sigma_o &= q\mu_p (p_o + bn_o) \\ \Delta\sigma &= q\mu_p (b + 1)\bar{p} \end{aligned} \tag{10.12}$$

Thus the voltage across the rectangular bar can be written as

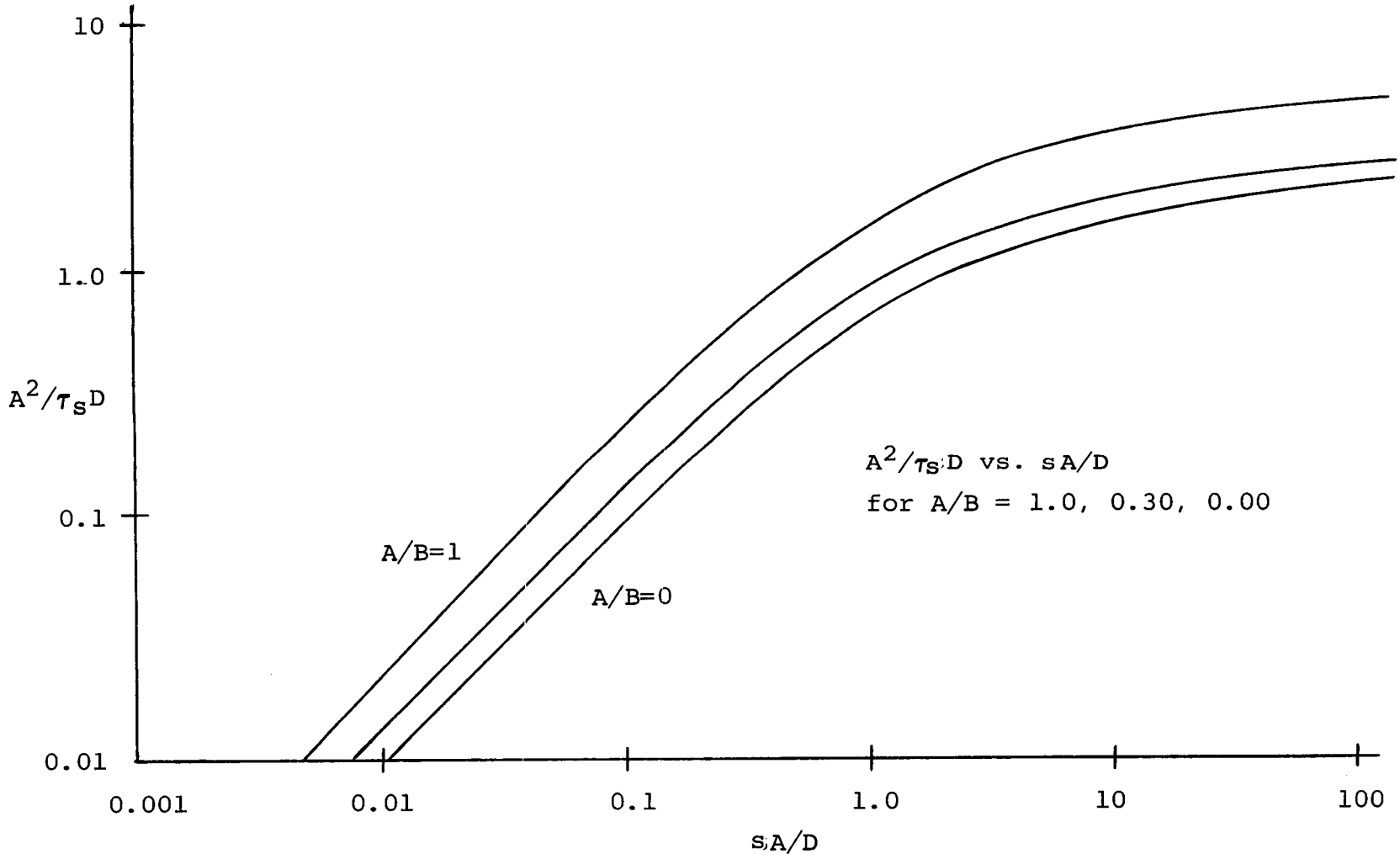

Figure 10.3. $A^2/\tau_S D$ vs. sA/D where A is the smallest sample dimension, D the ambipolar diffusivity, τ_S the surface lifetime and s the surface recombination velocity

$$V = \frac{\text{constant}}{1 + \frac{(b + 1)}{p_o + bn_o}\ \overline{p}} \tag{10.13}$$

If we assume low level injection such as $\overline{p} << p_o + n_o$, then

$$V \approx \text{constant}\ (1 + \frac{b + 1}{p_o + bn_o}\ \overline{p})$$

or

$$V \approx V_o - \Delta V \tag{10.14}$$

The change in voltage is proportional to the change in excess carrier concentration.

To obtain an expression for the excess carriers in the bar, the continuity equation must be solved.

$$\frac{\partial \overline{p}}{\partial t} = \frac{p - p_o}{\tau_p} - \mu_p E_x \frac{\partial \overline{p}}{\partial x} + D_p \left(\frac{\partial^2 \overline{p}}{\partial x^2} \quad \frac{\partial^2 \overline{p}}{\partial y^2} \quad \frac{\partial^2 \overline{p}}{\partial z^2}\right) \tag{10.15}$$

Using separation of variables, one solution of this equation is

$$\overline{p}(x,y,z,t) = e^{-vt}e^{-ax}\cos b_y \cos c_z \tag{10.16}$$

where a, b, c, and v are defined by the equation

$$v - \frac{1}{\tau_p} + \mu_p E_x a + D_p\ (a^2 - b^2 - c^2) = 0 \tag{10.17}$$

Assuming the surface recombination velocity, s, is the same on all surfaces and using the boundary conditions discussed in Chapter VI

$$J_{py} = \pm\ qs\overline{p} \quad \text{at } y = \pm\ A$$

$$J_{pz} = \pm\ qs\overline{p} \quad \text{at } g = \pm\ B$$

in equation 10.7 gives

$$bA \tan bA = \frac{sA}{D_p} = \alpha \tan \alpha$$
$$cB \tan cB = \frac{sB}{D_p} = \eta \tan \eta \qquad (10.18)$$

There are an infinite number of roots of these transcendental equations and in general the solution is an infinite series of solutions of the form of equation 10.7. However, for photoconductive decay, the first order solution is the most important (See Blakemore, 1962). Equation 10.8 becomes

$$V + D_p a^2 + \mu_p E_x a = \frac{1}{\tau_p} + D_p \left(\frac{\alpha_o^2}{A^2} + \frac{n_o^2}{B^2}\right) \qquad (10.19)$$

If V_f is defined as

$$V_f = \frac{1}{\tau_p} + D_p \left(\frac{\alpha_o^2}{A^2} + \frac{n_o^2}{B^2}\right), \text{ then}$$

$$D_p a^2 + \mu_p E_x a = V_f - V$$

or

$$a(D_p a + \mu_p E_x) = V_f - V \qquad (10.20)$$

Thus if $a = 0$ or $a = -\frac{\mu_p E_x}{D_p}$, then $V_f = V$. In reality, another condition is needed to completely determine both a and V. This condition is the assumption that end effects in the X direction can be neglected, which was never explicitly stated in a mathematical form. Assuming that the carrier distribution in the X direction is uniform and requires $a = 0$ and then

$$V = V_f = \frac{1}{\tau_f} + \frac{1}{\tau_s} \qquad (10.21)$$

where

$$\frac{1}{\tau_s} = D_p\left(\frac{\alpha_o^2}{A^2} + \frac{\eta_o^2}{B^2}\right)$$

The filament lifetime, V^{-1}, is then a sum of a bulk contribution and a surface contribution. Figure 10.3 shows a graph of $A^2/\tau_s D_p$ versus sA/D_p for several values of dimension ratio A/B.